José Eduardo Ferreira Araújo

Mestre em Genética Molecular Comparativa e Tecnológica

Peptidome and Proteome Peritoneal Dialysate Evolutionary Atlas (P3DEVOATLAS)

Dissertação para obtenção do Grau de Doutor em Química

Orientador: Doutor Hugo Miguel Baptista Carreira dos Santos,
Investigador Auxiliar, Faculdade de Ciências e Tecnologia, Caparica
Universidade NOVA de Lisboa, Portugal

Coorientadores: Doutor Janne Lehtiö, Professor e Diretor Científico,
Science for Life Laboratory, Karolinska Institutet, Suécia

Doutor Carlos Lodeiro Espiño, Professor Associado com Agregação,
Faculdade de Ciências e Tecnologia, Caparica
Universidade NOVA de Lisboa, Portugal

Júri:

Presidente: Doutora Ana Aguiar-Ricardo

Arguente: Doutor José Luís Gómez-Ariza

Arguente: Doutora Deborah Penque

Vogais: Doutor Hugo Miguel Santos

Doutor José Luís Capelo-Martínez

FACULDADE DE CIÊNCIAS E TECNOLOGIA
UNIVERSIDADE NOVA DE LISBOA

Março 2020

José Eduardo Ferreira Araújo

Mestre em Genética Molecular Comparativa e Tecnológica

Peptidome and Proteome Peritoneal Dialysate Evolutionary Atlas (P3DEVOATLAS)

Dissertação para obtenção do Grau de Doutor em Química

This thesis was supported by the Foundation for Science and Technology, with the fellowship, reference number SFRH/BD/109201/2015 and by the ProteoMass Scientific Society and Lehtiö Lab

Março 2020

Peptidome and Proteome Peritoneal Dialysate Evolutionary Atlas (P3DEVOATLAS)

ACKNOWLEDGEMENTS

No decorrer da realização deste trabalho, inúmeras pessoas e instituições intervieram, através da colaboração, disponibilidade, apoio e ensinamentos, quer diretamente como indiretamente. A todas essas pessoas presto os meus sinceros agradecimentos.

Ao Doutor Hugo Miguel Baptista Carreira dos Santos, pela orientação, pela sua disponibilidade e apoio laboratorial sempre que necessário e ensinamentos transmitidos no decorrer deste projeto.

Ao Professor Doutor Janne Lehtiö, pela coorientação, voto de confiança em aceitar como seu orientando, revisão crítica deste trabalho que contribuiu para um maior rigor científico e apoio financeiro no âmbito do trabalho desenvolvido no seu grupo de investigação.

Ao Professor Doutor Carlos Lodeiro Espiño, pela coorientação, conselhos dados e disponibilidade sempre que necessária, boa disposição e o apoio financeiro no âmbito do projeto.

Ao Professor Doutor José Luís Capelo Martínez, pelo voto de confiança, aceitando-me no seu grupo de investigação para realizar o Mestrado, que após concluído, deu a continuidade para o desenvolvimento deste projeto. Agradeço ainda, a contribuição para a minha formação como investigador e revisão crítica deste trabalho.

Ao Doutor Rui Mamede Branca, pela orientação e ajuda dada durante o meu período de adaptação na instituição de acolhimento estrangeira, pela sua disponibilidade, apoio e ensinamentos transmitidos.

Ao Hospital Garcia da Orta, mais concretamente ao Serviço de Nefrologia e em especial ao Sr. Doutor Fernando Teixeira e Costa e Sra. Doutora Aura Ramos, pela colaboração e disponibilização das amostras para este estudo.

A todos os meus colegas dos grupos de investigação Bioscope e LehtiöLab, pelo companheirismo, entreajuda e convívio dentro e fora do trabalho.

Aos meus Amigos e Família, pela amizade, confiança, carinho e apoio incondicional, o meu mais sincero Obrigado!

Pelo suporte financeiro agradeço à FCT, no âmbito do projeto SFRH/BD/109201/2015, assim como aos grupos de investigação LehtiöLab e Bioscope e à Associação Científica Proteomass

ABSTRACT

Peritoneal membrane (PM) failure in patients with end stage renal disease submitted to peritoneal dialysis (PD) cannot be predicted and does not occur in every patient in the same sequence and to the same extent. Moreover, long-term PD leads to morphological and functional alterations in the PM, reducing the lifespan of this dialysis up to five years, and forcing the replacement of PD by other renal replacement therapies. This represents a lower quality of life for the patients and extra cost of tens of million euros per year for the Portuguese National Health System.

Peritoneal dialysis effluent (PDE) represents an underestimated biochemical window into the peritoneum and a useful reservoir of potential clinical biomarkers. Therefore, this work aims to develop longitudinal studies to unravel the evolution of the peptidome and proteome of the PDE with time, to identify specific molecular changes that can be particularly interesting for the understanding and early detection of long-term PM alterations. To achieve this goal, mass spectrometry (MS)-based methods are needed to improve PDE proteome and peptidome analysis and to overcome some drawbacks that can arise from such a complex biological sample that can hamper the proteome and peptidome coverage.

For this reason, this thesis is focused also in the use of sample treatments and methodologies to reduce PDE sample complexity prior to MS analysis. Therefore, different methods of sample treatment were assessed with success as proteomics tools for getting insight into the PDE proteome and peptidome. Furthermore, this research constitutes the first proteome and peptidome-based longitudinal study of PD patient. In addition, the results represent the highest proteome and peptidome coverage ever achieved for this complex sample. Hence, this knowledge could be useful for the proteomic and clinical PD-devoted research community.

Keywords: Peritoneal dialysis effluent, Sample preparation, Mass spectrometry, Proteome analysis, Peptidome analysis, Longitudinal studies

RESUMO

A falha da membrana peritoneal (MP) em pacientes submetidos a diálise peritoneal (DP), não é um fenómeno possível de predizer, não ocorrendo de forma uniforme em todos os pacientes. A DP prolongada no tempo induz alterações morfológicas e funcionais na MP, o que reduz o tempo útil de tratamento a um máximo de 5 anos. Após este período, o paciente é forçosamente transferido para outro tipo de terapia de substituição renal, perdendo qualidade de vida e aumentando os custos de tratamento em dezenas de milhões de euros para o Serviço Nacional Saúde.

O efluente de diálise peritoneal (EDP), quando não menosprezado, representa um *reservoir* de potenciais biomarcadores que poderá ser útil para entender a bioquímica do peritoneu. Assim, este trabalho pretende efetuar um estudo temporal de modo a avaliar o conteúdo peptidómico e proteómico do EDP. A identificação de proteínas e péptidos indicadores de alterações da MP é particularmente interessante para compreender os mecanismos de alterações da MP ao longo do tratamento. No entanto, é necessário desenvolver métodos que melhorem e permitam ultrapassar algumas das dificuldades que advém da complexidade biológica deste tipo de amostra e que impedem a análise apropriada destas.

Por as razões acima mencionadas, esta tese é focada também na investigação e aplicação de metodologias para o tratamento de amostra de forma a reduzir previamente a complexidade das amostras de EDP antes da análise por espectrometria de massa. Diferentes metodologias foram testadas e permitiram com sucesso a análise proteómica e peptidómica das amostras de EDP. A investigação desenvolvida representa o primeiro estudo longitudinal neste tipo de amostra em pacientes de DP e com o maior número de proteínas e péptidos alguma vez identificados. Este conhecimento poderá ser útil para a comunidade proteómica e médica que desenvolvem investigação nesta área.

Palavras-chave: Efluente de diálise peritoneal, Preparação de amostra, Espectrometria de massa, Análise proteómica, Análise peptidómica, Estudo Longitudinal.

SUBJECT INDEX

FIGURES INDEX

Annex I

TABLES INDEX

Annex I

Electronic Supplementary Material Tables

Electronic Supplementary Material of Chapter VI can be assessed at ProteomeXchange:

Project Name: In-Depth Analysis of Peritoneal Dialysis Effluent Proteome and Peptidome: A Longitudinal Follow-Up Study

Project accession: PXD016853

Username: reviewer78275@ebi.ac.uk

Files:

Table ESM1- Detailed clinical information of the patient's cohort. File name: "Clinical_information_PDE_patients_cohort".

Table ESM2- Table with all the proteins identified and quantified with TMT labelling for all patients. File name: "TMT_quantification_PDE_study".

Table ESM3- Protein ranking abundance, proteins ¬ quantified and summarized are ranked according to their MS1 intensities and divided into four groups –(non-)unique for PDE, (non-) shared across patients– with neuropathy plasma dataset proteins as background. File name: "Proteome_rank_PDE_nephro2_protein_categories".

Table ESM4- Proteasix protease prediction analysis of the endogenous peptides acquired and identified with the CID fragmentation method. File name: "Proteasix_CID_input_observed".

Table ESM5- Proteasix protease prediction analysis of the endogenous peptides acquired and identified with the HCD-EThcD fragmentation method. File name: "Proteasix_HCD_EThcD_input_observed".

SYMBOLS, UNITS AND ABBREVIATIONS

A

Å	Ångström
ACE	Angiotensin converting-enzyme
ACN	Acetonitrile
ACS	Acute coronary syndromes
ADAMTS13	A disintegrin and metalloproteinase with thrombospondin motifs 13
AEBSF	Aminoethyl benzylsulfonyl fluoride
AGEs	Advanced glycation end products
AKT	Protein Kinase B
Ambic	Ammonium bicarbonate
AMI	Acute Myocardial Infarction
AngII	Angiotensin II
APD	Automated Peritoneal Dialysis
ADPKD	Autosomal dominant polycystic kidney disease
AQP	Aquaporin
ARB	Angiotensin II receptor blockers

B

BCA	Bicinchoninic acid
BMP	Bone morphogenic protein
BSA	Bovine serum albumin
BSG	Basigin

C

C18	18 carbon aliphatic chains
C8	8 carbon aliphatic chains
CA125	Cancer antigen 125
CAMs	Cell adhesion molecules
CAPD	Continuous ambulatory Peritoneal Dialysis
CAV-1	Caveolin-1
CBB	Coomassie brilliant blue
CCT/TRiC	Chaperonin-containing t-complex polypeptide 1
CCL18	CC chemokine ligand 18
ClAA	Chloroacetamide
CCPD	Continuous cycling peritoneal dialysis
CHAPS	3-[(3-cholamidopropyl)dimethylammonio]-1-propanesulfonate.

CHF	Congestive heart failure
CI	Chemical ionization
CID	Collision induced dissociation
CKD	Chronic kidney disease
CKs	Cytokines
COX-2	Cyclooxygenase-2
CPB2	Carboxypeptidase B2
CPD	Chronic peritoneal Dialysis
C_{pd}	Solute concentration in the dialysate
C_{plasma}	Solute concentration in plasma
CREB	cAMP-responsive element binding protein
CTGF	Connective tissue growth factor
CTSF	Cathepsin F
CTSL	Cathepsin L1
CTSK	Cathepsin K

D

D/D_0	$Dialysate_{240}$/initial dialysate ratio of glucose
D/P_{Cr}	Dialysate/plasma ratio of creatinine
D/P_{urea}	Dialysate/plasma ratio of urea
Da	Dalton
DI	Desorption ionization
DN	Diabetic Nephropathy
DOC	Deoxycholate
DTT	Dithiothreitol

E

ECD	Electron capture dissociation
ECM	Extracellular matrix
ECs	Endothelial cells
ECW	Extracellular water
EDTA	Ethylene diamine tetraacetic acid
EGF	Epidermal growth factor
eGFR	Estimated glomerular filtration rate
EI	Electron ionization
EMT	Epithelial-to-mesenchymal transition
eNOS	Endothelial NO synthase
EPS	Encapsulating peritoneal sclerosis
ERK	Extracellular signal–regulated kinase
ESI	Electrospray ionization

ESRD	End stage renal disease
ETD	Electron transfer dissociation
EThcD	Electron-transfer/higher-energy collision dissociation
EuTRiPD	European Training and Research in Peritoneal Dialysis Network

F

F10	Coagulation X
F2	Prothrombin
FASP	Filter-aided sample preparation
FGB	Fibrinogen beta chain
FGF	Fibroblast growth factor
FGG	Fibrinogen gamma chain
Fig.	Figure
FWHM	Full width at half-maximum
FWT	Free water transport

G

g	Gravitational force equivalent
GCNT1	Beta-1,3-galactosyl-O-glycosyl-glycoprotein beta-1,6-N-acetylglucosaminyltransferase
GDPs	Glucose degradation products
GFR	Glomerular filtration rate
GNC	Glomerular chronic nephritis
GPMDB	Global Proteome Machine Database
GRB2	Growth factor receptor-bound protein 2
GSEA	Gene set enrichment analysis
GSK	Glycogen synthase kinase
GSK3β	Glycogen-synthase kinase-3β

H

h	Hours
H.	High peritoneal transport patients
H.A.	High-average peritoneal transport patients
HA	Hyaluronan
HAP	High abundance proteins
HCD	Higher-energy collisional dissociation
HD	Hemodialysis
HEPES	4-(2-hydroxyethyl)-1-piperazineethanesulfonic acid
HGF	Hepatocyte growth factor
HIF-1α	Hypoxia inducible factor
HiRIEF	High resolution isoelectric focusing
HPMCs	Human peritoneal mesothelial cells

I

IAA	Iodoacetamide
ICAM-1	Intercellular adhesion molecule-1
ICAT	Isotope coded affinity tags
IEF	Isoelectric focusing
IFN-γ	Interferon-γ
IGF-I	Insulin-like growth factor-I
IGFBPs	Insulin-like growth factor binding proteins
IL	Interleukin
ILK	Integrin-linked kinase
IPG	Immobilized pH gradient
ITGB1	Integrin beta-1
ITIH3	Inter-alpha-trypsin inhibitor heavy chain H3
iTRAQ	Isobaric tag for relative and absolute quantification)

K

K	Lysine
KDa	kilodalton
K_f	Membrane filtration coefficient
KNG1	Kininogen-1
Kt/V_{urea}	K, the clearance of urea (mL/min) multiplied by t, the time of dialysis treatment (min) by the coefficient of V, the volume of distribution of urea (mL)

L

L2	Neural cell adhesion molecule L1
L	Litters
L.	Low peritoneal patients transport
L.A.	Low-average peritoneal patients transport
LAP	Low abundance proteins
LC	Liquid chromatography
Lef/Tcf	Lymphoid enhancer factor/T cell factor
LMWH	Low molecular weight heparin
LP	Large Pores
LpS	Hydraulic condunctance or ultrafiltration coefficient
LPS	Lipopolysaccharide

M

m	Minutes
m/Z	Mass-to-charge ratio
M1	Macrophages with a proinflammatory phenotype
m^2	Square meters

M2	Macrophages with a profibrotic phenotype
MALDI	Matrix-assisted laser desorption ionization
MALDI-TOF	Matrix-assisted laser desorption ionization time of flight
MAPK	Mitogen-activated protein kinase
MARS	Multiple Affinity Removal System
MCP	Monocyte chemoattractant protein
MCs	Mesothelial cells
MEA	Modular enrichment analysis
MEK	Mitogen-activated protein kinase
MET	Mesenchymal-to-epithelial transition
MHC	Major histocompatibility complex
mm	Millimetre
mmHg	Millimetre of mercury
mM	milliMolar
mmol	Millimole
MMPs	Matrix Metalloproteinases
MMT	Mesothelial-to-mesenchymal transition
mOsm	Milliosmole
MS	Mass spectrometry
MS/MS	Tandem mass spectrometry
MTAC	Mass transfer-area coefficient
mTOR	Mammalian target of rapamycin
MW	Molecular weight
MYL	Myosin light chain
MUC16	Mucin-16
Mφ	Macrophages

N

NaF	Sodium fluoride
Net UF	Net ultrafiltration
NF-kB	Nuclear factor-kB
NIPD	Nocturnal intermittent peritoneal dialysis
NO	Nitric Oxide
Notch-IC	Intracellular fragment of Notch
Nrps	Neuropilins
NT-proBNP	N-terminal brain natriuretic peptide

P

P	Hydrostatic pressure
PAI-1	Plasminogen activator inhibitor 1

PAMSs	Phenotype-associated molecular signatures
PAMSs	Phenotype-associated molecular signatures
PCA	Principal component analysis
PD	Peritoneal dialysis
PDE	Peritoneal dialysis effluent
PDF	Peritoneal dialysis fluid
PDGFRB	Platelet-derived growth factor receptor beta
PET	Peritoneal equilibration test
PGE2	Prostaglandin E2
PLG	Plasminogen
PLAU	Urokinase-type plasminogen activator
PKCα	Protein kinase C
PM	Peritoneal membrane
PMF	Peptide mass fingerprints
PMN	Polymorphonuclear neutrophils
PMSF	Phenylmethylsulfonyl fluoride
PPAR-γ	Peroxisome proliferator-activated receptor-γ
PPCl	Peritoneal protein clearance
PPI	Protein-protein interaction
ppm	Parts per million
PRIDE	Proteomics identifications database
PROC	Vitamin k-dependent protein C
PROS	Vitamin k-dependent protein S
PSTR	Peritoneal solute transport rate
PTH	Parathyroidism hormone
PTM	Post-translational modifications

Q

Q	Quadrupole

R

R	Arginine
RAGE	Receptors of advanced glycation end products
RAS	Renin-angiotensin system
RF	Radio frequency
Rhoa	Ras homolog gene family member A
RKF	Residual kidney function
ROCK	Rho-associated protein kinase
RORγt	Retinoic acid-related orphan receptor-γt
RP-HPLC	Reverse Phase High-Performance Liquid Chromatography

RRT	Renal replacement therapies
RTKs	Receptor tyrosine kinases

S

s	Seconds
SD	Standard deviation
SEA	Singular enrichment analysis
SERPINA11	Serpin A11
SERPINC1	Antithrombin-III
SERPIND1	Heparin cofactor 2
SERPINF2	Alpha-2 antiplasmin
SERPING1	Plasma protease C1 inhibitor
SHCA	Adaptor protein SRC homology 2 domain-containing-transforming A
SI	Spray ionization
sIL-6R	Soluble interleukin-6 receptor
SILAC	Stable isotope labelling by amino acids in cell culture
SN	Supernatant
SOS	Son of sevenless
SP	Small pores
SP3	Single-Pot Solid-Phase-enhanced Sample Preparation
SPUF	Small-pore ultrafiltration
SS	Simple peritoneal sclerosis
SSP	Severe sclerosing peritonitis
STAT3	Signal transducer and activator of transcription 3

T

TAK1	Tumor growth factor-β-activated kinase 1
TBW	Total body water
TCA	Trichloroacetic acid
TCEP	Tris(2-carboxyethyl)phosphine
TFA	Trifluoroacetic acid
TGF	Transforming growth factor
Th	T helper cells
TIMP	Inhibitors of metalloproteinase
TMED	N, N, N’, N’-tetramethylethylene-diamine
TMP	Three pore model
TMT	Tandem mass tags
TNF	Tumor necrosis factor
TOF	Time-of-flight
tPA	Tissue plasminogen activator

TRAF6	Tumor necrosis factor receptor-associated factor 6

U

UF	Ultrafiltration
UFF	Ultrafiltration failure
US	Ultrasounds

V

VCAM-1	Vascular cell adhesion molecule-1
VEGF	Vascular endothelial growth factor
VEGFRs	Vascular endothelial growth factor receptors

W

WBC	White blood cell

Others

1D-SDS-PAGE	One-dimensional sodium dodecyl sulfate/polyacrylamide gel electrophoresis
2D-SDS_PAGE	Two-dimensional sodium dodecyl sulfate polyacrylamide gel electrophoresis
Å	Ångström
α-SMA	α-smooth actin
β1-AR	β1-adrenergic receptor
π	Effective osmotic pressure

CHAPTER I. GENERAL INTRODUCTION

1-A general revision of chronic kidney disease and renal replacement therapies

Chronic kidney disease (CKD) is a general term for heterogeneous disorders affecting kidney structure and function [1]. Currently, the international guidelines define CKD as decreased kidney function shown by a glomerular filtration rate (GFR) of less than 60 mL/min per 1.73 m^2, or markers of kidney damage (albuminuria), or both, of at least 3 months duration, regardless of the underlying cause [2]. Given the important of the GFR in the pathophysiology of the complications, the disease is classified into five stages based on GFR: Stage 1 (> than 90 mL/min per 1.73 m^2); Stage 2 (60–89 mL/min per 1.73 m^2); Stage 3 (30–59 mL/min per 1.73 m^2); Stage 4 (15–29 mL/min per 1.73 m^2) and stage 5 (< than 15 mL/min per 1.73 m^2) (Figure 1). Also, albuminuria stages should be taken into account for prognosis, since increased albuminuria is correlated with mortality and kidney outcomes [1].

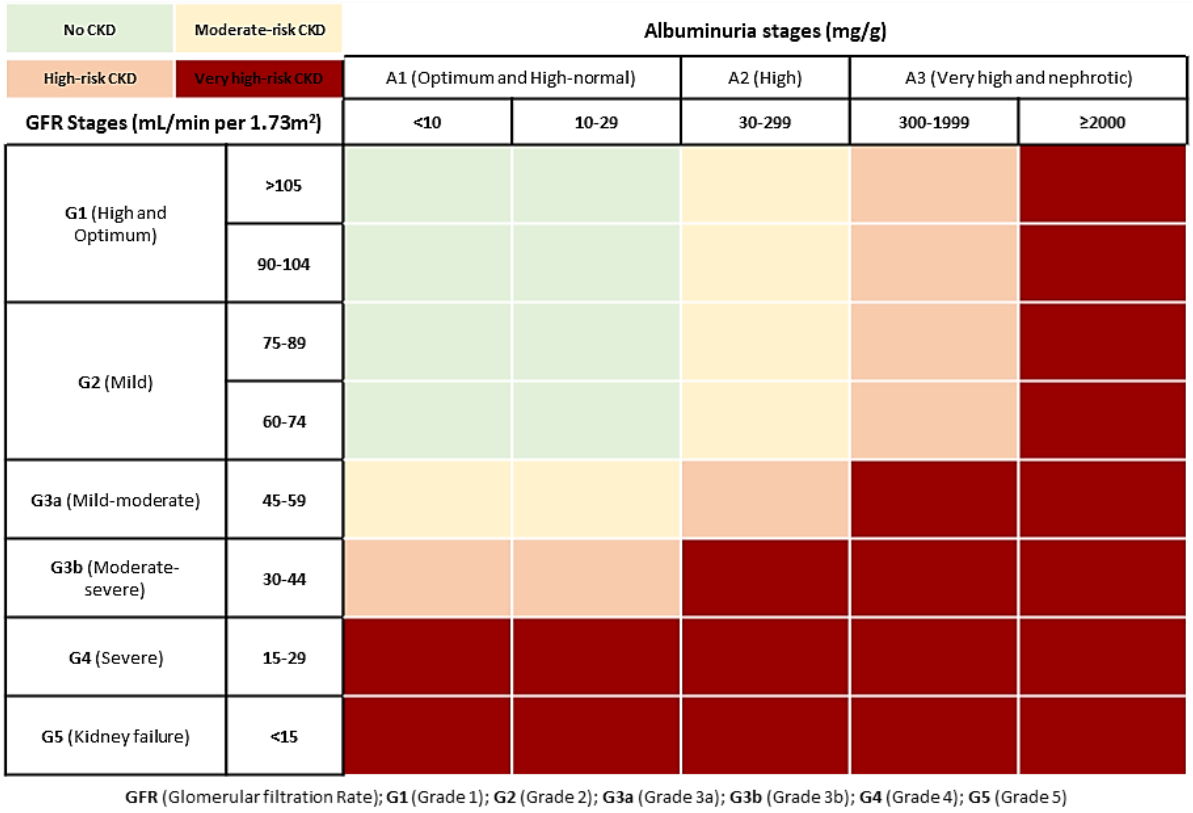

Figure 1 – Prognosis of CKD based on GFR and albuminuria stages. Image adapted from Levey and Coresh, 2012 [1].

Additionally, CKD is a leading cause of end stage renal disease (ESRD) and cardiovascular morbidity and mortality worldwide, resulting in a growing social and economic burden [3]. ESRD is the irreversible loss of kidney function, which is fatal if not treated with renal replacement therapies (RRT) or renal transplantation [4].Thus, kidney failure is defined as a GFR of less than 15 mL/min per 1.73 m^2, or the need for treatment with dialysis or transplantation [5]. However, for patients with ESRD unable to receive a kidney transplant, replacement of kidney function with dialysis is necessary to extend life, hemodialysis (HD) and peritoneal dialysis (PD) being the two major forms of therapy.

HD involves the passage of blood via an extracorporeal circuit whereby removal of small solutes, toxins, and water is achieved across a synthetic, semipermeable dialysis membrane [6].Given the technical differences between dialysis and ultrafiltration, patients can undergo solute clearance, volume removal, or both simultaneously [7]. In PD, the dialysis membrane is the highly vascularized internal lining of the peritoneal cavity. Intraperitoneal installation of hypertonic high glucose PD solution creates a transmembrane osmotic and diffusive gradient that facilitates water removal (ultrafiltration), convection and diffusion of uremic toxins [6]. Each year over 100.000 Americans and similar number of Europeans move from advanced non-dialysis-dependent CKD to RRT, these patients usually have an GFR <25 mL/min 1.73 m^2 at the time of the transition. From these patients, <5% undergo kidney transplantation and the majority move on to renal replacement therapy (RRT) [5]

Nowadays, the number of people worldwide suffering from chronic kidney diseases and requiring dialysis treatment is rising at a constant rate of around 6% annually, with more than 3.4 M patients expected in 2018 and approximately 4.9 M by 2025 [8]. Likewise, as the global burden of CKD continues to increase, so does the need for a cost-effective RRT [9]. To-date there is a focus of interest in peritoneal dialysis (PD), as it provides a better quality of life and autonomy for the patients than other renal replacement therapies (RRT) such as hemodialysis and represents a cost-effective RRT. Despite these benefits, the utilization of PD has not always increased [9],[10]. In the last decade, approximately 196,000 end stage renal disease (ESRD) patients were performing PD worldwide, representing 11% of the dialysis population [11].

Therefore, to move the PD therapy forward some strategies need to be implemented to facilitate PD utilization, such as, policies and incentives to favour this therapy, appropriate training for nephrologists to increase the use of the therapy and to decrease the rates of technique failure. In addition, the PD community should undertake clinically meaningful studies with a strong focus on technique survival [9] [10].

2-Peritoneal Dialysis: a peritoneal membrane-based treatment technique

Peritoneal dialysis (PD) is a life-sustaining therapy that involves solute and fluid exchange, mainly between peritoneal capillary blood and dialysis solution in the peritoneal cavity [12]. This therapy is based on using the peritoneum, defined as the serosal membrane that covers the peritoneal cavity, because it is a semipermeable membrane through which ultrafiltration and diffusion of circulating compounds occur[10],[11],[13].

The peritoneum is composed of two principal parts, (i) the parietal peritoneum, which covers the inner surface of the abdominal and pelvic walls including the diaphragm, and (ii) the visceral peritoneum, which covers visceral organs, forms the visceral mesentery that connects loops of bowel, and reflects over and covers the inner surface of the abdominal wall. In the physiological state, the peritoneal cavity retains 50–100 mL of peritoneal fluid. This space can be enlarged by the instillation of fluid, normal-sized adults can tolerate 2 or more liters of fluid without discomfort [5][13][14]. In PD

patients, the compact zone of the visceral peritoneum is ~20 μm thicker and the parietal peritoneum can be thickened up to 500 μm in long-term PD patients when compared with 50 μm of a normal parietal peritoneum [15].

The PD efficiency is dependent of important anatomic components of the PM, such as, the mesothelium, the insterstitium, the microcirculation and the visceral lymphatics. The mesothelial cell monolayer, mesothelium, lines the peritoneal cavity [14]. These cells secrete lubricants, anticoagulants and surface-lowering substances for the peritoneum, minimizing the friction between intra-abdominal organs, caused by intestinal peristalsis or respiratory movement [16]. In the steady state, mesothelial cells produce 5-100 mL of peritoneal fluid containing complement factors, immunoglobulins, defensins, and immune cells such as macrophages, lymphocytes, eosinophils, and mast cells that exert anti-infection actions and regulate the inflammatory response [17].

The homogenous basement membrane underling the mesothelial cells (MC), is between 25 and 40 mm thick, and is believed to be composed of type IV collagen, proteoglycogens, and glycoproteins [14]. Below the mesothelium is the submesothelial compact zone. It contains the interstitium, which is the supporting structure of the peritoneum and is primarily composed of a mucopolysaccharide matrix, contains bundles of collagen fibers, blood vessels, the lymphatics, occasional macrophages, glycosaminoglycans, and fibroblasts. There are aqueous and lipophilic phases. The aqueous phase mediates transport of water, electrolytes, protein, nutrients, and hormones [6][14].

The blood supply to the visceral and parietal peritoneum (that constitute 60% and 40% of the total surface area of peritoneum, respectively) arises from 2 sources: (1) the celiac and mesenteric arteries, with venous drainage via the portal vein; and (2) the circumflex, iliac, lumbar, intercostal, and epigastric arteries draining directly into the systemic circulation, bypassing the hepatic portal system. The number of perfused capillaries determines the functional area for the exchange between blood and dialysate. The solute exchange occurs according to the three pore model (TMP) (described below in section 2.1), in which ultra-small pores (aquaporin (AQP)-1) mediate water flux along osmotic gradients, small pores (40-60 Å) transport readily dialyzable molecules (sodium and urea) and large pores (100-200 Å) are responsible for movement of macrolecules (β-2 microglobulin) [6] [7] [14].

In addition, a network of lymphatic vessels aids in the removal of fluids and solutes from the interstitium. The fluid absorption occurs primarily through stomata in the subdiaphragmatic area. Several physiologic factors can alter the rate of lymphatic uptake, such as, intraperitoneal hydrostatic pressure, body posture, and pharmacological agents [14].

PD involves the insertion of a permanent abdominal catheter through which the peritoneal cavity is filled with dialysis fluid, left to dwell and then drained out, removing uraemic toxins and excess water (Figure 2). This home-based treatment is undertaken daily by the patients, who can perform continuous ambulatory PD (CAPD) during the day, or use a machine overnight to perform automated PD (APD), also referred to as continuous cycling PD (CCPD). Both methods enable the patient to remain at home, promoting self-management and preserving vascular access, which hemodialysis diminishes

[4][18].Thus, this enables patient autonomy and reduces the cost of the medical treatment compared with hemodialysis.

In conclusion, the peritoneal dialysis system has three major components: the peritoneal microcirculation, the peritoneal membrane, and the dialysate compartment, which includes the composition of the solution and the modalities of delivery. All of these components may have an important effect on the final performance of the technique [19].

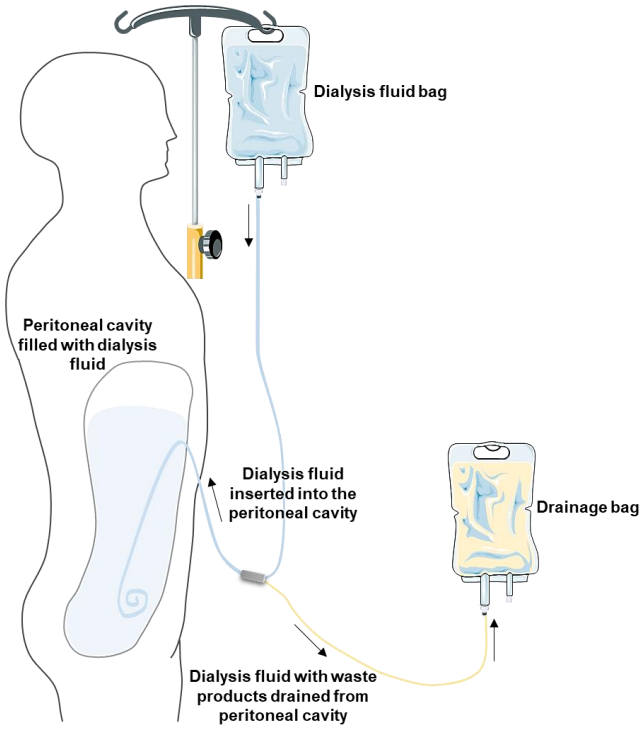

Figure 2 – Peritoneal dialysis representation and principle, from the insertion of dialysis fluid, solute and fluid exchange between peritoneal capillary blood and dialysis solution to final drainage.

2.1- Solute and water transport across the PM

The PD involves diffuse and convective transports as well as osmosis through the highly vascularized PM [20]. Solute and fluid transport through diffusion is driven by a concentration gradient (from the high-concentration to a lower-concentration compartment), whereas convection (ultrafiltration) is driven by osmotic or hydrostatic pressure gradients [18]. Ultrafiltration, i.e., the amount of water removed from the patient, depends on the presence of an osmotic agent (most often glucose) in the PDF [21]. The pathways available for solute and water exchange between the plasma in the peritoneal capillaries and the fluid in the peritoneal cavity include, i) anatomic peritoneum (more precisely the mesothelium), ii) the cell-interstitial matrix or space, and iii) blood capillary endothelium lining vasculature, which is distributed within the tissue, and can be functionally described as TMP (Figure 3A and 3B) [16] [22].

The solute exchange occurs according to the TPM, through ultra-small pores, small pores and large pores. The ultra-small pores located in endothelial cells account (the only ones located inside the endothelial cells) for about of 2% of the total ultrafiltration (UF) coefficient (LpS, or hydraulic

conductance) and are permeable to water but impermeable to solutes (Figure 3B and 3C-i)[16]. The transcellular water permeability is mediated by AQP-1 channels, a membrane protein essential for water removal across the PM that allows transport of solute-free water in response to a crystalloid-induced osmotic pressure. In clinical practice, such water movement is termed free water transport [18]. The small pores (located between the endothelial cells) account for ~90% of the LpS and 99.5% of the total pore area available for solute transport. The large pores (thought to correspond to interendothelial gaps) account for 5–8% of the LpS, occupying <0.5% of the total pore area[16][23] (Figure 2.1B).

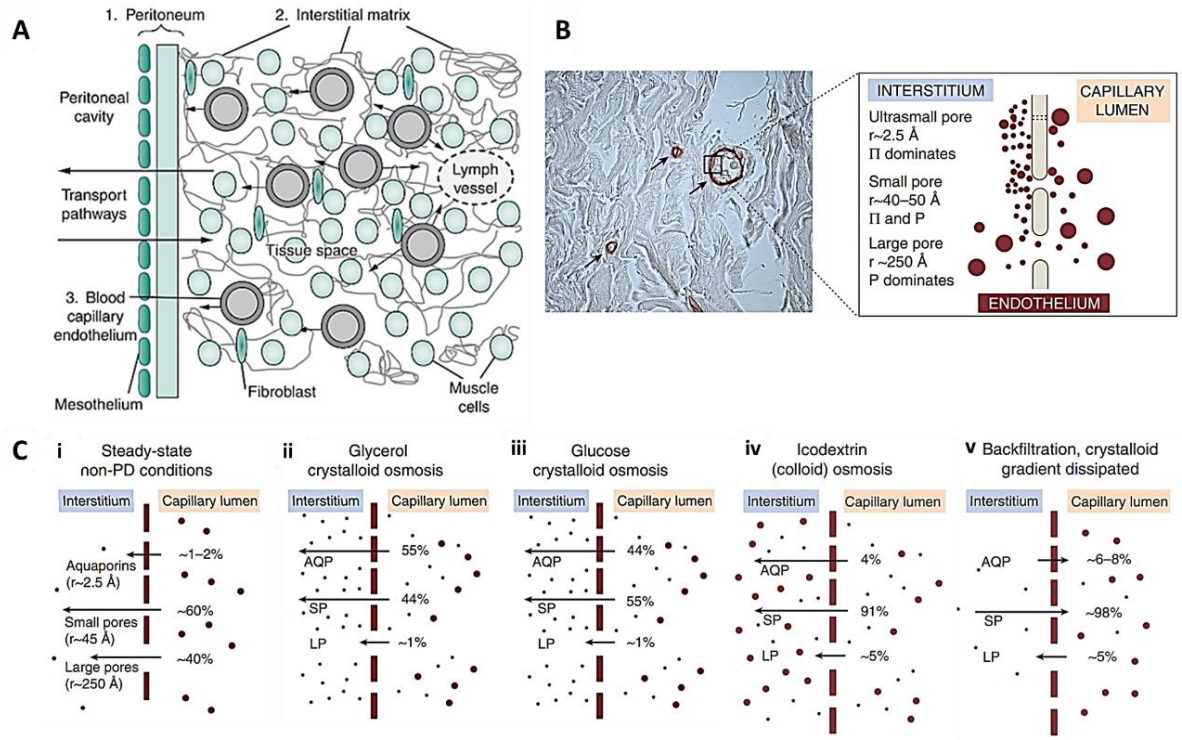

Figure 3- A- The capillary dialysis system: capillary, interstitium, mesothelium, and peritoneal cavity. Potential barriers separating the dialysis solution in the peritoneal cavity from plasma flowing within the microvasculature distributed within the subperitoneal tissue. B- Structure of the PM and representation of the TPM. During PD, the microvascular endothelium (arrows, stained in red) represents the functional barrier for the transport of solutes and water from the blood of the patient to the dialysate that has been instilled in the peritoneal cavity. The Starling forces (P, hydrostatic pressure; Π, oncotic pressure) operating across each type of pore are indicated. Å, angström (10−10m); r, functional radius. C-Transcapillary UF in the TPM, i) Fractional fluid flows across the peritoneum under normal conditions with no dialysis. In the absence of an osmotic agent, (ii) With glycerol as the osmotic agent, (iii) With glucose as the osmotic agent, (iv) In a conventional icodextrin PD solution and v) Backfiltration after gradient dissipation. Aquaporin (AQP), Small Pore (SP) and Large Pore (LP). Figure adapted from Devuyst *et al.* [16] and Flessner *et al*. [22].

The Starling forces (P, hydrostatic pressure; Π, oncotic pressure) can be considered as the forces operating across each different type of pore. Under normal conditions, with no dialysis and in the absence of an osmotic agent, ~60% of the transcapillary fluid flow occurs through small pores, where the Starling forces are close to equilibrium. Approximately 40% of the capillary UF occurs across large pores where there is hardly any colloid osmotic pressure counteracting the transcapillary hydrostatic pressure gradient (Figure 3C-i)[16].

However, transcapillary UF in the TPM can change in different conditions of PD. That is, fluid removal can be markedly enhanced by the presence of an osmotic agent in the peritoneal cavity. With

glycerol and glucose as the osmotic agent, ~55% and ~45% of the transperitoneal water flow occurs through water-only pores (AQP), respectively; and 45% and 55% through the small pores, respectively. Glucose is relatively inefficient as an osmotic agent across the small-pore pathway. However, when compared with glycerol (also relative inefficient) it is 50% more efficient than glycerol (Figure 3C-ii and 3C-iii)[16].

The glucose in the dialysis solution, once introduced into the peritoneal cavity, generates crystalloid osmotic pressure which, along with transmembrane hydrostatic pressure, promotes convective water and solute transport from the capillary blood to the dialysis solution. The effectiveness of glucose in promoting water and solute transport during convection is determined by the resistance offered by the PM to glucose transport from the peritoneal cavity to the capillaries. This resistance is expressed as the osmotic reflection coefficient. By definition the reflection coefficient is 1.0 for a solute with complete resistance, such that the solute cannot cross the membrane, and 0 when the membrane offers no resistance to solute movement. [18].

Icodextrin, a glucose polymer, has been introduced as an alternative to the glucose in PD solutions because it provides better UF during long dwells and reduces the metabolic effects [24]. Being a macromolecule, induces colloidal osmosis. Due to its size, is unable to cross capillary walls, generating an oncotic pressure that pulls fluid in its direction. Icodextrin induces fluid transport in its direction at the capillary level even in an isotonic or hypotonic state. Consequently, dialysis solution containing icodextrin draws fluid out of capillary blood despite low osmotic force, through the small pores. In contrast, icodextrin fails to draw water via AQP due to low numbers relative to electrolytes and extremely low osmotic force compared to glucose. In addition, icodextrin stays in the PD fluid for long periods due to extremely slow metabolism and poor absorption from the peritoneal cavity, drawing fluid into the peritoneal compartment for a longer period than glucose-based solution and does not cause sodium sieving [18]. Therefore, with a conventional icodextrin PD solution, ~25–30% of the molecules (~3mm) act as a colloid, implying a reflection coefficient close to unity. A 3 mM of high-molecular-weight icodextrin produce approximately, a colloid osmotic pressure of 58mmHg (3 × 19.3mmHg (for solutes with a reflection coefficient of 1, each 1 milliosmole (mOsm) exerts an osmotic pressure of 19.3 mm Hg according to Van't Hoff's law [18]), which is sufficient to counteract the plasma colloid osmotic pressure (22–26mmHg) exerted by ~1mm of negatively charged plasma proteins (Figure 3C-iv). Thus, the type of osmotic agent used markedly affects the mechanisms of osmosis [16].

Back absorption of fluid into capillaries follows Starling forces, whereas lymphatic absorption is convective and driven by the negative force created by expansion of the chest wall during inspiration. Back absorption across the small pores occurs when the crystalloid (glucose) osmotic gradient has totally dissipated, usually after 4h. The net Starling fluid balance is biased toward reabsorption across the small pores in PD and some across AQP-1. On the other hand, a minute UF still occurs across the large pores (figure 3C-v) [16].

In conclusion, transport of solutes and water across the peritoneal membrane during PD can be

influenced by, i) the exchange frequency and volume of the dialysate; ii) the osmolality of the dialysate; (iii) the peritoneal blood flow; iv) the effective peritoneal vascular surface area (EPSA) and v) the microvascular intrinsic permeability [25]. The main transport parameters across the PM are routinely evaluated using the peritoneal equilibration test (PET), which is based on the rate of small solutes transport during an exchange (described in section 2.2). Therefore, and based on these basic principles, any increase in the transport of small solutes across the membrane leads to a rapid dissipation of the osmotic gradient (due to increased reabsorption of glucose, the osmotic gradient) and loss of the UF, causing fluid overload in uremic patients [21]. Thus, the capacity of osmotically-induced UF across the PM is a major predictor of outcome and mortality in PD patients, and failure of the UF capacity the most frequent abnormality and the main reason for technical failure in long-term PD patients [21].

2.2- Peritoneal equilibration test

The peritoneal equilibration test (PET) is a standardized test used to assess the transport properties of the PM in individual patients treated with PD enabling the characterization of the functional state of this biological membrane and the assessment of the required dialysis dose. These measurements are useful due to intra- and inter-individual variabilities of the patients [26]. The principle of PET was standardized by Twardowski et al in 1987 as explained below [27].

Firstly, the exchange preceding PET must dwell for 8-12 hours, this pre-test exchange is completely drained over 20 min with the patient in the sitting position, a dialysate and a blood sample are obtained at the end of drainage. Then a sample of dialysis solution is taken from the test bag to be infused, and a 2 L of 2.5% dialysis solution is infused with the patient in the supine position in portions of 400 mL every 2 min. The patient is rolled from side to side after each infusion to mix residual volume and infused solution, and this procedure takes a total of 10 min. Exactly 10 min after the start of infusion, when the infusion is completed (0 dwell time), 200 mL of solution is drained into the bag, mixed well, a 10 mL sample of dialysate is taken and the remaining 190 mL reinfused. Posteriorly, samples of dialysate are taken with the same technique after 30 min, 60 min, 120 min, and 180 min of dwell time. After a 4-hour dwell time, the dialysate is drained over 20 min with the patient in the sitting position. At the end of the drainage, the total volume drained is measured and a dialysate and blood sample are taken. The total time of the equilibration exchange is 270 min. Finally, a sample of dialysis solution is taken from a post-test exchange bag to be infused, and 2 L of fresh solution is infused over 10 min with the same technique as for the equilibration exchange; 200 ml of dialysate is immediately drained into the bag, a 10 ml sample is collected and the remaining 190 ml reinfused [27].

After a PET has been performed it is possible to measure the low molecular weight solute transfer and net ultrafiltration. Details of the process of fluid transport are important from a clinical point of view because of the high prevalence of complications related to water removal which is the reason for the change of PD modality and/or schedule or the change from PD to HD [28]. The PET was the

first standardized method to evaluate PM characteristics but there are numerous techniques for measuring peritoneal transport, based on the measurement of parameters, such as, PM transport, total protein clearance, residual renal function, ultrafiltration and nutritional status.

Summing up, the aims of evaluating PM function are:

- Optimization of the treatment prescription with regard to small-solute clearances, volume regulation and reduction of uraemic toxicity;
- To assess membrane characteristics not related to small solutes: osmotic conductance of glucose, aquaporins, hydraulic conductance, large-solute flow, lymphatic reabsorption;
- To evaluate the evolution of peritoneal function over time.

Therefore, assessment of PM characteristics, specifically solute transport rate and UF capacity, is fundamental to PD prescription, as this will guide the prescription [29]. Some of the parameters assessed are described in the following sections.

2.2.1-Dialysate/plasma ratios and peritoneal transporter classification

Measurements performed during PETs include dialysate-to-plasma ratios of urea (D/P_{urea}), creatinine (D/P_{Cr}) at 4 h and the ratio of dialysate glucose concentrations at 0 and 4 h, $dialysate_{240}$/initial dialysate ratio of glucose (D/D_0) (Figure 4). These are calculated and used as parameters of solute transport [26][30].

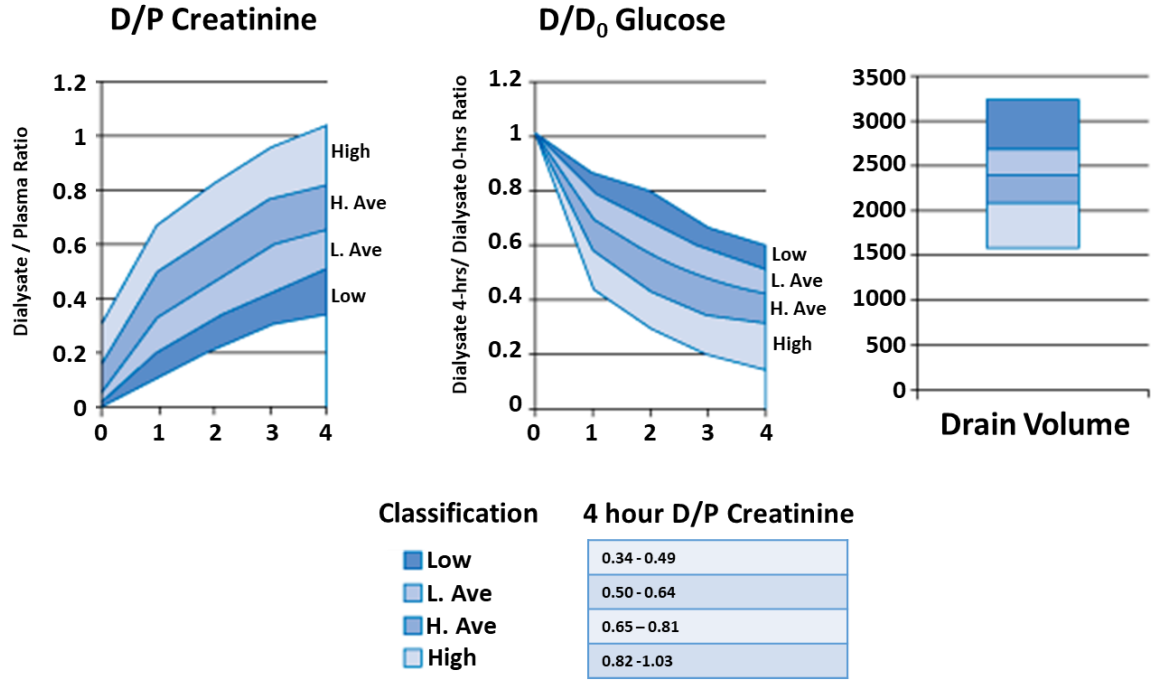

Figure 4- Twardowski Curves: Transport status based on the PET. (Left) dialysate creatinine versus plasma creatinine at 4-hours (D/P); Middle) ratio of dialysate glucose at time zero (D/D_0); (Right) Drain volume after 4-hours for the different membrane classifications. The figure was adapted from Hoffman *et al*. [31].

Patients are categorized into low (L), low-average (L.A.), high-average (H.A.) and high (H) transporters according to the values of solute transport calculated after PET procedure. A patient with H transporter is defined with either a D/P_{Cr} exceeding the mean + 1 SD, or a D/D_0 of less than the mean D/D_0 -1 SD. H.A transporters have a D/P_{Cr} between the mean and mean + 1 SD, or a D/D0 between the mean and mean -1 SD. The L. and L.A are defined in the same way [26].

There is a considerable variability for both solute transport and UF capacity among PD patients. Therefore, the PD therapy should be tailored to the specific needs of the patients in terms of ideal length of dwell, the number of dwells and the type of dialysis solutions used, as described in Table 1. An inappropriate prescription can lead to substantial underachievement in terms of solute clearance an UF or unnecessary exposure to hypertonic solutions. [29].

Table 1- Dialysis regimen based on PET procedure. Adapted from Twardowski [33].

Transport type	D/P creatinine	UF	Solute clearance	Preferred Regimen
High (Fast)	>0.80	Poor	Adequate	APD regimens (eg, NIPD, CCPD, PD plus)
High-average	0.65-0.80	Adequate	Adequate	Standard PD (any regimen)
Low-average	0.55-0.64	High	Adequate	Standard dose CAPD
		High	Inadequate	High dose PD
Low (slow)	<0.55	Excellent	Inadequate	High dose PD, longer dwell CAPD (or hemodialysis)

Abbreviations: PD (peritoneal dialysis); APD (automated peritoneal dialysis); NIPD (nocturnal intermittent peritoneal dialysis); CCPD (continuous cyclic peritoneal dialysis); CAPD (continuous ambulatory peritoneal dialysis)

It is important that, PETs carried out within the first month of PD are considered as preliminary and are confirmed by a PET 4 weeks later, because peritoneal transports characteristics change significantly within the first month of PD. This has been shown in a prospective study of 50 patients in whom the results of PETs obtained after 1 week and 1 month were compared. Significant differences were observed in the measurement of D/P_{urea}, D/P_{Cr} and D/D_0 glucose between 1 week and 1 month. In addition, PET measurements performed more than 1 year following PD commencement generally agreed closely with 1-month measurements, and poorly with 1-week measurements [30].

Peritoneal transport has an impact on clinical outcomes, however it is not constant in PD patients [32] since PM characteristics can change with time in therapy. Some patients develop neo-angiogenesis, vasculopathy and submesothelial and interstitial fibrosis, that leads to decreased UF capacity and an increase in the transport rate for small solutes. Therefore, membrane transport characteristics should be evaluated at least once a year in order to make sure that the prescription still matches the needs of the patient [29].

In addition, large-scale longitudinal studies focusing in the differences of peritoneal transport among patients are needed. Recently, a study was published by Jiang *et al.* [32] with the aim of elucidating the changing trend of peritoneal transport and its impact on patient outcomes. For this purpose, survival rates of a cohort of 470 patients, with a mean age of 63.2 ± 14.3 years and a 40%

diabetes occurrence, were analysed for up to 10 years. The main conclusion based in D/P_{Cr} were that, (i) D/P_{Cr} mean dropped significantly in the first year and remained constant thereafter; (ii) a slow increasing trend was observed after year 5 and (iii) in the first few years, D/P_{Cr} declined significantly in the H. and H.A. transport patients and increased in the L.A. and L. transport patients. Interestingly, there was no significant difference in patient and technique survival rates according to baseline transport groups. Moreover, D/P_{Cr} only was considered a significant risk factor for mortality from year 3 onwards. Additionally, H.A. patients were associated with poorer outcomes only after the first few years of PD. Finally, the authors concluded that the initial peritoneal transport status was not a determinant factor of patient survival in long-term PD [32]

In addition, a meta-analysis study carried out to characterize the relationship between D/P_{Cr} and mortality and technique failure in PD patients, showed a relative risk of 1.15 for every 0.1 increase in D/P_{Cr}. This result equated to an increased mortality risk of 21.9 % for L.A, 45.7 % for H.A, and 77.3% for H, as compared with patients with L. transport status. Regarding the relative risk for death-censored technique failure was 1.18, for every 0.1 increase in the D/P_{Cr}. This meta-analysis demonstrated that a H.A. solute transport rate is associated with a higher mortality risk and a trend to higher technique failure [34].

Nevertheless, deterioration of clinical parameters (volume overload, UFF and malnutrition) and biochemical parameters (haemoglobin, serum albumin, urea and creatinine) can be caused by an inappropriate PD regimen, as a consequence of a change in PM characteristics. Thus, is very important to re-evaluate the PM characteristics and to adapt the treatment accordingly [29].

2.2.2- Ultrafiltration capacity /Net ultrafiltration

PD needs to provide patients with both solute clearance and fluid removal, that is, UF. Failure to provide adequate levels of either or both of these parameters accounts for approximately 18% of overall technique failure and transfer to HD [35].

Net ultrafiltration (net UF) in PD refers to the difference between the osmotically induced UF into the peritoneal cavity and the fluid loss from the cavity during dialysis [36]. Fluid loss is made up primarily of hydrostatic pressure-driven convection to the tissues surrounding the peritoneal cavity and a lesser amount of lymph flow. The cellular and blood capillary sources of water are distributed in an interstitial matrix, which decreases the effective osmotic pressure in the vicinity of the microvasculature. The interstitial matrix makes the process of fluid removal far less efficient than it would be if the blood capillaries were actually in direct contact with the peritoneal fluid. Osmotically driven water transport occurs chiefly across the blood capillary endothelium into the interstitium and ultimately out into the peritoneal cavity [37]. Net UF is calculated as the difference between the drained and the instilled volume [26],[37], as can be seen in the following equation:

$$\text{Net UF} = \frac{Drain\ volume - Fill\ volume}{Dwell\ time} \quad (1)$$

This equation does not tell what mechanisms or forces govern the transfer of fluid. Small solute (MW=6,000 Da) transfer occurs in both directions across the membrane in accordance with the mass transfer-area coefficient (MTAC),

$$\text{Solute transfer} = MTAC \cdot (C_{plasma} - C_{pd}) \quad (2)$$

where C_{plasma} = solute concentration in plasma; C_{pd} = solute concentration in the dialysate. UF across any membrane follows the classic Starling equation,

$$\text{Fluid transport} = K_f A \cdot [P_{plasma} - P_{pd} - (\pi_{plasma} - \pi_{pd})] \quad (3)$$

where K_f = membrane filtration coefficient; P = hydrostatic pressure; π= effective osmotic pressure. However, the simple membrane model cannot account for all processes that ultimately result in the measured net UF [37].

The transfer of fluid to and from the peritoneal cavity is more complex than the simple membrane model. The net UF is made up of two components,

$$\text{Net UF} = \text{Osmotically-driven filtration} - \text{fluid loss} \quad (4)$$

where fluid loss = fluid transfer from the cavity = direct lymph flow + hydrostatic pressure (P)-driven convection to the surrounding to the surrounding tissues. From the tissue, transfer into the blood capillaries or intra-tissue lymphatics carries the fluid back to the plasma compartment [37].

Importantly, the amount of UF rate has been correlated with patient survival in PD patients [38]. Signs of UFF include loss of solute-free UF and general decrease in UF below 400 ml with a 4-h dwell of hypertonic dialysate [37].

2.3- Dialysis dose adequacy

One of the most important parameters measurements in PD, is the Kt/V_{urea}, this unit-less measurement is determined by (i) K, the clearance of urea (mL/min) during a dialysis treatment; (ii) t, the time (min) of the treatment and (iii) V, the volume of distribution of urea (mL), which is approximately the total body water. Given that several factors can affect Kt/V_{urea} (blood flow rate, dialysate flow rate and the size of the PM) the time spent on treatment is the most easily modifiable variable to achieve for the dialysis dose adequacy [39].

Following the recently reviewed and published clinical practice guidelines for peritoneal dialysis a combined urinary and peritoneal Kt/V_{urea} of 1.7/week or a creatinine clearance of 50L/week/1.73 m^2 should be considered as minimal treatment doses for adults [40]. Despite the fact that

many guidelines agree with the minimum target of total weekly Kt/V_{urea} of >1.7, it has been evidenced that increasing small solute clearance beyond this level does not guarantee better survival. Furthermore, dialysis adequacy cannot be merely determined by one biochemical marker. Instead, comprehensive understanding of dialysis adequacy is required to improve clinical outcomes. This should encompass adequate fluid balance, optimal blood pressure control, maintaining acid-base homeostasis, correction of anemia, malnutrition, and calcium-phosphorus mineral disturbances, decreasing inflammation, and improving middle molecule clearance [41].

2.4- Peritoneal protein clearance

Peritoneal protein clearance (PPCl) is another clinical parameter that must be taken in consideration, being dependent on vascular supply and size selective permeability [42]. Recently, a multivariate analysis study correlated some factors associated with increasing PPCl, such as, (i) longer dwell times of CAPD, (ii) greater peritoneal creatinine clearance and faster PET transport, (iii) increased log N-terminal brain natriuretic peptide (NT-proBNP), (iv) extracellular water (ECW)/total body water (TBW) ratio and (v) estimated dietary protein intake and muscle mass, suggesting a link to sodium intake and sodium balance, increasing both ECW and conduit artery hydrostatic pressure resulting in greater vascular protein permeability [42].

In addition, protein/albumin loss it is an important predictor of survival in PD patient, and presumably a marker of endothelial dysfunction and, as such, a reflection of general atheromatosis or of subclinical inflammation. [29]. Therefore, peritoneal protein loss can be determined to discriminate fast transport status caused by large surface area (low protein loss) from fast transport status due to inflammation (high protein loss) [29]. Moreover, PPCl rather than faster transport status was suggested as an outcome predictor in PD patients, since a higher PPCl was associated with increased risk of death, even after patients underwent transplantation or transferred to hemodialysis [43]. Furthermore, given the fact that fast PM transport status may be due to inflammation or increased peritoneal membrane surface area, PPCl has been purposed to distinguish fast PM transport status as a consequence of PM inflammation and assess its impact on patient survival. The results show that peritoneal transport status no longer predicted survival, whereas PPCl remained a predictor [44].

2.5- Peritoneal dialysis effluent CA 125 marker

The loss of MCs from the basement membrane is one of the major characteristics in peritoneal membrane structural change. Thus, if the reduction of peritoneal MC mass in PD patients is monitored, signs of UFF and peritoneal fibrosis can be detected early [45]. MCs secrete surfactant-like lubrication for the peritoneum, are active in modulating host defence, and have been shown to produce cancer antigen (CA) 125 [46]. Therefore, concentration or appearance rate of CA125 in peritoneal dialysis effluent (PDE) has been used for many years as a biomarker for mesothelial cell mass in patients on PD

[47]. The concentration of this high molecular weight glycoprotein is determined after a standardized dwell. Serum CA125 is normal in PD patients, but its concentration in PDE suggests local release. Besides that, large amounts are found during peritonitis, due probably to necrosis of mesothelial cells. However, a decrease with time on PD suggests loss of MCs [42]. The CA125 concentration can be measured directly in U/mL or calculated as the CA125 appearance rate, which is the amount of CA 125 in the total drained effluent volume divided by the dwell time [45]. The CA125 appearance rate can be calculated using the following equation:

$$\text{CA125 appearance rate (U/min)} = \frac{CA125\left(\frac{U}{mL}\right)\times volume\ effluent\ (mL)}{dwell\ time\ (\text{min})}$$

2.6 -Residual kidney function

Residual kidney function (RKF) is another parameter that must be taken into consideration with incremental of PD The RKF, both in terms of clearance and in terms of diuresis, should be monitored on a regular basis by 24-h urine collection and calculation of the mean of urea and creatinine clearance. The rationale of incremental PD is to treat symptoms of renal failure by a combination of dialysis and RKF. Thus, with the further decline of kidney function the dialysis dosage should be continually increased [29],[39]. This approach brings several advantages: (i) given significant RKF (3-10 mL/min) even a small amount of PD tends to improve uremic symptoms; (ii) a reduced burden/ less intensive regimen, gives the patient time to adjust to PD; (iii) Glucose exposure of peritoneum can be minimized from the beginning and (iv) rationale incremental PD might better conserve RKF [39].

However, intentionally leaving patients overhydrated to preserve RKF is strongly discouraged. Overhydration also results in faster decline of RKF and is by itself an important factor leading to cardiovascular mortality. On other hand, dehydration should be avoided, since it can also cause faster deterioration of RKF [29].

Patients with a rapidly declining RKF often also have a faster deterioration of the PM [29]. Patients with preserved RKF are more likely to have well-controlled blood pressure, euvolemia, better nutritional status, less inflammation, and better phosphate and middle molecule clearance as compared to anuric patients. Maintaining euvolemia is also of extreme importance as fluid overload is associated with an increased cardiovascular risk such as high blood pressure, cardiac dilatation and hypertrophy, and congestive heart failure. Therefore, RKF and fluid balance are indeed two most important determinants of clinical outcomes in dialysis patients. For this reason, these two should be incorporated into measures of dialysis adequacy [41].

3- Complications related to Peritoneal Dialysis therapy

During the early years of RRT, PD provides an equivalent, if not superior, mode of dialysis when compared with HD, for a substantial number of patients. However, this appears to be limited to

the first three or four years, and the majority of patients switch therapy to HD due to treatment failure. [15]. PM degrades with time and its short-to-medium survival outcome is up to five years [48]. PM failure increases from 5% patient-years in the beginning of the treatment to 25% patient-years in the third year [48]. The causes of this treatment failure are multifactorial and include recurrent episodes of peritonitis, loss of RKF, and loss of peritoneal function [15]. Additionally, continuous exposure to bio-incompatible PD solutions (hyperosmotic, hyperglycemic, and acidic dialysis solutions), mechanical stress connected with dwelling practice, and episodes of peritonitis or hemoperitoneum may cause acute and chronic inflammation and injury to the PM, which progressively undergoes fibrosis, angiogenesis, vasculopathy, loss of the protective hyaluronan layer on the peritoneal peritoneal surface of mesothelium, loss of MCs, mesothelial-to-mesenchymal transition (MMT), ultimately, leading to UFF [49][50][51]. Importantly, all these changes are interconnected factors associated with alterations on fluid and solute removal. These changes ultimately lead to different spectra of PM ultrafiltration failure (UFF) types (type I–IV) (Figure 5) (described in Section 3.2), which compromises treatment efficacy (due to extracellular volume overload) and patient outcomes.

3.1-Inducers of peritoneal membrane degradation

The efficacy of the PD depends on the morphological and functional PM integrity. However, this integrity is compromised during long-term PD due to different factors such uremia, recurrent peritonitis (bacterial and fungal infections), hemoperitoneum, and especially, long-term exposure to large volumes of bio-incompatible solutions containing glucose degradation products (GDPs) [23],[52]. GDPs that are potentially toxic to the PM are formed during heat-sterilization and prolonged storage. GDPs are rapidly absorbed into the circulation and increase systemic advanced glycation end products (AGEs)[17]. In turn, AGEs can bind to receptors of AGE (RAGE), activating intracellular signals that produce oxidative stress and synthesis of inflammatory cytokines, growth factors, and ECM components, contributing to PM alterations [50],[53].

Moreover, AGEs appearance in peritoneal effluents of PD patients is correlated with the time on PD treatment. Biopsy studies have confirmed the accumulation of AGE in peritoneal tissues of PD patients and the intensities of AGE accumulation is associated with fibrosis and ultrafiltration dysfunction [50]. In addition, the uremic status contributes to AGE accumulation and some circulating mediators such as, nitric oxide (NO), VEGF and inflammatory cytokines (IL-1β, tumor necrosis factor-alpha (TNFα), IL-6) that can significantly increase, influencing the structure and function of PM [52]. Uremia per se leads to thickening of the sub-mesothelial zone and mild vasculopathy [38] (Figure 5).

Furthermore, some factors other than those related to the PDF can have important effects on the PM, and can result in variability in peritoneal function. For example, i) the degree of glycaemic control rather than diabetes *per se* can cause changes to the PM, ii) a high salt intake can induce changes in hypertonic exchanges leading to PM changes and iii) PM characteristics can be influenced by genetic

polymorphisms. However, many of these factors are modifiable, and attention should be given to them in clinical practice in order to maintain the PM integrity [54]. Altogether, these factors lead to morphological alterations of peritoneum, undergoing inflammation and infection, MC loss, mesothelial to mesenchymal transition, increase of the submesothelial extracellular matrix (ECM) deposition (fibrosis), angiogenesis and lymphangiogenesis, as described in the following sections.

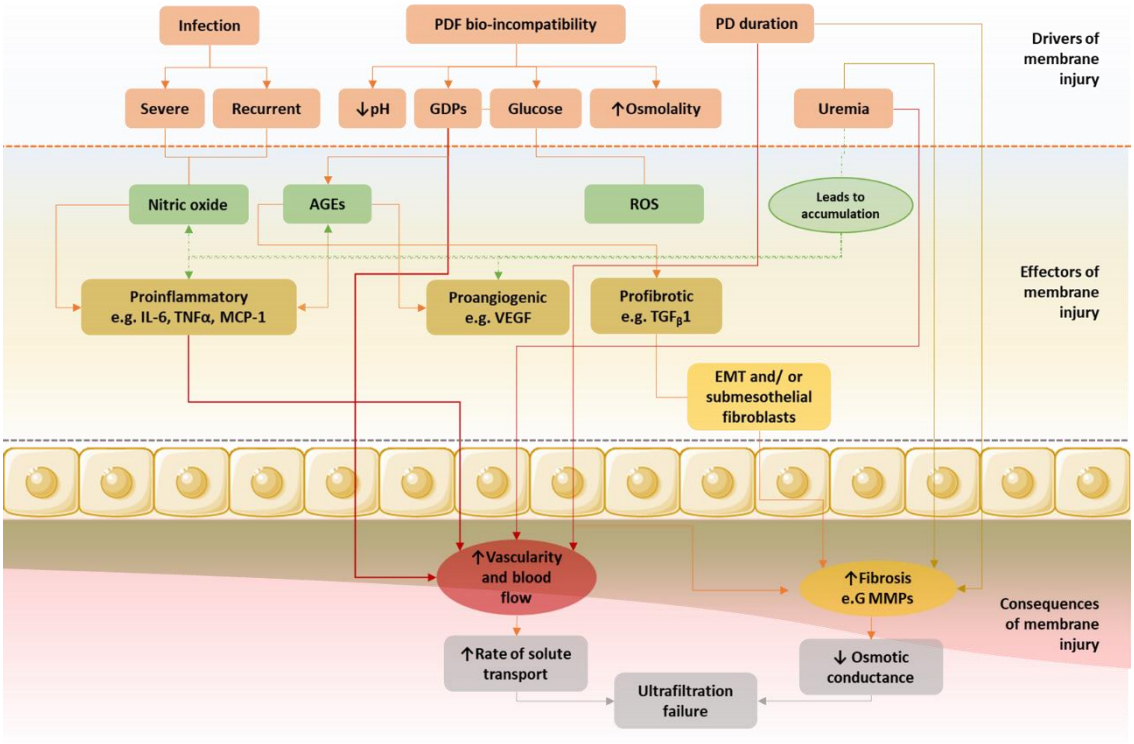

Figure 5- The pathways of PM injury and progressive UFF can be divided into 3 phases: drivers, mechanisms, and functional consequences. EMT, epithelial-to-mesenchymal transition; GDPs, glucose degradation products; IL, interleukin; MCP, monocyte chemoattractant protein; TGF, transforming growth factor; TNF, tumor necrosis factor; VEGF, vascular endothelial growth factor. The figure was adapted from Davies [53].

3.1.1- Inflammation and infection

As described in the previous section, several factors can trigger peritoneal inflammation, inducing an immunological response in the peritoneal cavity that involves MCs, mast cells dermal fibroblast, macrophages, lymphocytes and neutrophils. When stimulated, these cells produce a wide variety of cytokines, chemokines and growth factors, such as TNFα, interleukin (IL)-1, IL-6, IL-8, IL-17, TGFβ, VEGF, fibroblast growth factor (FGF)-2, monocyte chemotactic protein (MCP)-1 and many others (Table 2), thereby increasing inflammation and causing structural and functional alterations [50].

The MCs are capable of recognizing pathogen and tissue damage, and initiating inflammatory response through antigen presentation, cytokine production, interaction with immune cells like macrophages, and through tissue repair and adherence formation [56].

In acute peritonitis, a first wave of polymorphonuclear neutrophils (PMN) recruited by chemoattractants of bacterial origin (lipopolysaccharide (LPS)) is progressively replaced by a

population of mononuclear cells, composed of monocytes/macrophages and lymphocytes[49]. This temporal switch in the pattern of leukocyte is crucial in the clearance of infection, with involvement of the IL-6 as a key mediator in this regulation. This IL-6 response depends on the presence of the soluble IL-6 receptor (sIL-6R), to form the sI-6RL/IL-6 complex (transsignaling mechanism), allowing IL-6 signaling in cell types lacking the cognate IL-6R, through the ubiquitously expressed transducing molecule, gp130. The transsignling mechanism, modulates the expression of specific chemokines and adhesion molecules, and regulates the process of apoptosis, thereby influencing the leukocyte recruitment [49], [57]. This control primarily results from chemotactic cytokine production by MCs, contributing to proinflammatory cytokine-driven activation and synthesis of a large amount of IL-6 during inflammation. However, MCs not express the cognate IL-6R, so they regule chemokine synthesis only when exposed to the agonistic sIL-6R/IL-6 complex [57].

Table 2- Types of cytokines produce by different cells in peritoneum, their relevance to PD. Adapted from Shi *el al.*[55]

Types of cytokines	Cellular source in peritoneum	Relevance to PD
VEGF (angiogenic factor)	Mast cells	VEGF and VEGFR are crucial for angiogenesis
	ECs	
	MCs	
Angiopoietin2 (angiogenic factor)	ECs	Angiopoietin2 signalling involved in TNF-α induced peritoneal angiogenesis
IL-6 (angiogenic/inflammatory factor)	Macrophages	IL-6 is positively correlated with VEGF in plasma and dialysate
	ECs	
	MCs	
IL-1 (inflammatory factor)	Macrophages	IL-1 increases vessel-like structures by enhancing VEGF production, and augments proliferation when added to ECs
	MCs	
IL-8 (inflammatory factor)	Macrophages	IL-8 enhances EC proliferation and capillary tube formation
	Mast cells	
	MCs	
TNF-α (inflammatory factor)	Macrophages	TNF-α causes neoangiogenesis both in *vitro* and *vivo*
	Mast cells	
	MCs	
MCP-1 (chemokine)	Macrophages	MCP-1-induced protein enhances ECs proliferation, migration, and other pro-angiogenic genes, leading to capillary-like tube formation
	ECs	
ICAM-1 (adhesion molecules)	ECs	Induced by IL-6 and TNF-α after EC injury, promoting new capillary formation
VCAM-1 (adhesion molecules)		
TGF-β (growth factor)	Mast cells	TGF-β triggers the expression of VEGF via EMT and conversely amplifies its own secretion
	MCs	

Abbreviations: VEGF (vascular endothelial growth factor); IL-1 (interleukin-1); IL.6 (interleukin-6); IL-8 (interleukin-8); TNF-α (tumor necrosis factor –α); MCP-1 (monocyte chemotactic protein-1); ICAM-1 (intercellular adhesion molecule-1); VCAM-1 (vascular cell adhesion molecule-1); TGFβ (transforming growth factor-β); MCs (mesothelial cells); ECs (endothelial cells).

In summary, as can be seen in Figure 6, during acute inflammation, leukocyte recruitment is characterized by an initial infiltration of neutrophils, which are later replaced by a more sustained mononuclear cell influx [58]. This process is mediated through activation of proinflammatory cytokines (TNF-α, IL-1, and IFN-γ) and subsequent changes in chemokine expression. In addition, it is believed that the initial attraction of neutrophils by proinflammatory cytokine-driven expression of CXC chemokine, MIP-1/KC, is followed by the release of sIL-6R shed from neutrophils, facilitating the formation of sIL-6R/IL-6 complexes [58]. On the other hand, these complexes suppress the release of other CXC chemokines, ensuring clearance of neutrophils, and simultaneously promoting the secretion of the CC chemokines, such MCP-1 and RANTES, triggering the recruitment of mononuclear leukocytes [57]. Involvement of the IFN-γ in the control of PMN recruitment and modelling of IL-6

signalling through sIL-6R to promote their apoptosis and clearance has also been demonstrated. Thus, IFN-γ has an important role in regulating innate immunity through control of both the recruitment and clearance phases of PMN trafficking [59]. Another study, using knock-in mice expressing mutant forms of the IL-6 signal transducer molecule gp130 [60], showed that IL-6/sIL-6R signalling also selectively promotes T cell recruitment into the peritoneal membrane through a gp130-dependent, STAT1/3-dependent activation pathway [57].

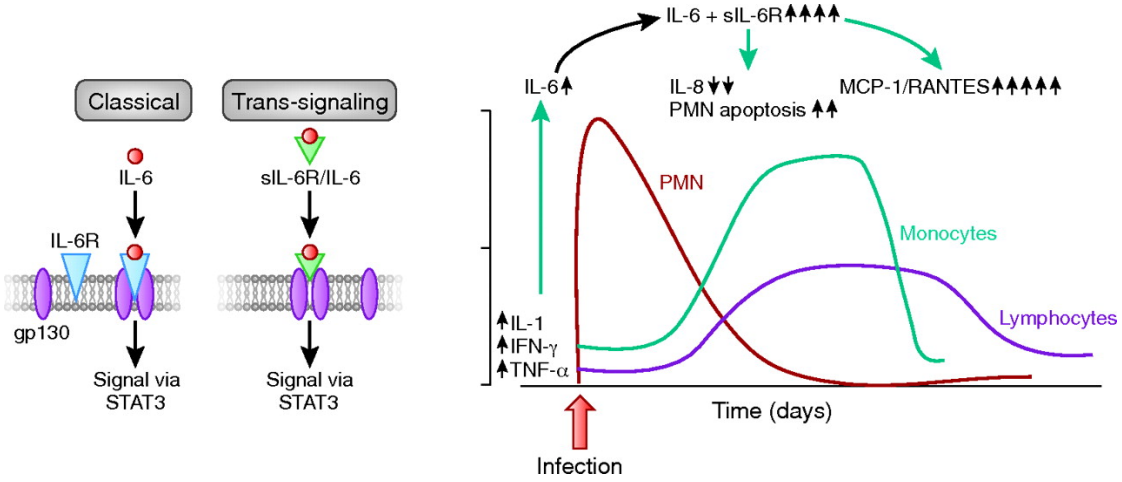

Figure 6- Representation of IL-6 and sIL-6R signaling in the regulation of leukocyte trafficking. The regulation of leukocyte trafficking in the peritoneal cavity is mediated by proinflammatory cytokine–driven (IL-1, TNF-α, and IFN-γ) activation of IL-6/sIL-6R transsignaling mediated through control of STAT3 activation that results in differential control of chemokine secretion (that is responsible for mononuclear leukocyte and T cell recruitment) and polymorphonuclear neutrophils (PMN) apoptosis. Image taken from Devuyst *et al.* with permission [57].

However, the unphysiologic composition of PDFs used adversely affects peritoneal host defence and may thus contribute to the development of PD-related peritonitis [61]. The viability of PMN, monocytes, peritoneal macrophages and MCs is severely depressed by conventional PDFs, and therefore the production of inflammatory cytokines and chemoattractants by these cells are markedly affected. The recruitment of circulation leukocytes in response to an infectious stimulus is also hampered, and phagocytosis, respiratory burst, and bacterial killing are lower when PMN, monocytes, and peritoneal macrophages are exposed to these solutions [61].

Summing up, while the transition from innate immunity to acquired immunity facilitates the resolution of inflammation and the clearance of bacterial infection in the peritoneum during acute inflammation, through the sI-6RL/IL-6 complex, dysregulation of this pathway as occurs in chronic inflammation or after repeated infections also contributes to inflammation-induced peritoneal damage [57].

3.1.2- Mesothelial to Mesenchymal Transition

Epithelial and mesenchymal cells have distinct characteristics. Epithelial cells form layers of cells that are closely adjoined through tight junctions, adherens junctions, desmosomes and gap

junctions. In addition, epithelial cells have apical–basolateral polarization, which manifests itself through the localized distribution of adhesion molecules (cadherins and certain integrins), the organization of cell–cell junctions as a lateral belt, the polarized organization of the actin cytoskeleton, and the presence of a basal lamina at the basal surface [62]. Contrarily, mesenchymal cells do not form an organized cell layer, nor do they have the same apical–basolateral organization and polarization of the cell-surface molecules and the actin cytoskeleton as epithelial cells. They contact neighbouring mesenchymal cells only focally, and are not typically associated with a basal lamina [62].

Regarding cell motility, epithelial cells are motile and can move away from their nearest neighbours while remaining within the epithelial layer, but do not detach and move away from the epithelial layer under normal conditions. Contrarily, mesenchymal cells present high motility *in vitro*, but not necessarily *in vivo*. In fact, there is plasticity in the way that mesenchymal cells migrate. These cells might migrate together as chains, or as individual cells that exhibit either cyclic extension–adhesion–retraction translocation or amoeboid-type crawling. [62].

These cell types can be partially or fully interconverted through the processes of epithelial-to-mesenchymal transition (EMT) and mesenchymal-to-epithelial transition (MET) [62]. EMT is an essential process in embryogenesis, and is beneficial in normal wound healing, but is pathogenic in fibrosis [57]. The reverse process, MET, occurs during somitogenesis and nephrogenesis. EMT is characterized by disrupted cell–cell adhesion and apical–basolateral polarity, cytoskeletal reorganization, detachment from basement membranes, and the generation of motile mesenchymal cells [63]. Therefore, EMT can be described as a series of events during which epithelial cells lose many of their epithelial characteristics and take on properties that are typical of mesenchymal cells, which require complex changes in cell architecture and behaviour. However, this does not necessarily refer to a lineage switch, given that the transition from epithelial- to mesenchymal-cell characteristics encompasses a spectrum of inter- and intracellular changes, all of which are not always seen during EMT [62],[64].

As described in the previous sections, MCs are epithelial-like cells lining the peritoneal cavity. MCs have junctional complexes and apical–basolateral polarity, and adhere to a basement membrane. In normal development, some MCs undergo MMT to form vascular smooth muscle. MCs are not typical epithelial cells, so the biological characteristics of MMT and EMT may not be identical [63]. Therefore, the EMT of MCs is more properly named as MMT [64].

The pathophysiologic mechanisms that are involved in peritoneal structural alterations can have origins from new fibroblastic cells that may arise from local conversion of MCs by MMT during the inflammatory and repair responses induced by PD [50]. These alterations happen soon after PD is initiated, with peritoneal MCs showing a progressive loss of epithelial morphology through the dissociation of intercellular junctions, as a result of downregulation of adhesion molecules (such, E-cadherin, claudins, occludins, zona occludens-1, and desmoplakin), and with the loss of microvilli and apical-basal polarity [50], [64]. Then the cells adopt a front-back polarity as a result of cytoskeleton reorganization, and acquire myofibroblast-like characteristics with migratory and invasive capacities

with the up-regulation of α_2 integrins and α-smooth actin (α-SMA). In the latest stages the cells acquire the capacity to degrade the basement membrane and to invade the fibrotic stroma by upregulating the expression of MMPs. In addition is also observed during the transition is a downregulation of cytokeratins, upregulation of vimentin, N-cadherin, and transcription factor snail; and increased production of ECM components (Figure 7)[50], [64]. The decrease in the expression of cytokeratins and E-cadherin occurs through and induction of the transcriptional repressor *snail* [64]. The objective of this process is to repair tissue wounds by promoting the recovery of ancestor capabilities of epithelial cells. The process is conducted by TGF-β and the representative cell form is the myofibroblast [65].

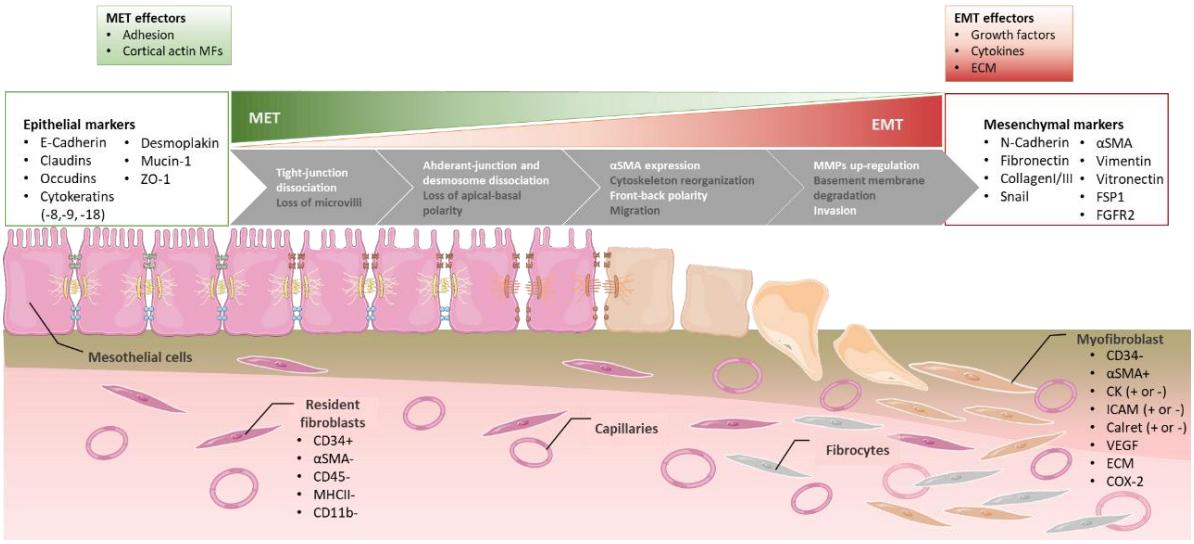

Figure 7- Representation of the peritoneal membrane suffering structural abnormalities such as, loss of mesothelial cells monolayer, increasing number of fibroblasts, submesothelial fibrosis, and augmented number of vessels. The key steps and effectors for the epithelial-to-mesenchymal transition (EMT) and for mesenchymal-to-epithelial transition (MET) are also represented. Furthermore, common markers for epithelial and mesenchymal cells, resident fibroblasts and myofibroblasts, are also represented. Figure adapted from Aroeira *et al.* [50].

The myofibroblast can be defined as cells with intermediate features between a fibroblast and smooth muscle cells and are characterized by the expression of α-SMA. The submesothelial myofibroblasts can originate from activated resident fibroblasts, fibrocytes (circulating cells that are recruited to injured tissues), and from MCs through MMT. The myofibroblastic conversion of MCs can be observed by immunohistochemical analysis, which reveals the presence of fibroblast-like cells embedded in the compact zone expressing mesothelial markers such as cytokeratins, intercellular adhesion molecule-1 (ICAM-1), and calretinin. Peritoneal myofibroblasts express VEGF, ECM, and cyclooxygenase-2 (COX-2), indicating that these cells are implicated in peritoneal structural alterations that are induced by PD [50].

Interestingly, these fibroblasts present different markers. Resident fibroblast show an intense expression of CD34, and antigen characteristic of bone marrow stem cells. On the other hand, expression of CD34 gradually disappears in PD patients with the degree of peritoneal fibrosis and it seems to correlate with the appearance of myofibroblast phenotype [66]. Moreover, tissue $CD34^+$ fibroblasts are closely related to circulating $CD34^+$ fibrocytes and reflect a bone marrow origin. Fibrocytes represent a

small subpopulation of circulating leukocytes that express collagen I, CD45RO, CD13, CD11b, CD34, CD86, and MHC class II, which transform into myofibroblasts when exposed to TGF-β in vitro. In contrast, peritoneal CD34+ fibroblasts do not express these fibrocyte markers, suggesting that they are simply residual embryonic mesenchymal cells that remained in the peritoneal tissue after organogenesis [50] (Figure 7).

As was already discussed, several endogenous and exogenous factors can stimulate the immune system and MCs in the peritoneal cavity to induce MMT. The MMT progression is regulated by complex signaling pathways that together accelerate or complete the transdifferentiation. These signaling pathways are, i) inflammation ii) delta-like jagged Notch, iii) integrins, iv) receptors for TGF/Smads, and v) tyrosine kinase receptors and vi) Janus kinase (JAK)- signal transducer (Figure 8).

Inflammatory cells (as described in Section 3.1.2.1) secrete large numbers of cytokines, growth factors, and chemokines to establish a complex network that feeds back, resulting in sustained chronic inflammation. In addition, during inflammation, IL-6 can promote EMT through JAK-signal transducer and activator of transcription (STAT)3-induced SNAIL1 expression [67].

In Notch and Hedgehog signalling, glioma 1 can induce SNAIL1 expression, and the intracellular domain of Notch can activate SNAIL2 expression, hence downregulating E-cadherin, by inducing growth arrest and survival, which confer selective advantage to migrating trans-differentiated cells. In turn, the integrin pathway is able to activate the integrin-linked kinase (ILK), by β1 integrins, inducing the serine/threonine kinase AKT, which inhibits glycogen synthase kinase (GSK)-3β inducing MMT. Phosphorylated-AKT triggers NF-kB activation, which in turn induces the expression of Smad 7, an inhibitory Smad molecule that interferes with the phosporylation of Smad 2 and 3, and of snail, a key regulator of MMT. The phosphorylation of GSK-3 by ILK results in its inhibition and subsequent stabilization of β-catenin, released from the adherent junction, and of AP-1. Stabilized b-catenin, in conjunction with Lef-1/Tcf, may by itself induce MMT, and AP-1 activates MMP-9 expression inducing the invasion of ECM [65], [67].

The TGFβ/Smads pathway is able to activate different routes, such as, i) through the phosphorylation of the adaptor protein SRC homology 2 domain-containing-transforming A (SHCA), that creates a docking site for growth factor receptor-bound protein 2 (GRB2) and son of sevenless (SOS), which initiates the RAS-RAF-MEK-ERK pathway (also necessary for the induction of snail expression) or, ii) through the p38 MAPK and JNK activation, another TGFβ-induced route, resulting from the association of TNF receptor-associated factor 6 (TRAF6) with the TGFβ receptor complex, which activates TGFβ-activated kinase 1 (TAK1) and, as a result, p38 MAPK and JNK[67] In addition, a Smad-independent signalling cascade triggered by TGF-β receptor I ligation, is the RhoAp160ROCK pathway that regulates cytoskeleton remodelling and cellular migration/ invasion. Moreover, RhoA induces the expression of α-SMA in a ROCK-independent manner [65].

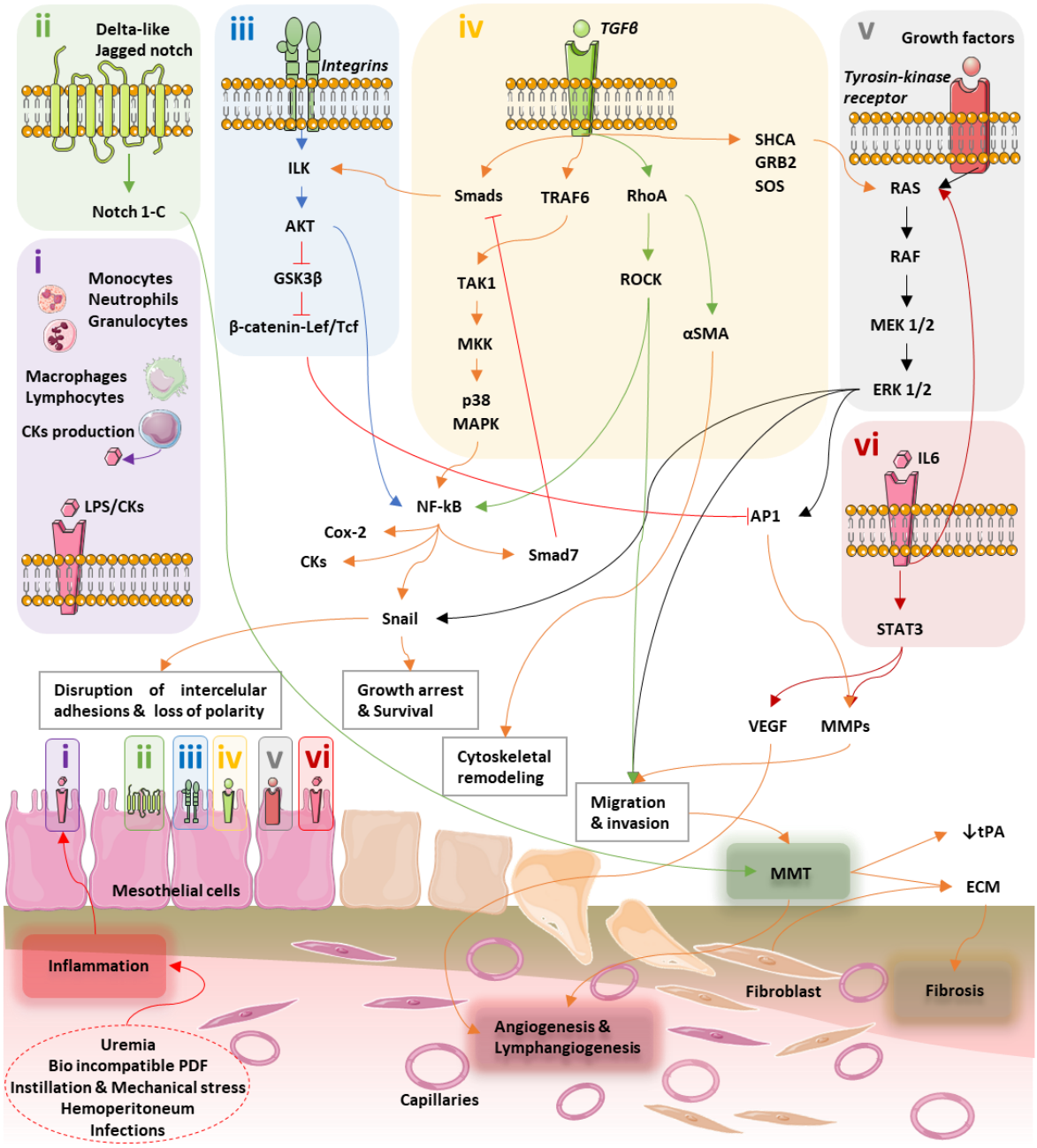

Figure 8- Representation of the signalling pathways that regulate MMT progression. These signalling pathways are, i) inflammation ii) delta-like jagged Notch, iii) integrins, iv) receptors for TGF/Smads, and v) tyrosine kinase receptors and vi) Janus kinase signal transducer. Abbreviations: MMT (mesothelial-to-mesenchymal transition); TGFβ (transforming growth factor-β); MMPs (matrix metalloproteinases); GSK3β (glycogen-synthase kinase-3β); β-catenin-Lef/Tcf (lymphoid enhancer factor/T cell factor); ILK (integrin-linked kinase); MAPK (mitogen-activated protein kinase); RAS–RAF–MEK–ERK pathway, extracellular signal-regulated kinases (MEK: Mitogen-activated protein kinase kinase. ERK: extracellular signal–regulated kinase); NF-kB (nuclear factor-kB); TAK1 (TGF-beta activated kinase 1); VEGF (vascular endothelial growth factor); ECM (extracellular matrix); Notch-IC (intracellular fragment of Notch); COX-2 (cyclooxygenase); CKs (cytokines); SHCA (adaptor protein SRC homology 2 domain–containing-transforming A); GRB2 (growth factor receptor–bound protein 2); SOS (son of sevenless); TRAF6 (TNF receptor-associated factor 6); α-SMA (alpha smooth muscle actin); AKT (protein kinase B); RhoA (Ras homolog gene family member A); ROCK (Rho-associated protein kinase); STAT3 (signal transducer and activator of transcription 3); t-PA (tissue plasminogen activator); AP-1 (activator protein-1); and LPS (lipopolysaccharide). Figure adapted from Aguilera *et al*. [65] and González-Mateo *et al*. [67].

The activation of the receptor tyrosine kinases (RTKs) can occur in response to several growth factors, such as epidermal growth factor (EGF), fibroblast growth factor (FGF), hepatocyte growth factor (HGF), and VEGF, leading to the activation of a major pathway, the RAS-RAF-MEK-ERK

MAPK signalling cascade. Once this pathway is activated, ERK1 and ERK2, MAPK pathway cell motility and invasion are activated [67].

Finally, MCs lose their basoapical and basolateral polarity, acquire migratory capacity to synthesize large amounts of ECM and angiogenesis through increased synthesis of VEGF [67].The increase in total VEGF production may increase the VEGF-C levels, which are directly implicated in lymphogenesis [68].

3.1.3- Angiogenesis and Lymphangiogenesis

Blood vessels deliver oxygen and nutrients, remove waste and CO_2, whereas lymphatic vessels drain the interstitial fluid collected in the tissues to maintain the interstitial environment, and serve as conduit for immune cell trafficking and fat absorption [69].

In regard to peritoneal angiogenesis, it is a process characterized by the formation of new capillaries, increasing the effective surface area of exchange, which results in a decrease in the glucose-driven osmotic pressure [23]. Besides that, it has been shown that local production of the proangiogenic and vasoactive factor VEGF during PD plays a central role in increased solute transport across the peritoneum and ultrafiltration failure [50]. The biological effect of VEGF is mediated by three VEGF receptors (VEGFRs): VEGFR-1/Flt-1, VEGFR-2/KDR, and VEGFR-3/Flt4, which share a similar structure composed by seven extracellular immunoglobulins (Ig)-like domains, one transmembrane region, and an intracellular tyrosine kinase domain that, once activated via ligand-triggered dimerization, leads to different signal transduction pathways (Figure 9) [70]. The VEGFR2 is the specific receptor distributed on the surface of the ECs that binds VEGF and recruits EC migration to anoxic and vascular areas. As the ECs proliferate and differentiate, angiogenic remodelling occurs where the vessels enlarge and mature [55].

Additionally, VEGF activity is also regulated by neuropilins (Nrps), a family of cell surface glycoproteins composed of two members, Nrp1 and Nrp2 (Figure 9). The Nrp-1 has been described as an isoform-specific VEGF co-receptor expressed in endothelial and tumour cells, enhancing VEGF binding to VEGFR-2 and its bioactivity. On another hand, Nrp-1 may also signal independently of VEGFR-2 in endothelial cells to VEGF-triggered migration and adhesion. Moreover, Nrp-1 may also interact with other growth factors, such as FGF and TGF-β1. Besides the neurons and ECs, Nrp-1 expression was also described in MCs [70]. Remarkably, in a study performed by Pérez-Lozano *et al.*, it has been shown that the expression patterns of VEGFRs and co-receptors change in MCs during MMT, with a strong induction of VEGF and Nrp-1, and downregulation of VEGFR-1 and VEGRF-2. In addition, MCs which have undergone an MMT proliferate less and acquire an increased invasion capacity compared with epithelial-like MCs. Furthermore, it has been shown that this enhanced invasion

could be partially inhibited by treatment with anti-VEGF or anti-Nrp-1b antibodies, strongly suggesting that the interaction of VEGF with Nrp-1 may have a role in MCs invasion [70].

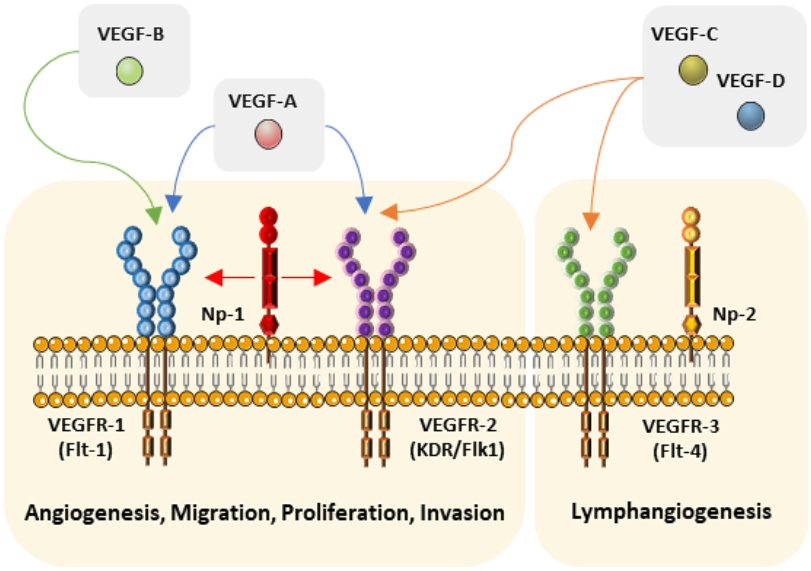

Figure 9- Scheme of VEGF receptors and co-receptors and processes in which they are involved. Figure adapted from Pérez-Lozano *et al.*[70].

Lymphangiogenesis, which represents the growth of lymphatic vessels from pre-existing vessels [71] is a poorly analysed process in PD. However, it is known that excessive lymphatic fluid drainage from the peritoneal cavity may be related with the macromolecule and isosmotic solutions reuptake and convective reabsorption of solutes that were cleared from plasma by diffusion [23]. The lymphatic capillaries develop during the progression of tissue fibrosis in various clinical and pathological situations, such as CKD, peritoneal injury PD, tissue inflammation, and tumour progression [72]. Therefore, inflammation is an important contributor to lymphangiogenesis in PD, and macrophages in particular have been suggested to stimulate lymphangiogenesis through the production of VEGF-C and VEGF-D. VEGF-C is one of the most important mediators of lymphangiogenesis, and it has been shown that its content in the PDE is positively correlated with the membrane transport rate. Thus, if VEGF-C concentration in the PDE increases, the PM transport rate will be higher [23].

Interestingly, VEGF production is associated with blood and lymphatic vessels proliferation, while lymphangiogenesis specifically is mainly regulated by VEGF-C and VEGF-D [23]. In addition, VEGF receptor (VEGFR)-3 is also part of this signalling pathway, in that it represents the central molecular mechanism for lymphangiogenesis [72].

Importantly, TGF-β is another key player, and is responsible for inducing peritoneal fibrosis in association with PD, and also peritoneal neoangiogenesis through interaction with VEGF-A. On the other hand, TGF-β has a direct inhibitory effect on lymphatic endothelial cell growth. Therefore, a possible mechanism of the TGF-β–VEGF-C pathway in which TGF-β promotes VEGF-C production in tubular epithelial cells, macrophages, and MCs, leading to lymphangiogenesis in renal and peritoneal fibrosis, has been recently proposed [72].

Moreover, it has been shown in cultured macrophages and fibroblasts that VEGF-D increases by prostaglandin E2 (PGE2) and by inflammatory cytokines, while VEGF-D has been reported to be down-regulated by TGF-β. In addition, although cultured human MCs strongly express VEGF-C, they do not express VEGF-D. Thus, either VEGF-C or VEGF-D induce growth of the lymphatic vessels via activation of VEGFR-3, which is localized on the surface of lymphatic ECs [23]. In addition, CTGF is also involved in fibrosis-associated renal lymphangiogenesis through interaction with VEGF-C, in part by mediating TGF-β signalling [72]. Therefore, signalling via VEGF-C and VEGF-D/VEGFR3 represents the most central pathway for lymphangiogenesis and survival of ECs, providing a new therapeutic target to increase net UF by suppression of lymphangiogenesis and lymphatic absorption [23].

Furthermore, angiogenesis and fibrosis seem to be intimately linked through common initiating growth factors and inflammatory cytokines and the EMT process. Understanding the mechanisms of fibrosis and the interaction with angiogenesis is, therefore, important to developing therapeutic strategies to preserve the peritoneum as a dialysis membrane [57].

3.1.4- Peritoneal fibrosis, sclerosis and EPS

Peritoneal fibrosis (or sclerosis) consists of the deposition of ECM proteins (collagen I, III, V, VI, fibronectin, tenascin) in the interstitium, with increased number of fibroblasts (some presenting myofibroblastic characteristics) and inflammatory cell infiltration. In addition, it is usual to find extracellular accumulation of collagen IV and laminin in the basement membrane, proteoglycans, polysaccharides, and glycoproteins [67]. The fibrotic thickening of the peritoneum increases resistance to fluid flux and ultimately decreases water flow through the interstitium. Thus, it appears that the gradual loss of peritoneal UF with time is initially related to increased solute transport leading to proportional dissipation of the osmotic gradient. Fibrosis that develops at later stages affects the osmotic conductance from solute transport, resulting in the reduction of UF. Neovascularization plays also a key role in this scenario, both contributing to increased small-solute transport and fuelling fibrosis[73].

Peritoneal fibrosis is a term that includes a wide spectrum of structural alterations, ranging from mild inflammation to severe sclerosing peritonitis (SSP) and encapsulating peritoneal sclerosis (EPS), the most severe and dangerous manifestation [67]. The most commonly used criteria for differential diagnosis is the peritoneal thickness. The normal thickness of human peritoneum is 20 μm, but after a few months on PD, it may reach up to 40 μm in simple peritoneal sclerosis (SS) cases. The SSP is a progressive sclerosis characterized by a dramatic thickening of the peritoneum (up to 4000 μm), accompanied by inflammatory infiltrate, calcification, angiogenesis, and vasodilatation of blood and lymphatic vessels [67][74].

In regard to signs of peritoneal fibrosis, these are detected in 50% to 80% of patients within one to two years. Usually, peritoneal alterations are limited and a result of SS, generally correlated with the

length of exposure to PD solutions, being reversible when PD is interrupted [49]. Moreover, SS can be considered as an intermediate stage of peritoneal fibrosis, it is the most common lesion found in patients after few months on PD and may represent the beginning of SSP [67]. Long-term PD treatment can lead to EPS, an exaggerated fibrogenic response of the PM, that leads to encapsulation of the bowels and intestinal obstruction and progresses even if the patient is removed from PD [12][50].Therefore, while it is generally accepted that PD should be discontinued in patients with EPS, the utility of continuing intermittent peritoneal lavage may aid in the removal of noxious mediators such MMPs, that have been implicated in the pathogenesis [75]. The observation that some cases of EPS arise after cessation of PD has also contributed to the notion that continued peritoneal lavage may be beneficial[35]. The frequency of EPS increases with the duration of PD, patients on for > 8 years are at higher risk [76].

Regarding the mechanism behind the aberrant response to injury through fibrosis, some pathways and molecules have been found to be associated with this process. The MMT of MCs is an important mechanism involved in peritoneal fibrosis, and the TGF-β1 is considered central in this process [77]. As described in Section 3.1.2, MMT generates some myofibroblasts that can drive the fibrosis through the expressing α-Smooth muscle actin (αSMA)[63]. In the case of TGF-β1, the upregulation has been correlated to worse PD outcomes. In addition, other proinflammatory and profibrotic cytokines, as well as angiotensin II (AngII) have shown to be upregulated during peritonitis episodes and may contribute to peritoneal fibrosis [50].

A key role for macrophages (Mφ) in fibrosis has also been suggested. Depending on the cytokine microenvironment, Mφ can adopt a proinflammatory (M1) or a profibrotic (M2) phenotype characterized by the expression of cell surface proteins such CD206 and CD163 and soluble factors, such as CC chemokine ligand 18 (CCL18)[78]. Thus, M2 may participate in peritoneal fibrosis through the stimulation of fibroblast cell growth and CCL18 production. High concentrations of CCL18 are associated with functional deficiency and fibrosis of the PM[78], [79]. Furthermore, M2 expressing CD163+ have been demonstrated as one of the dominant cell populations in EPS peritoneal biopsies [80].

In addition, IL-17, a potent and best characterized member of the IL-17 family of cytokines, that led to the identification of a distinct type of T helper (Th) cells, may be critically involved in initiating peritoneal fibrosis. IL-17 is produced primarily by γδT cells and possibly by other innate-like tissue-resident lymphocytes. The increase in IL-17 is associated with increased peritoneal levels of IL-6, TGF-β, and retinoic acid-related orphan receptor-γt (RORγt), leading to the formation of additional IL-17-secreting Th17 cells in a vicious circle. Moreover, Th17 cells release CCL20, a chemokine that boosts the recruitment of further Th17 cells. In the peritoneum of PD patients, IL-17 promotes thickening of the submesothelial compact zone. In rodents, the attenuation of IL-17-mediated responses reduces the extent of peritoneal fibrosis.[73].

3.2- Peritoneal membrane failure

Ultrafiltration failure (UFF)/membrane failure is one of the important reasons for technique failure in PD [38]. UFF is the commonly used term for a situation, where netUF, i.e., the difference between the drained and the instilled volume is less than expected in the PD population. As the glucose concentration of the dialysis solution is an important determinant of netUF by osmosis, normal values are related to the glucose concentration of the dialysate [81]. UFF should be considered in patients presenting clinical findings of volume overload in whom noncompliance with diet or the dialysis regime, defects of the abdominal cavity boundary, and uncompensated loss of kidney function have been eliminated as possible causes [35]. Although the original PET allows accurate estimation of small-solute transport (expressed by D/P_{creat} and D/D_0) and ultrafiltration capacity, it does not provide sufficient information to discriminate between causes of UFF. To assess that information a PET with a 3.86% glucose solution is recommended in order to determine the evolution of D/P_{sodium} during the dwell. This allows evaluation of the function of the aquaporins by the assessment of 'sodium sieving' [29] There are four main causes of UFF than can be distinguished: (a) fast transport of low molecular weight solutes, reflecting the presence of a large peritoneal vascular surface area; (b) decreased osmotic conductance to glucose; (c) an extremely small peritoneal surface area; and (d) the presence of a high disappearance rate of intraperitoneally administered macromolecules ("effective lymphatic absorption") (Figure 10) [82]. The true UFF is defined by the "rule of fours": failure to achieve at least 400 ml of netUF during a 4 h dwell using 4.25% dextrose [35].

These four types of UFF present different pathophysiologic features. Thus, knowing the specific pathophysiology of the various causes of UFF aids the diagnosis.

Increased peritoneal exchange surface area (type-I UFF) represents the most common form of UFF arising as a consequence of changes in the PM over time causing a transition to a very rapid transport status [35], and is characterized by a high solute transport, with a D/P of creatinine > 0.81. The PM shows an inflammatory process with subsequent hyper-permeability. This type of UFF can also be observed in patients with inherent high transport characteristics of PM and during the episodes of peritonitis [38]. These anatomical changes are probably due to both tissue fibrosis and angiogenesis giving rise to a large effective exchange surface area, which results in the rapid dissipation of the osmotic gradient and consequently poor ultrafiltration [23],[35]. This hyper permeability has been demonstrated as a predictor of an increase in the mortality and technique failure in long-term PD patients. Patients' survival is inferior in high / high average transport status groups as compared to patients in low/ low average transport status group [38].

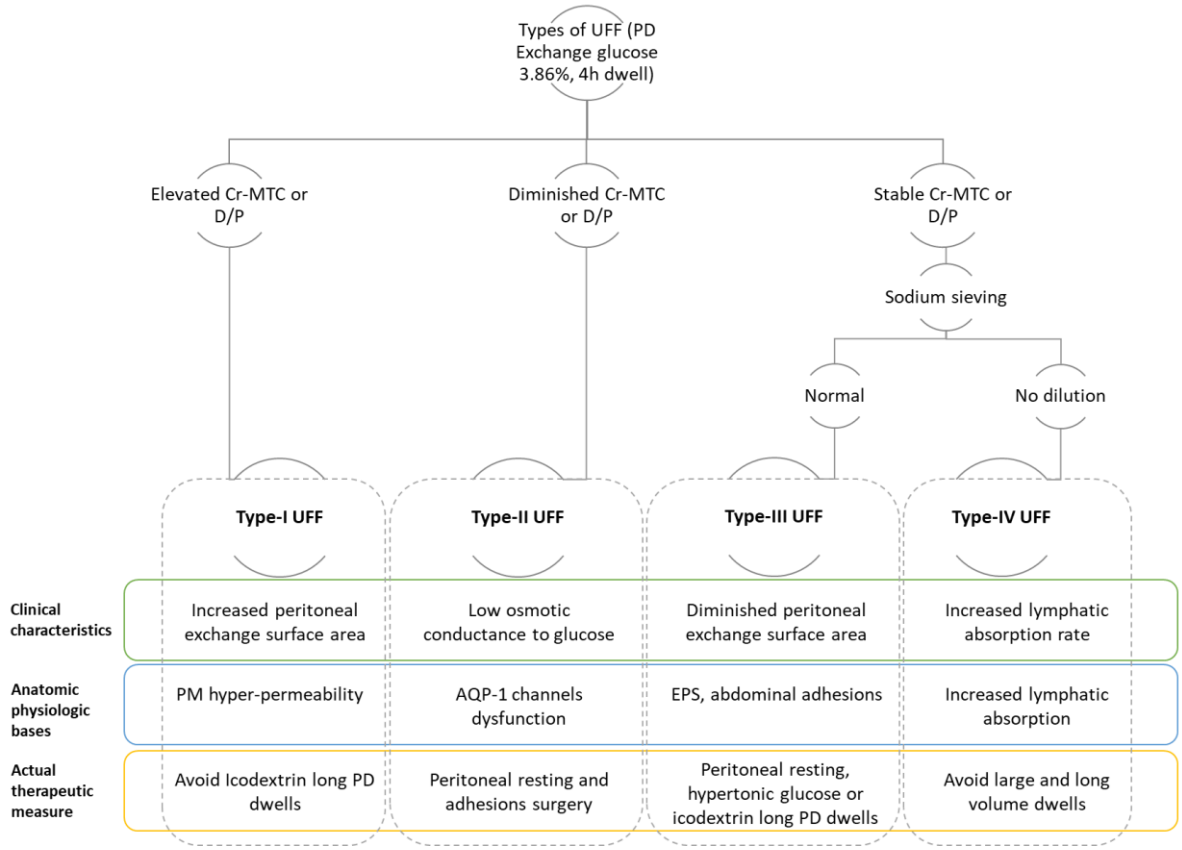

Figure 10-Clinical characteristics of the different types of UFF and accepted therapeutic option for UFF. Creatinine mass transfer coefficient (Cr-MTC); dialysate-to-plasma ratio (D/P). Adapted from González-Mateo *et al*.[23].

Low osmotic conductance to glucose (type-II UFF), leading to inadequate water removal via aquaporins (AQP-1 channels dysfunction), AQP-1 channels account for 40 to 50% of the total UF across the PM [23]. The clinical characteristic of this UFF is attenuation of sodium sieving, that is, the dampening of the decrease in dialysate sodium during the first hour of a dwell with 3.86% glucose [35].It is characterized by low/high average solute transport, with a D/P of creatinine =0.5-0.8 [23]. This selective defect in water transport has been attributed to AQP-1 dysfunction, rather than deficiency in PM [38]. The cause of the functional alteration is yet to be elucidated; there is much speculation on the roles of glycosylation or endothelial NO [35]. The NO regulates vascular tone and permeability [83] whereas, endothelial NO synthase (eNOS) is a dimeric enzyme that is likely to be uncoupled in pro-oxidant states, thus changing its functional activity, giving rise to superoxide formation instead of NO [84]. AQP1 and eNOS show a distinct regulation within the endothelium lining peritoneal capillaries. In acute peritonitis, the upregulation of eNOS and increased release of NO dissipate the osmotic gradient and result in UFF, despite the unchanged expression of AQP1. Giving the critical role of AQP1 in PD, manipulating AQP1 expression may be used to increase water permeability across the peritoneal membrane [21].

Diminished peritoneal exchange surface area (type-III UFF) represents the least common form of UFF, and is characterized by a low solute transport rates, with a D/P of creatinine < 0.5[23].

Anatomically, there is a severe reduction in effective PM surface area and permeability. The clinical characteristics that may be present are, volume overload, symptoms of inadequate solute removal or both [35]. The diffuse hypo permeability of the PM appears to be caused by the effects of pro-fibrotic mediators such as TGFβ and as a consequence of MMT suffered by MCs [23]. This is observed in patients who have recurrent and relapsing peritonitis, sclerosis of PM (sclerosis peritonitis), and intra-abdominal adhesions [52]. In simple sclerosis of the PM, there is a diminution in peritoneal transport but without more serious clinical consequences. However, in a more severe form, this may culminate in the most extreme complication of PD, the EPS, characterized by bowel obstruction through persistent PM adhesions, frequently associated with calcification [35].

Increased lymphatic absorption rate (type-IV UFF), is responsible for low effective UF, with alterations in dialysate solute concentrations. The D/P creatinine ratio does not change with increased lymphatic flow, although net UF can be considerably reduced. Increased lymphatic flow, netUF and solute clearance are inversely related to lymphatic fluid absorption [52]. The total fluid that leaves the peritoneal cavity via lymphatics absorption is no more that 10-30% [37].The magnitude of fluid loss can be estimated by examining the rate of egress of radiolabelled albumin from the peritoneal cavity. Yet, this analysis is relatively difficult to perform and is not routinely available clinically. However, as icodextrin is removed from the peritoneal cavity via the lymphatics, and since even rapid transporters will usually achieve UF with the use of icodextrin, it has been suggested that failure to achieve UF with icodextrin may be construed as indirect evidence for a high rate of fluid absorption from the peritoneal cavity [35]. The pathogenesis of this form of UFF is poorly understood. It has been suggested that TGF-β1 may play a role in promoting lymphangiogenesis in a rat model [85].This condition is relatively rare, which is fortunate as there is little to offer therapeutically and PD must often be discontinued [35].

Therefore, functional alterations in the dialysis capacity of the membrane, leading to UFF, are associated with increased morbidity and mortality and represent a major obstacle to successful long-term PD therapy [16]. UFF diagnosed at the initiation of PD has been insufficiently characterized and few longitudinal studies have analysed the time course of water transport in patients with this complication. A recent prospective study shows that patients with UFF at the start of PD, suffer from a disorder of peritoneal water transport affecting both free water transport (FWT) and small-pore ultrafiltration (SPUF). After 1 year of follow-up the FWT increased systematically. In contrast, the evolution of SPUF was less predictable. However, an improvement of SPUF seemed to reverse this complication [86].

NetUF has been shown to decrease by as much as 30%-40% from the baseline in most patients on PD for more than 3-4 years, with peritoneal clearance of small solutes increasing or being stable. A study conducted by Prakash *et al.* [87] has reported UFF as the most common (15.5%) non-infectious complication of CAPD in their study[38].

Therefore, to improve PM longevity in PD, it is mandatory to diminish or block the up-

regulation of the molecular mechanisms implicated in the onset of the UFF [23].

3.3- Stability of peritoneal membrane transport over time

PM function at the start of PD treatment, measured as solute transport rate and UF capacity, varies considerably between individuals, and even if this can be correlated to clinical factors such as age and body habitus it accounts for little of the variance seen. [88]. Additionally, the underlying pathophysiology that leads to morphologic and functional changes in the PM over time among patients on PD is not well understood [89]. Transport characteristics and UF capacity of the PM vary among patients, and deleterious changes in the membrane occur over time. The degree to which these changes are a direct consequence of currently available PD solutions, recurrent infectious episodes, genetic differences among patients, or a combination thereof is the subject of intense study[6]. In addition to these factors, adverse consequences resulting from systemic and local metabolic effects of intraperitoneal glucose exposure, infection of the PDF, PD catheter dysfunction, and patient burnout from self-care affect the long-term success of the therapy [6].

Although, initial PM changes are not life threatening, they tend to cause an increase in transport of solute both to and from the peritoneal cavity. As a result of the increased glucose uptake, UF becomes difficult, but can usually be managed by a change in prescription and occasional “resting” the peritoneal membrane with transient HD [90]. In addition, one PD-patient’ prescription does not fit all. The potential ultrafiltration volume/dwell varies based on dwell time, transport type, instilled volume, and the osmotic agent used in that instilled dialysis fluid. Thus, optimization of drain volume and the sodium content in that drain is dependent on the physician being aware of these factors and adjusting the prescription to be able to accomplish these patient specific goals [90]

Importantly, some conventional interventions can be conducted to attenuate progressive peritoneal membrane injury and preserve peritoneal function, such as i) prevention of peritonitis, ii) timely removal of the peritoneal catheter in the face of non-resolving peritonitis, iii) use of biocompatible PDF, and iv) limitation of total glucose exposure by avoiding hypertonic dextrose solutions. In addition, some other attempts to preserve PM consist in; i) inhibition of the renin-angiotensin-aldosterone and vascular endothelial growth factor systems, ii) peritoneal resting, iii) combined PD and HD, and N-acetylcysteine, and iv) gene therapy [89].

Summing up, the most common change in peritoneal function is a loss of UF capacity, although a reduction in solute clearance is not an infrequent occurrence. There is increasing evidence that such functional changes are related to changes in the structure of the PM, which correlates in most patients with the longevity of dialysis. Structural changes include loss of MCs, thickness of the submesothelial compact zone, and a plethora of vascular changes [15], as already described.

Therefore, to improve PM longevity in PD it is important to monitor its functional characteristics with respect to time. The data obtained could be useful for tailoring dialysis adequacy, analysis of clinical problems such as ultrafiltration failure or to predict the development of peritoneal sclerosis [91]. The fight against PM damage begins with the improvement in PDF biocompatibility, as described in the following section [67]. In addition, an alternative approach to preserve the PM might be the use of pharmacological agents or molecular strategies, as presented in Section 3.3.2.

3.3.1- Biocompatibility of the Peritoneal Dialysis Fluids

PDF can be broadly divided into conventional PDF and novel solutions with more biocompatible characteristics (e.g. neutral-pH, low GPDs solutions). Conventional PDF are characterized by several undesirable characteristics, including acidic pH (5.2-5.5), high glucose concentrations (13.6-42.5 g/L), hyperosmolarity (360-511 mOm/ kg) and relatively high concentration of GDPs. Conventional PDF contain an osmotic agent, electrolytes, and lactate as a buffer [92], as follows:

Osmotic agent: high levels of glucose (dextrose; 75.5–214 mmol/L) are used in conventional PDF in order to achieve fluid removal, with different dextrose concentrations (e.g. 0.5 or 0.55%, 1.36 or 1.5%, 2.27 or 2.5% and 3.86 or 4.25% for anhydrous or hydrous dextrose, respectively) and with varying osmolalities (345–484 mOsm/L). Whilst glucose is a reasonable osmotic agent because it is cheap, easily metabolized, readily available [93], easily sterilized and associated with an excellent long-term safety profile, the quantity of glucose required for effective UF can be problematic [92]. Absorption of 100-200 g of glucose per day from PDF worsens metabolic and nutritional problems, such as impaired glucose tolerance, hyperinsulinemia, hyperlipidaemia, and, in some patients, abdominal obesity [93].

Buffer: conventional PDF contain lactate (30–40 mmol/L) as a buffer and are acidic (pH 5.2–5.5). Lactate diffuses into the bloodstream and is rapidly metabolized into bicarbonate. As conventional PDF use a single-chamber delivery system, it is not possible to store bicarbonate-buffered solutions, since calcium and bicarbonate will precipitate to form calcium carbonate. Lactate has been shown to inhibit key cellular functions involved in peritoneal defence mechanisms, including phagocytosis, bacterial killing and secretion of cytokines [92].

Electrolyte composition: the concentrations of Na^+, Cl^-, Ca^{2+} and Mg^{2+} are kept close to those of serum concentrations. Removal of these ions is therefore almost completely dependent on convection due to the low diffusion gradient. For a decilitre of fluid removed in a 4-h dwell, approximately 10 mmol of Na^+ and 0.1 mmol of Ca^{2+} are removed, given that serum Na^+ and Ca^{2+} are within the reference ranges [92].

GDPs: include 3-deoxyglucose, 3,4-dideoxyglucosone-3-ene (3,4-DGE), 5-hydroxymethyl furaldehyde, formaldehyde and acetaldehyde, which have been shown to have adverse effects on both

the peritoneal membrane and systemically, are produced during the heat sterilization process and/or prolonged storage [92].

In summary, conventional PDF are characterized by several undesirable characteristics that have been shown to result in adverse clinical outcomes, including PM injury. To diminish PM alterations related to the use of conventional glucose-based PDF, newer PDF has been developed. They are more biocompatible, having fewer negative local and systemic effects than conventional PDFs (Figure 11) [92], [93]. Some of these new PDFs have a neutral pH with low content of GDPs and bicarbonate-lactate as buffers [94]. Other strategies include the use of non-glucose osmotic agents, such icodextrin and amino acid-based formulae, and the use of modern double chamber PDF with fewer GDPs, for the achievement of long-term preservation of the PM [52], [94].

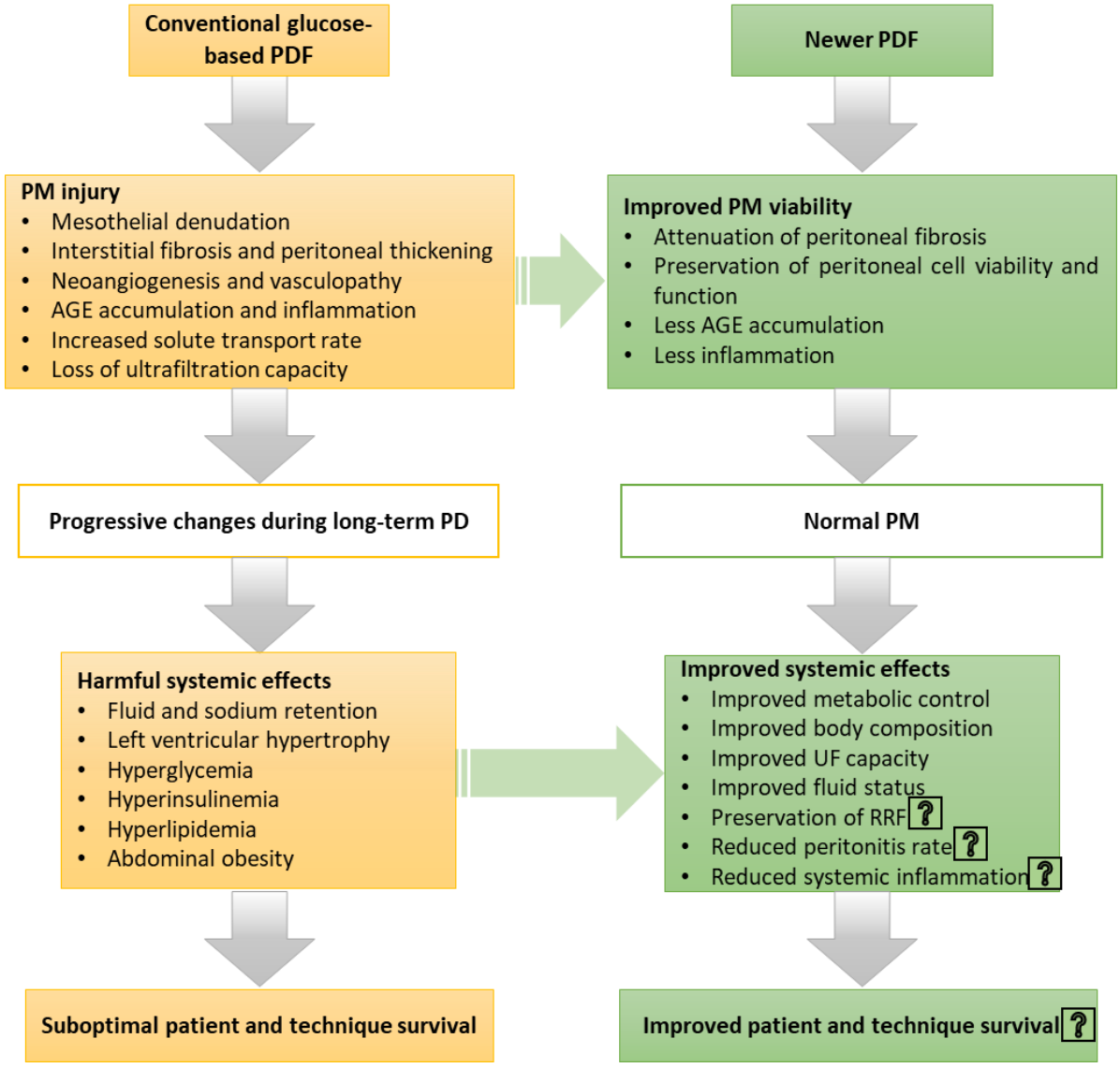

Figure 11- Schematic presentation of the potential beneficial effects of newer PDF. Abbreviations: AGE, advanced glycation end products; PD, peritoneal dialysis; PDF, peritoneal dialysis fluid; PM, peritoneal membrane; RRF, renal residual function; UF, ultrafiltration. Adapted from García-Lopez *et al*. [93].

Neutral-pH with low GDP solutions: was achieved through the development of a multi-chamber technology, where lactate and/or bicarbonate are separate, from the glucose, which is kept in a different chamber and sterilized at a very low pH (2.8–4.2), minimizing GDPs production. The remaining solution is kept at an alkaline pH (8.0–8.6) in the other compartment. Prior to administration, the contents of the two compartments are allowed are mixed, resulting in the infusion of neutral pH (6.8–7.3) [17],[92]. Depending on the manufacturing process, GDP formation is substantially reduced but still varies considerably between different brands [17].

Icodextrin and amino acid-based formulae: along with modern multi-chambers, are suggested as the first step to achieve long-term preservation of the PM, avoiding the use of glucose [52]. PDF with an alternative osmotic agent contain icodextrin, a glucose polymer, is slowly absorbed via the lymphatics and the resultant osmotic gradient dissipates slowly compared to glucose, which is absorbed via the small pores of the PM. This provides a much greater net UF during the long dwell and can therefore be used for a single long dwell per day, especially in patients with high transporter status [94], thereby improving the patient´s hydration status. In addition, treatment using icodextrin has been shown to achieve UF equivalent to fluid removal achieved with 4.25% glucose exchange during longer PD dwells (10–16 h) [17],[92].

Another alternative to glucose-based PDF are solution containing amino acid, which are free of GDP and with a slightly acidic pH of 6.7 [17]. As already described, PD causes loss of protein and amino acids in the dialysate and so contributes to the development of protein and energy malnutrition in PD patients. Amino acids-based PDF are osmotically equivalent to 1.5% glucose PDF, although their use is limited to a single daily exchange due to a risk of worsening systemic acidosis and uraemia [95]. For optimized nutrition of malnourished patients and to prevent increased serum nitrogen levels and metabolic acidosis, they should be applied at a ratio of 1–4 with glucose-containing PDF [17].

Glucose- or GDP-sparing strategies are often hypothesized to confer clinical benefits to PD patients. Icodextrin solution seems to improve peritoneal UF and reduce the risk of fluid overload, but these beneficial effects are probably the result of better fluid removal rather than being glucose sparing [96]. Although frequently used for glucose sparing, the role of amino acid–based solution in this regard has not been thoroughly tested. Regarding the use of glucose-free solutions in a combination regimen, results suggested that glycemic control was improved significantly in diabetic PD patients, and there are probably beneficial effects on peritoneal function[96].

Limited progress has been achieved during the past 50 years of PD treatment regarding PDF technology and mainly consists of a reduction of the GDP content, pH neutralization, introduction of a bicarbonate buffer and of two alternative osmotic compounds. Glucose-based PDF still predominates, and PD treatment still confers major local peritoneal and systemic toxicity [17]. Therefore, newer PDF seems to have systemic benefits, as represented in Figure 11; however, it is still not clear whether the newer PDF can exert beneficial effects on patient-level outcomes, such as peritonitis, technique and

patient survival [93],[96],[97]. A recent study performed by Tawada *et al.* suggested that pH-neutral solution prevents the morphological and functional peritoneal changes induced by long-term PD treatment [98]. Moreover, neutral pH–low GDP fluids have been convincingly shown to preserve RRF and urine volume [96],[97].

As suggested by Misra *et al*. an ideal biocompatible PDF solution is one that delivers: i) prolonged and sustained UF and solute clearance, ii) no adverse consequences with absorption, and possible beneficial nutritional and metabolic effects if absorbed, iii) no alterations in peritoneal host defences, and no induction of peritoneal and systemic inflammation, and iv) no long-term alterations in PM function with use [99]. Since none of the currently available PDF are perfect, more biocompatible PDF, ideally using a non-glucose osmole agent, which is non-toxic, easily metabolized, easily manufactured, cost-effective and metabolically efficient needs to be developed [92]. Complementary to this, an alternative approach to preserve the PM might use pharmacological agents or molecular strategies, as described in following section.

3.3.2-Pharmacological preservation of the peritoneal membrane

As already described in the previous sections, several processes are involved in the deterioration of the PM. However, different strategies have been tested *ex vivo*, *in vivo*, and *in vitro* targeting different processes to achieve PM amelioration [67]. Thus, the use of pharmacological agents to protect the mesothelium or targeting inflammation and fibrosis is an alternative and complementary approach to the effort aimed at improving PDFs biocompatibility. These drugs might be administrated orally or intraperitoneally, but most of the experiments are performed in animal models [100].

Pharmacological agents might interfere in several ways, such as, i) playing a direct role in lessening chronic inflammation; ii) acting on several mediators such cytokines, growth factors and hormones that play a key role in PD-mediated tissue remodelling and iii) they can up- or down regulate cellular signalling pathways induced by activation of peritoneal cells (MCs and recruited leukocytes) during PD therapy [101]. Some interventional studies have explored the efficacy of peroxisome proliferator-activated receptor-γ (PPAR-γ) agonists, cyclooxygenase (COX)-2 inhibitors, renin–angiotensin system (RAS) targeting and bone morphogenic protein (BMP)-7 in protecting the PM [100], and many more agents with different mechanisms of action as described in Table 3.

Although therapeutic interventions have been investigated with the aim of preventing complications such as inflammation, fibrosis and angiogenesis involved in peritoneal remodelling [101], the efficacy of many therapeutic agents is uncertain because there are insufficient good-quality clinical studies [102]. In addition, most studies are performed *in vitro* or *in* animals and less is known about the effects that these pharmacological interventions may have on human peritoneum[101]. Therefore, it is important to perform better quality clinical and basic research studies within this area, in order determine the most appropriate therapeutic approach for processes of PM damage [23], [102].

Table 3 Potential pharmacological interventions to block different processes implicated in the alterations suffered in the peritoneal membrane during peritoneal dialysis. Adapted from Gónzalez-Mateo [23].

Agents	Drug	Mechanism	Target molecules	Other processes blocked/ Other actions
Targeting AGEs	Benfotiamine	Transketolase activation and direct anti-oxidative effects	AGEs	Reduction of inflammation and angiogenesis [103]
	Rosiglitazone	PPAR-γ agonist	AGEs	Reduction of inflammation, angiogenesis and fibrosis [104]–[106]
	Aminoguanidine	Inhibition of diamine oxidase and NO synthase. Acts by lowering the levels of AGEs through interaction with 3-deoxyglucosone	AGEs	Reduction of angiogenesis and fibrosis [107]
	Alagebrium	AGE crosslink breaker, breaks preformed peritoneal AGEs	AGEs	Reduction of AGEs formation in the capillaries, enhancing of endothelial function [108], [109]
	Zopolrestat	Inhibitor of aldose reductase activity (glucose is reduced to sorbitol by aldose reductase, with the eventual formation of AGEs)	AGEs	Prevention of peritoneal fibrosis and angiogenesis [110]
	Pyridoxamine	Inhibitor of AGEs and "carbonyl stress," the inhibitory mechanism remains elusive	AGEs	Reduction of AGEs accumulation and angiogenic cytokine of VEGF and FGF-2 [111]
Anti-fibrotic	Captopril	ACE inhibitors	AngiotensinII	Less production of TNF-α and IL-1, attenuation of VEGF concentration [112]
	Enalapril	ACE inhibitors	AngiotensinII	Peritoneal thickness is not completely inhibited, peritoneal histology and function preserved [112]
	Losartan	ARB inhibitors	AngiotensinII	Less production of TNF-α and IL-1 [112]
	Pentoxifylline	Inhibition of ECM production	TGF-β	Inhibition human peritoneal MCs growth and collagen synthesis [113]
	Dipyrodamole	Inhibition of TGF-β production	TGF-β	Inhibits TGF-β–induced collagen gene expression in human peritoneal MCs [114]
	Emodin	Inhibition of ECM production	PKCα	Amelioration of the undesirable effects of concentrated glucose on human peritoneal MCs via suppression of PKC activation and CREB [115]
	Simvastatin	Increases fibrinolytic activity, through synthesis of the fibrinolytic enzyme tPA and decreases PA-1	PA-1	Prevent EMT, preserved UF and reduce the thickness of the PM [116]–[118]
	BMP-7	TGF-β blockade	TGF-β	Prevent and reduces fibrosis and negatively regulates EMT [64],[119]
	Tamoxifen	Estrogen receptor modulation	TGF-β, VEGF and leptin	Inhibition of MMT and angiogenesis [120], [121]
Anti-angiogenic and Anti-lymphangiogenic*	TNP-470	Decreases VEGF expression	VEGF	Reduction of fibrosis, suppression of myofibroblast proliferation [122]
	Celecoxib*	Inhibition of COX-2 , modulating the VEGF expression	VEGF	Reduction of lymphangiogenesis, fibrosis and inflammation. Improved UF [123], [124]
	Sunitinib*	Inhibits *tyrosine kinase*, blocking VEGF signalling	VEGF	Reduction of lymphangiogenesis [125]
	Endostatin peptide*	Inhibits VEGF-VEGFR-binding and ATPase activity	VEGF	Reduction of lymphangiogenesis and fibrosis [126], [127], [128], [129]
	Suramin	Inhibition of cytokines or growth factors/receptors interaction and ECM deposition	TGF-β and VEGF, α-SMA	Reduction of fibrosis and improve UF [103]
	FG-3019	CTGF antagonist	CTGF	Reduction of fibrosis [130]
	Fasudil, Y-27632	Inhibition of Rho/ROCK pathway	VEGF	Reduction of fibrosis [131]
	Blocking peptides (p17 and p144)	TGF-β blockade	TGF-β	Reduction of fibrosis [131]

	Calcitriol and paricalcitol	Vit D receptor activator	TGF-β (and inflammatory cells)	Reduction of proteinuria and improved UF (paricalcitol) [132].
	Smad7*	Inhibition of TGF-β/Smad pathway	TGF-β	Reduction of fibrosis [133], [134]
	Kallistatin*	Serine protease inhibition	VEGF and AGEs	Reduction of lymphangiogenesis [135], [136]
	LMWH*	HIF-1α blockade	VEGF and HIF-1α	Reduction of lymphangiogenesis and fibrosis [137], [138]
	mTOR blockade*	Rapamycin	HIF-1α	Reduction of lymphangiogenesis [139]–[142]
	Nebivolol	β1-AR blockade	β1-AR	Reduction of fibrosis, inflammation, MMT and increased fibrinolytic capacity [143]

Abbreviations: **ACE**, angiotensin converting-enzyme; **AGE**, advanced glycation end products; **ARB**, angiotensin II receptor blockers; **β1-AR**, β1-adrenergic receptor ; **CTGF**, connective tissue growth factor; **COX-2**, cyclooxygenase; **CREB**, cAMP-responsive element binding protein ; **HIF-1α**, hypoxia inducible factor; **IL-1**, Interleukin-1; **BMP-7**, bone morphogenetic protein 7; **ECM** , extracellular matrix; **PPAR-γ**, peroxisome proliferator-activated receptor-γ; **PKCα**, protein kinase C; **LMWH**, low molecular weight heparin; **PAI-1**, plasminogen activator inhibitor 1; **TGF-β**, transforming growth factor β; **TNF-α**, tumor necrosis factor α; **VEGF**, vascular endothelial growth factor; **VEGFR**, vascular endothelial growth factor receptor; **MMT**, mesothelial to mesenchymal transition; **FGF-2**, Fibroblast growth factor; **EMT**, epithelial-to-mesenchymal transition; **ROCK**, Rho-activated kinase; **α-SMA**, α-smooth muscle actin; **tPA**, tissue plasminogen activator; ***mTOR***, *mammalian target of rapamycin;* **MC**, mesothelial cell; **NO**, nitric oxide; **UF**, ultrafiltration.

4- Early detection of peritoneal response

Currently there are no non-invasive methods for early prediction of PM failure. Therefore, parameters such as urea and creatinine concentrations, glucose transport and net ultrafiltration are used to follow-up the PM outcome, yet they do not change until a very late stage, when PM function is no longer recoverable [10][144]. The only way to follow PM failure is based on peritoneal biopsies, which allow the assessment of morphologic changes. However, it is an invasive procedure that may lead to temporary discontinuation of PD therapy. Moreover, uncertainty exists about sampling errors, reproducibility, and the risk of scarring [144][145].

The understanding of peritoneal functional outcome in response to PD requires a deep knowledge of the starting point because of initial functional diversity of the human peritoneum. Moreover, it can be hypothesized that the diversity in solute and water transports at PD initiation may represent different tissue responses to similar components of dialysates. Furthermore, different starting points followed by diverse reactions to PD at midterm can generate a wide spectrum of peritoneal morphofunctional scenarios [50]. Finally, the recent development of PDE biomarkers in PD has predominantly been hypothesis driven and is based on pathologies and pathomechanisms that are found to be relevant to the course of PD disease [146].

Thus, the following section is shows some of the actual known biomarkers primarily associated with the process, such as, chronic inflammation and peritoneal infection., fibrosis, angiogenesis and peritoneal membrane remodelling.

4.1-Implementation of biomarker use in clinical practice

In a clinical context a biomarker is a characteristic that can be objectively measured and evaluated as an indicator of normal biological processes, pathogenic processes, or pharmacological response to a therapeutic intervention [146]. A good biomarker should have a large intra- and a low inter-individual variability, a high sensitivity and specificity for the clinical outcome of interest [147].

PDE represents an underestimated biochemical window into the peritoneum and a useful reservoir of potential clinical biomarkers [148] that have recently received attention by the medical community as a potential target to follow PM evolution. At present, integration of PDE biomarkers in the routine clinical practice of PD is still modest [144].

Implementation of effluent biomarkers in patient care is a goal for the near future as peritoneal transport studies provide insufficient information on the development of PM alterations (such as the, development of EPS). A feasible approach could include some biomarkers (limited to 2 or 3, easily measured in effluent) in routine clinical assessment of peritoneal function, providing more information than currently available [144]. Potential biomarkers can be divided in those that represent mesothelial mass, cytokines, growth factors and those that may represent tissue remodelling and peritoneal fibrosis,

some metalloproteinases and their inhibitors [147]. Currently, CA125, reflecting mesothelial cell mass, and IL-6, representing peritoneal inflammation, are at a stage at which their measurement can be easily included in peritoneal function tests [144].

CA125, a glycoprotein, is the most extensively studied biomarker whose levels may indicate severe mesothelial cell damage, trans-differentiation, or increased risk of the development of EPS [144]. However, it cannot be used as an early predictor. In addition, IL-6, an interleukin protein, is probably a biomarker for local peritoneal inflammation in the absence of clinical peritonitis. As yet, no good biomarker for the extent of peritoneal fibrosis has been identified with certainty [144]. Also hyaluronic acid and MMP2, initially from PD biocompatibility research, can be used to obtain information about peritoneal integrity. However, their potential information is unspecific and limited [52].

Recently, a consensus article was published by members of the European Training and Research in Peritoneal Dialysis Network (EuTRiPD) reviewing the current status of biomarker research in PD, suggested a selection of biomarkers that can be relevant to PD patient care and are directly accessible in PDE. The authors proposed a biomarker research defined by a hypothesis-driven approach in selected candidate biomarkers, reflecting cellular mechanisms of interest, in the experimental setting and then translated into the clinical context. Clinical phenotypes to be assessed with molecular signatures (PAMSs) as biomarkers were suggested to be divided into pro-inflammatory and PM damage-associated phenotypes. The pro-inflammatory phenotype was further divided into acute peritonitis and post-peritonitis–triggered chronic inflammation. The membrane-damage phenotype was further divided into MMT and changes in PM function determined by PET [146].

Therefore, combining clinical and peritoneal transport data with the measurement of molecular biomarkers would improve the complex diagnosis and management of PM failure. Recently, a study performed by Ossorio et al suggested that sustained low peritoneal effluent chemokine CCL18 levels are associated with the preservation of PM function in PD. The authors suggest CCL18 as a new marker and mediator of this serious condition as well as a new potential therapeutic target [79]. Similarly, other markers have been established or suggested as a potential target to follow PM evolution, as represented in Table 4.

The possibility of identifying and following changes in the PM at the molecular level by peptidomics and proteomics has been proposed through longitudinal studies, as being of prime importance to unravel morphological and biochemical changes in long-term PD [48]. **Hence, longitudinal studies to follow changes in PM at molecular level by peptidomics and proteomics was performed in chapter 6.**

Table 4- Candidate effluent biomarkers in peritoneal dialysis. Table adapted from Barreto *et al.* [144], Bajo *et al.* [94]

Processes	Biomarker	Involvement/Evidence	Local production (+/-)	Evidence
Coagulation and Fibrinolysis	Fibrin monomers	Coagulation and fibrinolysis	+	Decreasing tendency of FM in first 2 years of PD treatment [149]
	PA-1	Fibrosis (inhibitor of fibrinolysis)	+	Linear increasing tendency during 4-h PET [150]; during peritonitis, expression is augmented [151]; elevated levels are present in homogenates of peritoneal tissue of patients with intra-abdominal adhesions [152], [153]; Lower effluent concentrations with biocompatible PD solutions [154]; tendency to increase with PD duration [155]
Cytokines	IL-6	Pro- and anti-inflammation, induces synthesis of hepatic acute-phase proteins	+	Increased plasma concentrations during acute-phase reactions are associated with mortality in hemodialysis and PD patients; intraindividual coefficient of variation of 28% [156]; variable results with regard to correlations with peritoneal solute transport [157]–[160]; longitudinal and conventional vs biocompatible PDF [161]–[163]
	TNF-α	Angiogenesis, fibrosis, acute-phase inflammation	-	Signs of local production during acute phase of peritonitis; no difference between patients treated with biocompatible vs conventional PDF [164]
Growth Factors	CTGF	Angiogenesis, cell adhesions, and fibrosis	+	Increased levels in PD patients with high peritoneal transport*; In vitro* induction of ECM [165]
	TGF-β	Angiogenesis, fibrosis and ECM formation	+	Present in inactive form; induction of EPS-like peritoneal alterations after adenoviral vector gene transfer [166]; no difference in levels between conventional vs biocompatible PDF [167]; stimulation ECM formation [168]
	VEGF	Angiogenesis and increases vascular permeability	+	An increasing tendency with duration on PD [169] ; Not a predictor of EPS [170]; Increased dialysate VEGF concentrations associated with high peritoneal solute transport [157]
Matrix and Tissue Remodelling	CCL18	Fibrosis	-	Elevated levels in EPS patients [171]; Low levels are associated with preservation of PM function [79]
	HA	Connective tissue turnover, fibrosis	+	Elevated levels in the acute phase of peritonitis [172] and in patients with fast transport status [173], [174]; not a predictor of EPS, but low levels may predict survival of CAPD patients [175]; increased levels are associated with both high peritoneal transport and time in PD [173]
	MMP-2	EMT, fibrosis, tissue remodelling	+	High values of MMP-2 in patients with EPS were found in multicenter study [145]; positive relationship with PD duration and with tissue inhibitor of metalloproteinase 1 has been reported; also, a negative association with FWT in prevalent PD patients is present; associated with the amount of peritoneal fibrosis in EPS-like rat model [155]
	Procollagen peptides	Fibrosis	+	Modest elevation during peritonitis [176]; exposure to biocompatible PDF either led to an increase of effluent procollagen peptides [154] or had no effect[164]
Mesothelium	CA125	Mesothelial cell mass	+	Long-term PD may be associated with the loss of mesothelial cell mass [177] and may be absent or severely reduced in patients with abundant fibrosis [156]; Dialysate CA125 decreases during time on PD [178]; exposure to biocompatible PDF for up to 2 years led to increase in effluent CA125 [154], [167], [179]–[181]
Endothelial Dysfunction	E-selectin	Cell-adhesion	+/-	Correlation between percentage of FWT and E-selection attributed to local production [144]

Abbreviations: CA125, cancer antigen 125; **CAPD**, continuous ambulatory peritoneal dialysis; **CCL18**, CC chemokine ligand 18; **CTGF**, connective tissue growth factor; **ECM**, extracellular matrix; **EPS**, encapsulating peritoneal sclerosis; **HA**, hyaluronan; **IL-6**, interleukin 6; **MMP-2**, matrix metalloproteinase 2; **PAI-1**, plasminogen activator inhibitor 1; **PD**, peritoneal dialysis; **TGF-β**, transforming growth factor β; **TNF-α**, tumour necrosis factor α; **VEGF**, vascular endothelial growth factor; **EMT**, epithelial-to-mesenchymal transition; **MMP**, matrix metalloproteinase.

5-Mass spectrometry

Fundamentally, MS measures the mass-to-charge ratio (m/z) of gas-phase ions. This quantity is formed by dividing the mass of an ion (in Dalton (Da) units) by the number of charges carried by the ion [182]. Mass spectrometers consist of an ion source that converts analyte molecules into gas-phase, a mass analyser that separates ionized analytes on the basis of the m/z ratio, and a detector that records the number of ions at each m/z values [183]. The mass analyser is central to MS technology. For proteomic research, four types of mass analysers are commonly used, time-of-flight (TOF), quadrupole (Q), ion trap and orbitrap analysers. These are very different in design and performance, with their own strengths and weaknesses. In the context of proteomics, the key parameters are mass accuracy, mass resolution, sensitivity and the ability to generate information-rich ion mass spectra from peptide fragments (MS/MS spectra) [184].

The mass accuracy is usually the most important parameter and refers to the ability to assign the actual mass of an ion. Mass accuracy is usually presented in parts per million (ppm) and is typically expressed as an error value. For example, 20 ppm means that the real mass of an ion measured to 1000 Da has a predicted error margin of ± 0.020 Da. [185]. On the other hand, whereas mass accuracy is the closeness of the agreement between the result of a measurement and a true value (exact mass), **mass precision** is the closeness of agreement between independent mass measurement results [186]. Mass accuracy depends on mass spectral signal-to-noise ratio and digital resolution [187].

The mass resolution (resolving power), of a given ion signal is defined as the mass spacing at which peaks can be clearly separated, and is reported in Daltons. The term "resolution" actually refers to "resolving power", which is measured as $m/\delta m$, with m the mass of the peak center and δm the resolution (often defined as the width of a peak at half height or Full Width at Half-Maximum (FWHM)). Resolving power is a unitless parameter [185].

Sensitivity, is defined as the slope of intensity/moles of sample plot. It is often incorrectly used to refer to the limits of detection, which is the smallest amount of sample that can be used to achieve a detectable signal [185]. Therefore, sensitivity is the capability of responding reliably and measurably to changes in analyte concentration, and the detection limit of an analytical method must be lower than the concentrations to be measured [188].

In MS, mass resolving power, mass resolution, mass accuracy, and mass precision are used to characterize the performance of high-resolution accurate-mass mass spectrometers. For precise mass determination the mass spectrometer needs to pass through mass calibration to ensure the best mass precision and mass accuracy. Furthermore, the mass capacity of the analyser must be considered, if the mass resolution of the mass spectrometer is sufficient to separate ions of interest from the chemical background, the molecular ions can be measured with high precision and accuracy in a wide range of

complex samples in different matrices [186]. In addition, the recalibration of the data on "internal standards" contained in every proteomics data, is important to make the best use of the mass precision offered by the instrument. Each data set should also be accompanied by a plot of mass errors from which appropriate maximum mass deviation can be chosen [189]. Finally, satisfactory mass precision can be achieved only if the system provides enough mass resolution and thus the ability to distinguish and separate the peak of interest from adjacent signals [186].

5.1-Mass spectrometry analysers

A mass spectrometry analyser is defined as the section of the mass spectrometer where the ionized molecules of protein or peptides are separated based on their mass-to-charge ratio by electric and/or magnetic fields or by measuring the time taken by an ion to reach a fixed distance to the detector[190]. As already mentioned above and described herein, different types of analysers are available for the separation of molecules, as can be seen in Figure 12. The instrumentation represented in the Figure 12, was used in the PDE sample analysis, and the analyser types are described here.

A quadrupole mass analyser is a four-electrode device. The four rod-like electrodes are positioned symmetrically around the ion axis and parallel to one another. Quadrupole mass analysers, resolve m/z by applying radio frequency (RF) and DC voltages, allowing only a narrow mass/charge range to reach the detector. Ions with the incorrect m/z undergo trajectories that eventually cause them to presumably strike the rods where they are annihilated, never reaching a detector or a second mass analyser. These type of analysers are usually limited in mass range and have low resolution. However, it is a versatile and sensitive mass analyser for the mass range m/z 10-4000 and the MS/MS scan modes are powerful [191], [192].

TOF analysers, accelerate the ions by using a short voltage gradient and measure the time ions take to traverse a filed free flight tube, the flight time is proportional to the square root of the m/z, given a constant acceleration voltage (time of flight = $k\sqrt{(m/z)}$) [182], [192]. Thus, smaller the molecule the faster it will travel the distance of the flight tube to the detector. With respect to the resolution and hence mass accuracy, the performance of linear TOF analyser is related to the ionizing conditions within the ion source and to the length of the flight tube. TOF analysers afford a high sensitivity and theoretically and unlimited mass range (practical limit is determined by the detection efficiency of the ions arriving at the detector) [182].

An ion trap analyser consists of three electrodes with hyperbolic surfaces, the central ring electrode and two adjacent end-cap electrodes [193]. Ion traps analysers can trap and accumulate ions over time in a physical device. The ion trap technology is characterized by MS/MS capacities, by performing sequential mass analysis measurements, with unmatched sensitivity and fast data acquisition [194]. High mass resolution ($>10^6$ at m/z >1000) is accessible through slow scans, but mass measurement accuracy is relatively poor [193].

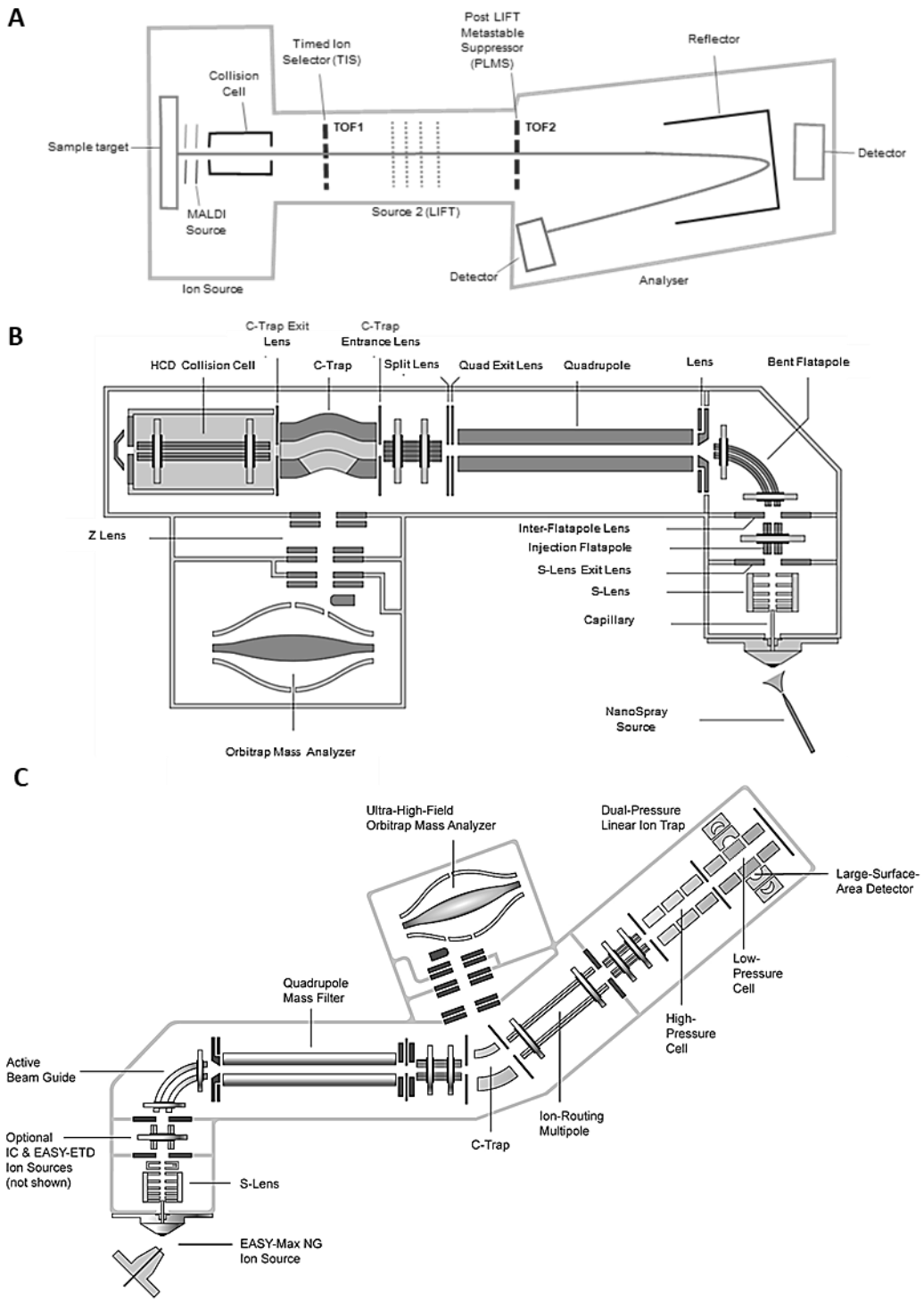

Figure 12- Schematic representation of three different MS instruments: A- MALDI LIFT-TOF/TOF; B-Q-Exactive HF (Hybrid Quadrupole-Orbitrap Mass Spectrometer); and C-Orbitrap Fusion (Tribrid Mass Spectrometer). Figure A, was adapted from Suckau *et al.* [195] and Figure B was taken with permission from, Michalski *et al*. [196] and Figure C was taken from the instrument view software. Thermo Fisher Scientific is acknowledged as an author of the Thermo Fisher material.

An orbitrap analyser can trap and separate ions in an oscillating electrostatic field. The electrostatic attraction towards the central electrode is compensated by a centrifugal force that arises from the initial tangential velocity, forcing the ions to move in complex spiral patterns. The axial component of the oscillations is independent of initial energy, angles and positions. A Fourier transform

is employed to obtain oscillation frequencies for ions with different masses, resulting in an accurate reading of their m/z. With respect to mass accuracy and resolution, measurements in the low ppm-sub ppm range can be achieved and with an extremely high resolution [194], [197]. **The MALDI TOF/TOF-MS mass spectrometer was used in articles 1-3 (Chapters 3-5), and Q-Exactive HF and Orbitrap Fusion in article 5 (Chapter 6).**

5.2-Ionization methods

MS spectrometry was restricted for a long time to small and thermostable compounds because of the lack of effective techniques to softly ionize and transfer the ionized molecules from the condensed phase into the gas phase without excessive fragmentation [194]. During the 1980s the study of proteins and peptides using mass spectrometry became popular as the electrospray ionization (ESI) technology was mature enough to allow reliable analysis of complex biological samples [198]. Also, during the same period the so called matrix-assisted laser desorption ionization (MALDI) method was developed [191].

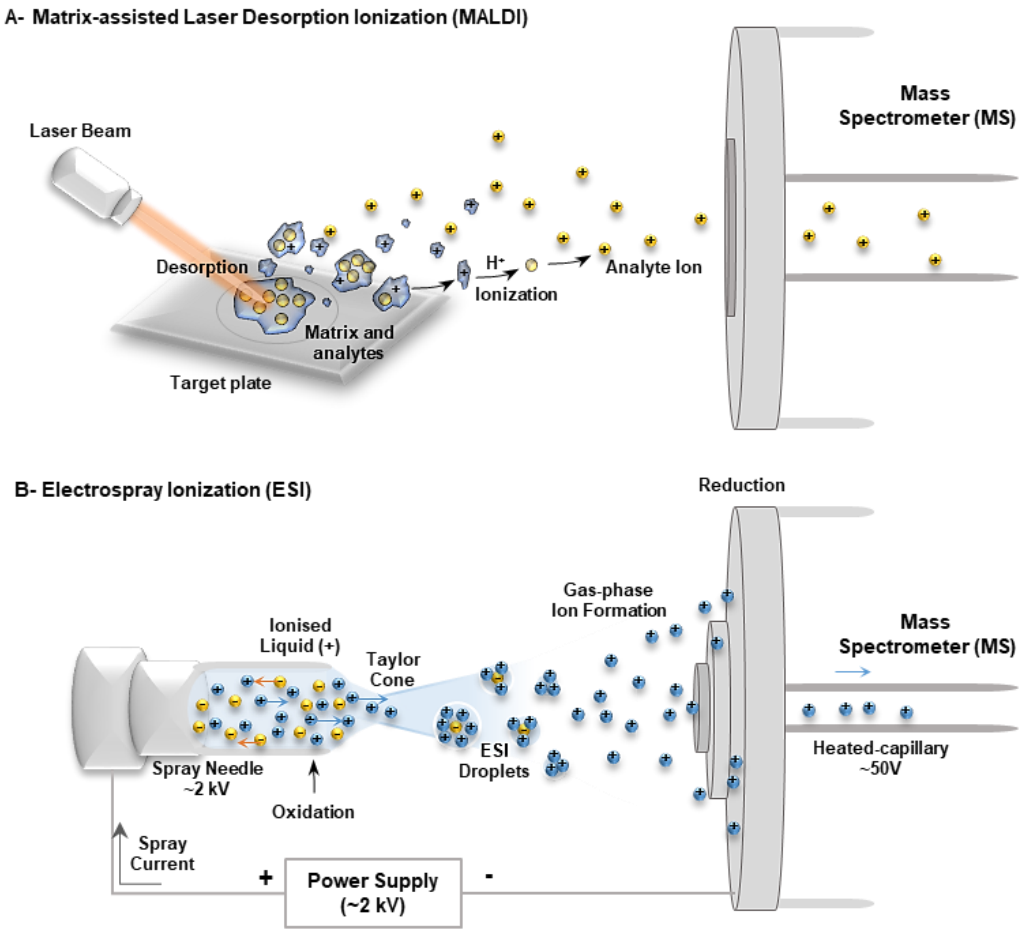

Figure 13- Soft ionization techniques, A- Matrix-assisted Laser Desorption Ionization (MALDI); B- Electrospray Ionization (ESI). Figure adapted from [199], [200].

In the case of MALDI, the ions are created by mixing the analyte with a small, organic molecule called a matrix, that absorbs light at the wavelength of the laser. The analyte becomes incorporated into

the crystallized matrix and is then irradiated with a laser, causing the desorption and ionization of the matrix and analyte, either by protonation (positively charged ions) or by deprotonation (negatively charged ions). The ions are then accelerated into a MS analyser [182], as can be seen in Figure 13-A.The ESI technique enables the formation of ions from molecules directly from samples in solution, that is then nebulized, with the resulting charged droplets being made to undergo desolvation and the resulting gas-phase ions being mass analysed [201], as can be seen in Figure 13-B. For a desorption (phase change) ionization (charge-state change) experiment, it has long been known that, precharged species give exceptionally high yields. On other hand, if the analyte is neutral when it leaves the surface, subsequent gas-phase chemical reactions are needed to yield ions and the yields drop correspondingly. The spray ionization experiments do not require matrix because this is essentially provided by the solvent in which the sample is carried [201]. In addition, another important difference between the MALDI and ESI methods is the charge state in which the analyte is formed, with MALDI experiments presenting spectra dominated by singly charged ions and ESI presenting multiply charged ions. These multiple charged ions are originated due to the evaporation of water from a microdroplet that has ionic constituents (buffer, a non-neutral pH), so the analyte tends to take a number of charges in proportion to the size of the molecule [201]. **MALDI was the ionization source used in articles 1-3 (Chapter 3-5) and ESI in article 5 (Chapter 6).**

5.3-Fragmentation methods

Fragmentation in a mass spectrometer consists of the physical process of dissociation of molecules into fragments, the spectrum thus obtained is unique to the molecule or ion. Collision induced dissociation (CID) it is a process whereby an ion of interest, named precursor ion, is selected, isolated, excited and fragmented by collisions with an inert gas within the mass spectrometer [182]. CID and higher-energy collisional dissociation (HCD) selectively cleave the most labile bonds in a protein, typically resulting in a limited sequence coverage [202]. In addition, alternative fragmentation techniques based on electron transfer of the ions present in the collision cell were developed to improve peptide sequencing. Electron capture dissociation (ECD)[203] and electron transfer dissociation (ETD)[204] yield fragments that are complementary to the CID fragmentation, these tend to be more evenly distributed over the entire peptide backbone and are particularly useful in localizing post-translational modifications (PTMs). [194]. However, ETD strongly depends on charge density, and ETD tandem mass spectra are often dominated by unreacted and charge reduced precursors [202]. New-generation mass spectrometers (such as, Orbitrap Fusion) introduced an electron-transfer/higher-energy collision dissociation (EThcD) peptide fragmentation methodology that combines HCD and ETcaD (also called ETciD) into one fragmentation event [205]. The advantage is that the peptide backbone fragmentation is improved and that dual fragmentation generates data-rich MS/MS spectra containing

both b/y and c/z ions, improving peptide sequence coverage and PTM localization confidence [206]. **The CID and HCD-EThcD were the fragmentation methods used in article 4 (Chapter 6).**

6-Mass spectrometry-based proteomics

The term "proteome" represents the entire collection of proteins encoded by a genome, cell, tissue or organism at a certain time, under defined conditions. Proteomics is the study of the proteome, the understanding of the structure, function, and interactions of the entire protein content of an organism [182] and it requires modern technology for the identification and quantification of the proteins present in a cell tissue or an organism [207]. Mass spectrometry (MS) has evolved into an indispensable tool for proteomics research, and the desire to understand the proteome has led to the development of new technologies that push the boundary of MS capabilities and allowed MS to address an ever-increasing array of biological questions [183]. Nowadays, proteomics comprises the large-scale analysis of proteins by modern mass spectrometry analysis methods capable of identifying and quantifying thousands of peptides/proteins in a fast high-throughput manner [208]. However, this task is challenging because the proteome has a large and unknown complexity, with the number of proteins far exceeding the number of correlated genes. This diversity arises from the fact that a particular gene can produce multiple distinct proteins, as a result of alternative splicing, the presence of sequence polymorphisms, PTMs and other protein-processing mechanisms [194].

There are two general approaches in proteomics for identification and characterization of proteins. On the one hand, the bottom-up (peptide level) or shotgun proteomics is based on the mass spectrometry sequencing of tryptic peptides derived from a proteolysed proteome and relies on algorithms for amino acid sequence assignments [209][192]. This approach is often referred to as liquid-based protein discovery. On the other hand, the top-down (intact protein level) approach separates/analyses intact proteins prior to proteolysis and MS identification mainly by two-dimensional gel electrophoresis [210].

MS can be used in two different ways, firstly to indicate the composition and secondly the structure of a given analyte. The first instance is performed in MS mode, where the actual mass of the analyte is measured [182]. However, this single-stage mass spectrum is composed of peaks corresponding to peptide precursor ions and is insufficient for distinguish ambiguous protein identification [211]. In the second instance the mass spectrometer is used in MS/MS mode, in this mode, the analyte is fragmented within the mass spectrometer to yield structural information [182]. In other words, after selection and further fragmentation of the single precursor ion a MS/MS spectrum is generated. In a MS/MS spectrum, there are generally two types of peaks: peaks generated from amino-terminal fragment ions ("b" ions) and peaks generated from carboxyl-terminal fragment ions ("y" ions). The combination of precursor m/z and its MS/MS spectrum is used to determine peptide sequences, and proteins are then inferred from the identified peptides [211].

The application of mass spectrometry and MS/MS to proteomics takes advantage of the vast and growing array of genome and protein data stored in databases. The information obtained by the mass spectrometer, list of peak intensities and mass-to-charge (m/z) values, can be used and compared with a "theoretical, *in-silico*" digestion of a protein or a "theoretical, *in-silico*" fragmentation of a peptide [192]. Therefore, in shotgun proteomics, the computational procedure for protein identification has two main steps, the protein identification and protein inference. In peptide identification, the experimental MS/MS spectra is searched against a protein sequence database to obtain a set of peptide-spectrum matches (as described above), or using the *de novo* sequencing to determine the peptide sequences without using the protein database. On the other hand, protein inference assembles identified peptides into a set of confident proteins [211].

In summary, MS-based shotgun proteomics is a strategy that offers fast, high-throughput characterization of complex protein mixtures [211]. An example MS-based shotgun proteomics experiment is based on, i) enzymatic digestion of proteins into peptides, with a protease, such trypsin (because it is stable, cost-effective, and relatively specific), ii) the peptides generated are subsequently separated using an isoelectric focusing technique; iii) analyse by Reverse Phase High-Performance Liquid Chromatography (RP-HPLC) coupled to tandem MS (MS/MS) and finally, iv) the resulting peptide sequence data generated from MS/MS spectra are compared through using sophisticated mathematical algorithms against protein databases [212].

Ideally, all peptides eluted from the RP-HPLC should be captured by the mass spectrometer. However, this does not happen because peptides compete for efficient ionization and therefore, abundant peptides are more likely to be analysed by the mass spectrometer than those less abundant peptides. Finally, peptides are quantified (either relatively or absolutely) to generate protein abundance. These protein abundances are then interpreted and further used for biomarker discovery or protein–protein interaction network construction [211].

6.1-Mass spectrometry-based approach to study the PDE proteome and peptidome

Prior to mass spectrometry sample analysis some pre-analytical factors influencing the results must be considered, namely sample collection, sample processing and sample storage [210]. A challenge when working with complex proteomes, is that proteins span a concentration range that exceeds the dynamic range of any single analytical method or instrument [194]. The concentration range of plasma proteins for example, can exceed more than 10 orders of magnitude in concentration from the high abundance proteins (HAP) to the low abundance proteins (LAP) [213]. This problem, to some extent, can be expected for PDE samples [214]. However, MS instrumentation performs analysis with up to four orders of magnitude of the dynamic range in the untargeted mode, in a stark mismatch with the proteome dynamic range. Moreover, in shotgun proteomics, the dynamic range of signal intensities of

peptides resulting from the proteome's digestion is at least an order of magnitude larger than that of the original proteome, which makes the above mismatch even more contrasting [215].

Another major drawback associated with the analysis of complex biological samples is the wider range of protein abundance, with a particular cell having only few copies of a given protein, but with millions of copies of other ones [216]. This complexity of proteome translates into analytic complexity for individual proteins, especially LAP [217]. As can be seen in Figure 14, a proteome's abundance distribution represents a nearly symmetric bell-shape curve on the logarithmic copy number scale [215]. Regarding the most abundant proteins, for every order of magnitude increase in sensitivity or sample amount, the number of proteins detected increase. However, when approximately half of the expressed cellular proteome (i.e. approximately 5000 proteins) is detected, the slope of the distribution inverts, and every order of magnitude increase yields progressively smaller increments in protein number. The challenge is the analysis of the approximately 1000 least abundant proteins, and the increasing sample size required to reach the depth of >9000, with >1 mg of sample corresponding to >5 million cells [215].

Therefore, an inherent challenge when working with complex samples is the issue of HAP. More than 95% of serum proteome is composed of HAP, that hampers the detection of LAP, which are most likely to be biologically relevant as markers of a disease state. To address the issue of HAP, MS instruments with wider dynamic ranges have been developed [218]. Additionally, to have a complete as possible portrait of the proteome of any type of samples, the HAP should be, at least partially removed so the complexity of the sample can simplified [216]. The removal of HAP from complex proteomes samples can be done using different methods of protein fractionation or protein depletion, which are generally followed by concentration of the fractionated/depleted fraction [219].

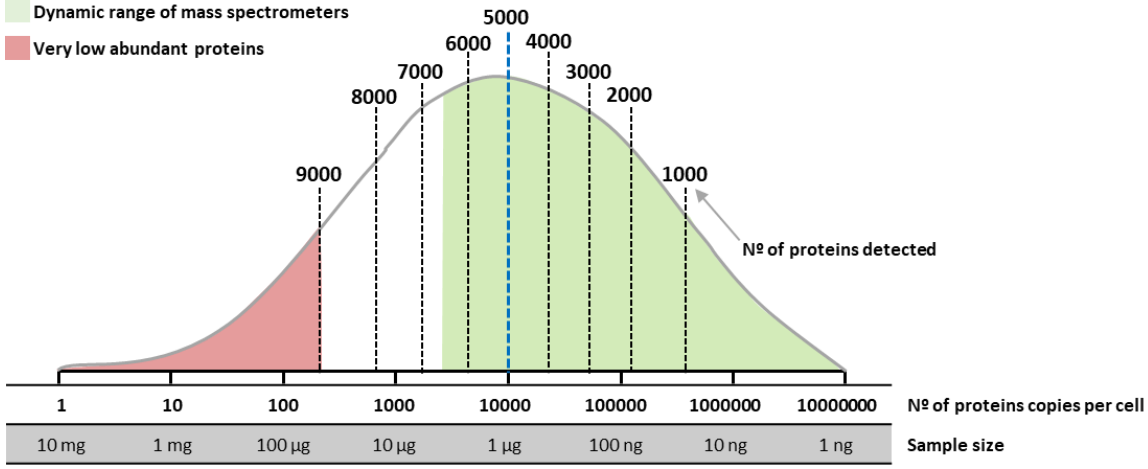

Figure 14-Distribution of protein abundances is a bell-shape curve on a logarithmic copy number scale. Conventional proteomics analysis detects highly abundant proteins (about four orders of magnitude). Deeper proteome analysis requires a much larger sample size. The very low abundant proteins (red part) is the most challenging detection part of the proteome (approximately 1000 least abundant proteins). Figure adapted from Zubarev *et al.*[215].

Summing up, MS is the most powerful tool for systematic and unbiased detection of a full set of proteins present in tissues and cells. However, it is limited by the need for multiple sample preparation stages, including depletion of HAP, liquid chromatography, and trypsin digestion, resulting in multiple analytic steps. [217]. Therefore, in order to improve resolution, sensitivity and reproducibility of peptide

identification and protein matches, a combination of depletion, fractionation prior to MS/MS is recommended [216], as described in the following section.

6.1.1-Sampling strategy and sample preservation

Body fluids are an important source of information about the biochemistry of living organisms. For example, cerebrospinal fluid is in direct contact with the central nervous system and thus has long been considered as a biopsy reflecting dynamic changes in this system. Other body fluids such blood, saliva and urine, are easily available and commonly used for clinical proteomics [216]. Although a PDE sample is not a "pure" body fluid (it is peritoneal fluid highly diluted in PDF), it presents the same advantages as those described above because it is in direct contact with the peritoneum and it is easily accessible. Therefore, PDE should be an excellent fluid to disclose what it is happening to the peritoneum when it is chronically exposed to PDF. It could allow i) follow-up the evolution of each patient's therapy, ii) search for candidate biomarkers and iii) performing a case-by-case therapy.

Some factors during sampling and then during sample preservation, must first be taken into consideration prior to further sample handling to effectively process the sample. Transport of samples from the hospital to the laboratory must be done in a standardized manner (on ice) and as quickly as possible, and long-term storage should be in low temperature-controlled freezers [220]. After a 4 -hour PD session~ 2300 mL of PDE are drained from the patient. Of this volume, only 100 mL are collected in two 50 mL tubes supplemented with protease inhibitors (sodium fluoride and ethylene diamine tetra acetic acid, EDTA). Before storage at -80 °C samples are centrifuged to remove *cell debris*. Then, each 100 ml sample is aliquoted into subsamples of 10 mL.

In general, supplementation of specific protease inhibitors, such as, phenylmethylsulfonyl fluoride (PMSF), aminoethyl benzylsulfonyl fluoride (AEBSF), EDTA, pepstatin, benzamidine, leupeptin, aprotinin or cocktails with a broader activity spectrum is recommended. This supplementation during sample preservation is important because, if not inhibited, liberated/activated endogenous proteases are responsible for uncontrolled enzymatic proteins degradation. Such proteolysis may produce artefacts and hence further complicate the analysis [216].

In addition, PDE samples are highly diluted due to the high volume of PDF that is inserted per PD session (2000mL). Therefore, after 100 mL have been collected, centrifuged and aliquoted, PDE concentration and desalting have to be performed by centrifugal ultrafiltration. Thus, centrifugal concentrators with 10 KDa cut-off membrane have to be used in order to concentrate the samples prior to any proteomic step. After performing centrifugal ultrafiltration, this methodology enables the obtaining of two fractions, the proteome (> 10 kDa) and the peptidome (< 10 kDa), allowing thus further analysis of the proteome and the endogenous peptidome.

The performance of the PDE concentration and desalting using centrifugal concentrators is presented in Chapter III. The best conditions obtained then are used in the PDE proteome and PDE peptidome studies done in Chapters I-VI.

6.1.2- Protein depletion and protein concentration strategies applied to PDE samples

The challenges of complexity and dynamic range of protein concentrations can be addressed with different methods for reducing the HAP in biological fluids, including immune depletion or chemical assisted protein equalization and/or depletion.

The HAP tend to mask the presence of LAP since the loading capacity of analytical methods are limited. Therefore, the removal of human serum albumin together with immunoglobulin G, both representing between 60–80% of the total serum protein content, would increase the LAP loading capacity and would thereby contribute to improving the detection sensitivity of LAP [221]. To overcome the aforementioned problem, the Multiple Affinity Removal System (MARS) was developed, in both spin-column and LC column formats, combining polyclonal antibodies targeting seven, twelve, fourteen, or twenty of the most abundant proteins present in plasma. Of the MARS available, antibody columns for removal of fourteen, twenty or more medium and HAP are the most effective, removing circa 95% of the total protein content [222]. **In our case, the MARS LC column format targeting fourteen abundant proteins was the depletion method selected to be used with the PDE samples in study four (Chapter VI).**

Another alternative to deal with HAP is depletion, and rapid acetonitrile (ACN)-based depletion method was first reported by Kay *et al.* [223], which reproducibly deplete high abundance and high molecular weight proteins from serum prior to MS. The combination of ACN depletion and one-dimensional nano-LC/MS/MS enabled the detection of the low abundance serum protein, insulin-like growth factor-I (IGF-I), which has a serum concentration in the region of 100 ng/mL, in the region of the LAP. Moreover, the one-dimensional sodium dodecyl sulphate/polyacrylamide gel electrophoresis (1D-SDS-PAGE) analysis of the depleted serum demonstrated the efficiency of the method for the depletion of high molecular weight proteins, with the absence of bands corresponding to proteins with a MW above 75 kDa. Additionally, the total protein analysis of the ACN extracts revealed that approximately 99.6% of all protein is removed from the serum.

On the other hand, a chemical assisted equalization method was proposed by Warder *et al*. [224], and is based on the use of a low volume of concentrated reducing agent, such as dithiothreitol (DTT) or tris (2-carboxyethyl)phosphine (TCEP), to rapidly and reproducibly precipitate high-abundance disulphide-rich proteins, including albumin and transferrin, from serum and plasma. Further precipitate removal via centrifugation and identification of protein content revealed an albumin-enriched pellet. Moreover, the supernatant analysis by MALDI-TOF-MS afforded peptidome and small protein profiles

with enhanced features and minimal ionization of full-length albumin. In addition, the author considered that this method distinguishes itself from immunoaffinity resin-based approaches, since it could be scaled to large millilitre quantities and it is compatible with plasma.

Interestingly, the combination of a chemical sequential depletion method based in two protein precipitations with ACN and DTT was later suggested by Fernández-Costa *et al.* [225] as an alternative method for the depletion of HAP in human plasma. This method was proposed as as inexpensive, of easy implementation and allowing a fast sample throughput. In addition, for the MS analysis of human serum proteins Fernández-Costa *et al.* also reported the comparison of the two different chemical methods, using ACN or DTT, with the protein equalization obtained with the ProteoMiner kit (Bio-Rad) [226]. Results showed how ACN depletion was efficient for depleting high molecular weight proteins (over 75 kDa), whereas DTT depletion primarily promotes the precipitation of proteins rich in disulphide bonds (mainly albumin), as previously reported by Kay *et al.*[223] and Warder *et al.* [224]. In addition, it was further confirmed that the use of DTT produces an extract compatible with protein equalization rather than with protein depletion, as high abundant proteins are not fully depleted.

The performance on the PDE samples of the chemical assisted depletion with ACN and the chemical assisted equalization with DTT was investigated in Chapters IV and V, and in the Chapter III, IV and V, respectively.

6.1.3- Protein digestion strategies applied to PDE samples

Digestion of complex proteomes can be done through two main methods, the gel-based electrophoresis approach in the first or in the second dimension, and in the *in-solution* digestion. *In-gel* digestion specifically degrade proteins into fragments that fit the effective molecular mass separation range of the mass analysers [227]. The in-gel digestion method was established by Rosenfeld *et al.* [228]. Several changes in the method have contributed to increase peptide yield and improvement of the quality of MS data. Essential steps such as, destaining, reduction and alkylation of cysteines, enzymatic cleavage of proteins into peptides, and extraction of peptides from the gel, are crucial for the acquisition of high-quality mass spectra [227].

Therefore, a classical in-gel digestion protocol for a protein band or spot stained with Coomassie brilliant blue (CBB), consists of the following steps: i) protein bands or spots are excised from the polyacrylamide gel, ii) Destaining of the CBB stained proteins is achieved by incubation of the excised gel bands or spots in a mixture of an organic solvent (typically ACN) and ammonium bicarbonate, iii) in order to increase the digestion efficiency and the sequence coverage, reduction of disulphide bridges (e.g. with DTT) and to prevent reformation of disulphide bonds, successive alkylation of the SH groups is done with iodoacetamide, IAA; iv) proteins are subsequently digested with proteolytic enzymes, typically trypsin, cleaving at the amino acid residues arginine (R) and lysine (K), v) the resulting peptides are extracted from the polyacrylamide matrix, usually with two sequential steps performed to

ensure extraction of peptides with different properties, with ammonium bicarbonate and ACN, formic acid or trifluoroacetic acid, and then vi) the peptide solution can be further purified for analysis by MS [227].**The in-gel digestion was the methodology used in studies two and three (Chapter IV-V).**

The second most common method of complex proteome digestion is in-solution digestion. The conditions of digestion, i.e., pH, protein concentration, digestion buffers, additives, the proteolytic enzyme, and enzyme/substrate ratio, can be altered or adapted for in-solution digestions more easily than for in-gel digestion, and the recovery of the digestion products is more efficient [229]. Similarly, to in-gel digestion, prior to in-solution protein digestion the proteins need to be denatured, reduced and alkylated, for the proteolytic enzyme to be able to efficiently cleave the peptide chains of the proteins [230]. Trypsin is the most commonly used enzyme for in-solution digestion as it has a well-defined specificity, hydrolysing only the peptide bonds in which the carbonyl group is contributed by either an R or a K residue, except when they are bound to proline (P). Other enzymes like chymotrypsin, pepsin, Lys-C, Asp-N and Glu-C can also be used for protein digestion [231]. **In-solution digestion was used in the studies presented in Chapters III, IV and V.**

In-solution digestion with trypsin is performed at an optimal pH in the range 7.5-8.5, and is normally carried out overnight (12-16h) at 37 °C. Prior to the addition of trypsin, a buffer is added, usually 12.5 mM ammonium bicarbonate buffer to provide an optimal pH for the enzymatic cleavage [230]. The enzyme to protein ratio needed for digestion of a protein sample is crucial to ensure an enzyme amount sufficient to perform the digestion, but not so high as to produce trypsin autolysis products. Usually the ratio of enzyme to substrate is 1:20 [231]. The proteome digestion process is the most time consuming step in the proteomics sample preparation workflow and different techniques to accelerate this procedure have been developed [230], involving ultrasound-, heating-, infrared- and microwave-assisted digestion, immobilized digestion using, filter-aided sample preparation (FASP) and immobilized trypsin microreactors [231], [232].

Technological improvements in apparatus to deliver ultrasonic energy have led to the development of a device called a sonoreactor, that offers some advantages over the ultrasonic probe and the ultrasonic bath since it combines their benefits but not their drawbacks. The sonic energy generated by the sonoreactor is lower than an ultrasonic probe, but higher than the energy produced by a common ultrasonic bath, a fact that is critical, because it speeds in-gel protein digestion without the gel degradation that occurs when an ultrasonic probe is used. Thus, as suggested by Rial-Otero *et al.,* a fast and high-throughput in-gel trypsin digestion of proteins using sonoreactor technology can be achieved, with just 120 seconds to digest the sample, and able to handle up to six samples at once [233]. Interestingly, the sonoreactor and the ultrasonic probe devices were also suggested for in-solution protein digestion by Santos *et al.*[234]. Thus, it has been demonstrated that ultrasonic probe and sonoreactor can be used for accelerating the sample treatment for protein digestion for protein identification by PMF using MALDI-TOF-MS from 24 h to 15 min (5 min per each step of protein alkylation, protein reduction, and protein enzymatic digestion) without compromising the number of

peptides matched or the protein sequence coverage obtained [234]. **The performance of the sonoreactor device applied to PDE samples for ultrasonic in-solution digestion is presented in Chapters III, IV and V.**

Another methodology that provides favourable conditions for proteolytic digestion is a method developed by Hughes *et al.* [235], termed Single-Pot Solid-Phase-enhanced Sample Preparation (SP3). Basically, the method consists of the addition of an organic solvent (ACN) to an aqueous solution containing paramagnetic beads, in order to promote the trapping of proteins and peptides in a solvation layer on the hydrophilic surface of the beads. Thus, immobilization on the bead surface permits rinsing (while on a magnetic rack) and removal of contaminating substances (such as detergents and chaotropes) with a combination of solutions (70% ethanol and 100% ACN), prior to proteolysis, fractionation or MS analysis. Furthermore, all steps in a conventional proteomics protocol (cell lysis, protein clean up and digestion, peptide labelling, desalting, fractionation, and concentration) can be completed entirely in a single tube with SP3, maximizing throughput while minimizing potential sample loss [235]. **The performance of the SP3 methodology was also investigated on PDE samples in the study presented in Chapter VI.**

6.1.4- Gel-based electrophoresis strategies for protein and peptide fractionation of PDE samples

Gel-based electrophoresis is mainly used in proteomics to separate and interrogate the proteins of proteomes [236]. In polyacrylamide gel electrophoresis, also known as gel electrophoresis in the first dimension, 1D-PAGE, proteins migrate in response to an electrical field through pores present in a polyacrylamide gel matrix. The pores of the matrix size decrease with the acrylamide concentration. The combination of pore size and protein's charge, size, and shape determines the migration rate of the protein [236]. The denaturation of the proteins in a solution of sodium dodecyl sulphate (SDS) allows avoiding charge variation between proteins as charge density becomes the same. Therefore, the proteins are then separated only according to molecular weight [207]. **The 1D-SDS-PAGE method is presented in Chapters III and IV.**

On the other hand, two-dimensional sodium dodecyl sulphate polyacrylamide gel electrophoresis (2D-SDS-PAGE) separates proteins by molecular charge in the first dimension and by molecular size in the second one. The first-dimension consists of protein isoelectric focusing (IEF) in an immobilized pH gradient (IPG), with proteins submitted to a high voltage within a pH gradient [237]. Thus, amphoteric analytes, such as proteins and macropeptides, are separated according to their isoelectric point (pI) values in a stable and linear pH gradient. The gradient increases from a low pH (anodic end) to a high pH (cathodic end). When an electric field is applied, each protein migrates through the pH gradient, becoming increasingly less charged when arriving at a pH equal to its pI, where its net charge is zero, and therefore will not migrate further in the electric field. Thus, each protein is focused, into a narrow zone at its pI position, where it remains as long as the electric field is maintained [238].

Proteins present in complex to be separated are first denatured and then loaded onto the IPG strip, which has a linear pH gradient. IPG strips are polyacrylamide-based, and upon rehydration, proteins are driven into the strip along with the buffer [239]. Thus, proteins are first solubilised in a denaturing buffer, usually urea, keeping the hydrophobic proteins in solution and avoiding protein-protein interactions. However, because urea is not so effective at breaking hydrophobic interactions, membrane proteins can be poorly solubilised. Nevertheless, a urea/thiourea mixture can help with this matter. In addition, the denaturation buffer also contains a neutral chaotrope agent, a zwitterionic or neutral detergent. As a general rule, CHAPS is often the zwitterionic detergent chosen, because of its high purity and it increases the solubility of hydrophobic proteins. Additionally, a reducing agent, such as DTT, is also used [182].

Once proteins have been separated in the first dimension, the IPG strips containing the proteins need to undergo an equilibration step (with DTT and IAA), to ensure complete protein unfolding. Then, a second dimension, 2D, separates proteins by molecular size using gel polyacrylamide electrophoresis. Once the 2D had been completed, each protein has a unique isoelectric point/molecular size coordinate. After visualisation using a staining agent (generally CBB), proteome changes are revealed by gel image analysis. Then, the protein spots are excised, the pieces of gel are treated as explained in the Section 6.1.3, and the pools of peptides are used to identify the proteins by mass spectrometry analysis [237]. **The 2D-SDS-PAGE method is presented in Chapter III.**

High resolution isoelectric focusing (HiRIEF) is another prefractionation method based on the use of IPG strips [240]. This method allows sample complexity reduction prior to MS- analysis via reproducible fractionation of the proteome. In contrast to 2D-SDS-PAGE, and SP3 methods, the protein digestion is performed (as described in section 6.1.3) before employing the extensive separation of peptides on 24 cm HiRIEF IPG strips. Then the strip is divided into 72 fractions and the peptides contained in each fraction are extracted and subsequently analysed by LC-MS. Thus, when compared to a regular 2D-SDS-PAGE methodology, this methodology differs in the fractionation of peptides (after SP3 digestion) instead of proteins, and there is no need of performing a second dimensional fractionation step. **The results obtained using the HiRIEF method are presented in Chapter V.**

6.1.5-RP-HPLC strategy for fractionation of PDE samples

HPLC is currently the most used and versatile separation technique in proteomics. It can easily be coupled to MS, which makes it a perfect tool for separation of peptides directly prior to mass analysis [216]. Each chromatography involves two phases, the mobile phase and stationary phase. The mobile phase drives compounds to flow through the surface of the stationary phase and the movements of compounds are delayed by interaction with stationary phase. Hence, compounds are delayed differentially according to the interaction strength and finally are separated [241]. The RP-HPLC was named due to the reversed polarity between mobile phase and the stationary phase if compared with

normal phase chromatography. In normal phase chromatography, the mobile phase is an organic solvent and the stationary phase is hydrophilic resin, whereas RP-HPLC uses hydrophobic adsorbents as stationary phase [241].

Therefore, RP-HPLC separates proteins based on the hydrophobicity of the molecules, resulting in a separation based on the mass, because retention time increases with hydrophobic (non-polar) surface are of the molecule resulting in a separation based on the actual protein size. In this chromatography, the stationary phase consists of ligands that bind reversibly with the hydrophobic proteins [190]. The separation depends on the hydrophobic binding of the solute molecule of the mobile phase to the immobilized hydrophobic ligands attached to the stationary phase (the sorbent). Separations can easily be manipulated by changing the gradient slope, the operating temperature, the ionic modifier, or the organic solvent composition [242]. Elution can proceed either by isocratic conditions where the concentration of organic solvent is constant, or by gradient elution, in which the amount of organic solvent (usually acetonitrile) containing an ionic modifier (trifluoroacetic acid) is increased over a period of time. The solutes are thus, eluted in order of increasing molecular hydrophobicity[190], [242].

Regarding the type of stationary phase used in RP-HPLC, it consists of a nonpolar material such as, hydrocarbon chains containing eight carbon aliphatic chains (C8), 18 carbon aliphatic chains (C18 or ODS), or phenyl groups, bonded on a porous silica support. Concerning the mobile phase, it is a variable aqueous-organic solution and it is more polar than the stationary phase. The solute molecules are in equilibrium between the more polar mobile phase and the hydrophobic stationary phase. The retention depends mainly on three factors: structure of the analyte molecule, solvent polarity, and the type of stationary phase used [243]. **The results obtained with the RP-HPLC strategy for fractionation of PDE samples is presented in Chapter V.**

7-Quantitative mass spectrometry-based proteomics

Quantitative mass spectrometry-based proteomics can be absolute or relative. Absolute quantification determines changes in protein expression in terms of an amount or concentration of each protein present, whereas relative quantification determines the up- or down-regulation of a protein relative to a given control sample, and the results are expressed as “fold” increases or decreases [244],[245]. Quantification can be performed through labelling or by label free methodologies. Labelling can be achieved by the application of combinatorial isotopologues of C, H, N, and O. These can be introduced into proteins through chemical derivatization, using enzymes or through metabolic processes [246][247]. Chemical derivatization procedures can be applied to any sample at either the protein or the peptide level. Enzymatic labelling is probably the most straightforward and universal in vitro labelling method [216][247].

The isotope coded affinity tags (ICAT) was developed in the late 1990s as strategy of isotopic labelling for differential expression. The method consists in the mass spectrometry comparison of two-samples labelled separately with a molecular tag containing a heavy or light isotope, then mixed together and analysed simultaneously [248]. This approach was later refined with a method called iTRAQ (isobaric tag for relative and absolute quantification) [249]. Stable isotope labelling by amino acids in cell culture (SILAC) is also an MS-approach for quantitative proteomics that depends on metabolic labelling *in vivo* (metabolic derivatization) of whole cellular proteome. The proteomes of different cells grown in cell culture are labelled with a "light" or "heavy" form of amino acids and differentiated through MS [207].

Stable isotope derivatization methods (with the exception of isobaric mass tags) introduce a small mass difference to identical peptides from two or more samples so they can be distinguished in the MS1 spectrum. The relative-abundance ratio of peptides is experimentally measured by comparing heavy/light peptide pairs, and then protein levels are inferred from statistical evaluation of the peptide ratios [244], [246].

Isobaric mass tags include families of stable isotope chemicals that are used for labelling of peptides, generating relative quantitative information in an isobaric labelling-based quantification strategy [246]. The most commonly used isobaric mass tags are the iTRAQ and tandem mass tags (TMT). The iTRAQ method uses isobaric amine-specific to label all peptides in up to eight different samples simultaneously. TMT is a reproducible and highly accurate quantification method, that provides both comparative and absolute MS/MS-based quantification of proteins and peptides in biological samples. TMT labelling produces data to calculate the relative abundance of proteins, making it possible to evaluate differential protein expression in two to eleven samples in a single experiment [250].

The advantage of these methods is that tags are isobaric, meaning that peptides labelled with isotopic variants of the tag appear as a single composite peak at the same m/z value in an MS1 scan with identical liquid chromatography (LC) retention time. The fragmentation of the modified precursor ion during MS/MS event generates two types of product ions: (a) reporter ion peaks and (b) peptide fragment ion peaks [244],[246]. The quantification is accomplished by directly correlating the relative intensity of reporter ions to that of the peptide selected for MS/MS fragmentation. The fragment ion peaks observed at higher m/z are specific for peptide amino acid sequence and are used for peptide identifications, which are eventually assigned to the proteins that they represent. Since every tryptic peptide can be labelled in an isobaric labelling method, more than one peptide representing the same protein may be identified, thereby increasing the confidence in both the identification and quantification of the protein [246].

Label-free quantification is the quantification of MS peptide signals in LC/MS/MS data without an isotopic labelling reagent [250]. Label-free methods aim to compare two or more experiments by (i) comparing the direct mass spectrometric signal intensity for any given peptide or (ii) using the number

of acquired spectra matching to a peptide/protein as an indicator of their respective abundance in a given sample[251]. Interestingly, the principle of most label-free methods is the recognition that most complex samples have a large group of unchanging species that can be used as the source of normalizing factors (used to correct the sample-to-sample and run-to-run variation in signal intensities for the species of interest). However, a key barrier to quantitation with MS involves the fact that while the intensity of an ion does reflect its abundance, corrections must be made for differences in mass spectrometer response, sample loading, and ionization efficient that can occur between experiments [220]. Therefore, any variability in sample preparation, LC, or MS more strongly affects label-free quantification than it does isotopically labelled techniques where differently labelled peptides co-elute. In addition, it provides the lowest throughput because of a lack of multiplexing. Finally, peptides might have different levels of ion suppression across the various samples, leading to a decrease in quantification accuracy [250].

In summary, the great advantage of iTRAQ and TMT as compared to other quantification methods is the multiplexed analysis of several samples within a single LC–MS/MS run, decreasing MS time analysis and variations during sample preparation, chromatography and MS acquisition. On the other hand, commercial labelling reagents are expensive and an additional labelling step has to be introduced in the analytical workflow [252]. In addition, various factors, such as ratio compression, reporter ion dynamic range, and others, cause an underestimation of changes in relative abundance of proteins across samples, undermining the ability of the isobaric labelling approach to be truly quantitative [246].

Label-free proteomics is cost-efficient and no additional sample preparation steps are needed. However, samples need to be handled separately until the final LC–MS/MS analysis and all these steps ranging from sample preparation to MS acquisition can introduce variations that can bias the quantitative analysis. Furthermore, a quantitative analysis is comparatively time-consuming, as a multiplexed analysis is not possible in case of label-free proteomics [252]. Nevertheless, label-free quantification it still worth consideration because: (i) there is no principle limit to the number of experiments that can be compared, (ii) unlike most stable isotope labelling techniques mass spectral complexity is not increased which, in turn, might provide for more analytical depth because the mass spectrometer is not occupied with fragmenting all forms of the labelled peptide and (iii) label-free methods provide higher dynamic range of quantification than stable isotope labelling and therefore may be advantageous when large and global protein changes between experiments are observed [253].

In conclusion, each of these quantitative MS proteomic approaches have their particular strengths and weaknesses. However, MS is not inherently quantitative because proteolytic peptides exhibit a wide range of physicochemical properties such as size, charge, hydrophobicity, etc., together leading to large differences in mass spectrometric response. Therefore, accurate comparisons between two samples must be based on the same individual peptide in LC-MS/MS experiments conducted under

the same conditions [253], [254]. **The results obtained with the TMT and Label-free quantification approaches are presented in Chapter VI.**

8-Bioinformatic analysis of mass spectrometry-based data sets

The computer analysis of MS data is key for large-scale and high-throughput protein analysis and it has allowed proteomic studies. A principal method in shotgun proteomics analysis of proteins mixtures is the database searching of MS/MS data of peptides. The method is based on predicting the fragmentation pattern of the peptide and then comparing the predicted pattern to the fragments in the tandem mass spectrum. Scoring of a match based on cross-correlation, fragment ion frequencies, and hypergeometric probability, is then attributed [255]. Moreover, intensity models in correlation analyses improve matches between sequence and spectra and probability-based methods provide a statistical measure for the fit between sequence and spectrum. The statistical relevance for quantitative comparisons can be determined through empirical analysis of known data sets and establishing scoring cut-offs for a statistical confidence level [255].

However, proteomic analyses can generate large amounts of data and thus have a need for a high level of automation in the data analysis. Thus, the major bottlenecks in proteomics can be considered as the data processing and analysis, with a huge amounts of data generated, but with an enormous challenge to figure out how to actually analyse this data and generate real biological insights. Also, the necessity of an integrated pipeline for processing and analysis of complex proteomics data sets has therefore become critical [256]. In addition, to facilitate the dissemination of the raw experimental data and inferred biological results, centralized data repositories have been developed in order to make the data and results accessible to proteomics researchers and biologists alike [257]. The main existing repositories are: the Global Proteome Machine Database (GPMDB) [258], PeptideAtlas [259], the PRoteomics IDEntifications database (PRIDE) [260], Tranche, and NCBI Peptidome [261], providing a highly valuable source for bioinformatics data mining [262].

The information generated in a typical proteomics experiment can be organized in three different levels, i) raw data; ii) processed results, including peptide/protein identification and quantification values; and iii) the resulting biological conclusion obtained with Protein Knowledge-bases, such as, the Universal Protein Resource (Uniprot) [263]. Uniprot is among the most used of the protein sequence and functional annotation providers, it integrates, interprets and standardizes data from the literature and resources to achieve the most comprehensive catalogue possible of protein information [264], and is essential for the subsequent Gene Ontology term (GO-term) analysis, as described in the section below.

8.1- Gene Ontology term identification and enrichment analysis

The output of a proteome analysis is usually a long list of identified factors, that have a probability score and ideally also a quantitative value associated to them. In order perform a functional analysis of a large protein list, the list has to be further classified and filtered. Thus, the first step for a functional analysis is to connect the protein name to a unique identifier (specific for that given protein) [265]. Some databases like the Uniprot knowledge base [266] and Ensembl [267] can be used for this purpose, using protein identifiers as input to retrieve the corresponding Uniprot or Ensembl identifiers. Later, these identifiers can be used to perform the GO-term identification and enrichment analysis.

Therefore, the GO-term analysis, is obtained through the association of the protein identifiers with its associated Gene Ontology Terms [268]. These GO-terms, are associated with functional terms that describe the *biological process*, *molecular function* or *cellular component* which have a unique identification number. For larger data sets and systematic approaches some database search algorithms for proteomic data such as MaxQuant, Proteome Discoverer and X!tandem have implemented a GO-term annotation step [265]. After performing the GO-term annotation, the GO-term enrichment can be performed to compare the abundance of specific GO-terms in the dataset with the natural abundance in the organism or a reference dataset [265]. Software available for annotation enrichment analysis can be categorized into three major classes according to their underlying enrichment algorithms. These are the singular enrichment analysis (SEA), gene set enrichment analysis (GSEA), and modular enrichment analysis (MEA) [269].

The SEA enrichment is the most traditional approach (tools such, BinGO [270] and EasyGO [271]), that tests GO-terms one at time against a list of genes for enrichment. Annotation terms passing the enrichment *p-value* threshold are reported. This is a simple and very efficient strategy to extract the major biological meaning behind large gene list. However, the linear output of the terms can be very large and overwhelming. On the other hand, GSEA method (such as, GSEA/P-GSEA [272], [273] and GeneTrail [274]) adopts a “no-cut-off” strategy, taking all genes into account without selecting significant genes. GSEA methods need biological values such as fold changes for each of the genes as input. However, sometimes is difficult to summarize many biological aspects of a gene into one value when the experiment design is complex. Finally, the MEA method (such as, DAVID [275], Ontologizer [276], topGO [277]) considers relationships between GO-terms during enrichment, which can reduce redundancy and prevent the loss of potentially important biological correlations due to lack of relationships [265], [269]. The MEA disadvantage is that some terms or genes with weak relationships to neighbouring terms or genes could be left out from the analysis [269].

Another common approach for the analysis of large datasets is the pathways analysis, allowing a reduction of complexity and increasing explanatory power. Therefore, it has become good approach for gaining insight into the underlying biology for a given gene or protein list, similarly to the previously

described GO-term enrichment analysis. However, examining protein or gene lists for pathway abundances might be more meaningful because it moves the data interpretation away from the gene-centric view towards the identification of functional biological processes [265], [269]. A large number of resources and databases is available to extract pathways from biological data. Some of the popular and freely available pathway databases (for academic users) are KEGG [278], Reactome [279] and PANTHER [280], whereas other databases, such Ingenuity Pathways Knowledge Base [281] and iPath [282] are commercial [283]. Although, the enrichment analyses are available with almost all pathway database resources, the identification of pathways affected under certain conditions is highly dependent on the algorithm, similar to what happens regarding GO-term annotation [265].

Furthermore, the analysis of protein-protein interactions (PPIs), is also important, because the majority of proteins do not act as isolated entities, but rather function in complexes as multiprotein-protein machines. Since their assembly is largely mediated by PPIs, functional interactions within a proteome may revealed by PPIs analysis. Functional interactions include sharing a common substrate in a pathway, regulating each other at the transcriptional level or indirect binding through participation in larger multi-protein assemblies[283]. Therefore, information regarding PPIs is deposited in interaction databases, such as MINT [284], BioGRID [285], IntAct [286] or HPRD [287], associated with the biological process in which they are functionally important.

In addition, a resource used for PPIs data is STRING [288], which is a database itself, but is able to connect to other data resources and is also capable of literature mining. Moreover, is also capable of showing simple protein networks based on the provided gene list and the available interactions in its databases[265]. Another popular one-source program for visualizing protein or gene networks is Cytoscape [289], offering several plugins that can be useful for specific types of analysis. Similar platforms offer also the possibility to explore and manipulate large pathways and graphs, such Gephi [290] or the recent NeVOmics [291], that can also build different network-based graphical representations from the enrichment results.

Computational proteomics can be considered multidisciplinary, attracting scientists from many fields and incorporating other disciplines like statistics, machine learning, efficient scientific programming, and network and time series analysis. Additionally, the integration of proteomics data with other biological high-throughput data is increasingly gaining importance [292]. **The GO-term enrichment, pathways and PPIs analysis were used in Chapters IV and VI.**

9-References

[1] A. S. Levey and J. Coresh, “Chronic kidney disease,” *Lancet*, vol. 379, no. 9811, pp. 165–180, 2012.

[2] A. C. Webster, E. V. Nagler, R. L. Morton, and P. Masson, “Chronic Kidney Disease,” *Lancet*, 2017.

[3] Y. Sato and M. Yanagita, “Resident fibroblasts in the kidney: a major driver of fibrosis and inflammation,” *Inflamm. Regen.*, vol. 37, no. 1, p. 17, 2017.

[4] J. Baillie, P. Gill, and M. Courtenay, “Knowledge, understanding and experiences of peritonitis amongst patients, and their families, undertaking peritoneal dialysis: A mixed methods study protocol,” *J. Adv. Nurs.*, vol. 74, no. 1, pp. 201–210, 2018.

[5] K. Kalantar-Zadeh *et al.*, “Transition of care from pre-dialysis prelude to renal replacement therapy: The blueprints of emerging research in advanced chronic kidney disease,” *Nephrology Dialysis Transplantation*. 2017.

[6] J. Perl and J. M. Bargman, “Peritoneal dialysis: from bench to bedside and bedside to bench,” *Am. J. Physiol. - Ren. Physiol.*, 2016.

[7] M. Foy and C. J. Sperati, “What the non-nephrologist needs to know about dialysis,” *Semin. Dial.*, 2018.

[8] F. M. C. A. KGaA, “Fresenius Medical Care 2017. Annual Report,” 2017.

[9] P. K. T. Li *et al.*, “Changes in the worldwide epidemiology of peritoneal dialysis,” *Nature Reviews Nephrology*. 2017.

[10] S. J. Davies, “Peritoneal dialysis-current status and future challenges,” *Nature Reviews Nephrology*. 2013.

[11] A. K. Jain, P. Blake, P. Cordy, and A. X. Garg, “Global Trends in Rates of Peritoneal Dialysis,” *J. Am. Soc. Nephrol.*, 2012.

[12] K. D. Nolph and Z. J. Twardowski, “Peritoneal Dialysis System,” *Springer, Dordr.*, 1989.

[13] H. Terawaki, “Peritoneal Physiology and Peritoneal Membrane,” in *The Essentials of Clinical Dialysis*, Y.-L. Kim and H. Kawanishi, Eds. Springer, 2018, pp. 153–161.

[14] I. Teitelbaum and J. Burkart, “Peritoneal dialysis,” *Am. J. Kidney Dis.*, vol. 42, no. 5, pp. 1082–1096, Jan. 2018.

[15] J. D. Williams, K. J. Craig, C. von Ruhland, N. Topley, G. T. Williams, and for the Biopsy Registry Study Group, “The natural course of peritoneal membrane biology during peritoneal dialysis,” *Kidney Int.*, 2003.

[16] O. Devuyst and B. Rippe, “Water transport across the peritoneal membrane,” *Kidney International*. 2014.

[17] M. Bartosova and C. P. Schmitt, “Biocompatible Peritoneal Dialysis: The Target Is Still Way Off,” *Front. Physiol.*, 2019.

[18] R. Khanna, “Solute and Water Transport in Peritoneal Dialysis: A Case-Based Primer,” *Am. J. Kidney Dis.*, 2017.

[19] R. T. Krediet, “Choice of Peritoneal Dialysis Technique: Intermittent or Continuous,” *Crit. Care Nephrol.*, pp. 1102-1104.e1, Jan. 2019.

[20] R. Raaijmakers *et al.*, “Proteomic profiling and identification in peritoneal fluid of children

treated by peritoneal dialysis," *Nephrol. Dial. Transplant.*, 2008.

[21] O. Devuyst and J. Ni, "Aquaporin-1 in the peritoneal membrane: Implications for water transport across capillaries and peritoneal dialysis," *Biochim. Biophys. Acta - Biomembr.*, vol. 1758, no. 8, pp. 1078–1084, Aug. 2006.

[22] M. Flessner, "Solute and water transport across the peritoneal barrier," in *Critical Care Nephrology*, 3rd ed., C. Ronco, R. Bellomo, J. Kellum, and Z. Ricci, Eds. Elsevier - Health Sciences Division, 2017, pp. 1096–1102.

[23] G. T. González-Mateo *et al.*, "Angiogenesis and Lymphangiogenesis in Peritoneal Dialysis," in *Aspects in Dialysis*, no. 7, 2018, pp. 133–163.

[24] C. Prado-Uribe *et al.*, "Ultrafiltration and Dialysis Adequacy with Various Daily Schedules of Dialysis Fluids," *Perit. Dial. Int.*, vol. 32, no. 5, pp. 545–551, 2012.

[25] R. T. Krediet, "The physiology of peritoneal solute transport and ultrafiltration," in *Textbook of peritoneal dialysis*, R. Gokal, R. Khanna, R. T. Krediet, and K. D. Nolph, Eds. Kluwer Academic Publishers, 2000, pp. 135–172.

[26] M. M. Pannekeet *et al.*, "The standard peritoneal permeability analysis: A tool for the assessment of peritoneal permeability characteristics in CAPD patients," *Kidney Int.*, 1995.

[27] Z. Twardowski *et al.*, "Peritoneal equilibration test," *Perit. Dial. Int.*, 1987.

[28] J. Waniewski, "Peritoneal fluid transport: Mechanisms, pathways, methods of assessment," *Archives of Medical Research*. 2013.

[29] W. Van Biesen *et al.*, "Evaluation of peritoneal membrane characteristics: Clinical advice for prescription management by the ERBP working group," *Nephrology Dialysis Transplantation*. 2010.

[30] D. W. Johnson *et al.*, "A comparison of peritoneal equilibration tests performed 1 and 4 weeks after PD commencement," *Perit. Dial. Int.*, 2004.

[31] B. B. Hoffman, "Chapter 51. Peritoneal Dialysis," in *CURRENT Diagnosis & Treatment: Nephrology & Hypertension*, E. V Lerma, J. S. Berns, and A. R. Nissenson, Eds. New York, NY: The McGraw-Hill Companies, 2009.

[32] C. Jiang and W. K. Lo, "Trend of peritoneal transport and impact on patient survival: A 10-year follow-up cohort study.," *Clin. Nephrol.*, 2018.

[33] Z. J. Twardowski, "PET--a simpler approach for determining prescriptions for adequate dialysis therapy.," *Adv. Perit. Dial.*, 1990.

[34] K. S. Brimble, M. Walker, P. J. Margetts, K. K. Kundhal, and C. G. Rabbat, "Meta-analysis: peritoneal membrane transport, mortality, and technique failure in peritoneal dialysis.," *J. Am. Soc. Nephrol.*, 2006.

[35] I. Teitelbaum, "Ultrafiltration failure in peritoneal dialysis: A pathophysiologic approach," *Blood Purif.*, vol. 39, no. 1–3, pp. 70–73, 2015.

[36] M. F. Flessner, "Net ultrafiltration in peritoneal dialysis: Role of direct fluid absorption into peritoneal tissue," *Blood Purif.*, 1992.

[37] M. F. Flessner, "Peritoneal ultrafiltration: Mechanisms and measures," *Contrib. Nephrol.*, vol. 150, no. 1, pp. 28–36, 2006.

[38] N. Prasad and S. Gupta, "Ultrafiltration Failure In Peritoneal Dialysis: A Review," *Indian J. Perit. Dial.*, vol. 1, pp. 15–24, 2012.

[39] J. M. Bargman and M. Girsberger, "Visions in a Crystal Ball: The Future of Peritoneal Dialysis,"

Blood Purif., vol. 4, pp. 218–223, 2018.

[40] G. Woodrow, S. L. Fan, C. Reid, J. Denning, and A. N. Pyrah, "Renal Association Clinical Practice Guideline on peritoneal dialysis in adults and children," *BMC Nephrology*. 2017.

[41] T. I. Chang and S. H. Han, "Kinetic Modeling and Adequacy in PD," in *The Essentials of Clinical Dialysis*, Y.-L. Kim and H. Kawanishi, Eds. Singapore: Springer Singapore, 2018, pp. 215–241.

[42] S. Yoowannakul, L. S. Harris, and A. Davenport, "Peritoneal Protein Losses Depend on More Than Just Peritoneal Dialysis Modality and Peritoneal Membrane Transporter Status," *Ther. Apher. Dial.*, no. 10, 2018.

[43] G. Rajakaruna, B. Caplin, and A. Davenport, "Peritoneal protein clearance rather than faster transport status determines outcomes in peritoneal dialysis patients," *Perit. Dial. Int.*, 2015.

[44] J. Perl, K. Huckvale, M. Chellar, B. John, and S. J. Davies, "Peritoneal protein clearance and not peritoneal membrane transport status predicts survival in a contemporary cohort of peritoneal dialysis patients," *Clin. J. Am. Soc. Nephrol.*, 2009.

[45] P. Ditsawanon, O. Supasyndh, and P. Aramwit, "Dialysate cancer antigen 125 in long-term peritoneal dialysis patients," *Clin. Exp. Nephrol.*, vol. 18, no. 1, pp. 10–15, 2014.

[46] E. Ferrantelli *et al.*, "The dipeptide alanyl-glutamine ameliorates peritoneal fibrosis and attenuates IL-17 dependent pathways during peritoneal dialysis," *Kidney Int.*, Jan. 2016.

[47] H. Cheema and J. M. Bargman, "Cancer antigen 125 as a biomarker in peritoneal dialysis: Mesothelial cell health or death?," *Peritoneal Dialysis International*. 2013.

[48] R. T. Krediet and D. G. Struijk, "Peritoneal changes in patients on long-term peritoneal dialysis," *Nat Rev Nephrol*, 2013.

[49] R. Strippoli *et al.*, "Molecular Mechanisms Underlying Peritoneal EMT and Fibrosis," *Stem Cells International*. 2016.

[50] L. S. Aroeira *et al.*, "Epithelial to Mesenchymal Transition and Peritoneal Membrane Failure in Peritoneal Dialysis Patients: Pathologic Significance and Potential Therapeutic Interventions," *J. Am. Soc. Nephrol.*, 2007.

[51] J. Waniewski *et al.*, "Peritoneal Fluid Transport rather than Peritoneal Solute Transport Associates with Dialysis Vintage and Age of Peritoneal Dialysis Patients," *Comput. Math. Methods Med.*, 2016.

[52] A. Fusshoeller, "Histomorphological and functional changes of the peritoneal membrane during long-term peritoneal dialysis," *Pediatric Nephrology*. 2008.

[53] S. J. Davies, "Unraveling the mechanisms of progressive peritoneal membrane fibrosis," *Kidney International*. 2016.

[54] A. Pletinck, R. Vanholder, N. Veys, and W. Van Biesen, "Protecting the peritoneal membrane: Factors beyond peritoneal dialysis solutions," *Nature Reviews Nephrology*. 2012.

[55] J. Shi, M. Yu, and M. Sheng, "Angiogenesis and Inflammation in Peritoneal Dialysis: The Role of Adipocytes," *Kidney Blood Press. Res.*, vol. 42, no. 2, pp. 209–219, 2017.

[56] A. Isaza-Restrepo, J. S. Martin-Saavedra, J. L. Velez-Leal, F. Vargas-Barato, and R. Riveros-Dueñas, "The peritoneum: Beyond the tissue - A review," *Front. Physiol.*, vol. 9, no. JUN, pp. 1–12, 2018.

[57] O. Devuyst, P. J. Margetts, and N. Topley, "The Pathophysiology of the Peritoneal Membrane," *J. Am. Soc. Nephrol.*, 2010.

[58] S. M. Hurst *et al.*, "IL-6 and its soluble receptor orchestrate a temporal switch in the pattern of

leukocyte recruitment seen during acute inflammation," *Immunity*, 2001.

[59] R. M. McLoughlin *et al.*, "Interplay between IFN-γ and IL-6 signaling governs neutrophil trafficking and apoptosis during acute inflammation," *J. Clin. Invest.*, 2003.

[60] R. M. McLoughlin *et al.*, "IL-6 trans-signaling via STAT3 directs T cell infiltration in acute inflammation," *Proc. Natl. Acad. Sci.*, 2005.

[61] S. Mortier, N. H. Lameire, and A. S. De Vriese, "The effects of peritoneal dialysis solutions on peritoneal host defense," *Peritoneal Dialysis International*. 2004.

[62] J. P. Thiery and J. P. Sleeman, "Complex networks orchestrate epithelial-mesenchymal transitions," *Nature Reviews Molecular Cell Biology*. 2006.

[63] S. Namvar, A. S. Woolf, L. A. H. Zeef, T. Wilm, B. Wilm, and S. E. Herrick, "Functional molecules in mesothelial-to-mesenchymal transition revealed by transcriptome analyses," *J. Pathol.*, 2018.

[64] M. Yáñez-Mó *et al.*, "Peritoneal Dialysis and Epithelial-to-Mesenchymal Transition of Mesothelial Cells," *N. Engl. J. Med.*, 2003.

[65] A. Aguilera, J. Loureiro, G. Gnzalez-Mateo, R. Selgas, and M. Lpez-Cabrer, "The Mesothelial to Mesenchymal Transition a Pathogenic and Therapeutic Key for Peritoneal Membrane Failure," in *The Latest in Peritoneal Dialysis*, 2013.

[66] J. A. Jiménez-Heffernan *et al.*, "Immunohistochemical characterization of fibroblast subpopulations in normal peritoneal tissue and in peritoneal dialysis-induced fibrosis," *Virchows Arch.*, 2004.

[67] G. Gónzalez-Mateo *et al.*, "Pharmacological Preservation of Peritoneal Membrane in Peritoneal Dialysis," in *Some Special Problems in Peritoneal Dialysis*, R. Ekart, Ed. 2016, pp. 25–49.

[68] R. Selgas *et al.*, "Epithelial-to-mesenchymal transition of the mesothelial cell - Its role in the response of the peritoneum to dialysis," *Nephrol. Dial. Transplant.*, 2006.

[69] V. L. Bautch and K. M. Caron, "Blood and lymphatic vessel formation," *Cold Spring Harb. Perspect. Biol.*, 2015.

[70] M. L. Pérez-Lozano *et al.*, "Functional Relevance of the Switch of VEGF Receptors/Co-Receptors during Peritoneal Dialysis-Induced Mesothelial to Mesenchymal Transition," *PLoS One*, vol. 8, no. 4, 2013.

[71] W. Zheng, A. Aspelund, and K. Alitalo, "Lymphangiogenic factors, mechanisms, and applications," *Journal of Clinical Investigation*. 2014.

[72] H. Kinashi, Y. Ito, T. Sun, T. Katsuno, and Y. Takei, "Roles of the TGF-β–VEGF-C Pathway in Fibrosis-Related Lymphangiogenesis," *Int. J. Mol. Sci.*, 2018.

[73] J. Witowski, J. Kamhieh-Milz, E. Kawka, R. Catar, and A. Jörres, "IL-17 in Peritoneal Dialysis-Associated Inflammation and Angiogenesis: Conclusions and Perspectives," *Front. Physiol.*, 2018.

[74] "https://www.sartorius.com/fileadmin/fm-dam/DDM/Lab-Products-and-Services/Lab-Filtration/Ultrafiltration-Devices/Vivaspin-Centrisart/Manuals/Manual_Vivaspin_15R_SLU2003-e.pdf (last time accessed January, 2016)."

[75] I. Hirahara, M. Inoue, K. Okuda, Y. Ando, S. Muto, and E. Kusano, "The potential of matrix metalloproteinase-2 as a marker of peritoneal injury, increased solute transport, or progression to encapsulating peritoneal sclerosis during peritoneal dialysis - A multicentre study in Japan," *Nephrol. Dial. Transplant.*, 2007.

[76] H. Kawanishi *et al.*, "Encapsulating peritoneal sclerosis in Japan: A prospective, controlled, multicenter study," *Am. J. Kidney Dis.*, 2004.

[77] S. M. Han *et al.*, "Network-based integrated analysis of omics data reveal novel players of TGF-β1-induced EMT in human peritoneal mesothelial cells," *Sci. Rep.*, 2019.

[78] T. Bellón *et al.*, "Alternative activation of macrophages in human peritoneum: Implications for peritoneal fibrosis," *Nephrol. Dial. Transplant.*, 2011.

[79] M. Ossorio *et al.*, "Sustained low peritoneal effluent CCL18 levels are associated with preservation of peritoneal membrane function in peritoneal dialysis," *PLoS One*, 2017.

[80] S. M. Habib *et al.*, "CD4-positive T cells and M2 macrophages dominate the peritoneal infiltrate of patients with encapsulating peritoneal sclerosis," *PLoS One*, 2015.

[81] R. T. Krediet, "Ultrafiltration Failure Is a Reflection of Peritoneal Alterations in Patients Treated With Peritoneal Dialysis," *Front. Physiol.*, vol. 9, p. 1815, 2018.

[82] W. M. Michels *et al.*, "Does lymphatic absorption change with the duration of peritoneal dialysis?," *Perit. Dial. Int.*, 2004.

[83] P. Pacher, J. S. Beckman, and L. Liaudet, "Nitric Oxide and Peroxynitrite in Health and Disease," *Physiol. Rev.*, 2007.

[84] R. Rodrigo and D. Gil-Becerra, "Implications of Polyphenols on Endogenous Antioxidant Defense Systems in Human Diseases," in *Polyphenols in Human Health and Disease*, 2013.

[85] H. Kinashi *et al.*, "TGF-β1 Promotes Lymphangiogenesis during Peritoneal Fibrosis," *J. Am. Soc. Nephrol.*, 2013.

[86] D. Machado Lopes *et al.*, "Analysis of ultrafiltration failure diagnosed at the initiation of peritoneal dialysis with the help of peritoneal equilibration tests with complete drainage at sixty minutes. A longitudinal study," *Perit. Dial. Int.*, 2016.

[87] S. Mujais *et al.*, "Evaluation and management of ultrafiltration problems in peritoneal dialysis," *Peritoneal Dialysis International*, 2000.

[88] S. J. Davies, "Mitigating peritoneal membrane characteristics in modern peritoneal dialysis therapy," *Kidney Int.*, 2006.

[89] S. H. Sajwani and J. M. Bargman, "Novel ways to preserve the peritoneal membrane.," *Adv. Perit. Dial.*, 2012.

[90] B. John, "The future of peritoneal dialysis: PD in 2010 and beyond," *Dialysis and Transplantation*. 2010.

[91] D. G. Struijk, "Monitoring of the peritoneal membrane," in *NDT Plus*, 2008.

[92] C. P. Schmitt, "Peritoneal dialysis solutions," in *Pediatric Dialysis, Second Edition*, 2012.

[93] E. García-López, B. Lindholm, and S. Davies, "An update on peritoneal dialysis solutions," *Nature Reviews Nephrology*. 2012.

[94] M. A. Bajo, G. del Peso, and I. Teitelbaum, "Peritoneal Membrane Preservation," *Seminars in Nephrology*. 2017.

[95] T. H.L., S. R., van den B. J.W., and F. M.W., "Amino acid-based peritoneal dialysis solutions for malnutrition: New perspectives," *Perit. Dial. Int.*, 2009.

[96] C. C. Szeto and D. W. Johnson, "Low GDP Solution and Glucose-Sparing Strategies for Peritoneal Dialysis," *Seminars in Nephrology*. 2017.

[97] H. Htay *et al.*, "Biocompatible dialysis fluids for peritoneal dialysis," *Cochrane Database of*

Systematic Reviews. 2018.

[98] M. Tawada *et al.*, "Effects of long-term treatment with low-GDP, pH-neutral solutions on peritoneal membranes in peritoneal dialysis patients," *Clin. Exp. Nephrol.*, vol. 23, no. 5, pp. 689–699, 2019.

[99] P. S. Misra, S. J. Nessim, and J. Perl, "'Biocompatible' Neutral pH Low-GDP Peritoneal Dialysis Solutions: Much Ado About Nothing?," *Semin. Dial.*, 2017.

[100] G. T. González-Mateo, L. S. Aroeira, M. López-Cabrera, M. Ruiz-Ortega, A. Ortiz, and R. Selgas, "Pharmacological modulation of peritoneal injury induced by dialysis fluids: Is it an option?," *Nephrol. Dial. Transplant.*, 2012.

[101] K. Farhat, A. W. D. Stavenuiter, R. H. J. Beelen, and P. M. Ter Wee, "Pharmacologic targets and peritoneal membrane remodeling," *Perit. Dial. Int.*, 2014.

[102] P. Ditsawanon and P. Aramwit, "Preserving the peritoneal membrane in long-term peritoneal dialysis patients," *Journal of Clinical Pharmacy and Therapeutics*. 2015.

[103] N. Liu, E. Tolbert, M. Pang, M. Ponnusamy, H. Yan, and S. Zhuang, "Suramin Inhibits Renal Fibrosis in Chronic Kidney Disease," *J. Am. Soc. Nephrol.*, 2011.

[104] T. Kawai *et al.*, "PPAR-γ agonist attenuates renal interstitial fibrosis and inflammation through reduction of TGF-β," *Lab. Investig.*, 2009.

[105] J. E. Toblli, M. G. Ferrini, G. Cao, D. Vernet, M. Angerosa, and N. F. Gonzalez-Cadavid, "Antifibrotic effects of pioglitazone on the kidney in a rat model of type 2 diabetes mellitus," *Nephrol. Dial. Transplant.*, 2009.

[106] P. Sandoval *et al.*, "PPAR-γ agonist rosiglitazone protects peritoneal membrane from dialysis fluid-induced damage," *Lab. Investig.*, 2010.

[107] M. Zareie *et al.*, "Beneficial effects of aminoguanidine on peritoneal microcirculation and tissue remodelling in a rat model of PD," *Nephrol. Dial. Transplant.*, 2005.

[108] S. J. Zieman *et al.*, "Advanced glycation endproduct crosslink breaker (alagebrium) improves endothelial function in patients with isolated systolic hypertension," *J. Hypertens.*, 2007.

[109] Y. K. Lee *et al.*, "The breakdown of preformed peritoneal advanced glycation end products by intraperitoneal alagebrium," *J. Korean Med. Sci.*, 2009.

[110] R. van Westrhenen, J. Aten, M. Aberra, C. A. M. Dragt, G. Deira, and R. T. Krediet, "Effects of inhibition of the polyol pathway during chronic peritoneal exposure to a dialysis solution," *Perit. Dial. Int.*, 2005.

[111] T. Kakuta *et al.*, "Pyridoxamine improves functional, structural, and biochemical alterations of peritoneal membranes in uremic peritoneal dialysis rats," *Kidney Int.*, 2005.

[112] S. Duman *et al.*, "Does enalapril prevent peritoneal fibrosis induced by hypertonic (3.86%) peritoneal dialysis solution?," *Perit. Dial. Int.*, 2001.

[113] C. C. Fang *et al.*, "Pentoxifylline inhibits human peritoneal mesothelial cell growth and collagen synthesis: Effects on TGF-β," *Kidney Int.*, 2000.

[114] K.-Y. Hung, C.-T. Chen, J.-W. Huang, P.-H. Lee, T.-J. Tsai, and B.-S. Hsieh, "Dipyridamole inhibits TGF-β–induced collagen gene expression in human peritoneal mesothelial cells," *Kidney Int.*, 2003.

[115] T. M. Chan, J. K. H. Leung, R. C. W. Tsang, Z. H. Liu, L. S. Li, and S. Yung, "Emodin ameliorates glucose-induced matrix synthesis in human peritoneal mesothelial cells," *Kidney Int.*, 2003.

[116] S. Patel, R. M. Mason, J. Suzuki, A. Imaizumi, T. Kamimura, and Z. Zhang, "Inhibitory effect of statins on renal epithelial-to-mesenchymal transition," *Am. J. Nephrol.*, 2006.

[117] B. Haslinger, R. Kleemann, K. H. Toet, and T. Kooistra, "Simvastatin suppresses tissue factor expression and increases fibrinolytic activity in tumor necrosis factor-α-activated human peritoneal mesothelial cells," *Kidney Int.*, 2003.

[118] B. Haslinger, M. F. Goedde, K. H. Toet, and T. Kooistra, "Simvastatin increases fibrinolytic activity in human peritoneal mesothelial cells independent of cholesterol lowering," *Kidney Int.*, 2002.

[119] J. Loureiro *et al.*, "BMP-7 blocks mesenchymal conversion of mesothelial cells and prevents peritoneal damage induced by dialysis fluid exposure," *Nephrol. Dial. Transplant.*, 2010.

[120] J. Loureiro *et al.*, "Tamoxifen Ameliorates Peritoneal Membrane Damage by Blocking Mesothelial to Mesenchymal Transition in Peritoneal Dialysis," *PLoS One*, 2013.

[121] H. Dellê, J. R. C. Rocha, R. C. Cavaglieri, J. M. Vieira, D. M. A. C. Malheiros, and I. L. Noronha, "Antifibrotic Effect of Tamoxifen in a Model of Progressive Renal Disease," *J. Am. Soc. Nephrol.*, 2012.

[122] Y. Yoshio *et al.*, "TNP-470, an angiogenesis inhibitor, suppresses the progression of peritoneal fibrosis in mouse experimental model," *Kidney Int.*, 2004.

[123] L. S. Aroeira *et al.*, "Cyclooxygenase-2 Mediates Dialysate-Induced Alterations of the Peritoneal Membrane," *J. Am. Soc. Nephrol.*, 2009.

[124] P. Fabbrini *et al.*, "Celecoxib treatment reduces peritoneal fibrosis and angiogenesis and prevents ultrafiltration failure in experimental peritoneal dialysis," *Nephrol. Dial. Transplant.*, 2009.

[125] S. N. Tapiawala, J. M. Bargman, D. G. Oreopoulos, and M. Simons, "Prolonged use of the tyrosine kinase inhibitor in a peritoneal dialysis patient with metastatic renal cell carcinoma: Possible beneficial effects on peritoneal membrane and peritonitis rates," *Int. Urol. Nephrol.*, 2009.

[126] S. Wang *et al.*, "Endostatin Has ATPase Activity, Which Mediates Its Antiangiogenic and Antitumor Activities," *Mol. Cancer Ther.*, 2015.

[127] Y. M. Kim *et al.*, "Endostatin blocks vascular endothelial growth factor-mediated signaling via direct interaction with KDR/Flk-1," *J. Biol. Chem.*, vol. 277, no. 31, pp. 27872–27879, 2002.

[128] K.-Y. Han *et al.*, "Characterization of the Interaction Between Endostatin Short Peptide and VEGF Receptor 3," *Protein Pept. Lett.*, 2012.

[129] K. Tanabe *et al.*, "Endostatin peptide, an inhibitor of angiogenesis, prevents the progression of peritoneal sclerosis in a mouse experimental model," *Kidney Int.*, 2007.

[130] N. Sakai *et al.*, "Inhibition of CTGF ameliorates peritoneal fibrosis through suppression of fibroblast and myofibroblast accumulation and angiogenesis," *Sci. Rep.*, 2017.

[131] W. Peng, Q. Zhou, X. Ao, R. Tang, and Z. Xiao, "Inhibition of Rho-kinase alleviates peritoneal fibrosis and angiogenesis in a rat model of peritoneal dialysis," *Ren. Fail.*, 2013.

[132] F. Coronel *et al.*, "Changes in peritoneal membrane permeability and proteinuria in patients on peritoneal dialysis after treatment with paricalcitol – a preliminary study," *Clin. Nephrol.*, 2012.

[133] J. Nie *et al.*, "Smad7 gene transfer inhibits peritoneal fibrosis," *Kidney Int.*, 2007.

[134] W. Peng *et al.*, "Smad7 gene transfer attenuates angiogenesis in peritoneal dialysis rats," *Nephrology*, 2013.

[135] K. F. Huang, H. Y. Yang, Y. M. Xing, J. S. Lin, and Y. Diao, "Recombinant human kallistatin

inhibits angiogenesis by blocking VEGF signaling pathway," *J. Cell. Biochem.*, 2014.

[136] C. Ma *et al.*, "Kallistatin exerts anti-lymphangiogenic effects by inhibiting lymphatic endothelial cell proliferation, migration and tube formation," *Int. J. Oncol.*, 2017.

[137] J. U. Choi *et al.*, "A heparin conjugate, LHbisD4, inhibits lymphangiogenesis and attenuates lymph node metastasis by blocking VEGF-C signaling pathway," *Biomaterials*, 2017.

[138] J. Li *et al.*, "Low Molecular Weight Heparin (LMWH) improves peritoneal function and inhibits peritoneal fibrosis possibly through suppression of HIF-1α, VEGF and TGF-β1," *PLoS One*, 2015.

[139] G. T. González-Mateo *et al.*, "Rapamycin Protects from Type-I Peritoneal Membrane Failure Inhibiting the Angiogenesis, Lymphangiogenesis, and Endo-MT," *Biomed Res. Int.*, 2015.

[140] C. C. Hudson *et al.*, "Regulation of Hypoxia-Inducible Factor 1 Expression and Function by the Mammalian Target of Rapamycin," *Mol. Cell. Biol.*, 2002.

[141] M. Guba *et al.*, "Rapamycin inhibits primary and metastatic tumor growth by antiangiogenesis: Involvement of vascular endothelial growth factor," *Nat. Med.*, 2002.

[142] R. C. Ji and Y. Eshita, "Rapamycin inhibition of CFA-induced lymphangiogenesis in PLN is independent of mast cells," *Mol. Biol. Rep.*, 2014.

[143] G. Liappas *et al.*, "Nebivolol, a β$_1$-adrenergic blocker, protects from peritoneal membrane damage induced during peritoneal dialysis," *Oncotarget*, vol. 7, no. 21, May 2016.

[144] D. Lopes Barreto and R. T. Krediet, "Current status and practical use of effluent biomarkers in peritoneal dialysis patients," *Am. J. Kidney Dis.*, 2013.

[145] I. Hirahara, M. Inoue, T. Umino, O. Saito, S. Muto, and E. Kusano, "Matrix metalloproteinase levels in the drained dialysate reflect the peritoneal solute transport rate: A multicentre study in Japan," *Nephrol. Dial. Transplant.*, 2011.

[146] C. Aufricht *et al.*, "Biomarker research to improve clinical outcomes of peritoneal dialysis: consensus of the European Training and Research in Peritoneal Dialysis (EuTRiPD) network," *Kidney International*. 2017.

[147] R. T. Krediet, D. G. Struijk, S. van Esch, and R. T. Krediet, "Assessment of the Peritoneum by Biomarkers in Peritoneal Effluent," *Perit. Dial. Man.*, pp. 27–34, 2018.

[148] M. Bruschi *et al.*, "Combinatorial peptide ligand library and two dimensional electrophoresis: New frontiers in the study of peritoneal dialysis effluent in pediatric patients," *J. Proteomics*, 2015.

[149] T. Sakurada *et al.*, "Prothrombin fragment 1 + 2 (F1 + 2) in effluent is a useful marker for peritoneal permeability in peritoneal dialysis patients using neutral dialysate," *Adv. Perit. Dial.*, vol. 27, p. 2—5, 2011.

[150] M. Goedde, T. Sitter, H. Schiffl, U. Bechtel, W. Schramm, and M. Spannagl, "Coagulation and fibrinolysis-related antigens in plasma and dialysate of CAPD patients," *Perit. Dial. Int.*, 1997.

[151] A. W. De Boer *et al.*, "Intraperitoneal hypercoagulation and hypofibrinolysis is present in childhood peritonitis," *Pediatr. Nephrol.*, 1999.

[152] M. N. Vipond, S. A. Whawell, H. A. F. Dudley, and J. N. Thompson, "Peritoneal fibrinolytic activity and intra-abdominal adhesions," *Lancet*, 1990.

[153] R. F. Buckman, M. Woods, L. Sargent, and A. S. Gervin, "A unifying pathogenetic mechanism in the etiology of intraperitoneal adhesions," *J. Surg. Res.*, 1976.

[154] B. Rippe *et al.*, "Long-term clinical effects of a peritoneal dialysis fluid with less glucose

degradation products," *Kidney Int.*, 2001.

[155] D. L. Barreto, A. M. Coester, D. G. Struijk, and R. T. Krediet, "Can effluent matrix metalloproteinase 2 and plasminogen activator inhibitor 1 be used as biomarkers of peritoneal membrane alterations in peritoneal dialysis patients?," *Perit. Dial. Int.*, 2013.

[156] D. Lopes Barreto *et al.*, "Variability of effluent cancer antigen 125 and interleukin-6 determination in peritoneal dialysis patients," *Nephrol. Dial. Transplant.*, 2011.

[157] R. Pecoits-Filho *et al.*, "Plasma and dialysate IL-6 and VEGF concentrations are associated with high peritoneal solute transport rate," *Nephrol. Dial. Transplant.*, 2002.

[158] D. Zemel, R. J. ten Berge, D. G. Struijk, E. Bloemena, G. C. Koomen, and R. T. Krediet, "Interleukin-6 in CAPD patients without peritonitis: relationship to the intrinsic permeability of the peritoneal membrane," *Clin Nephrol*, 1992.

[159] A. S. Rodrigues *et al.*, "Peritoneal fast transport in incident peritoneal dialysis patients is not consistently associated with systemic inflammation," *Nephrol. Dial. Transplant.*, 2006.

[160] S. van Esch, M. M. Zweers, M. A. M. Jansen, D. R. de Waart, J. G. van Manen, and R. T. Krediet, "Determinants of peritoneal solute transport rates in newly started nondiabetic peritoneal dialysis patients," *Perit. Dial. Int.*, 2004.

[161] L. Weiss *et al.*, "Biocompatibility and tolerability of a purely bicarbonate-buffered peritoneal dialysis solution," *Perit. Dial. Int.*, 2009.

[162] S. Opatrna, D. Lysak, L. Trefil, C. Parker, and N. Topley, "Intraperitoneal il-6 signaling in incident patients treated with icodextrin and glucose bicarbonate/lactate-based peritoneal dialysis solutions," *Perit. Dial. Int.*, vol. 32, no. 1, pp. 37–44, 2012.

[163] C. L.A. *et al.*, "Interleukin-6 levels decrease in effluent from patients dialyzed with bicarbonate/lactate-based peritoneal dialysis solutions," *Perit. Dial. Int.*, vol. 21, no. SUPPL. 3, pp. S102–S107, 2001.

[164] J. D. Williams *et al.*, "The Euro-Balance Trial: The effect of a new biocompatible peritoneal dialysis fluid (balance) on the peritoneal membrane," *Kidney Int.*, 2004.

[165] M. Mizutani *et al.*, "Connective tissue growth factor (CTGF/CCN2) is increased in peritoneal dialysis patients with high peritoneal solute transport rate," *Am. J. Physiol. Physiol.*, 2009.

[166] P. J. Margetts, M. Kolb, T. O. M. Galt, C. M. Hoff, T. R. Shockley, and J. Gauldie, "Gene Transfer of Transforming Growth Factor-{beta}1 to the Rat Peritoneum: Effects on Membrane Function," *J Am Soc Nephrol*, 2001.

[167] S. Jones *et al.*, "Bicarbonate/lactate-based peritoneal dialysis solution increases cancer antigen 125 and decreases hyaluronic acid levels," *Kidney Int.*, vol. 59, no. 4, pp. 1529–1538, Apr. 2001.

[168] M. M. Zweers, D. R. De Waart, W. Smit, D. G. Struijk, and R. T. Krediet, "Growth factors VEGF and TGF-β1 in peritoneal dialysis," *J. Lab. Clin. Med.*, 1999.

[169] M. M. Zweers, D. G. Struijk, W. Smit, and R. T. Krediet, "Vascular endothelial growth factor in peritoneal dialysis: A longitudinal follow-up," *J. Lab. Clin. Med.*, 2001.

[170] D. E. Sampimon *et al.*, "Early diagnostic markers for encapsulating peritoneal sclerosis: A case-control study," *Perit. Dial. Int.*, 2010.

[171] S. Ahmad *et al.*, "CCL18 in peritoneal dialysis patients and encapsulating peritoneal sclerosis," *Eur. J. Clin. Invest.*, 2010.

[172] M. M. Pannekeet, D. Zemel, G. C. M. Koomen, D. G. Struijk, and R. T. Krediet, "Dialysate markers of peritoneal tissue during peritonitis and in stable CAPD," *Perit. Dial. Int.*, 1995.

[173] K. Yamagata, C. Tomida, and A. Koyama, “Intraperitoneal hyaluronan production in stable continuous ambulatory peritoneal dialysis patients,” *Perit. Dial. Int.*, 1999.

[174] K. N. Lai, C. C. Szeto, K. B. Lai, C. W. K. Lam, D. T. M. Chan, and J. C. K. Leung, “Increased production of hyaluronan by peritoneal cells and its significance in patients on CAPD,” *Am. J. Kidney Dis.*, 1999.

[175] C. C. Szeto, T. Yuk-Hwa Wong, K. B. Lai, C. Wai-Kei Lam, K. N. Lai, and P. Kam-Tao Li, “Dialysate hyaluronan concentration predicts survival but not peritoneal sclerosis in continous ambulatory peritoneal dialysis,” *Am. J. Kidney Dis.*, 2000.

[176] F. Perfumo *et al.*, “Effects of peritoneal effluents on mesothelial cells m culture: cell proliferation and extracellular matrix regulation,” *Nephrol. Dial. Transplant.*, 2012.

[177] J. D. Williams *et al.*, “Morphologic changes in the peritoneal membrane of patients with renal disease,” *J.Am.Soc.Nephrol.*, 2002.

[178] M. M. Ho-Dac-Pannekeet, J. K. Hiralall, D. G. Struijk, and R. T. Krediet, “Longitudinal follow-up of CA125 in peritoneal effluent,” *Kidney Int.*, 1997.

[179] S. Haas *et al.*, “Improved acidosis correction and recovery of mesothelial cell mass with neutral-pH bicarbonate dialysis solution among children undergoing automated peritoneal dialysis,” *J. Am. Soc. Nephrol.*, 2003.

[180] C. Y. le Poole, A. G. A. Welten, M. C. Weijmer, R. M. Valentijn, F. J. van Ittersum, and P. M. ter Wee, “Initiating CAPD with a regimen low in glucose and glucose degradation products, with icodextrin and amino acids (NEPP) is safe and efficacious,” *Perit. Dial. Int.*, 2005.

[181] C. C. Szeto *et al.*, “Clinical biocompatibility of a neutral peritoneal dialysis solution with minimal glucose-degradation products - A 1-year randomized control trial,” *Nephrol. Dial. Transplant.*, 2007.

[182] R. Westermeier and T. Naven, *Reiner Westermeier, Tom Naven Proteomics in Practice Proteomics in Practice: A Laboratory Manual of Proteome Analysis*, vol. 5. 2002.

[183] X. Han, A. Aslanian, and J. R. Yates, “Mass spectrometry for proteomics,” *Current Opinion in Chemical Biology*. 2008.

[184] R. Aebersold and M. Mann, “Mass Spec-based Proteomics,” *Nature*, 2003.

[185] F. Hillenkamp and J. Peter-Katalinic, *MALDI MS: A Practical Guide to Instrumentation, Methods and Applications*, 2nd Editio. 2013.

[186] K. Strupat, O. Scheibner, and M. Bromirski, “High-Resolution, Accurate-Mass Orbitrap Mass Spectrometry – Definitions, Opportunities, and Advantages,” *Thermo Sci.*, 2013.

[187] A. G. Marshall *et al.*, “Mass Resolution and Mass Accuracy: How Much Is Enough?,” *Mass Spectrom.*, 2013.

[188] D. C. Harris, “Quality Assurance and Calibration Methods,” *Quant. Chem. Anal.*, 2010.

[189] R. Zubarev and M. Mann, “On the proper use of mass accuracy in proteomics,” *Mol. Cell. Proteomics*, 2007.

[190] N. Mishra and G. Blobel, *Introduction to Proteomics: Principles and Applications*. Wiley, 2010.

[191] M. Karas and F. Hillenkamp, “Laser Desorption Ionization of Proteins with Molecular Masses Exceeding 10 000 Daltons,” *Analytical Chemistry*. 1988.

[192] V. H. Wysocki, K. A. Resing, Q. Zhang, and G. Cheng, “Mass spectrometry of peptides and proteins,” *Methods*, vol. 35, no. 3, pp. 211–222, Mar. 2005.

[193] P. S. H. and R. G. C. Wong, “Ion Trap Mass Spectrometry,” *Curr. Sep.*, 1997.

[194] B. Domon and R. Aebersold, “Mass spectrometry and protein analysis,” *Science*. 2006.

[195] D. Suckau, A. Resemann, M. Schuerenberg, P. Hufnagel, J. Franzen, and A. Holle, “A novel MALDI LIFT-TOF/TOF mass spectrometer for proteomics,” *Anal. Bioanal. Chem.*, vol. 376, no. 7, pp. 952–965, 2003.

[196] A. Michalski *et al.*, “Mass spectrometry-based proteomics using Q exactive, a high-performance benchtop quadrupole orbitrap mass spectrometer,” *Mol. Cell. Proteomics*, 2011.

[197] M. Scigelova and A. Makarov, “Orbitrap mass analyzer - Overview and applications in proteomics,” in *Proteomics*, 2006.

[198] J. B. Fenn, M. Mann, C. K. Meng, S. F. Wong, and C. M. Whitehouse, “Electrospray ionization for mass spectrometry of large biomolecules,” *Science*. 1989.

[199] A. T. Kicman, M. C. Parkin, and R. K. Iles, “An introduction to mass spectrometry based proteomics—Detection and characterization of gonadotropins and related molecules,” *Mol. Cell. Endocrinol.*, vol. 260–262, pp. 212–227, Jan. 2007.

[200] P. Kebarle and U. H. Verkerk, “On the Mechanism of Electrospray Ionization Mass Spectrometry (ESIMS),” in *Electrospray and MALDI Mass Spectrometry: Fundamentals, Instrumentation, Practicalities, and Biological Applications: Second Edition*, 2012.

[201] R. B. Cole, Ed., *Electrospray and MALDI Mass Spectrometry : Fundamentals, Instrumentation, Practicalities, and Biological Applications*, 2nd editio. John Wiley and Sons Ltd, 2010.

[202] A. M. Brunner *et al.*, “Benchmarking multiple fragmentation methods on an orbitrap fusion for top-down phospho-proteoform characterization,” *Anal. Chem.*, 2015.

[203] R. A. Zubarev, N. L. Kelleher, and F. W. McLafferty, “Electron capture dissociation of multiply charged protein cations. A nonergodic process,” *Journal of the American Chemical Society*. 1998.

[204] D. F. Hunt, J. J. Coon, M. J. Schroeder, J. E. P. Syka, and J. Shabanowitz, “Peptide and protein sequence analysis by electron transfer dissociation mass spectrometry,” *Proc. Natl. Acad. Sci.*, 2004.

[205] C. Panse, V. Bilan, M. O. Hottiger, M. Leutert, and P. Nanni, “Combining Higher-Energy Collision Dissociation and Electron-Transfer/Higher-Energy Collision Dissociation Fragmentation in a Product-Dependent Manner Confidently Assigns Proteomewide ADP-Ribose Acceptor Sites,” *Anal. Chem.*, vol. 89, no. 3, pp. 1523–1530, 2016.

[206] P. M. Remes *et al.*, “Novel Parallelized Quadrupole/Linear Ion Trap/Orbitrap Tribrid Mass Spectrometer Improving Proteome Coverage and Peptide Identification Rates,” *Anal. Chem.*, vol. 85, no. 24, pp. 11710–11714, 2013.

[207] B. Aslam, M. Basit, M. A. Nisar, M. H. Rasool, and M. Khurshid, “Proteomics: Technologies and Their Applications,” *J. Chromatogr. Sci.*, vol. 55, no. 2, pp. 182–196, 2017.

[208] M. R. Di Falco, “Mass spectrometry-based proteomics,” in *Methods in Molecular Biology*, vol. 1775, 2018.

[209] D. A. Wolters, M. P. Washburn, and J. R. Yates, “An automated multidimensional protein identification technology for shotgun proteomics,” *Anal. Chem.*, 2001.

[210] G. J. Ebrahim, “Clinical proteomics: from diagnosis to therapy Jennifer E. Van Eyk and Michael J. Dunn (eds) Weinheim.,” *J. Trop. Pediatr.*, vol. 55, no. 1, p. 68, 2008.

[211] Z. He and Z. He, “Protein inference in shotgun proteomics,” *Data Min. Bioinforma. Appl.*, pp.

39–49, Jan. 2015.

[212] L. Geiser, A. R. Vaezzadeh, J. M. P. Deshusses, and D. F. Hochstrasser, "Shotgun Proteomics: A Qualitative Approach Applying Isoelectric Focusing on Immobilized pH Gradient and LC-MS/MS," in *Protein Chromatography: Methods and Protocols*, D. Walls and S. T. Loughran, Eds. Totowa, NJ: Humana Press, 2011, pp. 449–458.

[213] N. L. Anderson and N. G. Anderson, "The Human Plasma Proteome: History, Character, and Diagnostic Prospects: Fig. 3.," *Mol. Cell. Proteomics*, 2003.

[214] R. Herzog *et al.*, "Effects of Alanyl-Glutamine Treatment on the Peritoneal Dialysis Effluent Proteome Reveal Pathomechanism-Associated Molecular Signatures," *Mol. Cell. Proteomics*, 2018.

[215] R. A. Zubarev, "The challenge of the proteome dynamic range and its implications for in-depth proteomics," *Proteomics*, 2013.

[216] A. Bodzon-Kulakowska *et al.*, "Methods for samples preparation in proteomic research," *Journal of Chromatography B: Analytical Technologies in the Biomedical and Life Sciences*. 2007.

[217] J. G. Smith and R. E. Gerszten, "Emerging affinity-based proteomic technologies for large-scale plasma profiling in cardiovascular disease," *Circulation*, 2017.

[218] R. E. Gerszten *et al.*, "Challenges in translating plasma proteomics from bench to bedside: update from the NHLBI Clinical Proteomics Programs.," *Am. J. Physiol. Lung Cell. Mol. Physiol.*, 2008.

[219] E. Mostovenko, C. Hassan, J. Rattke, A. M. Deelder, P. A. van Veelen, and M. Palmblad, "Comparison of peptide and protein fractionation methods in proteomics," *EuPA Open Proteomics*, 2013.

[220] S. Daoud, Ed., *Cancer Proteomics: From Bench to Bedside*, 1st Editio. Humana press, 2008.

[221] K. Björhall, T. Miliotis, and P. Davidsson, "Comparison of different depletion strategies for improved resolution in proteomic analysis of human serum samples," *Proteomics*, 2005.

[222] L. A. Beer, B. Ky, K. T. Barnhart, and D. W. Speicher, "In-depth, reproducible analysis of human plasma using IgY 14 and SuperMix immunodepletion," in *Methods in Molecular Biology*, 2017.

[223] R. Kay *et al.*, "Enrichment of low molecular weight serum proteins using acetonitrile precipitation for mass spectrometry based proteomic analysis," *Rapid Commun. Mass Spectrom.*, 2008.

[224] S. E. Warder *et al.*, "Reducing agent-mediated precipitation of high-abundance plasma proteins," *Anal. Biochem.*, 2009.

[225] C. Fernández-Costa, V. Calamia, P. Fernández-Puente, J. L. Capelo-Martínez, C. Ruiz-Romero, and F. J. Blanco, "Sequential depletion of human serum for the search of osteoarthritis biomarkers," *Proteome Sci.*, 2012.

[226] C. Fernández, H. M. Santos, C. Ruíz-Romero, F. J. Blanco, and J. L. Capelo-Martínez, "A comparison of depletion versus equalization for reducing high-abundance proteins in human serum," *Electrophoresis*, 2011.

[227] B. Granvogl, M. Plöscher, and L. A. Eichacker, "Sample preparation by in-gel digestion for mass spectrometry-based proteomics," *Anal. Bioanal. Chem.*, 2007.

[228] J. Rosenfeld, J. Capdevielle, J. C. Guillemot, and P. Ferrara, "In-gel digestion of proteins for internal sequence analysis after one- or two-dimensional gel electrophoresis," *Anal. Biochem.*, 1992.

[229] A. Shevchenko, H. Tomas, J. Havliš, J. V. Olsen, and M. Mann, "In-gel digestion for mass spectrometric characterization of proteins and proteomes," *Nat. Protoc.*, 2007.

[230] H. Kolsrud, H. Malerod, S. Ray, L. Reubsaet, E. Lundanes, and T. Greibrokk, "A Critical Review of Trypsin Digestion for LC-MS Based Proteomics," in *Integrative Proteomics*, 2012.

[231] H. K. Hustoft, L. Reubsaet, T. Greibrokk, E. Lundanes, and H. Malerod, "Critical assessment of accelerating trypsination methods," *J. Pharm. Biomed. Anal.*, 2011.

[232] J. L. Capelo *et al.*, "Overview on modern approaches to speed up protein identification workflows relying on enzymatic cleavage and mass spectrometry-based techniques," *Analytica Chimica Acta*. 2009.

[233] R. Rial-Otero *et al.*, "Sonoreactor-based technology for fast high-throughput proteolytic digestion of proteins," *J. Proteome Res.*, 2007.

[234] H. M. Santos *et al.*, "Improving sample treatment for in-solution protein identification by peptide mass fingerprint using matrix-assisted laser desorption/ionization time-of-flight mass spectrometry," *J. Proteome Res.*, vol. 6, no. 9, pp. 3393–3399, 2007.

[235] C. S. Hughes, S. Foehr, D. A. Garfield, E. E. Furlong, L. M. Steinmetz, and J. Krijgsveld, "Ultrasensitive proteome analysis using paramagnetic bead technology.," *Mol. Syst. Biol.*, 2014.

[236] S. R. Gallagher, "One-dimensional SDS gel electrophoresis of proteins," *Curr. Protoc. Protein Sci.*, 2012.

[237] R. Smith, "Two-Dimensional Electrophoresis: An Overview," in *Two-Dimensional Electrophoresis Protocols*, D. Sheehan and R. Tyther, Eds. Humana Press, 2009, pp. 3–17.

[238] L. P. Kihm *et al.*, "Benfotiamine Protects against Peritoneal and Kidney Damage in Peritoneal Dialysis," *J. Am. Soc. Nephrol.*, 2011.

[239] A. Drabik and A. Bodzoń-Kułakowska, "Gel Electrophoresis," *Proteomic Profiling Anal. Chem.*, pp. 115–143, Jan. 2016.

[240] R. M. M. Branca *et al.*, "HiRIEF LC-MS enables deep proteome coverage and unbiased proteogenomics," *Nat. Methods*, 2014.

[241] J. Li, W. Han, and Y. Yu, "Chromatography Method," in *Protein Engineering - Technology and Application*, T. Ogawa, Ed. 2013, pp. 33–61.

[242] M. Aguilar, *HPLC of Peptides and Proteins: Methods and Protocols*, vol. 251. 2004.

[243] S. C. Moldoveanu, V. David, S. C. Moldoveanu, and V. David, "Basic Information Regarding the HPLC Techniques," *Sel. HPLC Method Chem. Anal.*, pp. 87–187, Jan. 2017.

[244] T. Liu, C. H. Borchers, J. Pan, C. E. Parker, H. Li, and J. Han, "Current trends in quantitative proteomics - an update," *J. Mass Spectrom.*, vol. 52, no. 5, pp. ii–ii, 2017.

[245] N. Pappireddi, L. Martin, and M. Wühr, "A Review on Quantitative Multiplexed Proteomics," *ChemBioChem*, 2019.

[246] N. Rauniyar and J. R. Yates, "Isobaric labeling-based relative quantification in shotgun proteomics," *Journal of Proteome Research*. 2014.

[247] J. R. Yates, C. I. Ruse, and A. Nakorchevsky, "Proteomics by Mass Spectrometry: Approaches, Advances, and Applications," *Annu. Rev. Biomed. Eng.*, 2009.

[248] S. P. Gygi, B. Rist, S. A. Gerber, F. Turecek, M. H. Gelb, and R. Aebersold, "Quantitative analysis of complex protein mixtures using isotope-coded affinity tags," *Nat. Biotechnol.*, 1999.

[249] C. H. Becker and M. Bern, "Recent developments in quantitative proteomics," *Mutat. Res.* -

Genet. Toxicol. Environ. Mutagen., 2011.

[250] ThermoFisher Scientific, "Proteome Discoverer™ Software," *Thermofisher.Com*, no. June, 2017.

[251] B. Deracinois, C. Flahaut, S. Duban-Deweer, and Y. Karamanos, "Comparative and Quantitative Global Proteomics Approaches: An Overview," *Proteomes*, 2013.

[252] D. A. Megger *et al.*, "Comparison of label-free and label-based strategies for proteome analysis of hepatoma cell lines," *Biochim. Biophys. Acta - Proteins Proteomics*, 2014.

[253] M. Bantscheff, M. Schirle, G. Sweetman, J. Rick, and B. Kuster, "Quantitative mass spectrometry in proteomics: a critical review," *Anal. Bioanal. Chem.*, vol. 389, no. 4, pp. 1017–1031, 2007.

[254] V. C. Wasinger, M. Zeng, and Y. Yau, "Current Status and Advances in Quantitative Proteomic Mass Spectrometry," *Int. J. Proteomics*, 2013.

[255] J. R. Yates, "Mass Spectral Analysis in Proteomics," *Annu. Rev. Biophys. Biomol. Struct.*, 2004.

[256] K. Chandramouli and P.-Y. Qian, "Proteomics: Challenges, Techniques and Possibilities to Overcome Biological Sample Complexity," *Hum. Genomics Proteomics*, 2009.

[257] M. Riffle and J. K. Eng, "Proteomics data repositories," *Proteomics*. 2009.

[258] R. Craig, J. P. Cortens, and R. C. Beavis, "Open source system for analyzing, validating, and storing protein identification data," *J. Proteome Res.*, 2004.

[259] E. W. Deutsch, H. Lam, and R. Aebersold, "PeptideAtlas: A resource for target selection for emerging targeted proteomics workflows," *EMBO Reports*. 2008.

[260] L. Martens *et al.*, "PRIDE: The proteomics identifications database," *Proteomics*, 2005.

[261] L. Ji *et al.*, "NCBI Peptidome: A new repository for mass spectrometry proteomics data," *Nucleic Acids Res.*, 2009.

[262] J. A. Vizcaíno, J. M. Foster, and L. Martens, "Proteomics data repositories: Providing a safe haven for your data and acting as a springboard for further research," *Journal of Proteomics*. 2010.

[263] Y. Perez-Riverol, E. Alpi, R. Wang, H. Hermjakob, and J. A. Vizcaíno, "Making proteomics data accessible and reusable: Current state of proteomics databases and repositories," *Proteomics*. 2015.

[264] S. Pundir, M. J. Martin, and C. O'Donovan, "UniProt protein knowledgebase," in *Methods in Molecular Biology*, 2017.

[265] A. Schmidt, I. Forne, and A. Imhof, "Bioinformatic analysis of proteomics data," *BMC systems biology*. 2014.

[266] A. Bateman *et al.*, "UniProt: The universal protein knowledgebase," *Nucleic Acids Res.*, 2017.

[267] D. R. Zerbino *et al.*, "Ensembl 2018," *Nucleic Acids Res.*, 2018.

[268] M. Ashburner *et al.*, "The Gene Ontology Consortium. Gene ontology: tool for the unification of biology," *Nat. Genet.*, 2011.

[269] T. Zhou, J. Yao, and Z. Liu, "Gene Ontology, Enrichment Analysis, and Pathway Analysis," *Bioinforma. Aquac.*, pp. 150–168, 2017.

[270] S. Maere, K. Heymans, and M. Kuiper, "BiNGO: A Cytoscape plugin to assess overrepresentation of Gene Ontology categories in Biological Networks," *Bioinformatics*, 2005.

[271] X. Zhou and Z. Su, “EasyGO: Gene Ontology-based annotation and functional enrichment analysis tool for agronomical species,” *BMC Genomics*, 2007.

[272] A. Subramanian *et al.*, “Gene set enrichment analysis: a knowledge-based approach for interpreting genome-wide expression profiles.,” *Proc. Natl. Acad. Sci. U. S. A.*, 2005.

[273] A. Subramanian, H. Kuehn, J. Gould, P. Tamayo, and J. P. Mesirov, “GSEA-P: A desktop application for gene set enrichment analysis,” *Bioinformatics*, 2007.

[274] C. Backes *et al.*, “GeneTrail-advanced gene set enrichment analysis,” *Nucleic Acids Res.*, 2007.

[275] X. Jiao *et al.*, “DAVID-WS: A stateful web service to facilitate gene/protein list analysis,” *Bioinformatics*, 2012.

[276] S. Grossmann, S. Bauer, P. N. Robinson, and M. Vingron, “Improved detection of overrepresentation of Gene-Ontology annotations with parent-child analysis,” *Bioinformatics*, 2007.

[277] A. Alexa, J. Rahnenführer, and T. Lengauer, “Improved scoring of functional groups from gene expression data by decorrelating GO graph structure,” *Bioinformatics*, 2006.

[278] M. Kanehisa, S. Goto, Y. Sato, M. Furumichi, and M. Tanabe, “KEGG for integration and interpretation of large-scale molecular data sets,” *Nucleic Acids Res.*, 2012.

[279] D. Croft *et al.*, “Reactome: A database of reactions, pathways and biological processes,” *Nucleic Acids Res.*, 2011.

[280] P. D. Thomas *et al.*, “PANTHER: a library of protein families and subfamilies indexed by function.,” *Genome Res.*, 2003.

[281] D. Ficenec *et al.*, “Computational knowledge integration in biopharmaceutical research.,” *Brief. Bioinform.*, 2003.

[282] I. Letunic, T. Yamada, M. Kanehisa, and P. Bork, “iPath: interactive exploration of biochemical pathways and networks,” *Trends in Biochemical Sciences*. 2008.

[283] R. Malik, K. Dulla, E. A. Nigg, and R. Körner, “From proteome lists to biological impact- tools and strategies for the analysis of large MS data sets,” *Proteomics*. 2010.

[284] M. Persico, A. Ceol, C. Gavrila, R. Hoffman, A. Florio, and G. Cesareni, “HomoMINT: An inferred human network based on orthodology mapping of protein interactions discovered in model organisms,” *BMC Bioinformatics*, 2005.

[285] R. Oughtred *et al.*, “The BioGRID interaction database: 2019 update,” *Nucleic Acids Res.*, 2019.

[286] S. Kerrien *et al.*, “IntAct - Open source resource for molecular interaction data,” *Nucleic Acids Res.*, 2007.

[287] T. S. Keshava Prasad *et al.*, “Human Protein Reference Database - 2009 update,” *Nucleic Acids Res.*, 2009.

[288] D. Szklarczyk *et al.*, “The STRING database in 2017: Quality-controlled protein-protein association networks, made broadly accessible,” *Nucleic Acids Res.*, 2017.

[289] P. Shannon *et al.*, “Cytoscape: a software environment for integrated models of biomolecular interaction networks.,” *Genome Res.*, 2003.

[290] M. Bastian, S. Heymann, and M. Jacomy, “Gephi : An Open Source Software for Exploring and Manipulating Networks Visualization and Exploration of Large Graphs,” *Int. AAAI Conf. Weblogs Soc. Media*, 2009.

[291] E. Zúñiga-León, U. Carrasco-Navarro, and F. Fierro, “NeVOmics: An Enrichment Tool for Gene

Ontology and Functional Network Analysis and Visualization of Data from OMICs Technologies," *Genes (Basel).*, 2018.

[292] P. Sinitcyn, J. D. Rudolph, and J. Cox, "Computational Methods for Understanding Mass Spectrometry–Based Shotgun Proteomics Data," *Annu. Rev. Biomed. Data Sci.*, 2018.

CHAPTER II. OBJECTIVES, WORKING PLAN AND THESIS OUTPUT

1-Objectives

Although a number of molecules have been identified as being involved in PM alterations, a global peptidomics/proteomics study to identify biomarkers of PM alterations has not yet been fully addressed. The present project is aimed at revealing novel peptides and proteins involved in peritoneal changes in patients on long-term peritoneal dialysis, helping in the early detection of such alterations and delaying UFF. Moreover, the study is primarily focused towards proteins highlighting signs of peritoneal processes of lesion. The analysis of PDE based on peptidomics and proteomics is projected to allow identification of new biomarkers for the early detection of peritoneal changes in patients of long-term peritoneal dialysis. Thus, the objectives are:

- Elaborate an atlas of the evolution of the proteome and peptidome content of the peritoneal dialysate (P3DEVOATLAS) during PD, which is potentially valuable for clinical diagnosis and prognosis.
- Link the changes observed in the P3DEVOATLAS with other medical variables of the peritoneal membrane and some candidate biomarkers present on PDE, such as, cancer antigen 125, plasminogen activator inhibitor 1, and interleukin 6, etc. These are some examples of candidate effluent biomarkers in PD that have been already proposed, as can be seen in Table 4.1 (Section 4.1, Chapter I).
- Establish relative/absolute quantitative relations between peptides / proteins to unravel potential biomarkers of peritoneal changes in patients on long-term PD;
- Integration of the P3DEVOATLAS in the understanding of the global biochemistry processes involved in the evolution of the peritoneal membrane.

2-Working Plan

Pre-analytical considerations

A group of ten new patients in the first year of PD and ten others in the second year but still within the first stage of PD have been followed for 3 years. In addition, another 20 patients already at different stages of dialysis have been followed during the same period. For all the patients in the beginning of PD, samples were taken after the first month of dialysis, when the first peritoneal equilibration test (PET) was done. Then, samples were taken 6 months after the first PET, one year after the second PET and one year after the third PET. For those patients already at different stages of dialysis, samples have been taken once a year. Additionally, patients were grouped according to the peritoneal transport characteristics based on the PET into (i) fast, (ii) fast-average, (iii) slow-average and (iv) slow transporter.

Samples were collected at the Hospital Garcia de Orta, Portugal. A proteases inhibitor cocktail was added to the samples and then samples were preserved on ice until centrifugation. Once in the laboratory, the samples were centrifuged, aliquoted and then stored at -80ºC until further analysis. Afterwards the PDE was submitted to ultrafiltration with a 10kDa cut-off membrane, thus the peptidome fraction (MW<10 kDa) and the proteome fraction (MW>10 kDa) were obtained.

Work-package 1 – To elaborate a proteome atlas of peritoneal changes in patients on long-term PD (P3DEVOATLAS).

The proteome fraction (MW > 10 kDa) was studied and analysed using different proteomic techniques in order to evaluate sample complexity. Thus, different methodologies of protein depletion (to diminish/remove high abundance proteins) and protein/peptides fractionation techniques were assessed to improve the coverage of the proteome fraction.

Deliverables: Methodologies to diminish sample complexity and improve proteome coverage. List of proteins differentially expressed across time-points. Linking these proteins to membrane evolution for diagnostics and prognosis.

Work-package 2 – Development of a peptidome atlas of peritoneal changes in patients on long-term PD (P3DEVOATLAS).

The term peptidome refers to the study of naturally occurring peptides. These peptides present in the peptidome fraction (MW<10 kDa) were pre-concentrated and cleaned by strong cation-exchange solid-phase extraction (SCX-SPE), then resulting peptide mixtures were analysed by LC-MS/MS on an Orbitrap Fusion mass spectrometer. All MS/MS spectra data were processed with Proteome Discoverer

(v2.2) using the PMI-Byonic node (V3.2.0) and Data files were searched for in the UniProt human canonical database (November 2018; 42,344 entries).

Samples from different time-points were analysed and the number and class of peptides identified followed. Evolution over time was estimated with Label free quantification of peptides using the sample taken first within the sampling plan as reference.

Deliverables: List of peptides differentially expressed over time. Elaboration of a relative scale of peptide abundance linked to membrane evolution for diagnostic use.

Work-package 3 – Establish relative quantitative relations between proteins to unravel potential biomarkers of peritoneal changes in patients on long-term PD

Proteins were quantified using TMT10plex. The TMT quantification data was used to elaborate a scale of membrane evolution similar to the one done in work-package 1 to assists physicians in diagnosis and prognosis.

Deliverables: Quantitative Scale of membrane evolution as a function of differentially expressed proteins.

Work-package 4 – Integration of peptidome/proteome biomarkers for diagnosis and prognosis of peritoneal changes

Data analysis was carried out integrating the data obtained in the previous work-packages using data mining software such as Cytoscape and Reactome plug-in, in order to identify peptides and or proteins that may indicate and predict changes in the peritoneal membrane in patients on long-term peritoneal dialysis.

Deliverables: Final elaboration of the P3DEVOATLAS. Biochemical and medical integration of all data obtained in work-packages 1 to 3. Elaboration of a theory to explain peritoneal membrane degradation with time. Proposal of potential therapies to extend the lifespan of peritoneal dialysis.

3-Thesis Output

3.1-Papers published in international scientific journals

3- *Title*: Classifying patients in peritoneal dialysis by mass spectrometry-based profiling

Authors: J. E. Araújo, S. Jorge, R. Magriço, A. Ramos, F. Teixeira-Costa, M. Reboiro-Jato, F. Fdez-Riverola, C. Lodeiro, J. L. Capelo, H. M. Santos

Journal: Talanta (2016) DOI: 10.1016/j.talanta.2016.02.026

Presented in Chapter V

2- *Title*: A cost-effective method to get insight into the peritoneal dialysate effluent proteome

Authors: J. E. Araújo, S. Jorge, F. Teixeira-Costa, A. Ramos, C. Lodeiro, H. M. Santos, J. L. Capelo

Journal: Journal of Proteomics (2016) DOI: 10.1016/j.jprot.2016.05.010

Presented in Chapter IV

1- *Title*: Matrix-assisted laser desorption/ionization time-of-flight mass spectrometry-based profiling as a step forward in the characterization of peritoneal dialysis effluent

Authors: J. E. Araújo, T. Santos, S. Jorge, T. M. Pereira, M. Reboiro-Jato, R. Pavón, R. Magriço, F. Teixeira-Costa, A. Ramos, H. M. Santos

Journal: Analytical Methods (2015) DOI: 10.1039/C5AY00620A

Presented in Chapter III

3.2-Paper in preparation

1- *Title*: In-depth analysis of peritoneal dialysis effluent proteome and peptidome: a longitudinal follow-up study

Authors: J. E. Araújo, R.M. Branca, I. Siavelis, G. Mermelekas, M. Pernemalm, M. Stahl, M. Sousa,.F. Teixeira-Costa, A. Ramos, H. M. Santos, J. L. Capelo, J. Lehtiö

In preparation, Presented in Chapter VI

3.3-Participation in national and international conferences

7. *Title*: Proteomics analysis of the peritoneal dialysis effluent by HiRIEF and TMT: a longitudinal study

Authors: J. E. Araújo, R.M.M. Branca, F. Teixeira e Costa, A. Ramos, M. Pernemalm, C. Lodeiro, J. L. Capelo, J. Lehtio
Congress: XII Eupa Congress, Translating genomes into biological functions, June 16th – June 20th, Spain, EUPA 2018
Participation: Poster presentation

6. *Title*: Unraveling peritoneal dialysis effluent proteome through cost-effective sample treatment methods applied to biomarkers discovery and MALDI-MS-based profiling techniques
Authors: J. E. Araújo, S. Jorge, F. Teixeira e Costa, A. Ramos, H. M. Santos, C. Lodeiro, J. L. Capelo
Congress: 2nd International Caparica Christmas Congress on Translational Chemistry, December 4th – December 7th, Portugal, IC3TC 2017
Participation: Poster presentation

5. *Title*: Unraveling peritoneal dialysis effluent proteome evolution
Authors: J. E. Araújo, H. López-Fernández, S. Jorge, F. Teixeira e Costa, Aura Ramos, Anabela Rodrigues, Gert Mayer, H. M. Santos, J. L. Capelo
Congress: Sao Paulo School of Advanced Science on Mass Spectrometry-based Proteomics, August 28th – September 6th, Brazil, SPSAS-MS 2017
Participation: Poster presentation

4. Title: An open-source software for fast and automatic processing of 2D-Gel and MALDI-based mass spectrometry protein data
Authors: J. E. Araújo, H. López-Fernández, D. Glez-Peña, M. Reboiro-Jato, F. Fdez- Riverola, J. L. Capelo-Martínez
Congress: EuBIC Winter School on proteomics bioinformatics, 10th-13th, Semmering – Austria, EUBIC 2017
Participation: Poster presentation

3. Title: Fast processing of 2D-gel and MALDI-based mass spectrometry protein data
Authors: H. López-Fernández, J. E. Araújo, Daniel Glez-Peña, M. Reboiro-Jato, Florentino Fdez-Riverola, José L. Capelo-Martínez
Congress: 2nd International Caparica Christmas Conference on Sample Treatment, 5th-7th December 2016, Caparica – Portugal, IC3ST 2016
Participation: Poster presentation

2.Title: Estudo Longitudinal do Efluente de Diálise Peritoneal
Authors: J. E. Araújo; Teixeira e Costa; Hugo Miguel Santos; Rita Magriço; José Luís Capelo; Ricardo Macau; Aura Ramos

Congress: Encontro Renal 2015, Sociedade Portuguesa de Nefrologia, 15th -18thApril, Vilamoura – Portugal

Participation: Slide Poster presentation

1.Title: MALDI mass spectrometry-based profiling of peritoneal dialysis effluent

Authors: J. E. Araújo, T. Santos, S. Jorge, T. Pereira, M. Reboiro-Jato, F. Riverola, C. Lodeiro, J. L. Capelo, H.M. Santos

Congress: 2nd NanoDay "NanoAtlantic: Brazil@Portugal meets NanoBIOScience", 12th of September, Caparica – Portugal, 2014

Participation: Oral presentation

CHAPTER III. MATRIX-ASSISTED LASER DESORPTION/IONIZATION TIME-OF-FLIGHT MASS SPECTROMETRY-BASED PROFILING AS A STEP FORWARD IN THE CHARACTERIZATION OF PERITONEAL DIALYSIS EFFLUENT[1]

[1] Araújo JE, Santos T, Jorge S, Pereira TM, Reboiro-Jato M, Pavón R, Magriço R, Teixeira- F, Ramos A, Santos HM (2015) Analytical Methods, 7, 7467. DOI: 10.1039/c5ay00620a

Abstract

The aim of this study was to differentiate patients with glomerulonephritis and diabetic nephropathy using (i) peritoneal dialysate effluent, (ii) matrix-assisted laser desorption/ionization time-of-flight mass spectrometry (MALDI-TOF MS) and (iii) bioinformatics tools. Profiles of peritoneal dialysate effluent were obtained using (a) sample preparation consisting of protein concentration through centrifugal concentrators and chemical-assisted protein depletion using DL-dithiothreitol, and (b) MALDI-TOF MS. A free open-source bioinformatics tool, Mass-UP, was used to classify such profiles using principal component analysis and hierarchical clustering. The methodology proposed here allows for classifying two different groups of patients with kidney failure, one with chronic glomerulonephritis and other with diabetic nephropathy.

Keywords: N/A

1-Introduction

The utilization of profiles to classify samples has been used in analytical chemistry since decades ago [1]-[3]. In proteomics, mass spectrometry, MS, profiling of complex proteomes comprises three main steps. First, an appropriate sample treatment developed for each particular type of sample is needed. Second, an adequate mass spectrometer is necessary. High throughput, cost-effectiveness and robustness are characteristics of Matrix-Assisted Laser Desorption Ionization time of flight (MALDI)-based MS [4]. Third, bioinformatics tools are needed, either through commercial or free/open-source software to handle large sets of data provided by MALDI-MS-based profiling. As both, bioinformatics and MALDI-MS have reached maturity, currently the bottleneck in proteome profiling remains sample treatment. Recently, our group has proposed a number of fast, cheap and robust methods to deplete and/or to equalize the protein content of serum samples to speed disease profiling for patient classification and diagnostic purposes [5]. Renal insufficiency is a medical condition in which the kidneys fail to filter waste products adequately from the blood, eventually leading to death. Therapy for renal failure can be done by effective methods such as peritoneal dialysis (PD) and haemodialysis, both of which effectively remove waste products from blood [6]-[9]. Indeed, PD is a highly effective, convenient and reasonably safe treatment modality for patients with end-stage renal disease. PD is based on the use of the peritoneal membrane as a replacement of the kidney. This is possible because the peritoneal membrane can function as a dialyzing membrane, allowing it to mimic the kidney capabilities for cleaning solutes and waste products from the blood [10],[11]. Although PD replaces the function of the kidney, pathologic damage to the peritoneum frequently results in decrease of the dialysing capacity and then, the patient is forced to move to haemodialysis. At this stage, the patient's condition gets worst slowly but constantly, leading to the death of the patient [11]-[13].Peritoneal dialysate effluent (PDE) renders a sample rich in proteins and metabolites. This sample is a potential source of clinician information and, as such, it deserved to be interrogated for diagnosis and classification purposes. This

work presents a novel approach to such aims based first on protein separation and concentration using centrifugal concentrators and then on protein equalization using DL-dithiothreitol, DTT. Then, the samples are trypsinated using a fast ultrasonic approach reported by us previously [14]. Finally, the pool of peptides is profiled using MALDI-MS and then the sets of data generated are treated with free/open-source software by principal component analysis and hierarchical clustering (Mass-Up: http://sing.ei.uvigo.es/mass-up/ last time accessed June, 2015). As a proof-of-concept, peritoneal dialysate collected from patients with diabetic nephropathy and chronic glomerulonephritis was used.

2-Materials and methods

2.1-Reagents

All reagents used were of HPLC grade or electrophoresis grade. Albumin, from bovine serum (BSA), N, N, N', N'-tetramethylethylene-diamine (TMED), glycine, b-mercaptoethanol, glycerol 86–88%, acrylamide/bis-acrylamide 30% solution (37.5:1), mineral oil, the bradford reagent, DL-dithiothreitol (DTT), iodoacetamide (IAA), sodium fluoride (NaF), trifluoroacetic acid (TFA), trypsin (proteomics grade) and acetonitrile (ACN, LC-MS CHROMASOLV(R)) were purchased from Sigma-Aldrich (St. Louis, USA). EDTA and bromophenol blue were purchased from Riedel-de Haen (Seelze, Germany). Ammonium bicarbonate (Ambic) and formic acid were purchased from Fluka (Steinheim, Germany). α-Cyano-4-hydroxycinnamicacid puriss for MALDI-MS (Fluka, Germany) was used as the MALDI matrix. Peptide calibration standard II from Bruker Diatonic GmbH was used as the mass calibration standard for MALDI-TOF MS.

2.2-Peritoneal dialysate effluent samples

Peritoneal dialysis effluent samples from ten anonymous patients from the Garcia de Orta Hospital, Portugal were collected in centrifuge sterile tubes supplemented with sodium fluoride and EDTA. Four patients with glomerular chronic nephritis, GNC, and six with diabetic nephropathy, DN, were enrolled in this study. For further details, refer to Table 1 of the supplementary material. The patients were informed about the project and their consent was requested in written. Once in the laboratory, the samples were centrifuged at 9000g for 20 min to remove insoluble solids and stored at -80 ºC until use.

2.3-Apparatus

PDE samples were collected and aliquoted in centrifuge sterile tubes of 50 mL and 15 mL, respectively (Ratiolab, Germany). Protein concentration was done in Vivaspin centrifugal concentrators of 50 mL from Sartorius Stedim Biotech (Bohemia, U.S.A.) and protein digestion was done in safe-lock tubes of 0.5 mL from Eppendorf (Hamburg, Germany). A vacuum concentrator centrifuge model UNIVAPO 150 ECH SpeedVac and a vacuum pump model UNIJET II (Munich, Germany) were used

for sample drying and sample pre-concentration. A mini incubator from Labnet (New Jersey, U.S.A.) was used for protein reduction and for protein alkylation steps. Centrifuge MPW-350 from MPW Med. Instruments (Warsaw, Poland), vortex models ELMI CM70M-09 Sky Line (Southern California, U.S.A.) and Labnet vortex mixer VX-200 (New Jersey, U.S.A.) were used throughout the sample treatment. An ultrasonic bath, Elma model Transsonic TI-H-5 (Singen, Germany), was used to facilitate protein depletion and peptide solubilization. A sonoreactor model UTR200 from Dr Hielscher (Teltow, Germany) was used to accelerate enzymatic protein digestions. Protein identification was done in an Ultraflex II MALDI-TOF/TOF instrument from Bruker Daltonics.

2.4-Peritoneal dialysate concentration

PDE concentration and desalting was performed in centrifugal concentrators Vivaspin 15R MWCO 10 kDa. 10 mL of PDE were concentrated until a final volume ranging from 150 µL to 300 µL, by centrifugation at 5000 × g for 20 min at 4 ºC. The concentrated PDE was transferred into a clean safe-lock tube. The Vivaspin 15R MWCO 10 kDa membrane was washed with 50 mL of MQ-Water and then the water was added to the safelock tube with the concentrated PDE (Figure 1). The total protein content was determined using a Bradford protein assay. Once the samples were quantified, they were divided into aliquots of 20 µL and stored in 0.5 mL safe-lock tubes at -80 ºC.

2.5-Protein depletion with DTT

Protein depletion from sera samples was performed with DTT according to the protocol described by Warder et al.[15] with minor modifications as described by Fernández et al. [16]. In brief, to 20 mL of serum, 2.2 µL of 500 mM DTT were added and the resulting mixture was vortexed for 20 s. The samples were then incubated for 1 h until a white precipitate was observed. Then, the samples were pelleted by centrifugation at 14 000 × g (2 × 20 min at 18 ºC). This process was performed with five aliquots for each patient. Then, the supernatants were pooled in a clean safe-lock tube and the total protein content was determined using a Bradford protein assay, using BSA as the standard protein.

2.6-2D gel electrophoresis

The samples were resuspended in 8 M urea, 2% (w/v) CHAPS, 0.2% (v/v) IPG buffer pH 4–7, 50 mM DTT and traces of bromophenol blue. The samples were incubated on ice for 30 min and sonicated using a 1 mm diameter probe for 6 × 10 seconds on ice at 50% sonication amplitude. Insoluble matter was removed by centrifugation (20 minutes 14 000 × g at 20 ºC). The protein concentration was determined using a Bradford protein assay using BSA as the protein standard. IPG strips, pH 4–7 and 7 cm size, were rehydrated overnight at 20 ºC with 135 mL of rehydration

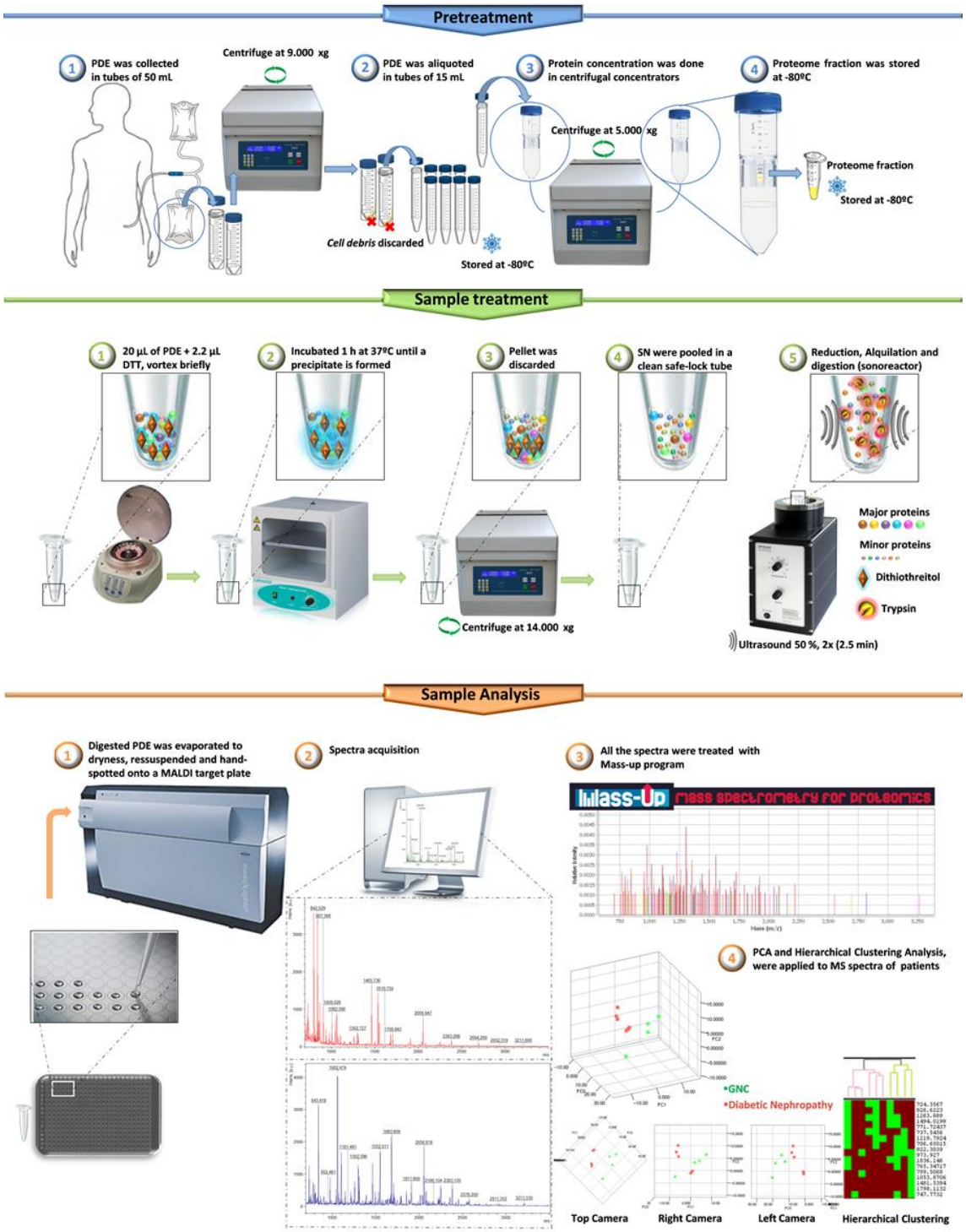

Figure 1- PDE sample treatment chart. (1) Concentration of proteins: the protein content of 10 mL of PDE is concentrated to *ca*. 150 µL using protein concentration tubes Vivaspin 15R MWCO 10 kDa. (2) Protein depletion: the sample treatment to equalize the proteome content consists of DTT depletion. The resulting pellet is discarded and the supernatant (SN) is withdrawn and stored at -80 ºC until analysis. (3) Sample trypsination: samples are digested using the ultrafast protein digestion, which was performed in a sonoreactor with the following operating conditions: 50% ultrasonic amplitude and 2.5 min ultrasonic time (twice). Then, the sample was vacuum centrifuged until dryness. (4) MALDI Profiling: for sample analysis, the peptides were re-suspended, hand-spotted onto a MALDI target plate and analyzed by MALDI-TOF MS. Finally, the Mass-Up program was used, as it was designed to support the pre-processing [(i) baseline correction; (ii) normalization; (iii) smoothing; (iv) peak detection; (v) peak matching] and analysis of MALDI-TOF mass spectrometry data through principal component analysis and hierarchical clustering analysis.

buffer containing 8 M urea, 0.5% (w/v) CHAPS, 0.2% (v/v) IPG buffer pH 4–7, 10 mM DTT and traces of bromophenol blue. Sample loading onto the IPG strip was carried out using the cup-loading method. IPG strips were removed from the rehydration tray; the oil was drained, and the gel was placed side up into the focusing tray's channels. The movable electrode assemblies were carefully positioned on top of the strips at the anode and cathode ends; after that, the sample loading cups were placed near the cathode. Afterwards, 50 mL of the protein-containing solution (2 mg mL -1) were loaded in the sample-loading cup and then overlaid with mineral oil. The focusing tray was placed into the PROTEAN IEF Cell. The isoelectric focusing was performed in three steps as follows: step 1: 250 volts for 30 min, rapid voltage ramping; step 2: 4000 volts for 60 min, slow voltage ramping; step 3: 4000 volts, 7468 | 10 000 V h. For the three steps, the current was limited to 50 mA per gel. After IEF, gel strips were removed and incubated with equilibration buffer (6 M urea, 75 mM Tris pH 8.8, 20% glycerol (v/v), 2% (w/v) SDS, and traces of bromophenol blue) and then again incubated with 2.5 mL of equilibration buffer containing 2% (w/v) of DTT for 15 min, followed by another 15 minutes' incubation with 2.5 mL of equilibration buffer containing 2.5% (w/v) of IAA. The IPG strips were removed from the equilibration tray and clipped briefly into a graduated cylinder containing running buffer. The strip was placed side up and onto the back plate of the SDS-PAGE gel. The IPG well of the gel was overlaid with agarose sealing solution (0.5% w/v prepared with 50 mL of Laemmli running buffer and traces of bromophenol blue). After agarose solidification, the electrophoresis was conducted at 200 V (constant voltage) for 55 minutes. After completion of the gel electrophoresis, the gel was mixed for 30 minutes with 40% (v/v) ethanol and 10% (v/v) acetic acid and then stained overnight with colloidal coomassie blue G-250. Gels were rinsed for 4 × 20 min with 100 mL of distilled water and further washed twice with 100 mL of 0.5 M sodium chloride until a clear background was observed. Gel imaging was carried out with a ProPicII-robot using 16 ms of exposure time and a resolution of 70 mm. Gel piking was done with the same equipment.

2.7-In-gel protein digestion

After spot piking, the spots were transferred to 0.5 mL low adhesion tubes. Gel spots were washed twice with 200 µL of water and then with 3 × 200 µL of 50% (v/v) acetonitrile/25 mM ammonium bicarbonate and sonicated at 60% ultrasonic amplitude for 10 min using an ultrasonic bath. Then, the gel pieces were dehydrated with 200 µL of acetonitrile. Subsequently, 15 µL of trypsin (20 ng mL^{-1} in ammonium bicarbonate 12.5 mM/2% (v/v) acetonitrile) was added to the gel spots and incubated for 60 min on ice, then covered with 20 mL of 12.5mM ammonium bicarbonate/2% (v/v) acetonitrile and incubated for 12 h at 37 ºC. Finally, 25 mL of 5% (v/v) formic acid was added and the supernatants were transferred to new low adhesion tubes. Peptides were further extracted from the gel matrix with 2 × 50 mL of 50% (v/v) acetonitrile/0.1% trifluoroacetic acid and sonicated at 60% ultrasonic amplitude for 5 min using an ultrasonic bath. The samples were dried-down and stored at -20 ºC until MALDI-TOF MS analysis.

2.8-In-solution protein digestion

Ultrasonic in-solution digestion was performed according to the ultrafast proteolytic digestion protocol previously developed in our laboratory [17]. Before protein digestion, the pH of the samples obtained in Section 2.5 was adjusted to 8.0 by adding 1 µL of 0.5 M Ambic. Protein disulfide bonds were reduced with 2 µL of 110 mM DTT, samples were then vortexed and incubated for 45 min at 37 ºC. The resulting cysteines were then blocked with 2 µL of 400 mM IAA. The samples were vortexed and incubated for 45 min at room temperature in the dark. For protein digestion, the reduced and alkylated samples were diluted to 0.04 mg mL^{-1} (2 mg of protein in a volume of 50 mL of 12.5 mM AmBic). Afterwards, trypsin was added twice according to the ratio 1:20 (w/w) (addition of 2.5 µL of trypsin, ultrasonic sonoreactor digestion, addition of another 2.5 µL of trypsin and then a final ultrasonic digestion with the sonoreactor). Once the trypsin was added, the digestion was performed in the sonoreactor with the following operating conditions: 50% ultrasonic amplitude and 2.5 min ultrasonic time. Finally, 5 µL of formic acid 50% (v/v) were added to stop the enzymatic activity (Figure 1), and the digested PDE was evaporated to dryness.

2.9-MALDI-TOF-MS analysis

Prior to analysis, samples were solubilized in 10 µL of 0.3% formic acid and 0.5 mL of sample was hand-spotted onto a MALDI target plate (384-spot ground steel plate) and then 1 µL of a 7 mg mL^{-1} solution of a-cyano-4-hydroxycinnamic acid matrix in 0.1% (v/v) TFA and 50% (v/v) ACN was added and allowed to air dry. The mass spectrometer was operated in positive ion mode using a reflectron, and thus, spectra were acquired in the m/z range of 600–3500. A total of 500 spectra were acquired for each sample at a laser frequency of 50 Hz. External calibration was performed with the $[M + H]^+$ monoisotopic peaks of bradykinin 1–7 (m/z 757.3992), angiotensin II (m/z 1046.5418), angiotensin I (m/z 1296.6848) substance P (m/z 1758.9326), ACTH clip 1–17 (m/z 2093.0862), ACTH18–39 (m/z 2465.1983) and somatostatin 28 (m/z 3147.4710). Peptide mass fingerprints (PMF) were searched with MASCOT search engine with the following parameters: (i) SwissProt Database2012_04 (535698 sequences; 190107059 residues); (ii) molecular weight of protein: all; (iii) one missed cleavage; (iv) fixed modifications: carbamidomethylation (C); (v) variable modifications: oxidation of methionine and (vi) peptide tolerance up to 100 ppm after close-external calibration. The significance threshold was set to a minimum of 95% (p # 0.05). A match was considered successful when the protein identification score is located out of the random region and the protein analysed scores first.

2.10-Principal component analysis (PCA)

Each sample was spotted in the MALDI plate five times. The corresponding raw-data spectrum of each sample was pre-processed with the Mass-Up open source program (http:// sing.ei.uvigo.es/mass-up/) using the following parameters: (i) intensity transformation (square root), (ii) smoothing (none),

(iii) baseline correction (snip), (iv) standardization (total ion current), (v) peak detection (MALDIquant: SNR (3), Half-WindowSize (60)), and (vi) minimum peak intensity (0.001). Peaks were matched with the following parameters: (i) intrasample matching (MALDIquant: tolerance (0.002)), without the selection of the "generate consensus spectrum" box, and (ii) inter-sample matching (MALDIquant: tolerance (0.002)). Then, the PCA was run with the following parameters: (i) max. components (-1, for no maximum number of components), (ii) variance covered (0.95), (iii) normalize, and (iv) discretize.

2.11-Hierarchical clustering analysis

An agglomerative hierarchical clustering analysis was applied as a complement to the PCA. Using the same handling of data as described above for the PCA, the clustering analysis operation of the Mass-Up software was executed with the following parameters: (i) minimum variance (0), (ii) peptide list (null), (iii) distance function type reference (average), (iv) conversion values (presence), distance function type function (hamming), and (v) intra-sample minimum presence (0), deep clustering (no).

3-Results and discussion

3.1-Sample treatment

Unravelling the peritoneal dialysate effluent, PDE, proteome presents some challenges in terms of sample treatment, as PDE is a relatively diluted solution of proteins, containing hundreds of them, with their concentrations spanning several orders of magnitude. To overcome this problem, concentrating low abundance proteins whilst diluting high abundance ones is mandatory. In our case, such tasks were accomplished as follows. First, we focused in concentrating the proteins. Proteins can be separated and concentrated from a solution using different approaches such as precipitation of proteins[18], using magnetic beads [19] or centrifugal concentrator tubes [20]. In previous reported work[18],we have used deoxycholate (DOC) / Trichloroacetic acid (TCA) precipitation to concentrate proteins from PDE, however this method requires chaotropic agents like urea or thiourea and detergents to solubilize protein pellets. The use of such reagents is required to solubilize protein samples before 2D gel electrophoresis. On the other hand, high concentrations of chaotropic agents and detergents are contaminants for mass spectrometry analysis, requiring a further purification step before analysis. To overcome the use of urea and detergents, concentration of proteins was accomplished using centrifugal concentrator tubes with a cut-off membrane of 10 kDa. Through this process, the protein content was concentrated from 10 mL to 150–300 mL. The second step was to overcome the problems related to high abundance proteins. For mass spectrometry-based applications, the presence of major proteins makes the detection of other less abundant proteins difficult [16], [20]-[22]. Different strategies are currently used to solve this problem, from which selective major protein depletion with chemical reagents, such as ACN or DTT, has been recently proposed as an economic and fast method to

accomplish this task [5], [23], [24]. Indeed, as we have suggested, the use of ACN to deplete proteins in sera samples renders an extract rich in apolipoproteins whilst the use of DTT renders an extract rich in immunoglobulins. Furthermore, depletion with DTT renders a serum with a higher concentration of high abundance proteins than when ACN is used [5], [23]. Because profiling is the main aim of this work, major proteins must be diluted from the target sample as much as possible but not totally. Through this way, the m/z signals originated from such proteins in the MALDI spectrum are drastically decreased, both in number and intensity, but are not totally eliminated. For the aforementioned reasons, the application of DTT was selected for this work. To this end, first the samples were concentrated with the centrifugal concentrators and then they were depleted using DTT as described in Section 2.5. The samples were then left to stand for about 1 h [23].We recommend making this process at temperatures above 25 ºC otherwise precipitation will take longer than 1 h. After depletion, the pellet was discarded and the supernatant was interrogated using 2D gel electrophoresis. The result of this study is presented in Figure 2, where a typical gel image from a pooled sample can be seen along with the distribution of the type of protein found. A complete list of the proteins identified is provided in Table 2 of the supplementary material. As may be seen in Figure 2, the type of protein present in the PDE clearly indicates a complex mechanism of membrane transportation through the peritoneum. It can be also noted that a significant fraction of those proteins are linked to regulation and response to a stimulus. A total of 50 proteins were identified, of which 12 (24%) were included in the top-20 of the most abundant proteins. This was an excellent result and further confirmed that DTT selectively depletes high abundance proteins from complex proteomes. Furthermore, protein AMBP, vitamin D-binding protein, α1-antitrypsin and pigment epithelium-derived factor, identified in our experiments, have been associated with diabetic nephropathy [24]. Moreover, the Ig mu chain C region and the fibrinogen gamma chain have been correlated with GNC [25].

3.2-Profiling PDE samples

Once confirmed the rationale of the method used for depleting major proteins from PDE samples, the next step was to apply the method to a number of samples from patients on PD treatment. The main aim of this work was to obtain for each patient a MALDI-MS profile of the pool of peptides belonging to the proteins obtained as described in Section 3.1. The number of patients as well as their individual characteristics is listed in Table 1 of the supplementary material. The complete sample treatment is depicted in Figure 1. The approach presented therein takes advantage of the ultrasonic energy as a tool to boost the enzymatic cleavage of proteins. Such approach is fast, cheap and easy to handle [14], [17], [26]. An additional advantage for clinical applications is that ninety-six samples can be treated in one day. This sample treatment has been described previously by our team [14], [17], [26], [27]. A typical MALDI-MS profile obtained using this protocol is shown in Figure 1. The profiling method renders a number of MALDI-m/z signals, which in practical terms can be considered as a series of numbers. For each sample, a series is obtained. Such series are interrogated with bioinformatics

programs using PCAs or hierarchical clustering analysis in our case, once all samples were profiled; a free/open-source software developed in collaboration with the SING group (http://sing.ei.uvigo.es) named Mass-Up was used. PCA and clustering analysis were the statistics tools used to study the samples. The Mass-Up software is available free of charge at http://sing.ei.uvigo.es/mass-up/ (last time accessed June, 2015). The software is easy to use and only requires to up-load the m/z values corresponding to the profiles as an excel file. A tutorial is available in the same web page from which the program is downloaded. Figure 1 shows the PCA analysis (Figure 1 of supplementary material) obtained for the two groups of patients profiled in this work. As may be seen, the groups are well classified. The two diseases assessed (a) diabetic nephropathy and (b) chronic glomerulonephritis alter the peritoneum membrane in a different way. As a consequence, the proteins that cross the membrane are also different. This difference is reflected in the pool of peptides obtained and thus the MALDI m/z values of each sample are also expected to have differences. The utility of the concept here proposed was further demonstrated by using hierarchical cluster analysis, which is shown in Figure 1 and in Figure 2 of supplementary material. As may be seen, the groups are again well classified. The hierarchical clustering suggests that both diabetic nephropathy and chronic glomerulonephritis can be readily distinguished.

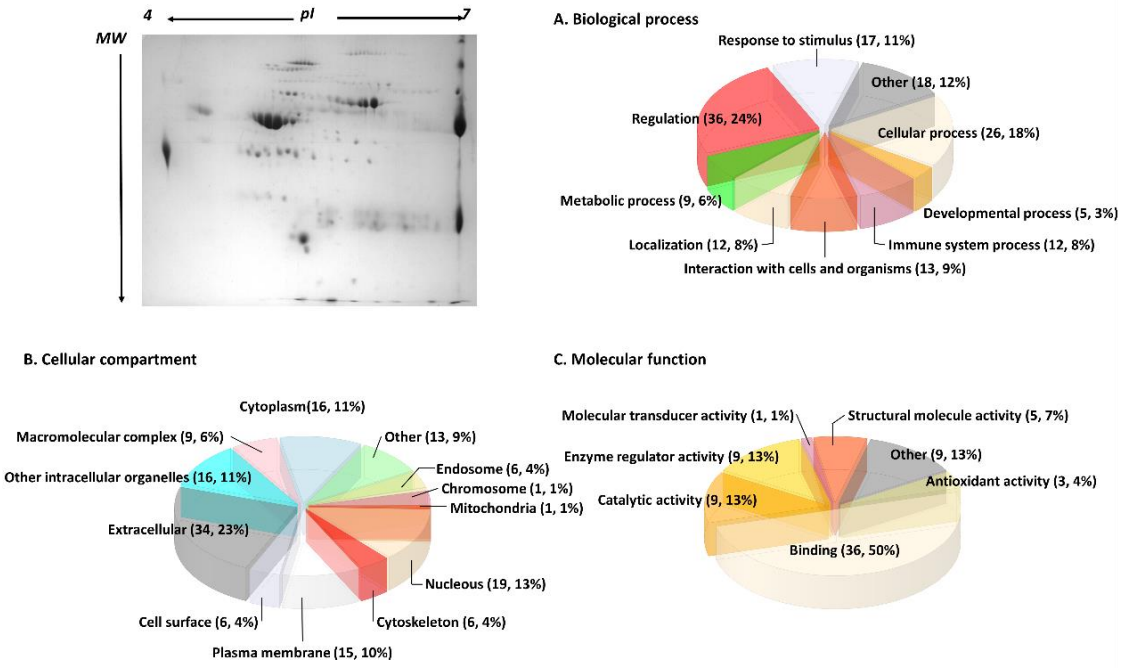

Figure 2- 2D-SDS-PAGE image from a pooled PDE sample of ten patients after protein concentration and depletion. Representative pie charts of: (A) biological processes; (B) cellular components; (C) molecular function of the identified proteins. The pie charts were generated with the STRAP 1.5 software.

This result opens new horizons in the research of the peritoneum degradation as a consequence of dialysis. Furthermore, differences in the peritoneum of each patient as a result of a long period of dialysis treatment are anticipated, thus helping physicians in preventing early peritoneum degradation.

4-Conclusions

We have demonstrated that the introduction of mass spectrometry-based profiling can provide a powerful, fast, cheap and accurate tool to classify patients with renal failure. It has been demonstrated that a workflow combining (i) sample preparation consisting in protein concentration through centrifugal concentrators and chemical-assisted protein depletion using DTT, and (ii) MALDI-TOF MS and the Mass-Up software is an effective method to classify patients with glomerular chronic nephritis, and diabetic nephropathy, thereby helping physicians in defining the etiology of the kidney disease. Although the approach is promising, large international trials to provide extensive spectra databases are needed to make this kind of profiling methodology a useful tool for the nephrology community. We are currently working to address this issue.

5-Conflict of interest

The authors declare no conflict of interest.

6-Acknowledgements

H. M. Santos acknowledges the post-doctoral grant SRFH/BPD/73997/2010 provided by Fundação para a Ciência e a Tecnologia, Ministério da Educação e Ciência (FCT–MEC, Portugal). This work was supported by PROTEOMASS Scientific Society (Portugal) and by the [14VI05] Contract-Programme from the University of Vigo. Authors thank LAQV/REQUIMTE (UID/QUI/50006/2013) and UCIBIO/REQUIMTE (UID/Multi/04378/2013) for general funding.

7-Data accessibility

Supplementary data to this article can be found online at the DOI: 10.1039/C5AY00620A.

8-References

[1] F. Adams and C. Barbante, “History and present status of imaging analysis,” *Talanta*. 2012.

[2] P. D. Rainville, G. Theodoridis, R. S. Plumb, and I. D. Wilson, “Advances in liquid chromatography coupled to mass spectrometry for metabolic phenotyping,” *TrAC Trends Anal. Chem.*, vol. 61, pp. 181–191, Oct. 2014.

[3] D. Cecconi and A. Zamò, “Proteomics of human cancer tissues and cells,” *TrAC Trends Anal. Chem.*, vol. 30, no. 2, pp. 346–359, Feb. 2011.

[4] M. A. Merlos Rodrigo, O. Zitka, S. Krizkova, A. Moulick, V. Adam, and R. Kizek, “MALDI-TOF MS as evolving cancer diagnostic tool: A review,” *J. Pharm. Biomed. Anal.*, vol. 95, pp. 245–255, Jul. 2014.

[5] C. Fernández-Costa, M. Reboiro-Jato, F. Fdez-Riverola, C. Ruiz-Romero, F. J. Blanco, and J. L. Capelo-Martínez, “Sequential depletion coupled to C18 sequential extraction as a rapid tool for human serum multiple profiling,” *Talanta*, 2014.

[6] Y.-C. Tyan, S.-B. Su, S.-S. Ting, and H.-Y. Wang, “A comparative proteomics analysis of

peritoneal dialysate before and after the occurrence of peritonitis episode by mass spectrometry," *Clin. Chim. Acta*, vol. 420, pp. 34–44, May 2013.

[7] N. Ghahramani, S. Shadrou, and C. Hollenbeak, "A systematic review of continuous renal replacement therapy and intermittent haemodialysis in management of patients with acute renal failure," *Nephrology*, 2008.

[8] P. L. Kimmel and S. S. Patel, "Quality of life in patients with chronic kidney disease: Focus on end-stage renal disease treated with hemodialysis," *Seminars in Nephrology*. 2006.

[9] S. M. A. De Lima *et al.*, "Inflammation, neoangiogenesis and fibrosis in peritoneal dialysis," *Clinica Chimica Acta*. 2013.

[10] Q. Wen *et al.*, "Proteomic analysis in peritoneal dialysis patients with different peritoneal transport characteristics," *Biochem. Biophys. Res. Commun.*, 2013.

[11] M. Lechner *et al.*, "A proteomic view on the role of glucose in peritoneal dialysis," *J. Proteome Res.*, 2010.

[12] D. Lopes Barreto and R. T. Krediet, "Current status and practical use of effluent biomarkers in peritoneal dialysis patients," *Am. J. Kidney Dis.*, vol. 62, no. 4, pp. 823–833, 2013.

[13] R. T. Krediet and D. G. Struijk, "Peritoneal changes in patients on long-term peritoneal dialysis.," *Nat. Rev. Nephrol.*, vol. 9, no. 7, pp. 419–29, 2013.

[14] J. E. Araújo *et al.*, "A journey through PROTEOSONICS," *Talanta*. 2014.

[15] S. E. Warder *et al.*, "Reducing agent-mediated precipitation of high-abundance plasma proteins," *Anal. Biochem.*, 2009.

[16] C. Fernández, H. M. Santos, C. Ruíz-Romero, F. J. Blanco, and J. L. Capelo-Martínez, "A comparison of depletion versus equalization for reducing high-abundance proteins in human serum," *Electrophoresis*, 2011.

[17] R. Rial-Otero *et al.*, "Sonoreactor-based technology for fast high-throughput proteolytic digestion of proteins," *J. Proteome Res.*, 2007.

[18] E. Oliveira *et al.*, "Proteomics analysis of the peritoneal dialysate effluent reveals the presence of calcium-regulation proteins and acute inflammatory response.," *Clin. Proteomics*, vol. 11, no. 1, p. 17, 2014.

[19] N. Guo, Q. Wen, Z.-J. Li, R.-C. Xu, F.-F. Peng, and X.-Q. Yu, "Optimization and evaluation of magnetic bead separation combined with matrix-assisted laser desorption/ionization time-of-flight mass spectroscopy (MALDI-TOF MS) for proteins profiling of peritoneal dialysis effluent.," *Int. J. Mol. Sci.*, vol. 15, no. 1, pp. 1162–75, 2014.

[20] L. Zhang *et al.*, "Developing a reproducible method for the high-resolution separation of peritoneal dialysate proteins on 2-D gels," *Protein Expr. Purif.*, 2013.

[21] S. Roche *et al.*, "Depletion of one, six, twelve or twenty major blood proteins before proteomic analysis: The more the better?," *J. Proteomics*, 2009.

[22] P. G. Righetti, A. Castagna, P. Antonioli, and E. Boschetti, "Prefractionation techniques in proteome analysis: The mining tools of the third millennium," *Electrophoresis*. 2005.

[23] R. Kay *et al.*, "Enrichment of low molecular weight serum proteins using acetonitrile precipitation for mass spectrometry based proteomic analysis," *Rapid Commun. Mass Spectrom.*, 2008.

[24] P. V. Rao *et al.*, "Proteomic identification of urinary biomarkers of diabetic nephropathy," *Diabetes Care*, 2007.

[25] H. Helin, J. Mustonen, A. Pasternack, and J. Antonen, "IgM-Associated Glomerulonephritis," *Nephron*, vol. 16, pp. 11–16, 1982.

[26] J. D. Nunes-Miranda *et al.*, "A mesofluidic platform integrating on-chip probe ultrasonication for multiple sample pretreatment involving denaturation, reduction, and digestion in protein identification assays by mass spectrometry," *Analyst*, 2014.

[27] C. Fernández-Costa, C. Ruiz-Romero, F. J. Blanco, H. M. Santos, and J. L. Capelo, "An assessment of the indirect high intensity ultrasonic assisted cleavage of complex proteomes with immobilized trypsin.," *Talanta*, 2013.

CHAPTER IV. A COST-EFFECTIVE METHOD TO GET INSIGHT INTO THE PERITONEAL DIALYSATE EFFLUENT PROTEOME[1]

[1] Araújo JE, Jorge S, Teixeira-Costa F, Ramos A, Lodeiro C, Santos HM, Capelo JL (2016) Journal of Proteomics, 145, 207-213. doi: 10.1016/j.jprot.2016.05.010.

Abstract

Protein depletion with acetonitrile and protein equalization with dithiothreitol have been assessed with success as proteomics tools for getting insight into the peritoneal dialysate effluent proteome. The methods proposed are cost-effective, fast and easy of handling, and they match the criteria of analytical minimalism: low sample volume and low reagent consumption. Using two-dimensional gel electrophoresis and peptide mass fingerprinting, a total of 72 unique proteins were identified. Acetonitrile depletes de PDE proteome from high-abundance proteins, such as albumin, and enriches the sample in apolipo-like proteins. Dithiothreitol equalizes the PDE proteome by diminishing the levels of albumin and enriching the extract in immunoglobulin-like proteins. The annotation per gene ontology term reveals the same biological paths being affected for patients undergoing peritoneal dialysis, namely that the largest number of proteins lost through peritoneal dialysate are extracellular proteins involved in regulation processes through binding. *Significance:* Renal failure is a growing problem worldwide, and particularly in Europe where the population is getting older. Up-to-date there is a focus of interest in peritoneal dialysis (PD), as it provides a better quality of life and autonomy of the patients than other renal replacement therapies such as haemodialysis. However, PD can only be used during a short period of years, as the peritoneum lost its permeability through time. Therefore, to make a breakthrough in PD and consequently contribute to better healthcare system it is urgent to find a group of biomarkers of peritoneum degradation. Here we report on two cost-effective methods for protein depletion in peritoneal dialysate effluent (PDE). The use of ACN and DTT over PDE to deplete high abundant proteins or to equalize the concentration of proteins, respectively, performs well and with similar protein profiles than when the same chemicals are used in human plasma samples. ACN depletes de PDE proteome from large proteins, such as albumin, and enriches the sample in apolipoproteins. DTT equalizes the PDE proteome by diminishing the levels of large proteins such as albumin and enriching the extract in immunoglobulins. Although the number and type of proteins identified are different, the annotation per gene ontology term reveals the same biological paths being affected for patients undergoing peritoneal dialysis. Thus, the largest number of proteins lost through peritoneal dialysate belongs to the group of extracellular proteins involved in regulation processes through binding. As for the searching of biomarkers, DTT seems to be the most promising of the two methods because acts as an equalizer and it allows interrogating more proteins in the same sample.

Keywords: Peritoneal dialysis effluent, Protein depletion, High-abundance proteins, Sample preparation, Acetonitrile, Dithiothreitol and Proteomics

1-Introduction

Peritoneal dialysis (PD) is a life-sustaining therapy used by more than 100,000 patients worldwide with end-stage renal disease and acute kidney injury [1]. During peritoneal dialysis, a

dialysate is introduced into the peritoneal cavity where it comes into contact with capillaries perfusing the peritoneum and viscera. Molecules and ions diffuse from the blood through the capillaries into the dialysate and, as a result, peritoneal dialysis effluent (PDE) is a rich source of potential biomarkers. As a matter of fact, PDE is easily accessible and contains a variety of protein and peptides for monitoring disease and therapy [2], [3]. However, medical-driven decisions based on proteomics analysis of PDE have been hampered by its complex plasma-like composition [4]. For example, detection and identification of proteins present in PDE, as in any other complex proteome, is often biased by the presence of high-abundance proteins, HAP. The performance of any downstream analytical workflow is challenged as the complexity of the proteome increases. For the particular case of human serum, it is known that the top 10 most abundant proteins account for about 90% of the total protein content, whereas other proteins are present in a very wide dynamic range, covering more than ten orders of magnitude [5]. For the reason mentioned above, depletion of HAP is often used as an efficient way to increase sensitivity in the detection and identification of low-abundance proteins. Nowadays, several methods are employed to compress the dynamic range of protein concentration in complex biological samples, the process being possible while maintaining the entire proteome [6]. Nevertheless, these work do not entirely solve the problem, mostly due to unspecific binding, which might result in partial or complete loss of proteins of interest. Furthermore, the proteins retrieved from different depletion methods are not the same since the type, and characteristics of the proteins depleted are different [7]. Recently, acetonitrile, ACN, and dithiothreitol, DTT, have been reported as simple, reproducible and cost-effective methods to remove high-abundance proteins from complex matrices, such as serum [7]-[9]. Indeed, serum protein depletion with acetonitrile or protein equalization with DTT has proven to be convenient to enrich selectively serum extracts in apolipoproteins and immunoglobulins, respectively. However, two questions remain to be answered. First, may ACN and DTT be used as proteomics tools in PDE? Second, is the information retrieved using each method the same? Herein, we report on the performance of ACN- and DTT-based methods over PDE samples as proteomics tools before analysis by two-dimensional gel electrophoresis and mass spectrometry.

2-Materials and methods

2.1-Reagents and apparatus

All reagents used were HPLC grade or electrophoresis grade. Albumin, from bovine serum (BSA), (N,N,N′,N′-tetramethylethylene-diamine (TMED), glycine, β-mercaptoethanol, glycerol 86–88%, Bradford reagent, coomassie blue R-250 (CBB), DL-dithiotreitol (DTT), iodoacetamide (IAA), trypsin sequencing grade, trifluoroacetic acid (TFA), acrylamide/bis- acrylamide 30% solution (37.5:1) and mineral oil were purchased from Sigma-Aldrich (Basel, Switzerland). Formic acid, ammonium bicarbonate (Ambic), ammonium persulphate (APS) and α-Cyano-4-hydroxycinnamic acid were purchased from Fluka (Basel, Switzerland). Hydrochloric acid (HCl), glacial acetic acid, tris–base,

sodium dodecyl sulphate (SDS), methanol and acetonitrile were purchased from Panreac (Barcelona, Spain). Bromophenol blue was from Riedel-de Haën (Basel, Switzerland). Molecular weight marker for gel electrophoresis Precision Plus Protein™ All Blue was purchased from Bio-Rad (USA). Vivaspin® 15R centrifugal concentrator 10,000 MWCO from Sartorius were used for protein pre-concentration. The ultrasonic processor UP50H from Dr. Hielschler (Germany) and multi-frequency ultrasonic bath Transsonic TI-H from ELMA Schmidbauer GmbH (Germany) was used for sample re-suspension and gel destaining, respectively. Protean IEF cell, IPG strips pH 4–7 (7 cm), cup loading tray and mini-PROTEAN Tetra Cell were from Bio-Rad (USA). Gel image acquisition and spot picking were performed using a PROPIC II DigiLab Genomic Solutions (USA). Protein digestion was done in low adhesion safe-lock tubes from Deltalab (Barcelona, Spain). A vacuum concentrator centrifuge model UNIVAPO 150 ECH SpeedVac and a vacuum pump model UNIJET II were used for sample drying and sample pre-concentration. A mini incubator from Labnet was used for gel washing, for protein reduction and for protein alkylation steps. The centrifuges MPW-350 and MPW-65R were from MPW Med. Instruments. A microplate reader LT4000 equipped with 595 nm filters from Labtech was used for Bradford protein assay. Mass Spectrometry protein identification was done in an Ultraflex II MALDI TOF/TOF instrument from Bruker Daltonics.

2.2-96-well plate Bradford protein assay

PDE samples were quantified using the Bradford protein assay adapted from [10]. Briefly, a BSA standard curve (0, 1, 5, 10, 15, 20, 25 μg/mL) was generated in duplicate. To each well being used, 150 μL of each standard were mixed with 150 μL Bradford reagent. The unknown samples were diluted with water to an approximate concentration between 5 and 20 μg/mL and then 150 μL of each unknown were mixed with 150 μL Bradford reagent. Finally, the samples were incubated at room temperature for 20 min, and then absorbances were measured at 595 nm.

2.3-Sample collection and pre-preparation

PDE samples were collected from consenting PD patients following a peritoneal equilibrium test. All the samples were supplemented with a protease inhibitor cocktail, 10 mM NaEDTA and 1 mM NaF and centrifuged within 30min of collection at 9000 ×g for 20min to remove insoluble solids. Before downstream use, 10mL of PDE were concentrated by duplicate using Vivaspin® 15R centrifugal concentrator 10,000 MWCO until approximately 300 μL [11]. The protein-enriched fractions were collected to clean low adhesion tubes and the centrifugal concentrators membrane were washed with 50 μL of water to maximize protein recovery. Finally, a Bradford protein assay (595nm) was carried out to determine the total amount of protein in the PDE concentrated samples.

2.4-Protein depletion with acetonitrile

Protein depletion with acetonitrile (ACN)was adapted from the protocol described by Kay *et al.* [12]. Briefly to 20 μL of concentrated PDE were diluted with 44 μL of ultrapure water and then 85μL of acetonitrile were added to obtain a solution containing 57% (v/v) of acetonitrile. Afterwards, samples were sonicated for 2 × 10 min in an ultrasonic bath (35 kHz and 100% ultrasonic amplitude) and then the protein precipitates were pelleted by centrifugation at 12,000 ×g for 10 min at 20 °C. The ACN depletion was done in quadruplicate. The four supernatants were transferred to a clean low adhesion tube and evaporated to dryness in a vacuum concentrator centrifuge without heating.

2.5-Protein depletion with DL-Dithiothreitol

Protein depletion with DL-Dithiothreitol (DTT) was performed as described by Fernández *et al.* [7]. Briefly, 2.2 μL of fresh DTT 500 mM was added to 20 μL of concentrated PDE and the samples were then incubated for 60 min at 37 °C until a viscous white precipitate persisted. The protein precipitates were pelleted by centrifugation at 14,000 ×g for 20 min. The protein depletion protocol was done in quadruplicate. The four supernatants were transferred to a clean low adhesion tube and evaporated to dryness in a vacuum concentrator centrifuge without heating.

2.6-1D-SDS-PAGE

Protein samples were re-suspended in 10 μL of water plus 10 μL of sample buffer (65.8 mM Tris–HCl pH 6.8, 2.1% SDS (w/v), 26.3% (w/v) glycerol, 0.01% (w/v) of bromophenol blue and 10% (v/v) β-mercaptoethanol) and then heated in a dry bath at 100 °C for 5 min. The denatured proteins were loaded in 12.5% polyacrylamide gels with 1 mm thickness. Proteins were separated at 200 V (constant voltage) until the tracking dye front reaches the bottom of the gel [13], [14].

2.7-2D-gel electrophoresis

Samples were re-suspended in 8M urea, 2% (w/v) CHAPS, 0.2% (v/v) ampholytes pH 4–7, 50mM DTT and traces of bromophenol blue. Samples were incubated on ice for 30 min and sonicated using a 1 mm diameter probe for 6 × 10 s on ice at 50% sonication amplitude. Insoluble mater was removed by centrifugation (20 min 14,000 ×g at 20 °C). Protein concentration was determined using a Bradford protein assay. IPG strips pH 4–7, 7 cm were rehydrated overnight at 20 °C with 135 μL of rehydration buffer containing 8 M Urea, 0.5% (w/v) CHAPS, 0.2% (v/v) ampholytes pH 4–7, 10 mM DTT and traces of bromophenol blue. Sample loading onto the IPG Strip was carried out using the cup loading method. IPG strips were removed from the rehydration tray; the oil was drained, and placed gel side up into the focusing tray's channels. The movable electrode assemblies were carefully positioned on top of the strips at the anode and cathode ends, after that, the sample loading cups were placed near the cathode. Afterwards, 50 μL of the protein containing solution (2 mg/mL) were loaded in the sample-

loading cup and then overlaid with mineral oil. The focusing tray was placed into the PROTEAN IEF Cell. The isoelectric focusing was performed in three steps as follows: step 1250 Volts for 30 min, rapid voltage ramping; step 2: 4000 Volts for 60 min, slow voltage ramping; Step 3: 4000 Volts, 10,000 V–hr. For the three steps the current was limited to 50 μA/gel. After IEF, gel strips were removed and incubated with equilibration buffer (6M urea, 75mMTris pH 8.8, 20% glycerol (v/v), 2% (w/v) SDS, traces of bromophenol blue) as follow 15 min incubation with 2.5 mL of equilibration buffer containing 2% (w/v) of DTT, followed by 15 min incubation with 2.5 mL of equilibration buffer containing 2.5% (w/v) of IAA. The IPG strips were removed from the equilibration tray and clip briefly into the graduated cylinder containing running buffer. The strip was placed side up and onto the back plate of the SDS-PAGE gel. The IPG well of the gel was overlay with agarose sealing solution (0.5% w/v prepared with 50 mL of Lammeli running buffer and traces of bromophenol blue). After agarose solidification, the electrophoresis was conducted at 200 V (constant voltage) until the tracking dye front reaches the bottom of the gel [12], [13].

2.8-Gel staining and image analysis

Finished the gel electrophoresis, the gel was fixed for 30 min with 40% (v/v) ethanol and 10% (v/v) acetic acid and then stained overnight with colloidal coomassie blue G-250. Gels were rinsed 4 × 20 min with 100 mL of distilled water and further washed twice with 100 mL of 0.5 M sodium chloride until a clear background was observed [15]. Gel imaging was carried out with a ProPicII–robot using 16 ms of exposure time and a resolution of 70 μm. Gel piking was done with the same equipment.

2.9-In-gel protein digestion

After spot piking the spots were transferred to 0.5 mL low adhesion tubes. Gel spots were washed twice with 200 μL of water and then with 3×200 μL of 50% (v/v) acetonitrile/25mM ammonium bicarbonate and sonicated at 60% ultrasonic amplitude for 10 min using an ultrasonic bath. Then the gel pieces were dehydrated with 200 μL of acetonitrile. Subsequently, 5 μL of trypsin (60 ng/μL in ammonium bicarbonate 12.5 mM/2% (v/v) acetonitrile) was added to the gel spots and incubated for 60 min on ice, then covered with 20 μL of 12.5 mM ammonium bicarbonate/2% (v/v) acetonitrile and incubated 12 h at 37 °C. Finally, 25 μL of 5% (v/v) formic acid was added and the supernatants were transferred to new low adhesion tubes. Peptides were further extracted from the gel matrix with 2 × 50 μL of 50% (v/v) acetonitrile/0.1% trifluoroacetic acid and sonicated using at 60% ultrasonic amplitude for 5 min using an ultrasonic bath. Samples were dried-down and stored at −20 °C until MS analysis.

2.10-Mass spectrometry analysis

Before MS analysis, samples were re-suspended in 10 μL of formic acid 0.3% (v/v) and 0.5 μL of sample was hand-spotted onto a MALDI target plate (384-spot ground steel plate) then 1 μL of a 5 mg/mL solution of α-cyano-4-hydroxycinnamic acid matrix in 0.1% (v/v) TFA and 50% (v/v) ACN was

added and allowed to air dry. The MALDI TOF/TOF mass spectrometer was operated in positive ion mode using a reflectron, and thus, spectra were acquired in the m/z range of 600–3500. A total of 500 spectra were acquired for each sample at a laser frequency of 50 Hz. External calibration was performed with the $[M+H]^+$ monoisotopic peaks of bradykinin 1–7 (m/z 757.3992), angiotensin II (m/z 1046.5418), angiotensin I (m/z 1296.6848) substance P (m/z 1758.9326), ACTH clip 1–17 (m/z 2093.0862), ACTH18–39 (m/z 2465.1983) and somatostatin 28 (m/z 3147.4710). Peptide mass fingerprints (PMF) were searched with MASCOT search engine with the following parameters: (i) SwissProt Database2012_04 (535,698 sequences; 190,107,059 residues); (ii) molecular weight of protein: all; (iii) one missed cleavage; (iv) fixed modifications: carbamidomethylation (C); (v) variable modifications: oxidation of methionine and (vi) peptide tolerance up to 50 ppm. The significance threshold was set to a minimum of 95% ($p \leq 0.05$). A match was considered successful when protein identification score is located out of the random region.

3-Results and discussion

3.1-Performance of centrifugal concentrators

There are some factors to consider when using protein concentrators that can affect sample treatment reproducibility. Such factors are (i) membrane pore size and material, (ii) range of molecular weight cut-off, (iii) sample volume range, (iv) centrifuge tube size and (v) concentration factor. Therefore, reproducibility of protein pre-concentration from PDE samples using 10,000 MWCO centrifugal concentrators, MWCO, was first investigated. To accomplish this task, samples collected from ten patients were first interrogated for total protein content. The protein concentration dynamic range was found to vary (n=2) between 0.40 ± 0.02 mg/mL and 1.80 ± 0.01 mg/mL. Then, the samples were ultrafiltrated as described in section 2.3. Two technical replicates were carried out for each sample. It was verified that the volumes obtained after pre-concentration were larger for those samples with higher protein content. This is in agreement with MWCO manufacturer specifications [16]. As the protein concentration of PDE samples was different for each patient as well as sample volume obtained after pre-concentration, it was necessary to normalize the final result somehow. Therefore, it was decided to present our data as the ratio between the protein content after and before sample pre-concentration. The results are presented in Figure 1A, and it is shown that when centrifugal concentrators are used, samples are pre-concentrated in a reproducible manner, as all samples were successfully pre-concentrated with relative standard deviations lower than 15%. Figure 1A also shows that pre-concentration factors have a large variation, ranging from one to two orders of concentration. Another question to be answered was how efficient and reproducible the protein recovery was through the pre-concentration process.

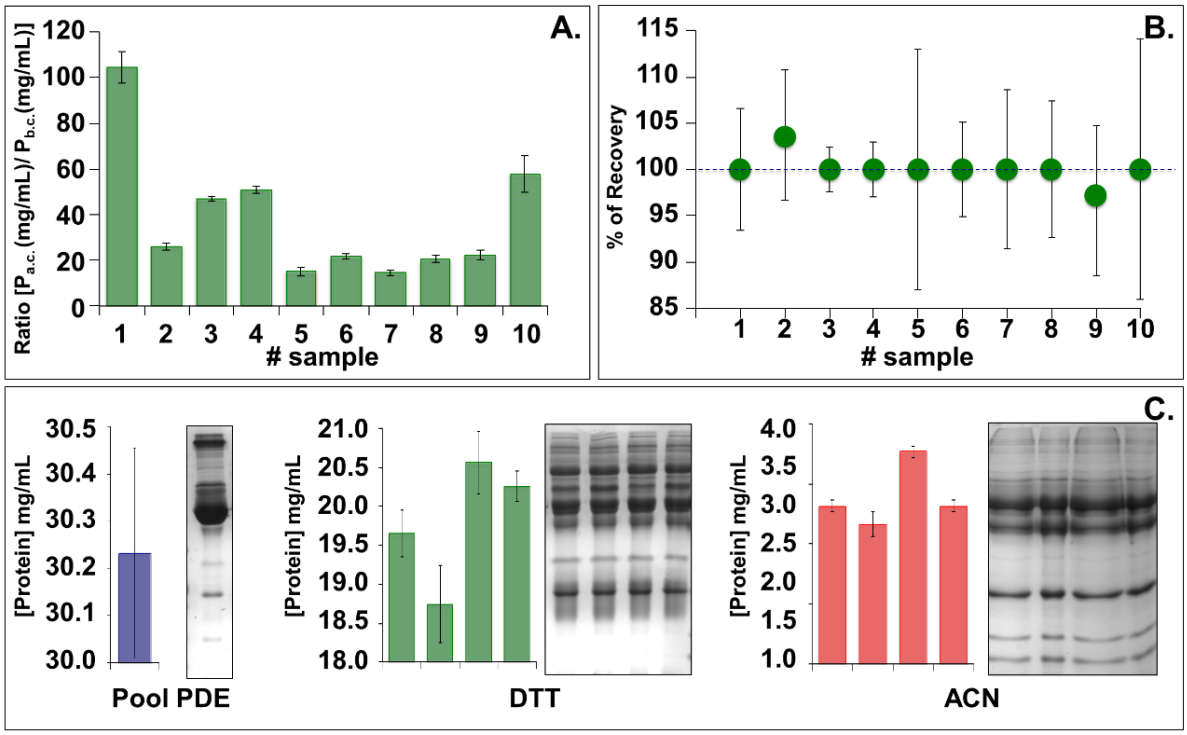

Figure 1- Reproducibility of protein recovery after centrifugal ultrafiltration: (A) Ratio of protein concentration after concentration ($P_{a.c}$) and before concentration ($P_{b.c}$). Protein concentrations were determined by Bradford Protein Assay (595 nm). Centrifugal ultrafiltration was performed in duplicates. The error bars represent the standard deviation of protein concentration between two replicates of the same sample. (B) % of protein recovery after centrifugal ultrafiltration. The error bars represent the standard deviation of recovery between two replicates.

The utilization of ultrafiltration devices to enrich the protein content in PDE samples reveals to be very effective with a mean protein recovery of 100% and with a mean standard deviation of 8 ± 4% (10 samples × 2 replicates). As may be seen in Figure 1B, protein recoveries were higher than 97%, which is in accordance to manufacturer's specifications. It is worth to mention that Zhang *et al.* reported a 2.14-fold lower recovery when they worked over PDE samples with 3000 MWCO centrifugal concentrators [17]. Furthermore, our results are in agreement with those previously reported by other authors [17], [18]. Therefore, once it was demonstrated that the pre-concentration step was done in an efficient and reproducible manner, we move forward to study the use of ACN- and DDT- based sample treatments over pre-concentrated PDE samples.

3.2-Use of acetonitrile- or dithiothreitol-based sample treatments over PDE samples

ACN- and DTT-based sample treatments have been reported in literature as tools to remove high abundant proteins or to equalize the sample's protein levels, respectively, in human biofluids like serum and plasma [7], [12], [19]. Notwithstanding this fact, the systematic assessment of both sample treatments over PDE samples has not been done yet. To cover this gap, a pool of PDE samples was prepared as described in sections 2.3–2.5. The protein content of this pool was 30 ± 1 mg/mL (Bradford protein assay). Then, eight aliquots of 20 µL of the PDE pool were used for studying the performance

of protein equalization using DTT (4 aliquots) or protein depletion using ACN (4 aliquots). Thus, first, the resulting supernatants after equalization or depletion were quantified. Results showed that equalization with DTT removes 34 ± 3% (n = 4) of the total amount of protein and that protein depletion with ACN removes 88 ± 8% (n = 4) of the total amount of protein present in PDE. Regarding protein concentration, it was found that both ACN- and DTT- based methods are highly reproducible, as the total protein content found in the supernatant after treatment was 20±1 mg/mL (n=4) and 3.8±0.3mg/mL (n=4), respectively. To further assess the reproducibility of the depletion process, the results were further confirmed using 1D SDS- PAGE. This study showed a similar profile among the four replicates (Figure 1C). As it can be seen, ACN promotes the depletion of proteins, mostly large ones, as it is revealed by the absence of intense bands in the zone corresponding to proteins with higher masses. On the other hand, it is possible to observe that DTT only partially removes proteins from the upper zone (in contrast with ACN), leading to a sample with a larger number of gel bands. Aimed at this excellent result, we evaluated the ACN- and DTT- based methods using 2D-GE. For comparative purposes, it was used a pool of samples over which no selective removal of proteins was done. 2D-gels are shown in Figure 2.

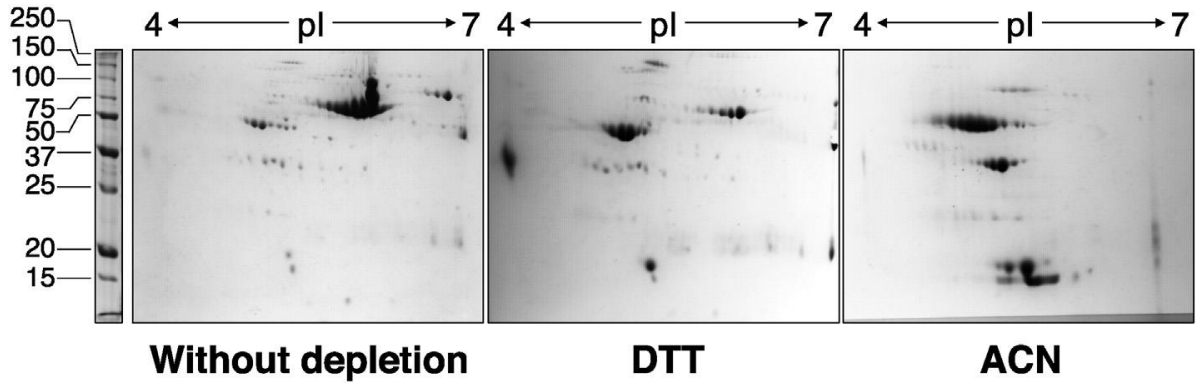

Figure 2- Colloidal coomassie stained 2D SDS-PAGE of a pool of peritoneal dialysate effluent without HAPs depletion and after HAPs depletion with DTT and ACN.

In-depth 2D-gel analysis using SameSpots software (TOTALLAB) revealed 112 ± 10 (n = 2) detected spots for the non-depleted sample whereas the gels of the samples depleted with ACN and DTT shown 119 ± 16 (n = 2) and 184 ± 12 (n = 2) detected spots, respectively, see Figure 3 for further details. All the detected 2D-spots were excised digested and analysed by MALDI-MS. Figure 3 illustrates the number of uniquely identified proteins obtained for each method: 54, 37 and 19 proteins for the DTT, no depletion- and ACN-based methods respectively. A group of 10 proteins are identified using any of the three methods, 26 proteins are unique for the DTT method, 10 proteins are exclusive for the method without depletion and six proteins are identified only in samples depleted with ACN. Immunoglobulins are abundant in the sample depleted with DTT while apolipoproteins are abundant in the sample depleted with ACN. This result is in agreement with the previous one reported by us using 1D gel electrophoresis and serum samples [7].

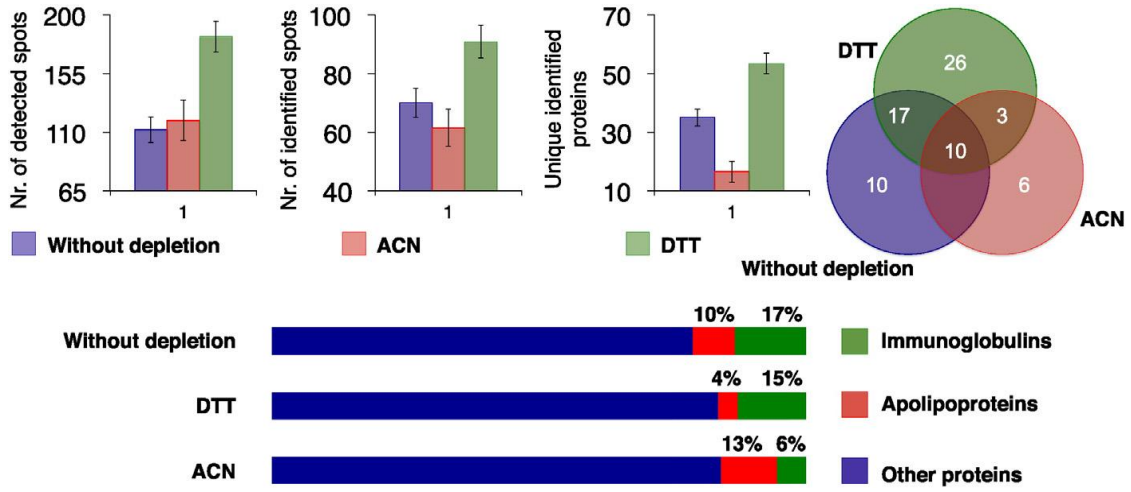

Figure 3- Number of detected spots, number of identified proteins and number of unique identified proteins for the samples without HAPs depletion, after depletion with ACN and DTT. Venn diagram of the unique identified proteins in each treatment and percentage of immunoglobulins and apolipoproteins enriched identified in each treatment.

3.3-Clinical significance

Removal of major abundant proteins, such as albumin, from complex samples, is a usual first step in the analysis of serum and serum like proteomes [20]- [22]. Albumin is known to bind other proteins and peptides. Therefore, it is expected to observe changes in the proteome upon removal of albumin and other major abundant proteins [20]. On the other hand, the albuminome proteins might provide relevant biological information in peritoneal dialysis. Our approach benefits from the combination of three methods that together provides a better comprehension of the peritoneal dialysate, as we have an overall representation of the proteins of the whole proteome, the DTT equalized proteome, and the ACN depleted sample, rendering the identification of 72 unique proteins (Supplementary Information). Although the number and type of proteins identified are different, the annotation per gene ontology term reveals the same biological paths being affected for patients undergoing peritoneal dialysate. Thus, each method, regardless the number of proteins identified, address the same information, namely that the largest number of proteins lost through peritoneal dialysate are extracellular proteins involved in regulation processes through binding, see Figure 4.

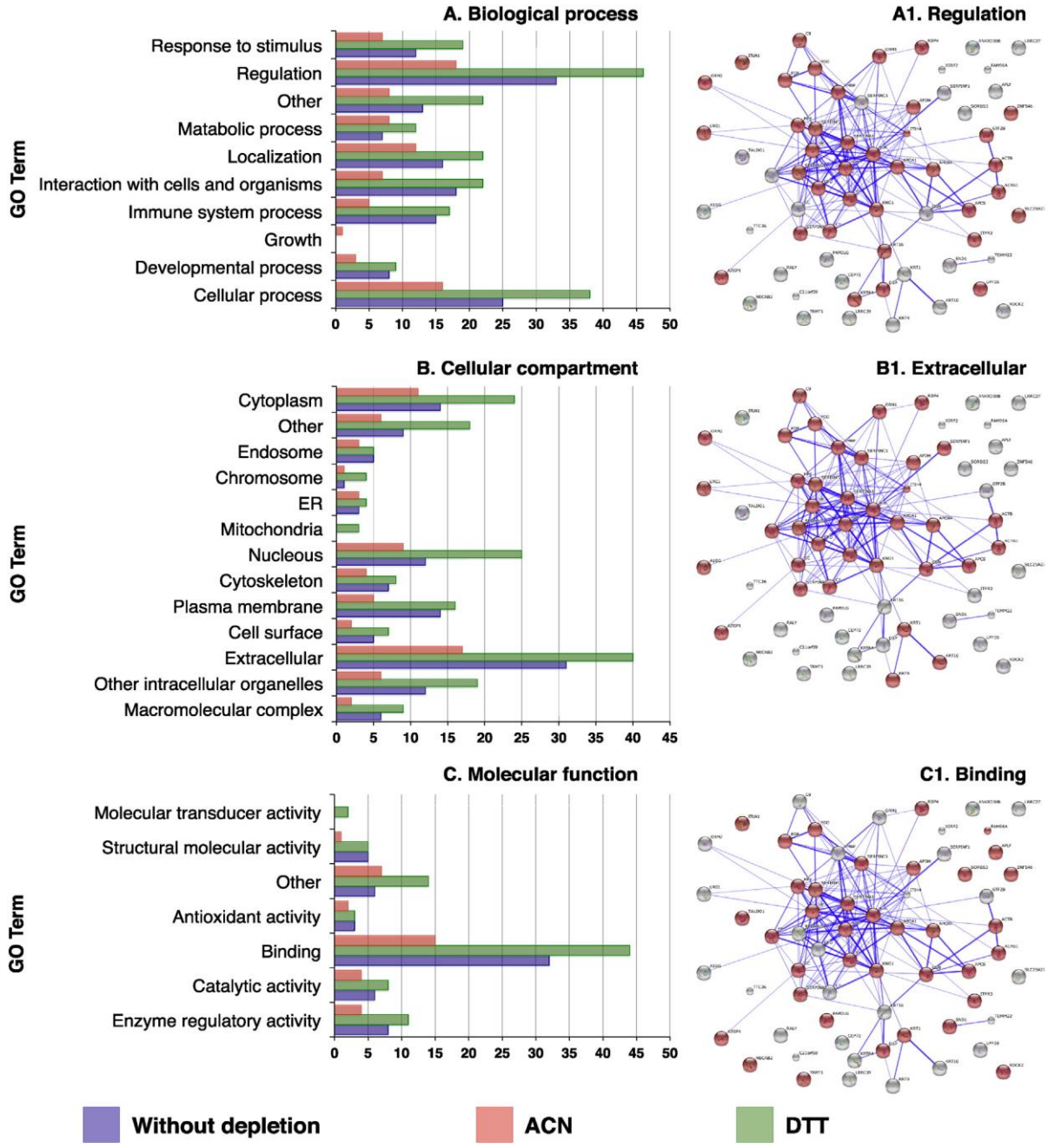

Figure 4- Annotation per gene ontology term obtained with the Software Tool for Researching Annotations of Proteins (STRAP). Bar chart of (A) Biological process GO term annotations, (B) Cellular component GO term annotations and (C)Molecular function GO term annotations. STRING Protein interaction network of the proteins identified in PDE. The proteins dashed in red denote involvement in (A1) Regulation, (B1) Extracellular and (C1) Binding. The network uses a confidence view. Thicker lines represent stronger associations.

Many proteins lost in PDE could have potentially harmful consequences. For instance, one of the proteins found in PDE is vitamin-D binding protein, which is involved in many regulatory processes, the most significant being calcium homeostasis and modulation of inflammatory responses, both playing an important role in the early morbidity and mortality of peritoneal dialysis patients [23]. We have identified several proteins that modulate the inflammatory response, including inhibition of lysosomal proteases that are released during the destruction of cells, namely (i) α-2-macroglobulin, (ii) α-1-

antitrypsin, and (iii) direct binding of lipopolysaccharide-like α-1-acid glycoprotein. Other proteins found were binding metals proteins with antioxidant action such as haptoglobin and ceruloplasmin[23]. Ceruloplasmin and haptoglobin are two proteins directly linked to iron transport and activity in blood. Low levels of these proteins might lead to an excess of free iron in the blood, which then gets deposited in the retina, liver, and pancreas leading to loss of vision, cirrhosis and endocrine abnormalities, respectively.

On the other hand, removal of other proteins such as adipokine proteins by peritoneal dialysis could have potential benefits. As an example, the accumulation of zinc-α2-glycoprotein in serum may have detrimental metabolic consequences [24]-[26]. Likewise, high levels of retinol binding protein 4 have been correlated with oxidative stress, inflammation, and metabolic syndrome [27]. Thus, removal of this protein by PD may be beneficial to acutely ill patients [25].

4-Concluding remarks

The use of ACN and DTT over PDE to deplete high abundant proteins or to equalize the concentration of proteins, respectively, performs well and with similar protein profiles than when the same chemicals are used in human plasma samples. ACN depletes de PDE proteome from large proteins, such as albumin, and enriches the sample in apolipoproteins. DTT equalizes the PDE proteome by diminishing the levels of large proteins such as albumin and enriching the extract in immunoglobulins. Although the number and type of proteins identified are different, the annotation per gene ontology term reveals the same biological paths being affected for patients undergoing peritoneal dialysate. Thus, the largest number of proteins lost through peritoneal dialysate belongs to the group of extracellular proteins involved in regulation processes through binding. As for the searching of biomarkers, DTT seems to be the most promising of the two methods because acts as an equalizer and it allows interrogating more proteins in the same sample.

5-Conflict of interest

The authors declare no conflict of interest.

6-Acknowledgements

J. E. Araújo acknowledges the Ph.D. grant SFRH/BD/109201/2015 and H. M. Santos acknowledges the post-doctoral grant SRFH/BPD/73997/2010, provided by Fundação para a Ciência e a Tecnologia –Ministério da Educação e Ciência (FCT-MEC, Portugal). This work was supported in part by PROTEOMASS Scientific Society (Portugal). The authors acknowledge the funding provided by UCIBIO, Unidade de Ciências Biomoleculares Aplicadas, which is financed by national funds from FCT/MEC (UID/Multi/04378/2013) and co-financed by the ERDF under the PT2020 Partnership Agreement (POCI-01-0145-FEDER-007728) and to the Associate Laboratory for Green Chemistry

LAQV which is financed by national funds from FCT/MEC (UID/QUI/50006/2013) and co-financed by the ERDF under the PT2020 Partnership Agreement (POCI-01-0145-FEDER-007265).

7-Data accessibility

Supplementary data to this article can be found online at http://dx. doi.org/10.1016/j.jprot.2016.05.010.

8-References

[1] O. Devuyst, P. J. Margetts, and N. Topley, "The Pathophysiology of the Peritoneal Membrane," *J. Am. Soc. Nephrol.*, 2010.

[2] A. M. Lichtenauer, R. Herzog, S. Tarantino, C. Aufricht, and K. Kratochwill, "Equalizer technology followed by DIGE-based proteomics for detection of cellular proteins in artificial peritoneal dialysis effluents," *Electrophoresis*, vol. 35, no. 10, pp. 1387–1394, 2014.

[3] V. Thongboonkerd, "Proteomics in extracorporeal blood purification and peritoneal dialysis," *Journal of Proteomics*. 2010.

[4] R. Raaijmakers *et al.*, "Proteomic profiling and identification in peritoneal fluid of children treated by peritoneal dialysis," *Nephrol. Dial. Transplant.*, 2008.

[5] R. Millioni *et al.*, "High abundance proteins depletion vs low abundance proteins enrichment: Comparison of methods to reduce the plasma proteome complexity," *PLoS One*, 2011.

[6] P. G. Righetti, A. Castagna, P. Antonioli, and E. Boschetti, "Prefractionation techniques in proteome analysis: The mining tools of the third millennium," *Electrophoresis*. 2005.

[7] C. Fernández, H. M. Santos, C. Ruíz-Romero, F. J. Blanco, and J. L. Capelo-Martínez, "A comparison of depletion versus equalization for reducing high-abundance proteins in human serum," *Electrophoresis*, 2011.

[8] C. Fernández-Costa, V. Calamia, P. Fernández-Puente, J. L. Capelo-Martínez, C. Ruiz-Romero, and F. J. Blanco, "Sequential depletion of human serum for the search of osteoarthritis biomarkers," *Proteome Sci.*, 2012.

[9] C. Fernández-Costa, M. Reboiro-Jato, F. Fdez-Riverola, C. Ruiz-Romero, F. J. Blanco, and J. L. Capelo-Martínez, "Sequential depletion coupled to C18 sequential extraction as a rapid tool for human serum multiple profiling," *Talanta*, 2014.

[10] R. M. M. Branca *et al.*, "HiRIEF LC-MS enables deep proteome coverage and unbiased proteogenomics," *Nat. Methods*, 2014.

[11] J. E. Araújo *et al.*, "Matrix-assisted laser desorption/ionization time-of-flight mass spectrometry-based profiling as a step forward in the characterization of peritoneal dialysis effluent," *Anal. Methods*, vol. 7, no. 18, pp. 7467–7473, 2015.

[12] R. Kay *et al.*, "Enrichment of low molecular weight serum proteins using acetonitrile precipitation for mass spectrometry based proteomic analysis," *Rapid Commun. Mass Spectrom.*, 2008.

[13] H. M. Santos *et al.*, "A novel 18O inverse labeling-based workflow for accurate bottom-up mass spectrometry quantification of proteins separated by gel electrophoresis," *Electrophoresis*, 2010.

[14] E. Oliveira *et al.*, "Proteomics analysis of the peritoneal dialysate effluent reveals the presence of calcium-regulation proteins and acute inflammatory response.," *Clin. Proteomics*, vol. 11, no. 1, p. 17, 2014.

[15] V. J. Gauci, M. P. Padula, and J. R. Coorssen, "Coomassie blue staining for high sensitivity gel-based proteomics," *J. Proteomics*, 2013.

[16] "https://www.sartorius.com/fileadmin/fm-dam/DDM/Lab-Products-and-Services/Lab-Filtration/Ultrafiltration-Devices/Vivaspin-Centrisart/Manuals/Manual_Vivaspin_15R_SLU2003-e.pdf (last time accessed January, 2016)."

[17] L. Zhang *et al.*, "Developing a reproducible method for the high-resolution separation of peritoneal dialysate proteins on 2-D gels," *Protein Expr. Purif.*, 2013.

[18] X. Zheng, H. Baker, and W. S. Hancock, "Analysis of the low molecular weight serum peptidome using ultrafiltration and a hybrid ion trap-Fourier transform mass spectrometer," *J. Chromatogr. A*, 2006.

[19] S. E. Warder *et al.*, "Reducing agent-mediated precipitation of high-abundance plasma proteins," *Anal. Biochem.*, vol. 387, no. 2, pp. 184–193, 2009.

[20] R. L. Gundry, Q. Fu, C. a Jelinek, J. E. Van Eyk, and R. J, "NIH Public Access," *System*, vol. 1, no. 1, pp. 73–88, 2010.

[21] P. Dowling *et al.*, "Transferrin-bound proteins as potential biomarkers for advanced breast cancer patients," *BBA Clin.*, vol. 2, pp. 24–30, Dec. 2014.

[22] R. L. Gundry, M. Y. White, J. Nogee, I. Tchernyshyov, and J. E. Van Eyk, "Assessment of albumin removal from an immunoaffinity spin column: Critical implications for proteomic examination of the albuminome and albumin-depleted samples," *Proteomics*, 2009.

[23] F. T. Stevenson, "Inflammation and End-Stage Renal Disease : Recent Insights."

[24] M. I. Hassan, A. Waheed, S. Yadav, T. P. Singh, and F. Ahmad, "Zinc 2-Glycoprotein: A Multidisciplinary Protein," *Mol. Cancer Res.*, 2008.

[25] I. Sörensen-Zender, J. Beneke, B. M. Schmidt, J. Menne, H. Haller, and R. Schmitt, "Zinc-alpha2-glycoprotein in patients with acute and chronic kidney disease," *BMC Nephrol.*, vol. 14, no. 1, pp. 1–6, 2013.

[26] D. M. Lefler, M. G. Pafford, N. A. Black, J. R. Raymond, and J. M. Arthur, "Identification of proteins in slow continuous ultrafiltrate by reversed-phase chromatography and proteomics," *J. Proteome Res.*, 2004.

[27] Y. Liu, D. Wang, D. Li, R. Sun, and M. Xia, "Associations of retinol-binding protein 4 with oxidative stress, inflammatory markers, and metabolic syndrome in a middle-aged and elderly Chinese population," *Diabetol. Metab. Syndr.*, 2014.

CHAPTER V. CLASSIFYING PATIENTS IN PERITONEAL DIALYSIS BY MASS SPECTROMETRY-BASED PROFILING[1]

[1] Araújo JE, Jorge S, Magriço R, Teixeira-Costa F, Ramos A, Reboiro-Jato M, Fdez-Riverola F, Lodeiro C, Capelo JL, Santos HM (2016) Talanta, 152, 364-370. doi: 10.1016/j.talanta.2016.02.026

Abstract

Protein equalization with dithiothreitol, protein depletion with acetonitrile and the entire proteome were assessed in conjunction with matrix assisted laser desorption ionization time of flight mass spectrometry-based profiling for a fast and effective classification of patients with renal insufficiency. Two case groups were recruited as proof of concept, patients with chronic glomerulonephritis and diabetic nephropathy. Two key tools were used to develop this approach: protein concentration with centrifugal concentrator tubes with 10 KDa cut-off membranes and chemical assisted protein equalization with dithiothreitol or chemical assisted protein depletion with acetonitrile. In-house developed software was used to apply principal component analysis and hierarchical clustering to the profiles obtained. The results suggest that chemical assisted protein equalization with dithiothreitol is a methodology more robust than the other two ones, as the patients were well grouped by principal component analysis or by hierarchical clustering.

Keywords: Peritoneal dialysate, Profiling, Mass spectrometry, MALDI, PCA and Hierarchical clustering

1-Introduction

In a typical matrix-assisted laser desorption ionization time of flight mass spectrometry, MALDI-TOF, experiment of trypsinated proteomes, first the proteome is treated to isolate the proteins from other molecules and then proteins are cleavage with an enzyme, commonly trypsin[1]. Through this way a pool of peptides is obtained which is then mixed with the so-called matrix and spotted in a MALDI target plate, where a sample-matrix crystal is formed [2]. Then a laser is fired over the sample and a plum of peptides is obtained, which is directed towards a time of flight analyser. Through the aforementioned process, a number of signals corresponding to the m/z peptide ratios are obtained. As for the majority of the peptides the net charge is +1, in practical terms each signal corresponds to the effective mass of the peptide. Such m/z signals can be treated as series of numbers. Each series can be considered as a “profile” of the sample under study [2], [3]. Profiles can be interrogated with modern bioinformatics tools using a number of features such as principal component analysis or clustering. However, both, the large number of proteins as well as the large variation in their concentrations make profiling of human samples by MALDI-TOF a challenge [4], [5]. The presence of the so-called major proteins severely affects profiling, hampering an effective implementation of this approach in large scale. As an example, 20 proteins accounts for more than 99% of the nominal mass of serum. If a sample containing these proteins is profiled, the majority of the m/z signals obtained using MALDI-TOF are anticipated to belong to them. Thus, the profiles between samples will be very similar and the possibility to work with them, for instance, for classification purposes, is severely limited. To overcome this problem different sample treatments have been developed by the analytical community. Thus, protein

depletion and protein equalization are ways to selectively deploy major proteins from human samples [6], [7]. Although these methods lack a standard definition there is a growing consensus about them. By protein depletion it is understood the selective removal of a protein or group of proteins from the sample of interest and by protein equalization it is understood the selective partial removal of a protein or group of proteins. Serum protein depletion with acetonitrile and protein equalization with DTT are convenient methods to selectively enrich serum extracts in apolipoproteins and immunoglobulins, respectively. As a matter of fact, the sequential use of both methods has been recently reported as a successful method in discovering new biomarkers for the diagnostic of osteoarthritis [8]. As a result, a new term has been coined called sequential depletion.

The bottleneck in proteomics uses to be sample treatment. The classic sample treatment for protein trypsination used to last for 12 h (overnight). However, ultrasonic energy and microwave energy have been proposed as a way to overcome this problem by boosting enzymatic protein cleavage from hours to some minutes [9]. Ultrasonic energy is gaining momentum in the proteomics arena as it can be delivered into the sample indirectly through the container´s walls, it allows high sample throughput, it is of easy handling and it can be afforded at a reasonable cost. A detailed step-by-step tutorial is available in literature [9].

Profiling cannot be accomplished without good bioinformatics tools, in other words, the amount of data generated when a high number of samples are profiled is too large to deal manually with it. This is the reason why there are many commercial software packages available to handle data. However, they are expensive and as a general role they require a training course. Currently, many labs develop their own in-house software to deal with their own samples.

Renal insufficiency is a medical condition in which kidneys fail to adequately filter waste products from the blood, eventually leading to dead. Therapy for renal failure can be done by methods such as peritoneal dialysis (PD) and haemodialysis, both of which effectively remove blood´s waste products [10]-[13]. PD is based on the use of the peritoneal membrane as a replacement of the kidney. This is possible because the peritoneal membrane can function as a dialyzing membrane, allowing to mimic the kidney capabilities for cleaning solutes and waste products from the blood [14], [15]. Although PD replaces the function of the kidney, pathologic damage of the peritoneum frequently results in decreasing of the dialysing capacity and then, patient is forced to move to haemodialysis. At this stage, the patient's condition gets worst slowly but constantly, leading to the death of the patient [16],[17]. To enlarge the lifespan of the peritoneum membrane the prediction of its degradation is of critical importance. The PD renders a sample reach in proteins and metabolites, which has been scarcely studied in terms of profiling.

The present work aims to compare the performance of chemical assisted depletion with acetonitrile versus equalization with DTT in PD extracts for MALDI-TOF-based profiling. For comparative purposes samples with the entire proteome are also used. In house made software is used to obtain principal component analysis and clustering [18]. To accomplish all these tasks two groups of

patients in peritoneal dialysis were recruited, patients with chronic glomerulonephritis and diabetic nephropathy.

2-Material and methods

2.1. Reagents

All reagents used were HPLC grade or electrophoresis grade. Albumin, from bovine serum (BSA), Bradford reagent, DL-dithiothreitol (DTT), iodoacetamide (IAA), trifluoroacetic acid (TFA), Trypsin (sequencing grade) and acetonitrile (ACN, LC-MS CHROMASOLV(R)), were purchased from Sigma-Aldrich (St. Louis, USA). Ammonium bicarbonate (Ambic) and formic acid were purchased from Fluka (Steinheim, Germany). α-Cyano-4-hydroxycinnamicacid puriss for MALDI-MS (Fluka,Germany) was used as MALDI matrix. Calibration 1, 4700 Proteomics Analyzer Calibration Mixture from ABSciex (Framingham, MA, USA) was used as a mass calibration standard for MALDI-TOF/TOF-MS measurements.

2.2-Samples

Peritoneal dialysis effluent samples from ten anonymous patients from the Garcia de Orta Hospital, Portugal were collected in centrifuge sterile tubes supplemented with sodium fluoride and EDTA. Four patients with glomerular chronic nephritis, GNC, and six with diabetic nephropathy, DN, were enrolled in this study. For further details, refers to Table 1 of supplementary information. The patients were informed about the project and their consent was requested in written. The local ethics committee approved the procedure. Once in the laboratory, the samples were centrifuged at 9000 g for 20 min to remove insoluble solids and stored at 80 °C until use.

2.3-Apparatus

PDE samples were collected and aliquoted in centrifuge sterile tubes of 50 mL and 15 mL, respectively (Ratiolab, Germany). Protein concentration was done in Vivaspin centrifugal concentrators of 50 mL from Sartorius Stedim Biotech (Bohemia, U.S.A.) and protein digestion was done in safe-lock tubes of 0.5 mL from Eppendorf (Hamburg, Germany). A vacuum concentrator centrifuge model UNIVAPO 150 ECH SpeedVac and a vacuum pump model UNIJET II (Munich, Germany) were used for sample drying and sample pre-concentration. A mini incubator from Labnet (New Jersey, U.S.A.) was used for protein reduction and for protein alkylation steps. Centrifuge MPW-350 from MPW Med. Instruments (Warsaw, Poland), vortex models ELMI CM70M-09 Sky Line (Southern California, U.S.A.) and Labnet vortex mixer VX-200 (New Jersey, U.S.A.), were used throughout the sample treatment. An ultrasonic bath, Elma model Transsonic TI-H-5 (Singen, Germany), was used to facilitate protein depletion and peptide solubilization step. A sonoreactor model UTR200 from Dr. Hielscher (Teltow, Germany) was used to accelerate enzymatic protein digestions. Protein identification was done in an Ultraflex II MALDI-TOF/TOF instrument from Bruker Daltonics.

2.4-Peritoneal dialysate concentration

After PDE centrifugation at 9000 ×g for 20 min at 4 °C cell debris was discarded. PDE supernatant (SN) was aliquoted in 15 mL tubes and stored at -80 °C. PDE concentration and desalting was performed in centrifugal concentrator's tubes with 10 KDa cut-off membrane. Centrifugation at 5000×g for 20 min at 4 °C was used to concentrate 10 mL of PD until a final volume ranging from 150 µL to 300 µL was obtained. Then, the concentrated PD was transferred into clean safe-lock tubes. Then, the 10KDa membrane was washed with 50 µl of MQ-Water and then the water was added to the safe-lock tube with the concentrated PDE (see Figure 1 for further details). Then, the sample was quantified using the Bradford method according to the protocol described by [19]. Once the samples were quantified, they were splitted in aliquots of 20 mL and stored in 0.5 mL safe-lock tubes at -60 °C.

2.5-Protein depletion with ACN

Protein depletion with ACN was performed according to the protocol described by Kay *et al.* with minor modifications [20], [21]. In brief, ten samples from the same number of patients were used. For each patient, five stored aliquots as described in 2.4 were used. Each aliquot was diluted with 44 µL of water and then samples were vortexed during 30 s. Then 85 µL of ACN were added to each aliquot and each sample was sonicated for 10 min in an ultrasonic bath (100% amplitude, 35 kHz, 50 W). Then, the samples were vortexed 30 s and then sonicated 10 min again. Once the precipitate was formed, the samples were pelleted by centrifugation at 14.000×g for 10 min at 18 °C. Then, the five supernatants were pooled into a clean safe-lock tube and then the pool was pre-concentrated until 10 µL, in a vacuum concentrator centrifuge without heating (Figure 1). Finally, this sample was then quantified using the Bradford method.

2.6-Protein equalization with DTT

Protein equalization from PDE samples was performed with dithiothreitol, DTT, according to the protocol described by Warder *et al.* [22] with minor modifications as described by Fernández *et al.* and Araújo *et al.*[21], [23]. Ten samples from the same number of patients were used. For each patient, five stored aliquots as described in 2.4 were used. In brief, to 20 µL of serum, 2.2 µL DTT 500 mM were added and the resulting mixture was vortexed for 20 s. The samples were then incubated for 1 h until a white precipitate was observed. Then the samples were pelleted by centrifugation at 14.000×g (2×20 min^2 at 18 °C) (Figure 1). This process was performed with five aliquots for each patient. Then, the supernatants were pooled in a clean safe-lock tube and total protein content was determined using a Bradford protein assay.

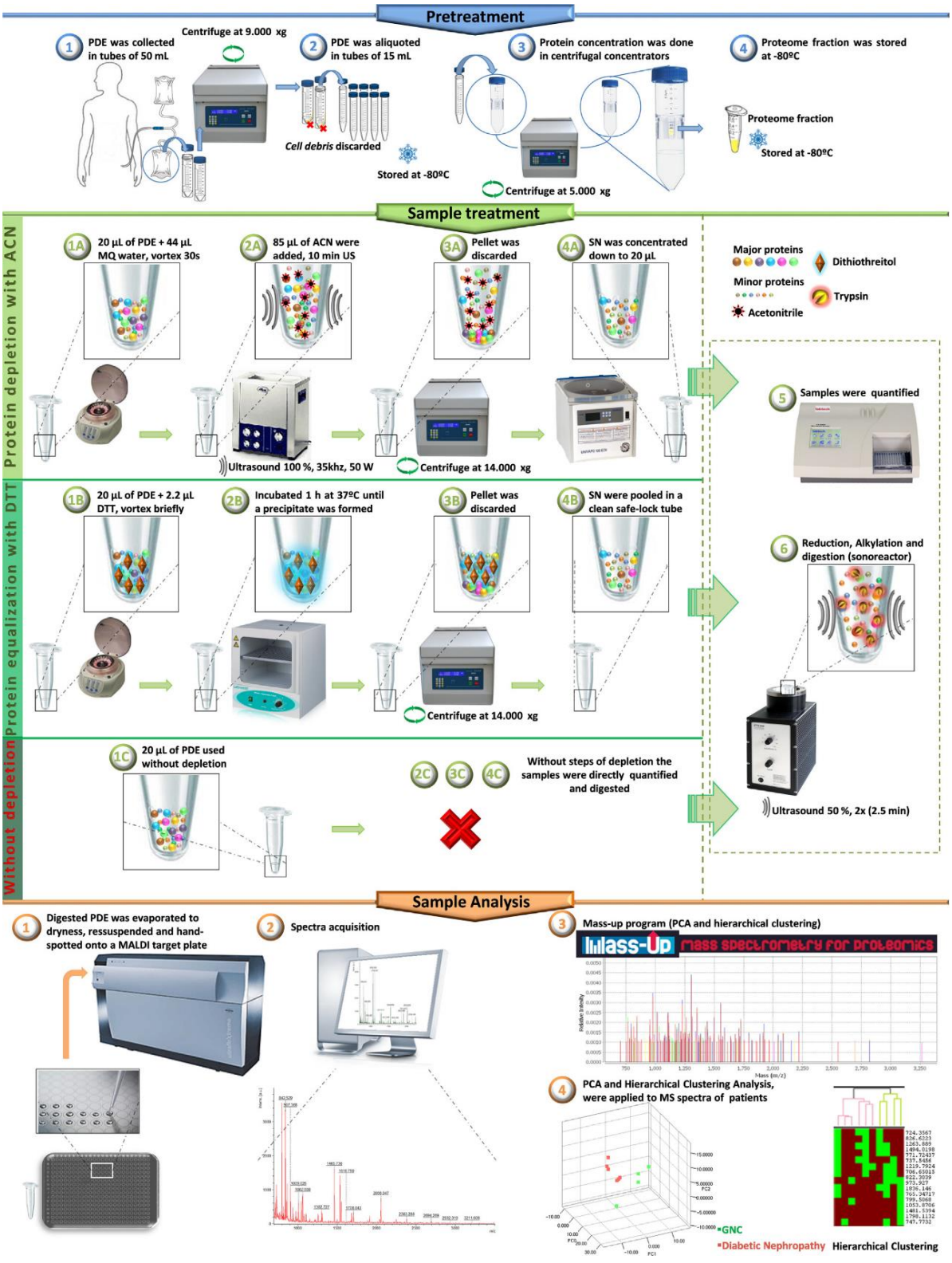

Figure 1- PDE sample treatment chart (Adapted from Araújo *et al.* [23]). **Sample pretreatment**: the protein content of 50 ml of PDE is concentrated to c.a. 150 µL using protein concentration tubes. **Sample treatment**: (A) Protein depletion with ACN, was used to avoid the presence of major protein. (B) Protein equalization with DTT, was used to equalize the proteome content. (C) Without depletion, no pre-treatment was used to avoid major protein or equalize the protein content. The pools of proteins obtained for all the three treatments were quantified and then trypsinated using ultrafast protein digestion. **Sample Analysis**: Peptides were analyzed by MALDI-TOF MS. Finally, the Mass- Up program was used to support the pre-processing and analysis of MALDI-TOF mass spectrometry data.

2.7-In-solution protein digestion

Ultrasonic in-solution digestion was performed according to the ultrafast proteolytic digestion protocol previously developed in our laboratory [24]. Before protein digestion, the pH of the samples obtained in 2.5 were adjusted to 8.0 adding 1 µl of Ambic 0.5 M. Protein disulfide bonds were reduced with 2 µl 110mM DTT, the sample was then vortexed and incubated (Labnet incubator) during 45 min at 37 °C. The resulting cysteines were then blocked with 2 µl IAA 400 mM, the sample was again vortexed and incubated during 45 min at room temperature in the dark. The sample was diluted to a final volume of 100 µl with AmBic 12.5 mM. For protein digestion, the reduced and alkylated samples were diluted to 0.04 mg/mL (2 mg of protein in a volume of 50 mL of AmBic 12.5 mM). Afterwards, trypsin was added according to the ratio 1:20 (w/w) twice (addition of 2.5 µL of trypsin, ultrasonic sonoreactor digestion, addition of another 2.5 µL of trypsin and then a final ultrasonic digestion with sonoreactor). Once the trypsin was added, the digestion was performed in the sonoreactor with the following operating conditions: 50% ultrasonic amplitude and 2.5 min ultrasonic time. Finally, 5 µl of formic acid 50% (v/v) were added to stop the enzymatic activity (Figure 1), and the digested PDE was evaporated to dryness.

2.8-MALDI-TOF-MS analysis

Prior to analysis, samples were resuspended in 10 µL of formic acid 0.3% and 0.5 µL of sample was hand-spotted onto a MALDI target plate (384-spot ground steel plate) then 1 µL of a 7 mg/mL solution of a-cyano-4-hydroxycinnamic acid matrix in 0.1% (v/v) TFA and 50% (v/v) ACN was added and allowed to air dry. The mass spectrometer was operated in positive ion mode using a reflectron, and thus, spectra were acquired in the m/z range of 600–3500. A total of 500 spectra were acquired for each sample at a laser frequency of 50 Hz. External calibration was performed with the $[M+H]^+$ monoisotopic peaks of bradykinin 1–7 (m/z 757.3992), angiotensin II (m/z 1046.5418), angiotensin I (m/z 1296.6848) substance P (m/z 1758.9326), ACTH clip 1–17 (m/z 2093.0862), ACTH18–39 (m/z 2465.1983) and somatostatin 28 (m/z 3147.4710). Peptide mass fingerprints (PMF) were searched with MASCOT search engine with the following parameters: (i) SwissProt Database2012_04 (535698 sequences;190107059 residues); (ii) molecular weight of protein: all; (iii) one missed cleavage; (iv) fixed modifications: carbamidomethylation (C); (v) variable modifications: oxidation of methionine and (vi) peptide tolerance up to 100 ppm after close external calibration. The significance threshold was set to a minimum of 95% (pr0.05). A match was considered successful when protein identification score is located out of the random region and the protein analysed scores first.

2.9-Principal component analysis (PCA)

Each sample was spotted in the MALDI plate five times. The corresponding raw-data spectrum of each sample was pre-processed with the Mass-Up v1.0.9 open source program (http://sing.ei.uvigo.es/mass-up/) using the following parameters: (i) Intensity transformation (Square root), (ii) Smoothing (None), (iii) Baseline correction (Snip), (iv) Standardization (Total Ion Current),

(v) Peak detection (MALDIquant: SNR (3), HalfWindowSize (60)), (vi) Minimum peak intensity (0.001). Peaks were matched with the following parameters: (i) Intra-sample matching (MALDIquant: tolerance (0.002)), without select the "generate consensus spectrum" box, (ii) Inter-sample matching (MALDIquant: tolerance (0.002). Then the PCA was run with the following parameters: (i) Max. Components (1, for no maximum number of components), (ii) Variance Covered (0.95).

2.10-Hierarchical clustering analysis

An agglomerative hierarchical clustering analysis was applied as a complement to the PCA. Using the same data as pre-processing as described above for the PCA, the clustering analysis operation of the Mass-Up software was executed with the following parameters: (i) Minimum variance (0), (ii) Peak List (NULL4for no peak filtering), (iii) Cluster Reference Value (Average), (iv) Distance Function (Hamming), (v) Conversion Values (Presence), (vi) Intrasample Minimum Presence (0) (vii) Deep Clustering (No).

3-Results and discussion

3.1-Sample treatments

The literature dealing with the protein content of peritoneal dialysate extract, PDE, is currently scarce. Cuccurullo *et al.* claim a number of proteins as large as 151 to be present in PD extract [25]. To avoid the presence of major proteins in serum we have previously reported protein depletion with acetonitrile, ACN, and protein equalization with dithiothreitol, DTT [21].With the aim to get insight into the proteome of PD extracts we tried the same approach. As can be seen in Figure 2a the use of ACN in concentration circa 57% V/V selectively depletes proteins with masses higher than 75KDa. The major proteins belong to this group. Although the mechanism involved in ACN-promoted protein depletion has not been well established yet, the supernatant is rendered reach in apolipo-type proteins when this depletion is used in PDE (see Figure 2b). Interestingly, DTT diminish the content of major proteins in sera samples as well, but only in some extent as can be seen in Figure 2a. Furthermore, DTT renders an extract reach in immunoglobulin-type proteins. These results are in agreement with the ones obtained previously by our team [21], [23] and they suggest that ACN and DTT perform in a similar manner when they are applied to complex proteomes. This is shown in Figure 2b. This conclusion is important because it suggests that both reagents can be universally used for protein depletion and equalization, respectively, regardless of the type of sample. A third sample treatment was also tested in this work in which the samples were used with the entire protein content. As the sample rendered by each method is rich in different types of proteins, it was anticipated different MALDI-TOF profiles for each one. An example of such profiles is presented in Figure 2c. Differences can be noted even by naked eye. As for previous works developed in our laboratory the number of times that one sample must be spotted in the MALDI-plate for profiling purposes is five [26]. Therefore, all the samples were spotted into the MALDI target five times, then the spectra were normalized and aligned with the Mass-Up

program [18]. Then the spectra were used for analysing the samples using principal component analysis and hierarchical clustering.

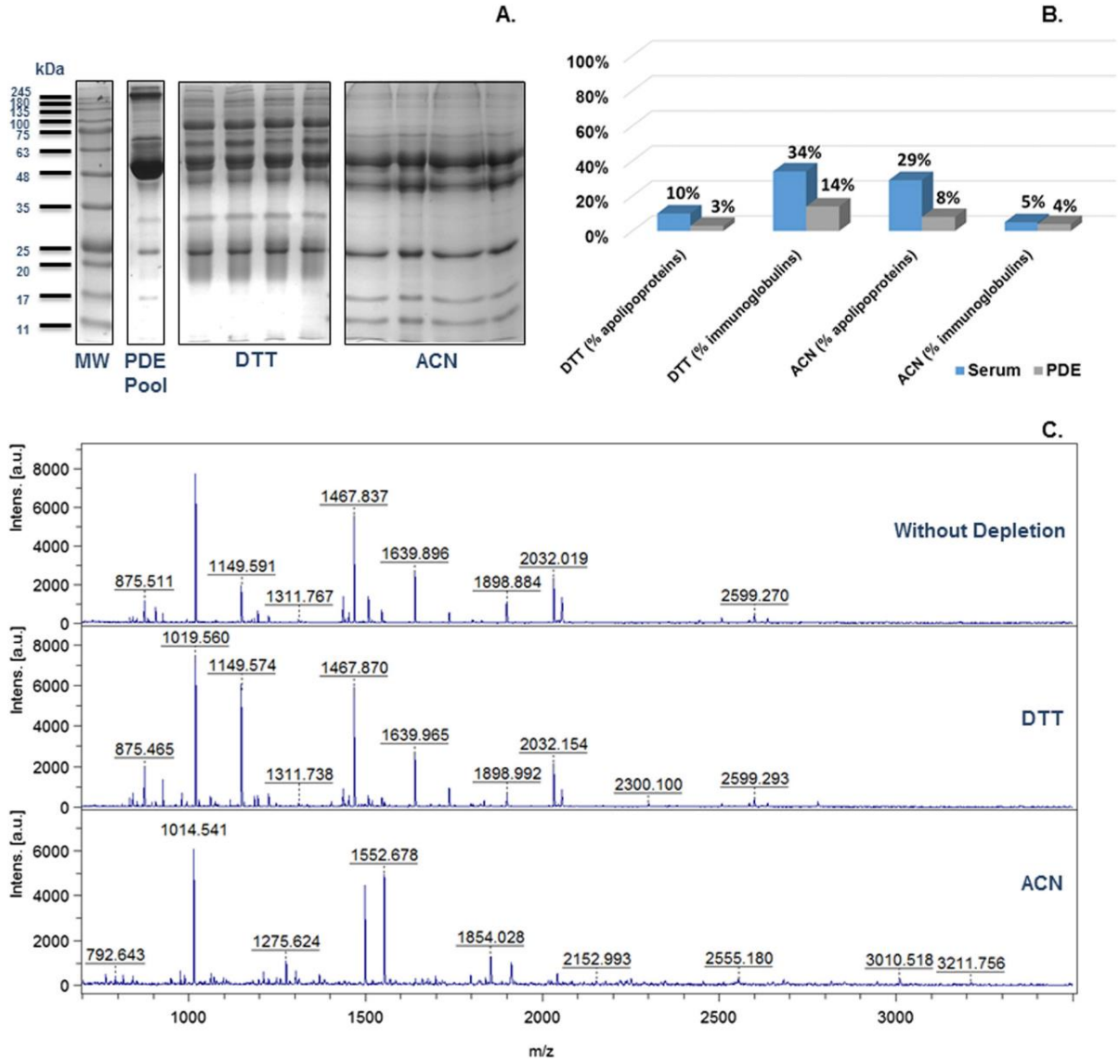

Figure 2-(A) 1D-SDS-PAGE, 12.5% polyacrylamide gels with 1 mm thickness: Molecular Weight standard (first lane), PDE Pool without treatment (second lane), DTT-treated samples (3–6 lanes) and ACN-treated samples (57%) (6–10 lanes). (B) Bar charts with the comparative percentage of immunoglobulins and apolipoproteins identified in each treatment (DTT and ACN) and for different samples (Serum and PDE). (C) MALDI-TOF-MS-based profiles obtained for the same patient with different treatment methods (without depletion, DTT, ACN).

3.2-Principal component analysis and hierarchical clustering analysis

Figure 3 shows the PCAs for the three sample treatments used in this work. The PCAs were obtained using the Mass-Up program[18]. It may be seen that the classification is only achieved with the profiles obtained using chemical assisted equalization with DTT. Depletion of major proteins using ACN does not bring benefits in terms of class separation and when the sample is used with the entire proteome the results are similar. This suggests that total removal of major proteins, such as when ACN

is used, or their non-removal, such as when all the proteome remains in the sample, are not adequate approaches if PDE samples are going to be classified using MALDI mass spectrometry-based profiling. The PCA result was further confirmed using hierarchical clustering.

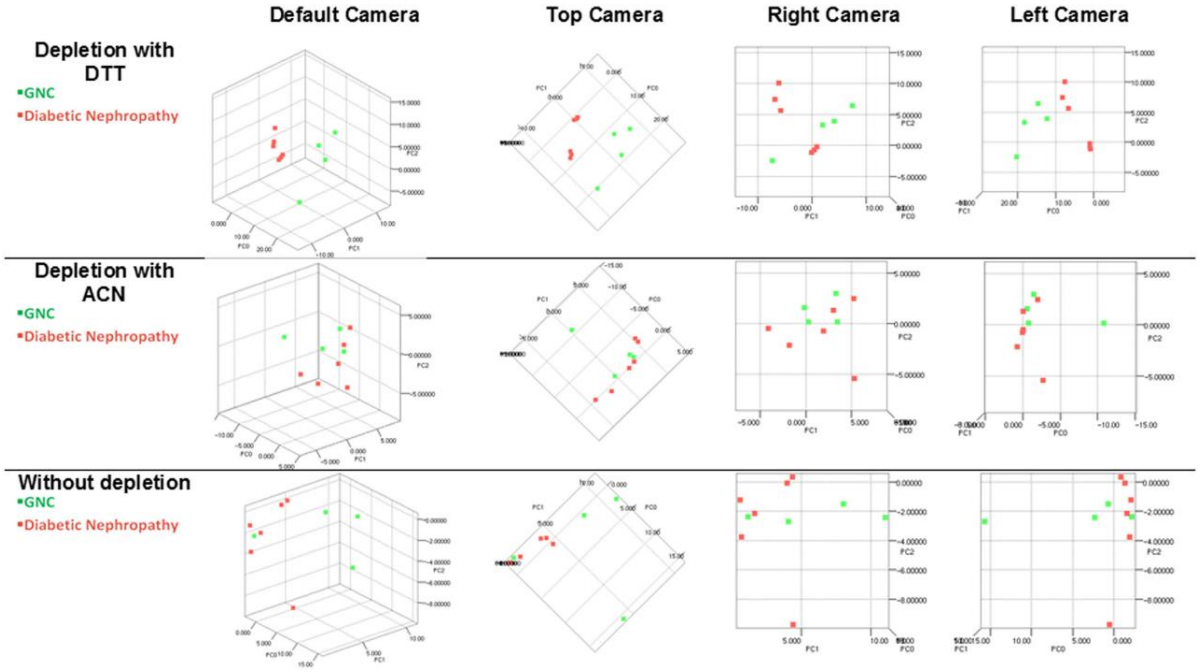

Figure 3- Mass-Up 3D Principal Component Analysis (PCA) for each sample treatment method.

As may be seen in Figure 4, only the profiles obtained with the DTT-chemical assisted equalization allows for classifying the patients correctly using either PCA or hierarchical clustering. For the case of ACN we hypothesize that depletion of mayor proteins concomitantly depletes some minor proteins as well, thus some important m/z signals for classification are then missed. When no depletion is used, the presence of peptides from major proteins hides the signals that are needed for classification. Because DTT only partially depletes major proteins, m/z signals for classification are retained.

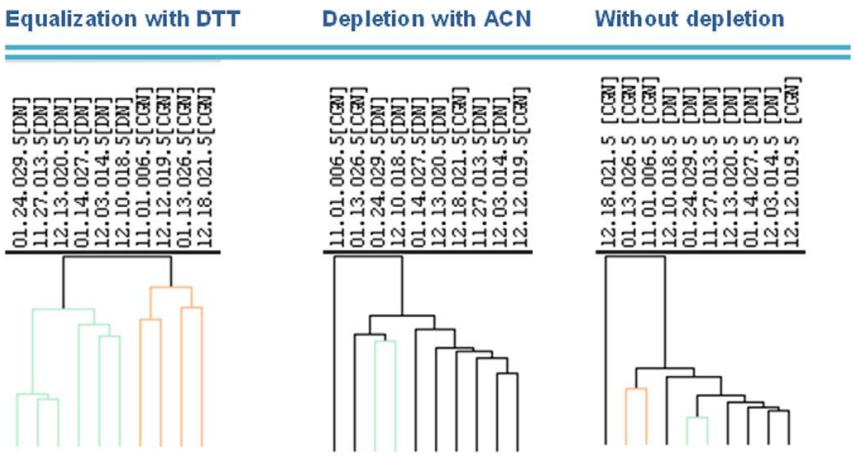

Figure 4- Mass-Up Hierarchical Clustering Analysis for each sample treatment method.

4-Conclusions

Chemical assisted depletion with acetonitrile, chemical assisted equalization with dithiothreitol and the use of the entire proteome were tested in peritoneal liquid extract to investigate their performance to obtain MALDI-TOF-MS-based profiles in order to classify two groups of patients, namely patients with chronic glomerulonephritis and diabetic nephropathy. The results suggest that chemical assisted protein equalization with DTT is a methodology more robust than the other two ones, as the patients were well grouped by principal component analysis or by hierarchical clustering. This result suggests that successful MALDI-MS-based profiling of PDE samples relies in the selection of an appropriate sample treatment to compress the complexity of the proteome appropriately. We propose protein depletion with DTT as such treatment.

5-Conflict of interest

The authors declare no conflict of interest.

6-Acknowledgments

J. E. Araújo acknowledges the doctoral grant SFRH/BD/109201/2015 and H. M. Santos the post-doctoral grant SRFH/BPD/73997/2010 both provided by Fundação para a Ciência e a Tecnologia Ministério da Educação e Ciência (FCT–MEC, Portugal). Dr. J. L.Capelo Acknowledges Associated Laboratory for Sustainable Chemistry-Clean Processes and Technologies- LAQV which is financed by national funds from FCT/MEC (UID/QUI/50006/2013) and co-financed by the ERDF under the PT2020 Partnership Agreement (POCI-01-0145-FEDER-007265). This work was supported by PROTEOMASS Scientific Society (Portugal). Authors thank REQUIMTE-FCT PEst-C/EQB/LA0006/2013 project.

7-Data Accessibility

Supplementary data to this article can be found online at http://dx.doi.org/10.1016/j.talanta.2016.02.026.

8-References

[1] J. S. Cottrell, “Protein identification using MS/MS data,” *J. Proteomics*, vol. 74, no. 10, pp. 1842–1851, Sep. 2011.

[2] F. Hillenkamp and J. Peter-Katalinic, *MALDI MS: A Practical Guide to Instrumentation, Methods and Applications*, 2nd Editio. 2013.

[3] R. B. Cole, Ed., *Electrospray and MALDI Mass Spectrometry: Fundamentals, Instrumentation, Practicalities, and Biological Applications*, 2nd Editio. 2010.

[4] H. Bensmail, O. J. Semmes, and A. Haoudi, “Clustering Proteomics Data Using Bayesian Principal Component Analysis,” in *Data Mining in Biomedicine*, P. M. Pardalos, V. L. Boginski, and A. Vazacopoulos, Eds. Boston, MA: Springer US, 2007, pp. 339–362.

[5] B. Meunier, E. Dumas, I. Piec, D. Béchet, M. Hébraud, and J. F. Hocquette, "Assessment of hierarchical clustering methodologies for proteomic data mining," *J. Proteome Res.*, 2007.

[6] N. L. Anderson and N. G. Anderson, "The Human Plasma Proteome: History, Character, and Diagnostic Prospects: Figure 3.," *Mol. Cell. Proteomics*, 2003.

[7] S. Roche *et al.*, "Depletion of one, six, twelve or twenty major blood proteins before proteomic analysis: The more the better?," *J. Proteomics*, 2009.

[8] C. Fernández-Costa, V. Calamia, P. Fernández-Puente, J. L. Capelo-Martínez, C. Ruiz-Romero, and F. J. Blanco, "Sequential depletion of human serum for the search of osteoarthritis biomarkers," *Proteome Sci.*, 2012.

[9] J. E. Araújo *et al.*, "A journey through PROTEOSONICS," *Talanta*. 2014.

[10] Y.-C. Tyan, S.-B. Su, S.-S. Ting, and H.-Y. Wang, "A comparative proteomics analysis of peritoneal dialysate before and after the occurrence of peritonitis episode by mass spectrometry," *Clin. Chim. Acta*, vol. 420, pp. 34–44, May 2013.

[11] N. Ghahramani, S. Shadrou, and C. Hollenbeak, "A systematic review of continuous renal replacement therapy and intermittent haemodialysis in management of patients with acute renal failure," *Nephrology*, 2008.

[12] P. L. Kimmel and S. S. Patel, "Quality of life in patients with chronic kidney disease: Focus on end-stage renal disease treated with hemodialysis," *Seminars in Nephrology*. 2006.

[13] S. M. A. De Lima *et al.*, "Inflammation, neoangiogenesis and fibrosis in peritoneal dialysis," *Clinica Chimica Acta*. 2013.

[14] W. Q. *et al.*, "Proteomic analysis in peritoneal dialysis patients with different peritoneal transport characteristics," *Biochem. Biophys. Res. Commun.*, vol. 438, no. 3, pp. 473–478, 2013.

[15] M. Lechner *et al.*, "A proteomic view on the role of glucose in peritoneal dialysis," *J. Proteome Res.*, 2010.

[16] D. Lopes Barreto and R. T. Krediet, "Current status and practical use of effluent biomarkers in peritoneal dialysis patients," *Am. J. Kidney Dis.*, 2013.

[17] R. T. Krediet and D. G. Struijk, "Peritoneal changes in patients on long-term peritoneal dialysis.," *Nat. Rev. Nephrol.*, vol. 9, no. 7, pp. 419–29, 2013.

[18] H. López-Fernández, H. M. Santos, J. L. Capelo, F. Fdez-Riverola, D. Glez-Peña, and M. Reboiro-Jato, "Mass-Up: An all-in-one open software application for MALDI-TOF mass spectrometry knowledge discovery," *BMC Bioinformatics*, 2015.

[19] M. M. Bradford, "A rapid and sensitive method for the quantitation of microgram quantities of protein utilizing the principle of protein-dye binding," *Anal. Biochem.*, 1976.

[20] R. Kay *et al.*, "Enrichment of low molecular weight serum proteins using acetonitrile precipitation for mass spectrometry based proteomic analysis," *Rapid Commun. Mass Spectrom.*, 2008.

[21] C. Fernandez, H. M. Santos, C. Ruiz-Romero, F. J. Blanco, and J. L. Capelo-Martínez, "A comparison of depletion versus equalization for reducing high-abundance proteins in human serum," *Electrophoresis*, vol. 32, no. 21, pp. 2966–2974, 2011.

[22] S. E. Warder *et al.*, "Reducing agent-mediated precipitation of high-abundance plasma proteins," *Anal. Biochem.*, vol. 387, no. 2, pp. 184–193, 2009.

[23] J. E. Araújo *et al.*, "Matrix-assisted laser desorption/ionization time-of-flight mass spectrometry-based profiling as a step forward in the characterization of peritoneal dialysis effluent," *Anal. Methods*, vol. 7, no. 18, pp. 7467–7473, 2015.

[24] R. Rial-Otero *et al.*, "Sonoreactor-based technology for fast high-throughput proteolytic digestion of proteins," *J. Proteome Res.*, 2007.

[25] M. Cuccurullo *et al.*, "Proteomic analysis of peritoneal fluid of patients treated by peritoneal dialysis: Effect of glucose concentration," *Nephrol. Dial. Transplant.*, 2011.

[26] J. D. Nunes-Miranda *et al.*, "Direct matrix assisted laser desorption ionization mass spectrometry-based analysis of wine as a powerful tool for classification purposes," *Talanta*, 2012.

CHAPTER VI. IN-DEPTH ANALYSIS OF PERITONEAL DIALYSIS EFFLUENT PROTEOME AND PEPTIDOME: A LONGITUDINAL FOLLOW-UP STUDY[1]

[1] Araújo JE, Branca RM, Siavelis I, Mermelekas G, Pernemalm M, Stahl M, Sousa M, Teixeira-Costa F, Ramos A, Santos, HM, Capelo JL, Lehtiö J (2019). *In preparation*

Abstract

Long-term peritoneal dialysis (PD) leads to morphological and functional alterations in the peritoneal membrane (PM), reducing the lifespan of this renal replacement therapy. Unfortunately, non-invasive ways to anticipate PM failure unavailable, and even though routine PD parameters are used to follow the PM condition, they may only change in a very late stage, when PM function is no longer recoverable. Peritoneal dialysis effluent (PDE) represents a useful reservoir of potential clinical biomarkers that may help to identify those patients at a higher risk for PD-related complications. Here, we perform for the first time longitudinal PDE proteomics and peptidomics studies on samples from 45 patients, attempting to unravel the morphological and biochemical changes occurring during long-term PD. We employed high-resolution peptide isoelectric focusing (HiRIEF) combined with LC-ESI-Q-Exactive Orbitrap MS/MS analysis. This approach rendered a total of 5478 proteins identified, greatly increasing the protein PDE coverage On the other hand, label-free quantitative approach was applied for the first time in the analysis of PDE endogenous peptides, rendering a total of 5246 peptides identified. Thus, this study represents the most complete proteome and peptidome coverage ever achieved.

Concerning the longitudinal analysis, three clinical case studies are discussed. For case study 1, with fungal peritonitis as a reason for PD therapy dropout, the proteome analysis revealed a diminished capacity of the peritoneal host response, with a decreasing trend of proteins within pathways of immune response, such as “class I MHC mediated antigen processing presentation” and the “Il-6, -7, pathway”. For this particular case, the proteomic analysis revealed that, for instance, following the IL-6 levels could have been useful for a clinical decision. On the other hand, for case study 2, with ultrafiltration failure as a reason for PD therapy dropout, the longitudinal analysis pinpointed a decreasing trend for protein homeostasis and a panoply of metabolic pathways; and an increased trend for pathways related with extra cellular matrix (ECM). In contrast, case study 3 represents a good patient response to PD therapy, in that many of the proteins and proteases identified orchestrate and regulate the process of both synthesis and degradation of matrix within the peritoneal cavity in a well-balanced way.

Thereby, this study sheds some light on the main molecular pathways associated with long-term PD, and contributes with valuable information for the proteomic and clinical research community in future studies using PDE samples.

Keywords: Peritoneal dialysis, Peritoneal dialysis effluent, HiRIEF, Longitudinal data, Proteomics, Peptidomics, Protease prediction.

1-Introduction

To date there is focus of interest in peritoneal dialysis (PD), as it provides a better quality of life and autonomy to patients than other renal replacement therapies (RRT) such as hemodialysis and is cost-effective. Despite these benefits, the utilization of PD has not been increasing [1], [2]. In the last decade, approximately 196,000 end stage renal disease (ESRD) patients were performing PD worldwide, representing 11% of the dialysis population [3].Nowadays, the number of people suffering from chronic kidney diseases and requiring dialysis treatment is rising at a constant rate of around 6% annually, with more than 3.4 million patients expected in 2018, and approximately 4.9 million by 2025 [4]. Therefore, to move PD therapy forward some strategies need to be implemented to facilitate PD utilization, such as, policies and incentives favouring PD, appropriate training for nephrologists to increase PD utilization and to decrease the rates of technique failure. In addition, the PD community should undertake clinically meaningful studies with a strong focus on technique survival [1], [2].

PD is based on using the peritoneum because it is a semipermeable membrane through which ultrafiltration (UF) and diffusion of circulating compounds occur [5], [6]. However, long-term PD leads to morphological and functional alterations in the peritoneum, reducing the lifespan of this dialysis to five years at most, and forcing the replacement of PD by other renal replacement therapies [6], [7]. The most commonly observed morphological and functional alterations in the peritoneal membrane (PM) of long-term PD patients are; peritoneal fibrosis varying from mild, moderate to severe cases [8]; progressive mesothelial cell loss, increase of submesothelial extracellular matrix (ECM) and mesothelial to mesenchymal transition (MMT)[9]; neovascularisation and thickening; chronic inflammation and angiogenesis [8], [10]. The PM failure due to fibrosis may potentially be induced by sterile inflammation caused by ongoing cellular stress due to prolonged exposure of the peritoneum to peritoneal dialysis fluids (PDFs) [11] with high concentrations of glucose, glucose degradation products (GDP), lactate and acidic pH [12]. The use of more biocompatible PD solutions to address this problem is promising, although further morphologic studies in patients using these solutions are needed [13]. In addition, the impact of neutral-pH, low-GDP fluids regarding PM long-term integrity and function remains uncertain [12]. Besides PDF composition, other risk factors need to be considered when assessing PM adequacy, such as, duration of end-stage renal disease, diabetes mellitus and time on PD that has been proved to be a significant factor [8].

Currently there are no non-invasive ways to predict PM failure; even though parameters such as urea and creatinine concentrations, glucose transport and net ultrafiltration are used to follow the PM condition, they do not change until a very late stage, when PM function is no longer recoverable [1], [14]. The only way to follow PM failure is based on peritoneal biopsies, that allow the assessment of morphologic changes. However, these are invasive procedures that may lead to temporary discontinuation of PD therapy. Moreover, uncertainty exists about sampling errors, reproducibility, and the risk of scarring [14], [15].

Nowadays, medical diagnostics and treatment is advancing from a one size fits all strategy to a case by case patient treatment. This transition to personalized medicine arises from incorporation of more analytical techniques into medical practice giving a holistic view of patient's condition [11]. Therefore, PD therapy requires biomarkers as tools to identify patients who are at the highest risk for PD-related complications and to guide personalized interventions that may improve clinical outcome in the individual patient [16]. In addition, peritoneal dialysis effluent (PDE) represents an underestimated biochemical window into the peritoneum and a useful reservoir of potential clinical biomarkers. The possibility to identify and follow changes in the peritoneal membrane at the molecular level by proteomics and peptidomics in a longitudinal setting has been proposed to be of prime importance to unravel morphological and biochemical changes in long-term PD [7].

The present work is such a longitudinal study aiming to unravel the evolution of the proteome and peptidome of the PDE over time, to identify specific molecular changes that can be particularly interesting for the understanding and early detection of long-term PM alterations. To achieve this goal, high-resolution peptide isoelectric focusing (HiRIEF) [17] was applied for the first time to PDE samples, allowing a reproducible fractionation and leading to a reduction of PDE proteome complexity prior to LC-ESI-Orbitrap MS/MS analysis. In parallel, label-free quantitative approach was applied for the first time in the analysis of PDE native peptides. Furthermore, protease prediction analysis was performed to extend our knowledge about proteases that might be related with protein cleavage occurring inside the peritoneum. This study sheds some light on the main molecular pathways associated with long-term PD, such as, dysregulated metabolic pathways, complement and coagulation cascades activation, ECM organization, formation of fibrin clot clotting cascade and contributes with valuable information for the proteomic and clinical research community in future studies using PDE samples. In addition, some longitudinal case studies are here discussed, presenting particular cases where the proteomic analysis gives some insights about patients' health condition.

2-Material and Methods

2.1-Reagents and apparatus

All reagents used were HPLC grade or electrophoresis grade. Albumin, from bovine serum (BSA), (N, N, N′, N′-tetramethylethylene-diamine (TMED), DL-dithiotreitol (DTT), Chloroacetamide (ClAA), trypsin sequencing grade, trifluoroacetic acid (TFA), Urea and 4-(2-hydroxyethyl)-1-piperazineethanesulfonic acid (HEPES) were purchased from Sigma-Aldrich (Basel, Switzerland). Formic acid and ammonium bicarbonate (Ambic) were purchased from Fluka (Basel, Switzerland). Hydrochloric acid (HCl), sodium dodecyl sulphate (SDS), methanol, ethanol and acetonitrile were purchased from Panreac (Barcelona, Spain). Bromophenol blue was from Riedel-de Haën (Basel, Switzerland). Amicon® Ultra-4 10 K Centrifugal Filter Devices 10,000 MWCO from Millipore were used for protein pre-concentration and buffer exchange. Immobilized pH gradient (IPG) strips pH 3–10

(24 cm-long IPG), IPG Pharmalyte carrier ampholytes (pH 3-10) and mineral oil were from GE Healthcare Bio-Sciences (Sweden). Strata™ -X-C 33 µm Polymeric Strong Cation and TMT10plex™ Isobaric Label Reagent Set were purchased from ThermoFisher Scientific (Massachussetts,USA).

The isoelectric focusing was performed using the Ettan IPGphor IEF cell from GE Healthcare (Sweden). Peptide extraction was performed using liquid-handling robotics (a modified GE Healthcare Ettan Digester). Protein digestion was done in eppendorf safe-lock tubes from Eppendorf (Germany, Hamburg). A vacuum concentrator centrifuge from Thermo Scientific, model Digital Series SpeedVac™ Systems SPD111V, was used for sample drying. An incubator-shaker CERTOMAT™IS from Sartorius was used for protein digestion. The refrigerated centrifuges, Thermo Scientific Sorvall™ ST 16R Centrifuge Series and ScanSpeed 1730R were used for sample preparation. A Thermo Scientific™ Multiskan™ GO Microplate Spectrophotometer reader was used for BCC protein assay.

2.2-Ethical statement and samples collection

The study was approved by the Hospital ethical committee and followed the Helsinki declaration. The patients were informed about the study and gave their written informed consent. PDE samples were collected from consenting PD patients from the Garcia de Orta Hospital (Portugal), following a peritoneal equilibrium test (PET). All the samples were collected in centrifuge sterile tubes supplemented with a protease inhibitor cocktail, 10 mM NaEDTA and 1 mM NaF. Once in the laboratory, samples were centrifuged at 9000 ×*g* for 20min at 4ºC to remove insoluble pellets. PDE supernatant was aliquoted in 15 mL tubes and stored at - 80 °C. Further details concerning the patients enrolled in this study can be seen in the Table 1, Figure 1 and in Electronic Supplementary material (ESM) Table ESM1.

2.3-PDE concentration

Before downstream use, PDE samples were desalted and concentrated using centrifugal concentrator's tubes with 10 kDa cut-off membrane (Amicon® Ultra-4 10 K Centrifugal Filter Devices), as previously described by Araújo *et al*. [18] with some minor changes. Centrifugation at 4000×*g* for 10 min at 4 °C was used to concentrate 5 mL of PDE by duplicate, until a final volume ranging from 50 µL to 100 µL was obtained. The protein-enriched fractions were collected to clean low adhesion tubes and the fraction below 10 kDa was stored at -80ºC for further use (peptidome analysis). Finally, a BCC protein assay (750 nm) was carried out to determine the total amount of protein in the PDE concentrated samples, as described in the section 2.4. From now on the Material and methods is distinct for the Proteome and Peptidome analysis, with the exception of the following section that is performed in the same way in both experiments (see Figure 2).

Table 1- Demographic data and clinical characteristics of the PD patients cohort at the baseline.

		Reference Values
Number of patients, N (%)	45 (100.0)	---
Age [years], mean ± SD		
<49 (n=9)	34.6 ± 8.1	---
>= 49 & <70 (n=18)	61.1 ± 6.7	
>=70 (n=18)	74 ± 3.20	
Male sex, N (%)	34 (75.5)	---
Height [cm], mean ± SD	167 ± 9	---
Weight [kg], mean ± SD	70.6 ± 11.4	---
Primary Renal Disease, N (%)		
ADPKD-Autosomal dominant polycystic kidney disease	4 (8.9)	
ANCA vasculitis	2 (4.4)	
Chronic glomerulonephritis	2 (4.4)	
Chronic interstitial nephritis	2 (4.4)	
Congenital Anomalies of the Kidney and the Urinary Tract (CAKUT)	3 (6.7)	
Diabetic nephropathy	11 (24.4)	---
Hypertensive nephrosclerosis	5 (11.1)	
IgA nephropathy	4 (8.9)	
Lupus Nephritis	2 (4.4)	
Obstructive uropathy	1 (2.2)	
Paroxysmal nocturnal hemoglobinuria	1 (2.2)	
Secondary focal segmental glomerulosclerosis	1 (2.2)	
Unknown	7 (15.5)	
Comorbidities, N (%)		
Diabetes	13 (28.9)	---
Ischemic heart disease	10 (22.2)	
Cerebrovascular disease	4 (8.9)	
D/P Creatinine at 4-hr PET (mL/min), mean ± SD	0.70 ± 0.11	>0.60 mL/min
Profile transporter, N (%)		
High	9 (20)	---
High-average	25 (55.6)	
Low-average	11 (24.4)	
Peritoneal ultrafiltration (mL/ 4h), mean ± SD	716.5 ± 399.6	>400 mL/4h
Diuresis (mL/day), mean ± SD	1232.5 ± 793.6	The higher the better
Creatinine clearance (mL/min), mean ± SD	90.7 ± 34.1	>60 mL/min
Kt/v, mean ± SD	2.4 ± 0.5	1.7
Serum albumin (mg/dL), mean ± SD	3.8 ± 0.3	> 3.0 (mg/dL)
CA 125 (kU/L), mean ± SD	18.9 ± 12.1	---
Parathyroidism hormone (PTH) (pg/mL), mean ± SD	419.2 ± 285.5	<800
Glomerular filtration rate (mL/min/1.73 m2), mean ± SD	6.5 ± 4.0	---
Darbepoetin-alfa, N (%)	27 (60)	---
Antagonists of the renin-angiotensin system, N (%)	29 (64.4)	---
Statins, N (%)	30 (66.7)	---
Beta Blockers, N (%)	21 (46.7)	---

2.4-96-well plate BCC protein concentration measurement assay

Peritoneal dialysis effluent (PDE) samples were quantified using the BioRad BCC assay according to the manufactures. Briefly, a BSA standard curve (8, 4, 2, 1, 0.5, 0.25, 0.125 mg/mL) was generated in triplicate. To each well being used, 25 µL of reagent A was added as described by manufactures. Then, 5 µL of each standard and samples were added and mixed with the already added reagent A. Finally, 200 µL of reagent B were added to each well used and the plate was gently agitated and left to incubated at room temperature for 15 min. After incubation absorbance's were measured at 750 nm. Once the samples were quantified, they were divided in aliquots and stored in safe-lock tubes at −80 °C until further use.

2.5-Proteome analysis of PDE samples

2.5.1-Multiple Affinity Removal Column Human 14

Given the plasma-like composition of PDE samples, with a very wide protein dynamic range covering more than ten orders of magnitude between high abundance proteins (HAPs) and the low abundance ones, it is crucial to compress the dynamic range so as not to hamper the proteomic analysis [19]. Thus, the Agilent Human 14 Multiple Affinity Removal Column (MARS14) was used to remove fourteen interfering high-abundance proteins following the manufacturer's instructions, in order to improve the subsequent HiRIEF LC/MS analysis by effectively expanding the dynamic range of the analysis. After depletion, a buffer exchange and sample concentration step through centrifugal concentrators was performed (as described in section 2.5.1.2) (see Figure 2).

2.5.2-Buffer Exchange/Concentration Samples

After the MARS14 runs, both fractions (depleted and bound) obtained per sample were collected to centrifugal concentrators of 10 kDa and reduced to ~100 µl by centrifugation for 30 min at 4000 ×*g*. Samples were diluted with 2 mL of 50mM HEPES buffer, pH 7.6 and then concentrated again to ~100 µl by centrifugation for 30 min at 4000 ×*g*. This step was repeated once and then samples were transferred to an Eppendorf and stored on ice for further protein concentration measurement.

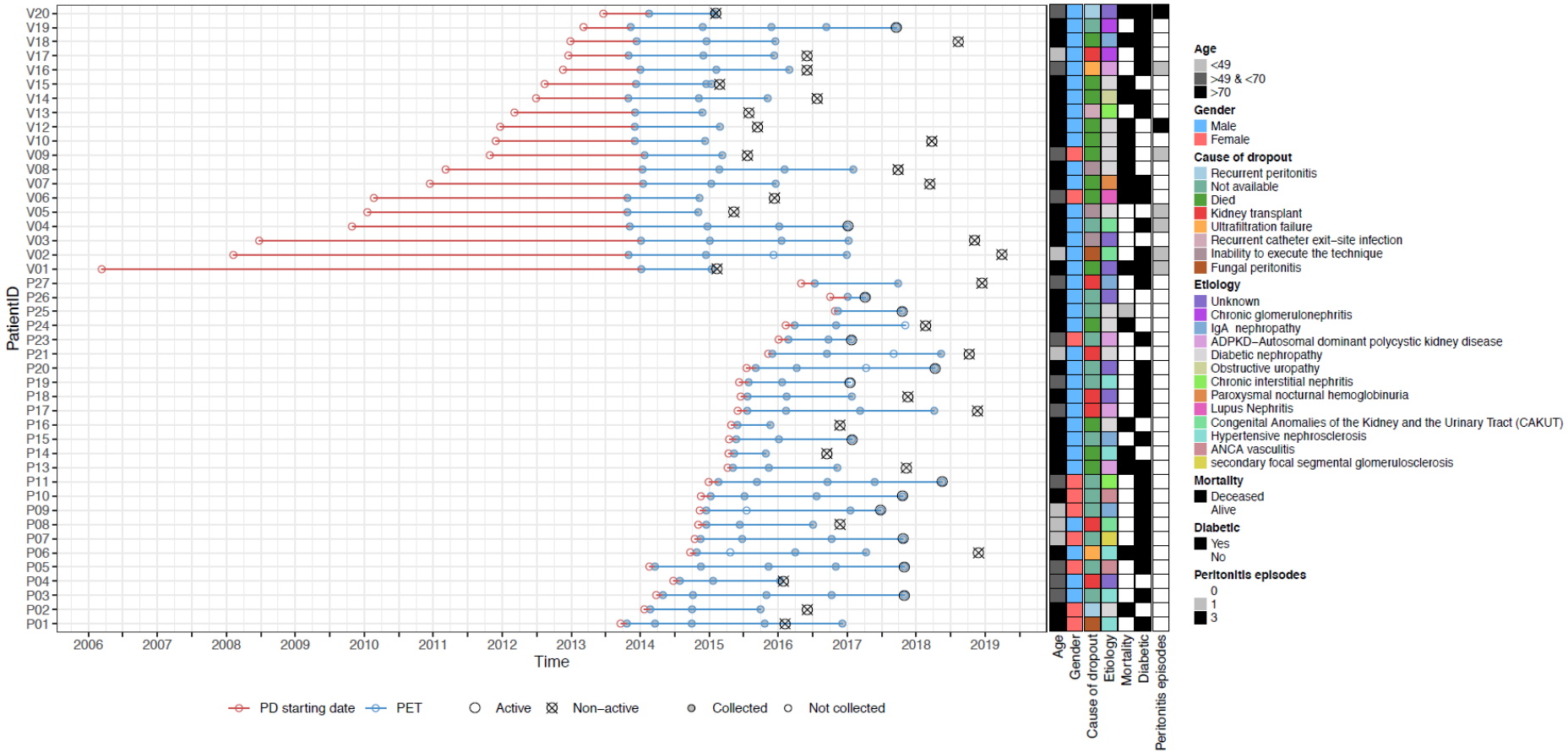

Figure 1. Longitudinal cohort description. Per patient starting date of peritoneal dialysis (PD) and Peritoneal Equilibration Test (PET) sample collection. Active and non-active patients are highlighted in different shapes. For non-active patients, the documented date of the last peritoneal dialysis is displayed.

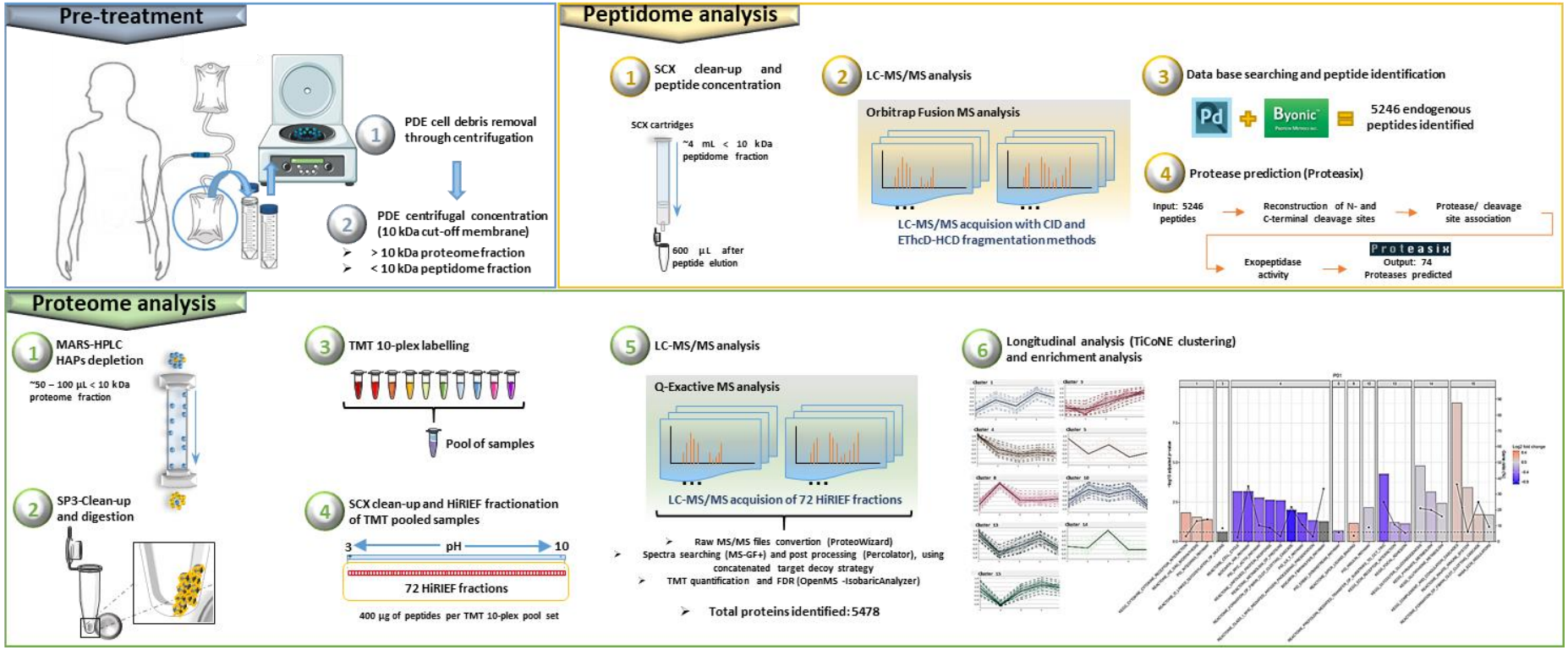

Figure 2- PDE sample treatment chart for the Proteome and Peptidome fractions. **Pre-treatment**: PDE samples are first centrifuged to remove insoluble pellets and then desalted and concentrated using centrifugal concentrator's tubes with 10 kDa cut-off membrane, thus obtaining the Proteome (> 10 kDa) and Peptidome (< 10 kDa) fractions. **The Proteome fraction (Proteome analysis)**, was subjected to protein depletion of the HAPs using the MARS14 approach. After the MARS14 runs, the depleted fraction was collected to centrifugal concentrators of 10 kDa to perform the buffer exchange and sample concentration before proceeding with the SP3-clean-up and digestion. Then, SP3-clean-up was performed and the peptides obtained after SP3 digestion were quantified and labelled with TMT 10-plex and the samples pooled. Afterwards, the pooled samples were fractionated with HiRIEF approach and then, the LC-MS/MS analysis (using Q-Exactive) of the 72 HiRIEF fractions performed. Finally, the longitudinal analysis of the data (using TiCoNE software) and the enrichment analysis were performed. **The Peptidome fraction (Peptidome analysis)** clean-up and peptide concentration was done using SCX cartridges. The concentration of the endogenous peptides was further quantified and analysed through LC-MS/MS (using Orbitrap Fusion), with CID and EThcD fragmentation methods. Finally, the data base searching and peptide identification was performed, and the peptides obtained were analysed with the Proteasix software (protease prediction tool).

2.5.3-Sample clean-up with Sera-Mag Speed beads (SP3) and protein digestion

The sample clean-up was performed following the protocol described by Hughes *et al.* with minor changes [20]. Firstly, all samples with a volume of approximately 50-100 µl and 200 µg of protein, were diluted in lysis buffer (4% SDS, 25mM HEPES pH 7.6, 1 mM DTT) in a ratio of 1:2 (protein solution: lysis buffer) and heated at 95ºC during 5 min with constant shaking. Then, 10µl of 0.4M chloroacetamide was added to every 100µl of protein solution (200µg of protein) to obtain a final concentration of 40mM Chloroacetamide, samples were vortexed and spun down. The SP3 beads solution was prepared according to the protocol described by Hughes *et al.* [20]. Briefly, after vigorously shaking the container bottles (until the suspensions look homogeneous), 50 µl of Sera-Mag speed beads P/N 65152105050250 and 50 µl of Sera-Mag speed beads P/N 45152105050250 (GE Healthcare) were collected to a fresh Eppendorf tube and were washed 3x with 500µl of milliQ water on the magnetic rack. The beads were finally resuspended in 500µl of milliQ water to make the stock SP3 bead suspension. This was added to protein solution at a ratio of 1:5 (beads suspension: protein solution) and mixed gently by pipetting. Then, ACN was added to the mixture to obtain a final ACN composition of 70% and mixed gently by pipetting, samples were incubated for 20min in the rotating rack. After incubation the tubes were placed in the magnetic rack and incubated for 2 min, the supernatant was removed and discarded. Then, 200µl of 70% EtOH was added and samples were incubated for 30s in magnetic rack, the supernatant was then removed and discarded. This EtOH wash step was repeated once. Then, 180µl of ACN was added to samples and incubated for 15s in magnetic rack, the supernatant was then removed and discarded, beads were allowed to air dry for 30s. Finally, 100µl of trypsin solution (50mM HEPES pH7.6, 4µg trypsin) was added to each sample and incubated at 37C for 14h with mild shaking. Peptide concentration was determined as described in 2.4 (see Figure 2).

2.5.4-TMT (10 plex) Labelling of peptides

The resulting peptides were labelled with TMT reagent 10 plex, accordingly manufactures' protocol. Each TMT set was loaded with eight samples and two internal pooled standards, which were prepared by equal mixing of peptide aliquots from all samples (see Figure 2). TMT reagents were allowed to reach room temperature before use. Regarding sample preparation, triethylammonium bicarbonate buffer (TEAB) was added to peptide samples to reach a final concentration of 100 mM and pH confirmed to be in the range of 8-8.5. TMT reagent vials preparation consisted in the addition of 250 µl of ACN to each TMT reagent vial with 5 mg. The reagent was dissolved for 5 min with occasional vortexing and spun briefly. Then, the content of each TMT reagent vial set was transferred to each sample tube accordingly with the study design. All tubes were vortexed, spinned and the pH confirmed to make sure that was above 7.5. Finally, tubes were incubated at room temperature for two hours, after half of the incubation time tubes were vortexed and the pH checked once again.

2.5.5-SCX cleaning of the proteome fraction

After pooling, all the TMT10plex peptide sets were cleaned by strong-cation exchange-solid-phase extraction (SCX-SPE, strata-X-C, P/N 8B-S029-TAK-TN from Phenomenex), as follows. Firstly, 10% formic acid was added to all the TMT10plex pools to ensure pH <3. Before adding the samples, the strata-X-C columns were washed with 600 µl 100% methanol and then equilibrated with 600 µl wash MilliQ water. Then, samples were added to the columns and after that step they were washed with 600 µl of washing solution (30% MeOH, 0.1% formic acid). Before eluting the peptides, tubes were prepared and then 600 µl of elution solution (30% MeOH, 5% ammonium hydroxide) was added (see Figure 2). The eluate containing the salted peptides was divided into different aliquots and dried in a speed vacuum.

2.5.6-High-resolution isoelectric focusing (HiRIEF)

The HiRIEF pH range employed was 3–10, 24-cm-long IPG (immobilized pH gradient) gel-strip (P/N GE-17-6002-44, GE Healthcare Bio-Sciences) (see Figure 2). Each peptide mixture set with 400 µg, was redissolved in 250 µl rehydration solution containing 8 M urea, 1% IPG Pharmalyte, pH 3–10 (P/N GE-17-0456-01, GE Healthcare Bio-Sciences). The peptide mixture set was loaded on the IPG tray, the IPG strip was placed above and allowed to absorb the sample overnight. The gel bridge was applied at the cathode (acidic) end of the IPG strip, and IEF was run on an Ettan IPGphor (GE Healthcare) until at least 150 kV-h. After focusing was complete, a well-former with 72 wells was applied onto each strip, and liquid-handling robotics (GE Healthcare prototype) proceeded with peptide extraction and transferred the 72 fractions into a microtiter plate (96 wells, V-bottom, Corning cat. #3894), which was then dried in a SpeedVac.

2.5.7-Proteome MS analysis

Prior to each LC-MS run of the 72 fractions, the auto sampler (Ultimate 3000 RSLC system, Thermo Scientific Dionex) dispensed 20 µl of mobile phase A (95% water, 5% dimethylsulfoxide (DMSO), 0.1% formic acid) into the corresponding well of the microtiter plate (96 well V-bottom, polypropylene, Greiner), mixed by aspirating/dispensing 10 µl ten times, and finally injected 10 µl into a C18 guard desalting column (Acclaim pepmap 100, 75 µm × 2 cm, nanoViper, Thermo). After 5 min of flow at 5 µl min−1 with the loading pump, the 10-port valve switched to analysis mode in which the NC pump provided a flow of 250 nL min−1 through the guard column. The slightly concave curved gradient (curve 6 in the Chromeleon software) then proceeded from 3% mobile phase B (90% acetonitrile, 5% DMSO, 5% water, 0.1% formic acid) to 45% B in 50 min followed by wash at 99% B and re-equilibration. Total LCMS run time was 74 min. We used a nano-EASY-Spray column (pepmap RSLC, C18, 2 µm bead size, 100 Å, 75 µm internal diameter, 50 cm long, Thermo) on the nano electrospray ionization (NSI) EASY-Spray source (Thermo) at 60 °C. Online LC-MS was performed using a hybrid Q-Exactive mass spectrometer (Thermo Scientific). FTMS master scans with 70,000 resolution (and scan range 300–1600 m/z) were

followed by data-dependent MS2 (35,000 resolution) on the top 5 ions using higher energy collision dissociation (HCD) at 30% normalized collision energy. Precursors were isolated with a 2 m/z window. Automatic gain control (AGC) targets were 1e6 for MS1 and 1e5 for MS2. Maximum injection times were 100 ms for MS1 and 450 ms for MS2. The entire duty cycle lasted ~1.5 s. Dynamic exclusion was used with 60 s duration. Precursors with unassigned charge state or charge state 1,7,8, >8 were excluded. An underfill ratio of 1% was used.

2.5.7.1-Proteome data search

All the raw MS/MS files were converted to mzML format and corrected for mass shifts using the msconvert tool (mzRefiner filter) from the ProteoWizard suite [21]. Spectra were then searched by MS-GF+[22], and post processed with Percolator [23] in a Nextflow [24] pipeline, using a concatenated target-decoy strategy. The full pipeline (version ee45bf6) is available at https://github.com/lehtiolab/galaxy-workflows/.

The reference databases used were the Swissprot human protein database downloaded from uniprot.org at 2018-07-18. MSGF+ settings included precursor mass tolerance of 10ppm, fully-tryptic peptides, maximum peptide length of 50 amino acids and a maximum charge of 6. Fixed modifications were TMT-10plex on lysines and N-termini, and carbamidomethylation on cysteine residues, a variable modification was used for oxidation on methionine residues. Quantification of TMT-10plex reporter ions was done using OpenMS project's IsobaricAnalyzer [25]. TMT ratios were calculated in each PSM using the average intensity of the two reporter ion channels loaded with internal pooled standard. PSMs found at 1% PSM- and peptide-level FDR (false discovery rate) were used to infer gene identities, which were quantified using the medians of per-channel median-normalised PSM quantification ratios. Inferred gene identity false discovery rates were calculated using the picked-FDR method [25], whereas the FDR for protein level identities was calculated using the -log10 of best-peptide q-value as a score [25]. The mass spectrometry proteomics data have been deposited to the ProteomeXchange Consortium via the PRIDE [26] partner repository with the dataset identifier PXD016853.

2.5.8-PDE vs plasma analysis

The PDE proteome dataset was compared with normal plasma (n=10) and nephropathy plasma (n=10) datasets. These datasets were in-house generated, for each plasma dataset, sample treatment was performed in the same way as was done for PDE samples. Thus, MARS14 depletion and HiRIEF approaches, were chosen for the protein depletion and peptides fractionation, respectively.

For the gene centric approach, quantified protein groups in at least one sample were median summarized by gene symbol or uniprot gene name depending on the analysis. MS1 set intensities (i.e. precursor peak areas) or MS2 sample intensities (i.e. TMT reporter ion ratios) were used as per need of absolute or relative quantification values, respectively. We note that the number of

quantified proteins differ in each level (MS1: n = 4549, MS2: 5338) because of inherent mass spectrometer limitations (e.g. ill-shaped MS1 peaks, not permitting area integration, but sufficient signal for decent MS2 fragmentation).

Datasets from nephropathy plasma data2 and normal plasma samples were in-house generated using HiRIEF method. Shared proteins across studies were identified and median MS1 intensity across sets was used as overall quantitative proxy to calculate Spearman correlations between the respective datasets. To detect outliers, we linearly regressed each protein profile from plasma dataset on PDE abundance values and highlighted estimated residuals lower than two standard deviations from the residuals' distribution.

For the protein abundance ranking abundance, proteins quantified and summarized as described above– were ordered according to their MS1 intensities and divided into four groups – (non-)unique for PDE, (non-)shared across patients– with neuropathy dataset 2 as mentioned before.

2.6-Peptidome analysis of PDE samples

2.6.1-SCX cleaning of the peptidome fraction

After centrifugal concentration, the fraction below the 10 kDa containing the PDE endogenous peptides was submitted to SCX-SPE in order to clean-up and concentrate the peptides. Therefore, to each 4 mL of PDE sample was added 800µL of 10% formic acid in order to reach a pH< 3. The acidified samples were then added to the cartridges and the same procedure was done as described before in the section 2.5.1.5 (proteome PDE analysis). After elution the supernatant was dried in a speed vacuum and the pellet resuspended in 100 µl Milli-Q water. The peptide concentration measurement was performed with BBC assay as described in section 2.4.

2.6.2-Peptidome MS analysis

For the peptidomics analysis, endogenous peptides were analyzed using a Ultimate 3000 RSLC system coupled to an Orbitrap Fusion mass spectrometer running in positive mode. LC-MS run was started with the injection of 5 µl into a C18 guard desalting column (Acclaim pepmap 100, 75 µm × 2 cm, nanoViper, Thermo). After 5 min of flow at 5 µl min−1 with the loading pump, the 10-port valve switched to analysis mode in which the NC pump provided a flow of 250 nL min−1 through the guard column. The slightly concave curved gradient (curve 6 in the Chromeleon software) then proceeded from 3% mobile phase B (90% acetonitrile, 5% DMSO, 5% water, 0.1% formic acid) to 45% B in 50 min followed by wash at 99% B and re-equilibration. Total LC-MS run time was 87 min. We used a nano-EASY-Spray column (pepmap RSLC, C18, 2 µm bead size, 100 Å, 75 µm internal diameter, 50 cm long, Thermo) on the nano electrospray ionization (NSI) EASY-Spray source (Thermo) at 60 °C. For each sample two different LC-MS runs were performed using two different fragmentation methods: i) CID only and ii) HCD

combined with EThcD. In both cases, FTMS master scans were performed with 60,000 resolution, a scan range 350-1550 m/z, an AGC target of 5e5, a maximum injection time of 100 ms, precursor isolation with a 2 m/z window, dynamic exclusion with 30 s duration, and precursors with unassigned charge state or charge state 1 were excluded. Then, for i), data-dependent MS2 acquisition was done with CID activation on the top 10 ions (10 scans) at 35% normalized collision energy, with an AGC target of 1e4, and a maximum injection time of 100msThe entire duty cycle lasted ~1.2 s. Regarding ii), HCD alternating with EThcD fragmentations were performed on the top 10 ions (10 scans), at a 40% and 25% normalized collision energy, respectively. For both HCD and EThcD AGC target was 2e5, and the maximum injection time was 120 ms. The entire duty cycle lasted ~2.4 s

2.6.2.1-Peptidome data search

All MS/MS spectra were processed with Proteome Discoverer (v2.2) using the PMI-Byonic node (V3.2.0) and Data files were searched against UniProt human canonical database (November 2018; 42,344 entries). Regarding spectrum selector and non-fragment filter node the parameters were set as default. For the Byonic analysis node, the precursor MS, HCD MS^2 and EThcD MS^2 tolerances were set to 10 ppm with non-specific enzyme searching. Some post-translational modifications (PTMs), such as, i) oxidation of methionine and proline, ii) amidated (C-Term), iii) acetyl (N-Term) and iv) Gln→pyro-Glu (N-term Q), were set as dynamic modifications. Data was searched as a single batch with PSM and peptide FDR set 1% using a target decoy approach in Byonic. The target decoy PSM validator node parameters were set as default.

2.6.3-Protease prediction analysis

The Proteasix tool was used in order to perform protease prediction analysis based on the naturally occurring peptides in the PDE Peptidome samples. Proteasix is an open-source peptide-centric tool that allows cleavage sites' retrieval and protease associations from a list of peptides [27]. Therefore, from an input peptide list, Proteasix enables the automatic reconstruction of N- and C- terminal cleavage sites and identification of observed and predicted proteases involved in the proteolysis of these cleavage sites. The Proteasix Knowledge Database supports two operational modes (observed and predicted) to find proteases. The observed mode was the one used in our study, and consists in matching against cleavage site associations collected from the literature to find proteases. The input list requires the following information of each peptide: i) Peptide identifier: useful to track the data with large list of peptides; ii) Parent protein: UniProt identifier (ID) or UniProt accession (AC); iii) Start amino acid position in the Parent protein sequence and iv) Stop amino acid position in the Parent protein sequence. Finally, the output data contains, i) peptide identifier, ii) Parent protein, iii) Start amino acid, iv) Stop amino acid, v) Protease, vi) Cleavage site, v) Source and the vi) Plausible proteolysis.

2.7-Longitudinal study: clustering and enrichment analysis

In order to perform the longitudinal analysis for each patient, we sorted each MS2 patient profile by time of collection and removed values above 0.1% percentile of the total quantified proteins that were considered as outliers. The remaining values were z-score transformed (mean = 0, standard deviation = 1).

The time-series expression data analysis was performed with TiCoNE [28], an expert-centred approach for discovering temporal response pathways. With this approach, time-series expression data is clustered to identify groups of biological entities with coherent temporal responses. It is also possible to add, remove, merge, or split temporal patterns. The clustering analysis was performed with the following parameters, i) Discretization (standard): negative (10) and positive (10); ii) Clustering method: CLARA, number of clusters (15 for patients with more than 3 time points, 10 for less than 3 time points); iii) Prototypes: Mean Time Series; iv) Similarities: Time series (Pearson correlation).

After obtaining the clusters, some cluster operations were performed, such as: i) Perform iteration until converge; ii) Modify clustering: Filter objects (least fitting objects sets) using as similarity method the “Shape (Pearson)” and selecting 10 percent of least fitting to be deleted. In addition, the cluster p-values were calculated selecting as a features for cluster fitness: Average object + prototype similarity, and as a conditional features: number of objects. The number of permutations was set for 5000. The resulting clusters for each patient, were subsequently enriched for gene sets in Molecular Signature Database (mSigDB) canonical pathways (v6.2) [29]. The enrichment analysis was performed patient- and cluster-wise using enricher function from ClusterProfiler R package with the following parameters: minGSSize = 10, maxGSSize = 200, pAdjustMethod = "BH", pvalueCutoff = 1, qvalueCutoff = 1 [30].

Background proteome (universe) was individually estimated for each patient according to the quantified proteins. P-values of the enriched terms were subsequently Benjamini-Hochberg (BH) corrected and those with adjusted p-value < 0.25 were retained.

3-Results and Discussion

3.1-In-depth proteome analysis.

PDE it is a useful reservoir for potential biomarkers, being easily accessible through a peritoneal equilibrium test and without constraints regarding the amount of sample that can be obtained, this sample represents and enormous and valuable source for long-term PD monitoring [7], [14]. However, PDE´s sample characteristics such as: i) highly diluted protein content, ii) complex plasma-like composition and iii) plasma-like wide dynamic range of concentrations between its component proteins, contribute to making the Proteome analysis a challenging task. The first step in sample preparation is to equalize the protein concentrations across all samples. Therefore, all

samples were first interrogated for the total protein content. The average of the protein concentration for the 136 samples analysed was 0.707±0.302 mg/mL and the range was found to vary between 0.327 and 1.913 mg/ml.

The Proteome analysis identified 5478 proteins (Table ESM 2) over all samples, of which 1828 were overlapped for all sets, with an average of 3119 proteins identified per set (ranging from 2803 to 3693), as shown in Figure 1 of the Supplementary Material. The total number of peptides were 59606, with an overlap of 9313 peptides between sets and an average of 26297 peptides per set (ranging from 24736 to 29602) as shown in Figure 1 of the Supplementary Material.

This is the largest number of proteins ever identified in a PDE Proteomics study, representing a 1.2-fold increase in PDE proteome coverage [31], [32]. An important PDE Proteomics study by Herzog *et al.* [32] applied a combinatorial peptide ligand library (CPLL) technique for depletion and enrichment approach, combining it with multiplex LC-MS analyses to explore the PDE [32], resulting in a total of 2506 proteins identified. Another important study, by Pearson *et al.* [31], determined the presence of extracellular vesicles (EVs) in PDE and subsequently characterized their proteome, identifying over 3700 proteins in total. The EVs in PDE were first isolated from PDE using differential centrifugation, then a further enrichment using size exclusion chromatography (SEC) and finally MS/MS were used to identify the marker proteins from the three types of EVs i.e. apoptotic bodies, ectosomes and exosomes.

We should also note the volumes of sample used in the previous studies for proteomic analysis [31], [32], in which a starting volume of at least 300 mL, and up to 1000 mL of PDE were used per sample. These large volumes seriously limit the implementation of proteomics studies with large sample cohorts, due to the obvious storage issue. In contrast, our proteomic analysis was performed with a smaller starting volume of 10 mL per sample, allowing also the parallel analysis of the endogenous peptides from precisely the same sample (fraction <10 kDa after centrifugal concentration step, section 2.3, and as can be seen in Figure 2).

Figure 3A shows an overview of the Proteome coverages of the present study compared to the two PDE Proteomics reference studies of Herzog *et al* and Pearson *et al*. The HiRIEF separation technique combined with the MARS14 depletion here proposed proved to be powerful tool obtain a deep insight into the PDE. Moreover, PDE HiRIEF-LC-MS analysis was compared with a previous data generated by our group (as described in section 2.5.1.9). Thus, two distinct groups of plasma samples (healthy donors and patients with nephropathy) were compared with PDE (Figure 3B). The previous study was performed under the same protocol conditions, with HiRIEF pH range of 3–10, 24-cm-long IPG gel-strip, allowing us to get some insights about how "plasma-like" are PDE samples when compared with plasma analysed under the same protocol conditions. The comparison allowed to discuss the pre-fractionation robustness of the HiRIEF technique. Moreover, the number of proteins found in PDE indicates that it is substantially more

complex than plasma, and suggests that it may not be as plasma-like as previously thought (Figure 3B).

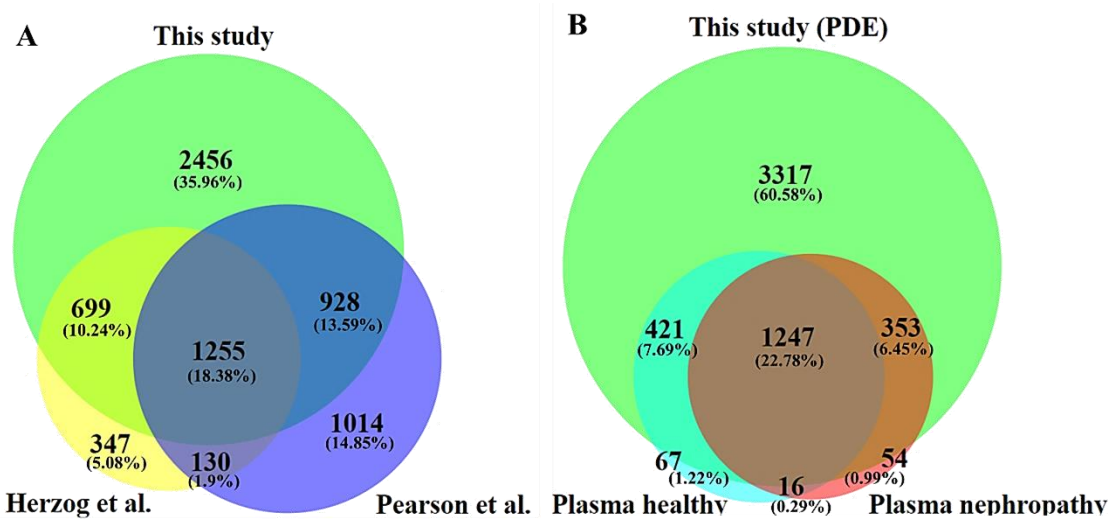

Figure 3- Venn's diagram comparison, **A-** This study vs PDE studies; **B-** PDE HiRIEF vs Plasma HiRIEF studies.

Additionally, when performing correlation analysis between the plasma HiRIEF datasets and PDE, the results shown that the highest Spearman´s correlation, was the correlation of plasma nephropathy HiRIEF and plasma normal HiRIEF analysis (0.68). This is not surprising, given the fact that both are plasma samples, and the sample treatment was performed with the same technique (Figure 4-A). From the point of view of the PDE HiRIEF data, it showed higher correlation (Spearman 0.61) with the plasma nephropathy HiRIEF data (Figure 4-C), and slightly worse correlation with the plasma normal HiRIEF data (Spearman 0.57) (Figure 3-B). Thus, we hypothesize that plasma nephropathy is more correlated with PDE samples, most likely because both are derived from patients with kidney disease (uremic patients). Hence, we have focused on outliers of this correlation analysis (PDE vs plasma nephropathy), which are exclusive to PDE samples, in order to focus on locally produced proteins, not plasma related ones.

Interestingly, when performing a correlation analysis of PDE and plasma nephropathy (HiRIEF), one of the outliers with highest score is SERPINE1 (plasminogen activator inhibitor (PAI-1)) (Figure 4-C). This glycoprotein functions as an inhibitor of fibrinolysis and is also involved in the inhibition of extracellular matrix turnover and stimulation of fibrosis, because it is upregulated by the transforming growth factor (TGF-β), an important mediator in many fibrotic processes. Furthermore, elevated levels of PAI-1 are present in intra-abdominal adhesions and the concentration of PAI-1 doubles transiently during acute peritonitis. Moreover, PAI-1 is present at higher levels with longer duration of PD and the appearance rate in effluent is a powerful predictor for encapsulating peritoneal sclerosis (EPS), with a predictive power of 0.77, sensitivity of 100%, and specificity of 54%, that increases to 94% when in combination with impaired free water transport[33]. Therefore, we demonstrate that HiRIEF-MS method has

the analytical depth and capability to detect tissue leakage or locally produced proteins, as recently described by Pernemalm *et al.* [34].

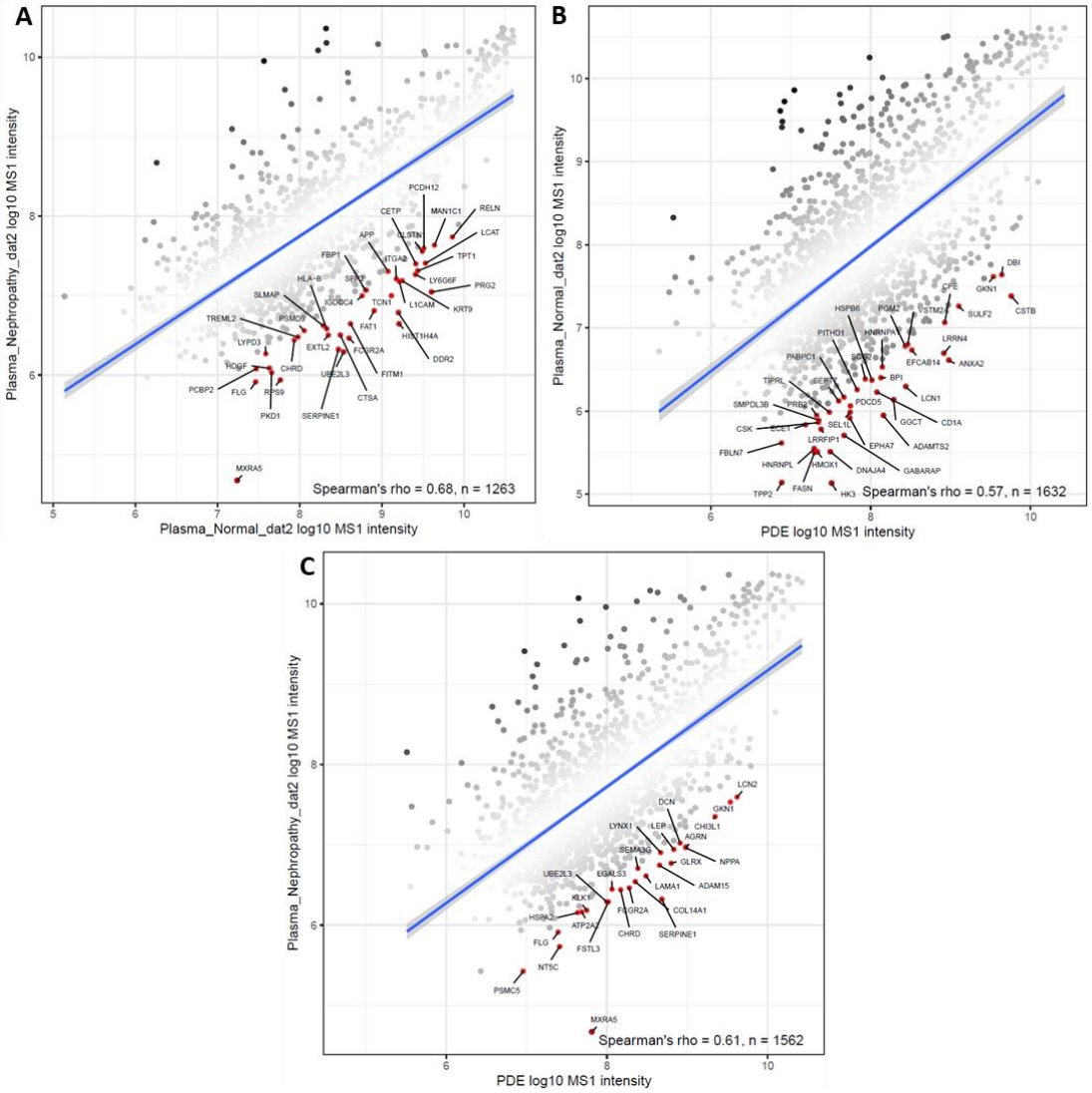

Figure 4- Correlation of PDE abundance (median MS1 intensity) and plasma abundance. **A**- HiRIEF plasma nephropathy versus normal plasma (plasma samples) (Spearman´s correlation =0.68). **B**- HiRIEF normal plasma versus PDE analysis (PDE vs plasma) (Spearman´s correlation =0.57). **C**- HiRIEF plasma nephropathy versus PDE (PDE vs plasma) Spearman´s correlation =0.61).

With the purpose of going into deeper considerations within PDE samples, we compared the number of proteins identified and quantified across the different time-points and patients. From 5338 proteins, 1807 are common across all time-points/patients, with some proteins unique for some patients or time points (Figure 5).

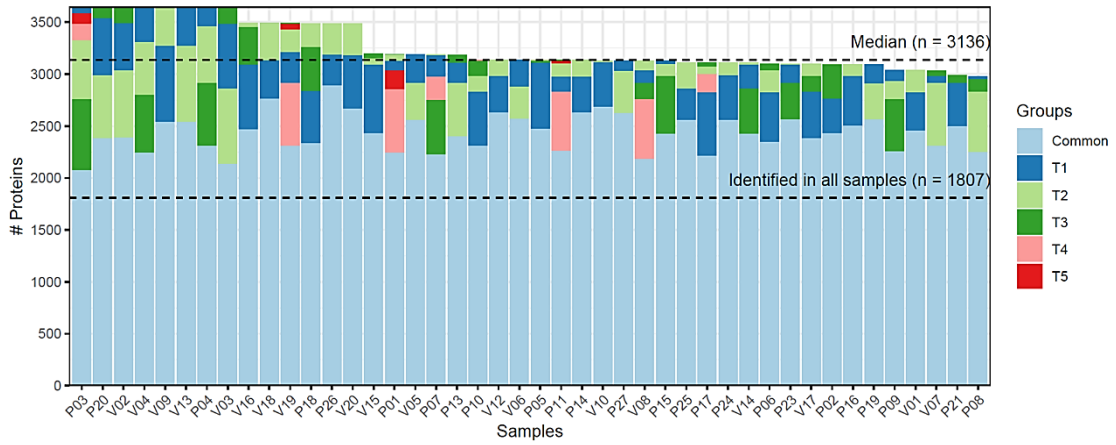

Figure 5- Bar chart with the number of proteins identified per patient for the different time points. The protein groups are coloured with, i) light blue: proteins common among time points of each patient; ii) dark blue: protein uniquely identified for the first time point (T1); iii) light green: protein uniquely identified for the second time point (T2); iv) dark green: protein uniquely identified for the third time point (T3); v) pink: protein uniquely identified for the fourth time point (T4); v) red: protein uniquely identified for the fifth time point (T5). Dashed lines indicate the number of common protein identified across all samples in the study (n=1807) and the median of proteins identified (n=3136).

Additionally, MS1 intensities of shared and unique proteins identified between time points/patients in the PDE samples as shown in Figure 6, were ranked and compared with the MS1 intensity of the plasma nephropathy HiRIEF dataset 2, because it was precisely the same method of fractionation, allowing us to have an idea of the technique reliability. Moreover, the plasma nephropathy HiRIEF dataset was the one chosen over the healthy plasma HiRIEF dataset, because of its closer correlation. Thus, this comparison was performed to get insights about the PDE proteins distribution, of proteins unique or shared across patients, that are found or not in plasma. The abundance ranking for a total of 4549 proteins is shown in Figure 6 (Table ESM 3).

As expected, in terms of abundance, the proteins shared across patients and found in plasma are the most abundant group, followed by the group of proteins shared across patients but not found in plasma. However, in terms of number of proteins represented per group, the proteins not shared across PDE samples and not found in plasma, comprise the group with the highest number of proteins, with 2384 proteins. This suggests the peritoneal effluent locally produced proteome provided by the current set of patients is rather varied. And it implies that a wide variety of peritoneal membrane conditions are found across the patients and time points of sample collection. Finally, we note that many more proteins were found to be exclusive to PDE than those common with plasma (2987 versus 1562) meaning that PDE samples are substantially more complex than was previously thought.

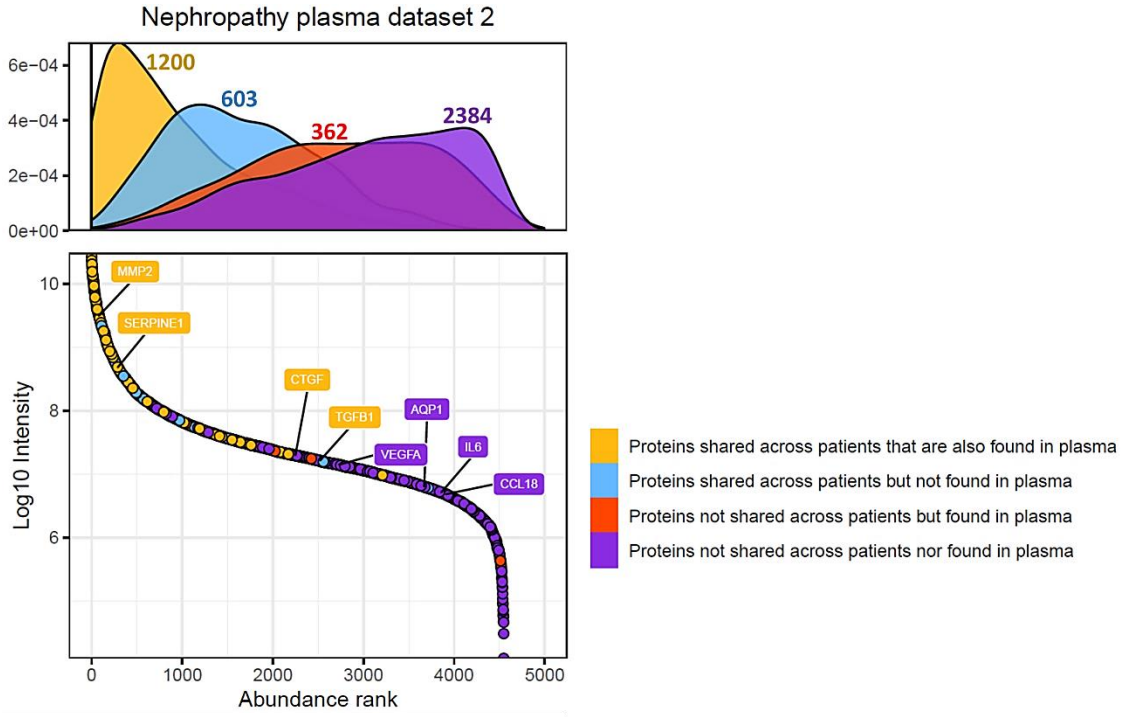

Figure 6- PDE proteins ranked (using nephropathy plasma dataset 2) according to abundance and coloured accordingly with, Yellow, proteins shared across patients that are also found in plasma (1200 proteins). Blue, proteins shared across patients but not found in plasma (603 proteins). Red, proteins not shared across patients but found in plasma (362 proteins). Purple, proteins not shared across patients nor found in plasma (2384 proteins). Some suggested literature PD candidate biomarkers that were identified and quantified with our methodology are highlighted in the abundance rank distribution. MMP-2, matrix metalloproteinase 2; SERPINE1, plasminogen activator inhibitor 1; CTGF, connective tissue growth factor; TGFB1, transforming growth factor beta 1; VEGFA, vascular endothelial growth factor A; AQP1, aquaporin-1; IL6, Interleukin-6; CCL18, C-C motif chemokine 18.

3.2-PDE peptidome analysis

In contrast to proteomics, peptidomics mostly aims to elucidate the exact form of each peptide detected in the sample, reflecting the proteolytic cleavages, PTMs and the co-existence of different versions of peptides derived from the same gene or precursor [35]. The network of complex interplays between proteins and peptides arises from the fact that there are over 560 genetically encoded proteases of different subfamilies and over 150 protease inhibitors encoded in the human genome. Thus, the peptidome is harder to predict in comparison with the genome and proteome [36]. Regarding PDE peptidome analysis, this presents also some challenges such as, i) complexity and large dynamic range of peptide concentration, ii) highly diluted peptide content, and iii) data analysis of the endogenous peptides.

Although endogenous peptides analysis does not require enzymatic digestion of the sample, the use of proteomic techniques applied to peptidomics is not as straightforward as it may seem, due to some challenges. Namely, the range size of the endogenous peptides, from 2 to over 100 amino acids (if precursor protein is cleaved into fragments, those are considered peptides); the charge state, which is not as uniform as for tryptic peptides. In other words, some endogenous peptides have no positive charge due to a blocked N-terminus and the absence of

Lys, Arg, or His residues, that make these peptides not detectable in positive ion mode. On the other hand, other endogenous peptides have charge states of 7+ or more [35]. Additionally, the endogenous peptides are originated from the activity of an array of often-unknown endogenous proteolytic enzymes, some without predictable cleavage sequence motifs [37]. Therefore, variations in peptide size and charge state and the lack of expected cleavage sites (such as K/ or R/ sites for tryptic cleavages used in trypsin-based Proteomics) complicate the analysis of endogenous peptides, and for these reasons, some adjustments to the proteomic analysis techniques used have to be done, in order to identify large numbers of endogenous peptides.

Peptides were analysed employing multiple fragmentation methods such as CID and HCD-EThcD, (see section 2.11.1.2.). The analysis of 136 samples covered a total of 5246 unique peptide sequences mapping to 444 protein groups with a high overlap between the different fragmentation approaches, namely 91% at peptide level and 96% at protein level (Supplementary Material Figure S2). To the best of our knowledge, this study represents the highest number of peptides ever identified in PDE samples and the first performing protease prediction analysis in PDE samples, as described in the section below.

3.2.1-Protease prediction

The “input” peptide list of native peptides identified in PDE with CID fragmentation was submitted to Proteasix analysis [27], allowing for automatic cleavage site reconstruction and protease association, as described in section 2.6.1.4.. The analysis rendered a total of 74 proteases (Figure S2). Concerning the number of cleavage events and substrates cleaved per protease it is possible to observe that despite the higher number of cleavage events related to some proteases, such as, plasminogen (PLG) and collagenase 13 (MMP13), these are not the proteases acting on a large number of protein groups (14 only), (Figure 7 and Table ESM 4). Thus, these proteases seem to have a higher specificity when compared for example to Cathepsin K (CTSK) and Cathepsin L1 (CTSL) (with 49 and 39 target proteins, respectively). Interestingly, the protease activity of several MMPs reflects their importance on the process of tissue injury and remodelling of PM, during its prolonged exposure to peritoneal dialysis fluids, as mentioned in case study number 3, in section 3.3.1. Another interesting remark is the number of cleavage events and variety of proteases acting in some specific protein groups. The fibrinogen alpha chain, serum amyloid A-1 protein and collagen alpha-1(III) chain are some of the proteins suffering a rather large number of cleavage events, with 620, 425 and 391 cleavage events, respectively. In addition, vimentin, actin cytoplasmic 1 and collagen alpha-1 (I) chain proteins appear to be a target for a high number of proteases, with 18, 17 and 16, respectively (Tables ESM 4 and ESM 5).

Additionally, is important to know that not all native peptides identified had an associated protease prediction, thus this protease prediction analysis does not cover all the data obtained and some of the endogenous peptides may arise from different processes of cleavage.

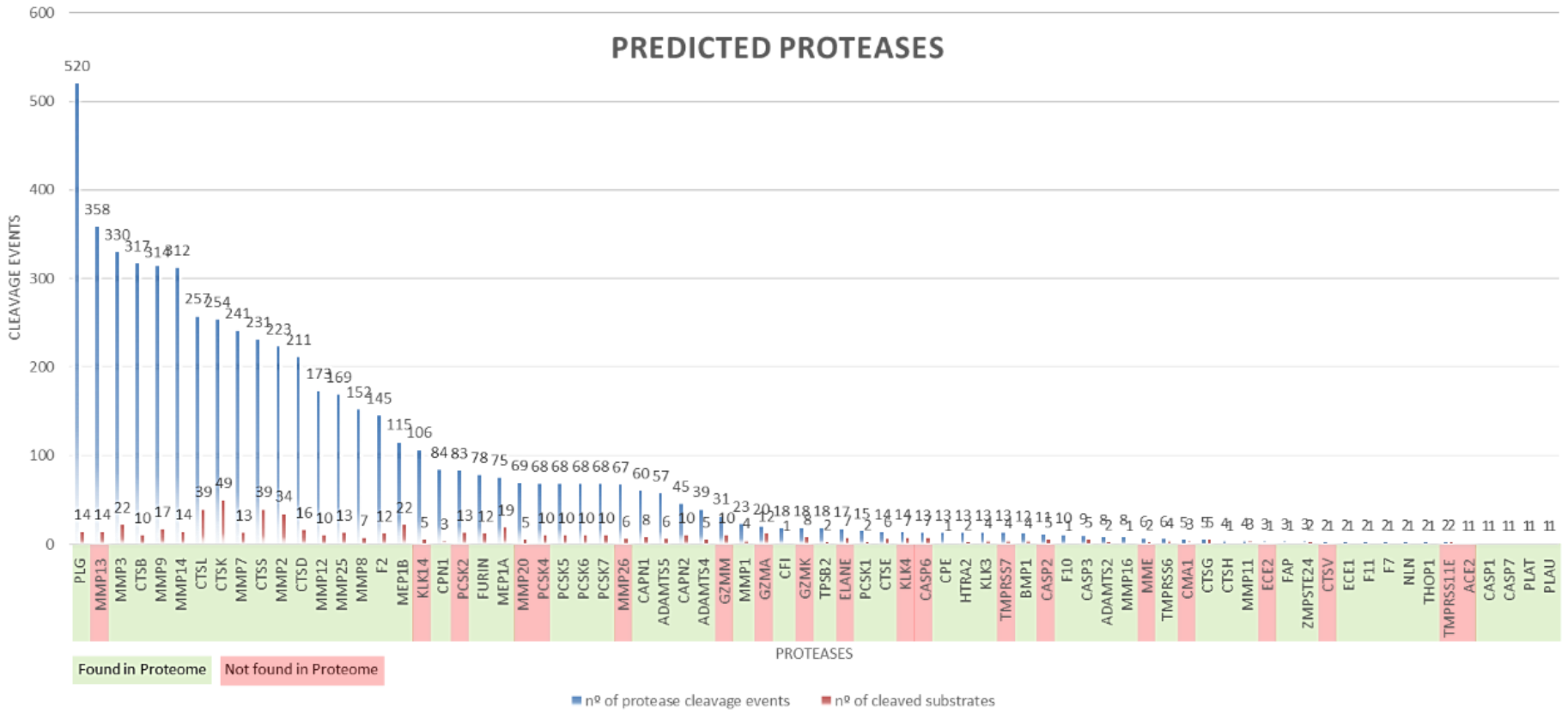

Figure 7- Bar chart with the predicted proteases for those peptides that had at least one protease prediction. For each protease the blue bar indicates the number of cleavage events, and the red bar the number of cleaved substrates that each protease is responsible for. The green and red labelling, means that the predicted protease is found or not found in the proteome, respectively.

Recently, in a work published by Magalhães and colleagues [38], the authors applied Proteasix software [27] to predict the proteases involved in the generation of the naturally occurring peptides in plasma, serum, CSF, saliva, urine and tears. The peptidome data of the most studied human body fluids was collected from public databases and from experimental studies. The analysis highlights 132 putative proteases from four families with the predominance of serine proteases and metalloproteases. From these, 49 proteases were common to all fluids and mostly associated to ECM as well as protein/peptide hormone processing [38]. Although PDE samples are not a truly human body fluid, 74 proteases were predicted as involved in the generation of endogenous peptides, and from those, 54 are identified and quantified in the proteome analysis.

3.3-Longitudinal study analysis.

Although it has been proven that long-term instillation of PDF into peritoneum causes morphological alterations in the PM, such as, detachment of the mesothelial layer, increased ECM deposition, fibrosis and angiogenesis [10], only some candidate biomarkers associated with these morphological alterations are currently being considered as valuable tools for improving patient management. These prognostic peritoneal biomarkers might be of prime importance to guide therapeutic decisions and to enable the early discrimination of patients that are at high risk of suffering complications (such PM deterioration or peritonitis), after PD therapeutic interventions [16]. Additionally, and due to a wide diversity of peritoneal function between patients, both before the start and in response to PD therapy, the detailed elucidation of the pathophysiological processes could provide a better understanding of ultrafiltration (UF) failure, allowing therapeutic options to be refined [31]. Some biomarkers, such as, IL-6, IL-8, CA125, have already been associated with relevant pathomechanisms arising from long-term PD, such as chronic peritoneal inflammation, infection and PM remodelling [16]. The longitudinal analysis of the PDE proteome for each patient, aimed to study the evolution of the PDE over time, to identify specific molecular changes that can be particularly interesting for the understanding and early detection of long-term PM alterations, and to understand the PM-dependent dynamic response among patients to PD therapy.

3.3.1-Clinical case studies

The analysis of longitudinal data consisted in clustering of proteins with similar expression patterns, followed by pathways' enrichment analysis of each cluster, revealing the most significant pathways related to these proteins, (see section 2.5.9.1.). This analysis was performed for patients with three or more time points and some of the most frequently significant pathways across patients are related with metabolic pathways, complement and coagulation cascades, ECM organization, formation of fibrin clot clotting cascade and integrin pathways

(Supplementary Table S1). For the clinical case examples described below, we focus particularly in vintage patients (those with more than 3 years of PD) or patients with at least three time points with particularly significantly enriched biological pathways. Thereby, with these case studies we intend to highlight the need of a case by case patient treatment, and the possibility of identifying and following changes in the PM during long-term PD.

Case 1-Fungal peritonitis as a reason for PD therapy dropout

The first case study (P01) represents a clinical case of a woman that initiated PD at age of 61 for the treatment of chronic kidney disease (CKD) due to hypertensive nephrosclerosis. This patient performed PD therapy for more than 3 years, experienced 2 episodes of peritonitis caused by *Acinetobacter spp.* and *pseudomonas* that were treated successfully. However, the patient was later on transferred from PD to hemodialysis (HD) therapy due to fungal peritonitis caused by *Candida Parapsilosis*. The peritoneal function, effluent biomarker CA125 and other clinical aspects such as serum albumin and parathyroidism hormone were assessed for each time point without any clinical alterations having been noted. The peritoneal function assessment showed a UF < 400 (ml/4h) for the last time point, and the patient performed PD therapy for two months before shifting to HD due to fungal peritonitis. The patient suffered from other comorbidities such as congestive heart failure (CHF) and stroke. In addition, statins and beta blocker drugs were prescribed as antagonists of the renin-angiotensin system. More details for this patient are noted in Figure 8 and Supplementary Table S2.

Concerning the peritonitis as a PD dropout reason, it is already known that severe or recurrent peritonitis can be a factor limiting long-term use of PD and causing the impartment of the anatomical and functional integrity of the PM. Moreover, several factors can trigger peritoneal inflammation, inducing an immunological response in the peritoneal cavity that involves mesothelial cells (MCs), fibroblast, macrophages, lymphocytes and neutrophils[39]. The MCs are capable of recognizing pathogens and initiating inflammatory response through antigen presentation, cytokine production and interaction with immune cells (e.g. macrophages) [40]. However, it is also known that the use of conventional peritoneal dialysis fluids (PDFs) with non-physiologic composition adversely affects the peritoneal host defence and may thus contribute to the development of PD-related peritonitis [41]. However, with the use of newer PDFs the peritoneal defence mechanisms may improve [42]. These considerations relate with some of the enriched pathways observed for patient P01, such as “class I MHC mediated antigen processing presentation” and “Il-6, -7 pathways”, both presenting a decreasing profile (cluster 4, Figure 8), with a steep decline in the levels of the proteins of these pathways already prominent at the second time point but continuing to increase over time. Thus, based on the clinical and proteomic information, it is possible to hypothesize that patient P01 suffered a continued

depletion of peritoneal host defence capabilities culminating in a more severe episode of peritonitis caused by *Candida Parapsilosis*. The proteomics analysis shows that these immune system pathways were already in severe decline as early as six months after the beginning of PD treatment, and had some of these components (e.g. IL6 levels) been monitored during treatment, clinicians would have been aware early on of the increased risk for peritoneal infection. The strongest risk factors for fungal peritonitis in PD patients are prolonged use of antibiotics and previous bacterial peritonitis [28], that in fact occurred before the event that caused the dropout.

In addition to the recognition of pathogens, MCs are also capable of recognizing tissue damage and initiating tissue repair and adherence formation [40]. The MCs play an important role in the adhesion formation via expression of cell adhesion molecules (CAMs), which also have an essential role in the inflammatory response. Some CAMS, such as selectins, integrins and immunoglobulin (Ig) gene family adhesion receptors, are selectively expressed by tissue cells, mediating the different steps of leukocyte attachment and migration to the inflammatory foci [43]. Some of enriched pathways such, "integrin3 pathway" and the "cytokine-cytokine receptor interaction" (presenting a stepwise increase, cluster 1, Figure 8) are related with the aforementioned process.

In PD, cytokines play a role both in defence against the development of peritoneal infection, in the course of peritoneal infection an in the processes related to peritoneal tissue repair. Peritoneal tissue repair consists in a series of events that culminate in inflammation and restoration, in which the balance of fibrin deposition and degradation is vital. In this context, the overall role of cytokines is to shift the balance of fibrin deposition and degradation in favour of fibrin residues [44]. In addition, coagulation, as well as fibrin generation, are key processes in the remesothelialization, whereas fibrinolysis (fibrin-dissolving) is instrumental in the degradation of fibrin deposits [44]. Interestingly, a decreasing trend is observed for the "formation of fibrin clot clotting cascade" and "fibrinolysis" pathways (cluster 4, Figure 8), that seems to have the tendency to stabilize after the first 6 months of PD, as observed in cluster 4 trend. Thus, we can hypothesize that these enriched pathways may be related with normal adaptive processes of the PM to the PD. In addition, it is known that following an injury to the peritoneum, fibrinolytic activity over the peritoneal surface decreases, leading to changes in the expression and synthesis of various cellular mediators and in the remodelling of the connective tissue [43].

Furthermore, pathways related with the metabolism of proteins were also found enriched in this case study. Concerning the enriched "metabolism of proteins" pathway (cluster 4, Figure 8), its components cover the full life cycle of a protein from its synthesis to its posttranslational modification (PTMs) and degradation at various levels of specificity. Also, within the "metabolism of proteins" a more specific pathway is enriched, "the unfolded protein response" (cluster 4, Figure 8) that is related to protein damage and protein turnover. However, this is not

surprising, because it is already known that PD has effects on protein metabolism by acutely inducing a new state in muscle protein dynamics, which is characterized by decreased turnover rates and a reduced efficiency of protein turnover, a condition which may be harmful in stress conditions, when nutrient intake is diminished or during superimposed catabolic illnesses [45]. In CKD patients, even a modest elevation in local insulin is followed by an anabolic muscle response, though the same effect is not observed during systemic hyperinsulinemia associated with substrate removal which occurs during PD. In this setting the anti-proteolytic effect of hyperinsulinemia is offset by a decrease in muscle protein synthesis due to amino acid deficiency. Thus, protein metabolism during PD is characterized not only by decreased, but also less efficient, turnover rates [46].

In addition, an enriched PTM pathway, more precisely, the *O*-linked glycosylation of mucins pathway, presents an increasing trend (cluster 3, Figure 8), with an overexpression of the MUC16 protein (see Supplementary Table 3 and Table ESM 2). Mucin-type *O*-glycans are found attached on the surface of secreted and extracellular matrix (ECM) proteins, and are thus positioned to modulate the recognition, adhesion, and communication events that occur between cells and the surrounding environment [47], [48]. Moreover, mucin-type O-glycosylation pathways have been associated with altered immune response, due to altered adhesive properties resulting in decreased (leukocyte) rolling on selectins[49].

On the other hand, GCNT1 was also found with an increasing profile over time (cluster 3, Figure 8). This glycosyltransferase catalyses the transfer of an N-acetylglucosamine moiety onto mucin-type core 1 O-glycan to form the branched mucin-type core 2 O-glycan [50]. Both core 1 and -2, are implicated in a diversity of immunological processes, such as, T cell contraction by apoptosis, antibody function, antigen receptor activation, and cell adhesion and trafficking [51]. In contrast to cells of the innate immune system, which often constitutively express the collection of enzymes that generate selectin ligands on their cell surface, the synthesis of core 2 O-glycans and the expression of L-selectin in T cells is highly dynamic. Importantly, the regulation of glycosyltransferase functional activity occurs largely at the transcriptional level, where the enhancement (or inhibition) of enzyme expression generally controls the surface glycan landscape of a cell. Thus, the signalling mechanisms that ultimately impact the transcriptional and/or epigenetic regulation of glycosyltransferase expression in both T cells and endothelial cell populations is critical for the overall understanding of how specific T cell populations are able to traffic into both lymphoid and non-lymphoid tissues [51]. Therefore, an increasing trend of MUC16 and GCNT1 within the "O-linked glycosylation of mucins pathway" may indicate an alteration of the recognition, adhesion, and communication events between cells and the surrounding environment altered by PDFs.

Furthermore, Acute Myocardial Infarction ("AMI") is another enriched pathway within cluster 4. Interestingly, this pathway may be related with congestive heart failure (CHF) and

stroke comorbidities. The adverse influence of CKD has been demonstrated in the setting of acute coronary syndromes (ACS), and among ACS patients, CKD doubles mortality rates and is third only to cardiogenic shock and CHF as a predictor of mortality [52]. Therefore, some drugs such as antagonists of the renin-angiotensin system (Valsartan), statins (Atorvastatin) and beta blockers (Carvedilol) were prescribed in order to ameliorate the patient's condition. Importantly, Valsartan, Atorvastatin and Carvedilol have been shown to reduce the cardiovascular morbidity and mortality [53]–[55]. Within the AMI pathway, there are many proteins enrolled in coagulation processes such as fibrinogen beta chain (FGB), fibrinogen gamma chain (FGG) and prothrombin (F2, the thrombin precursor). Thrombin converts fibrinogen to fibrin by cleaving bonds after Arg and Lys, and, in complex with thrombomodulin, activates vitamin k-dependent protein C (PROC). Also, coagulation factor X (F10), a vitamin k-dependent glycoprotein that converts prothrombin to thrombin is found enriched in this pathway. PROC itself and PROS1 (vitamin K-dependent protein S, an anticoagulant plasma protein that acts as a cofactor to activated PROC in the degradation of coagulation factors) are also enriched. All these proteins present a decreasing trend since the initiation of the PD therapy. This decreasing trend of proteins enrolled in the coagulation cascades is not all that surprising, considering the patient's clinical panel, with a predisposition for strokes as secondary comorbidity. Thus, it is interesting to observe that dysregulated pathways related to secondary comorbidities are also revealed by analysing the PDE proteome, and that proteins formed in other parts of the body (which in this case reflect the underlying vascular comorbidity) to the peritoneal membrane can also be monitored by the PDE Proteomics analysis.

After getting insights into the most significantly enriched pathways it is possible to conclude that for this particular case, as early as six months after commencing treatment, the patient showed predisposition to incur in peritonitis, and therefore, that the fungal peritonitis was not something unexpected, considering the proteomic panel here presented. The decreasing trend of proteins within pathways related with the immune response, such as, "class I MHC mediated antigen processing presentation" and "Il-6, -7, pathways", assessed by the proteomic analysis could have been useful for a clinical decision, especially the Il-6 levels. In addition to Il-6, STAT1 and STAT3 were also found with a decreasing profile within "Il-6, -7, pathways" (cluster 4, Figure 8), Supplementary Table S3. Il-6 trans-signalling is known to direct the transition between innate and acquired immune responses by orchestrating the chemokine-directed attraction and apoptotic clearance of leukocytes [56]. Moreover, Il-6 activation of STAT3 promotes T cell recruitment. Thus, Il-6 bioactivity is tightly linked to the homing or migratory capacity of T cells. Il-6 deficiency specifically disrupts chemokine control of T cell trafficking [57]. Therefore, we consider that monitoring Il-6 levels could have been informative for the clinicians, and alert them to the patient's increasing vulnerability to peritoneal infection caused by prolonged PD therapy.

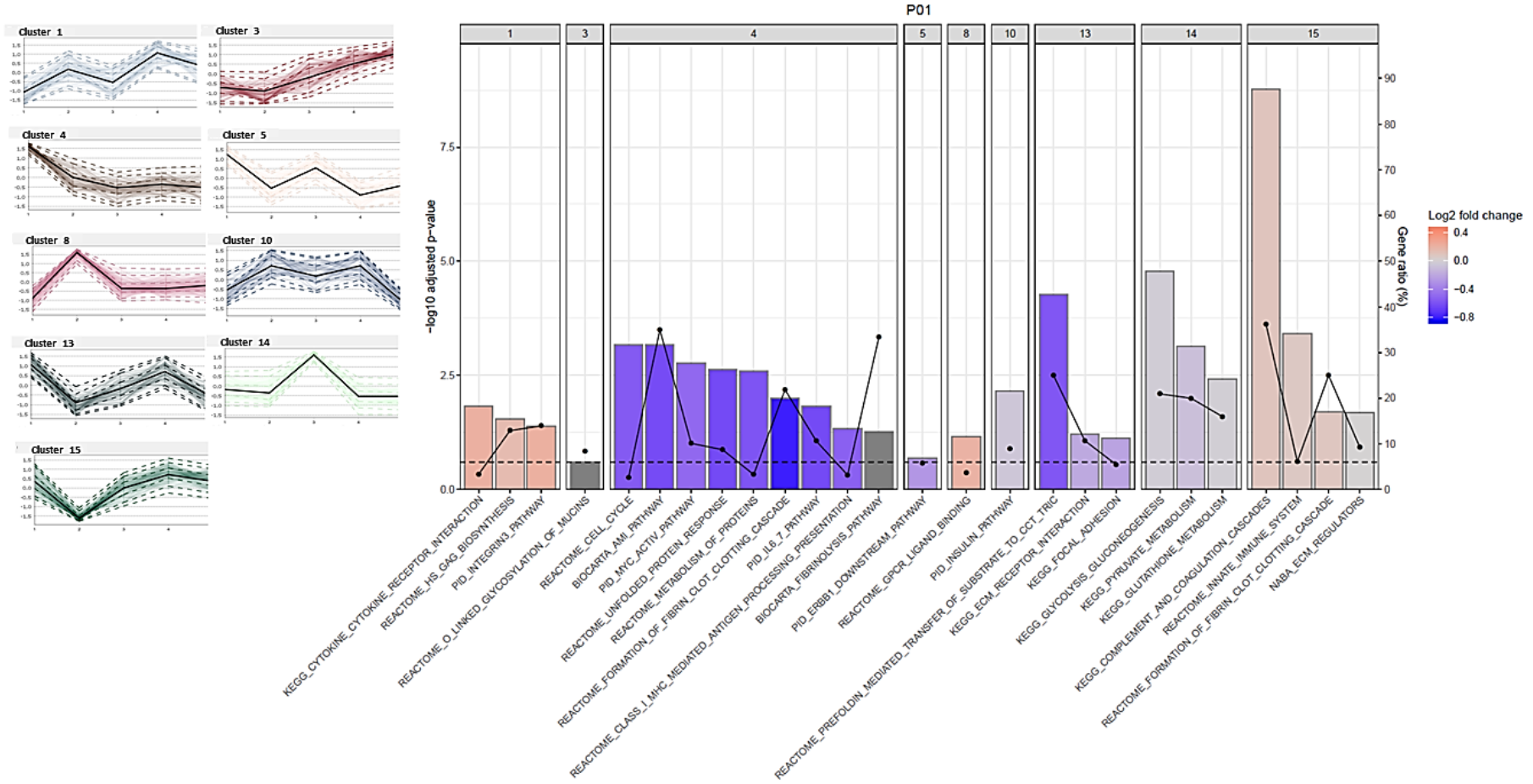

Figure 8- Case study 1 (P01)- Cluster trends (time profiles) and respective bar plot with the most significant (-log10 adjusted p-value) enriched pathways for each cluster. Bar heights represent the adjusted p-value for each pathway. The log2 fold change represents the median of the differences between all proteins enriched for that specific pathway at the last time-point and the same proteins at the first time-point. Blue means decrease, and red increase. The dots represent the number of proteins identified within the pathway in a specific cluster, divided by the total number of proteins identified in a specific pathway for this specific patient proteome background (universe). Dashed line represents the threshold of the p-adjusted value (0.25).

Case 2-Ultrafiltration failure as a reason for PD therapy dropout

Patient V16 is a clinical case of a man that initiated PD at age of 57 for the treatment of CKD due to autosomal dominant polycystic kidney disease (ADPKD). This patient performed PD therapy for more than 3 years. However, our proteomic follow-up for this patient started at month 14, and since then patient experienced one peritonitis episode caused by *Staphylococcus epidermidis* that was treated successfully. The peritoneal function, effluent biomarker CA125 and other clinical aspects such as serum albumin and parathyroidism hormone (PTH) were assessed for each time point. A change in the profile transporter from high average to high was observed, and also creatinine clearance was <60 ml/min in the last time point. Concerning other comorbidities, this patient suffered also from ischemic cardiomyopathy. Since the last time point of our study, the patient performed PD therapy for three months before developing ultrafiltration failure (UFF). In addition, some drugs such as statins and beta-blockers were prescribed. More details for this patient can be seen in Figure 9 and Supplementary Table 2

As already known [58], a progressive CKD results in retention of uremic toxins that can contribute to dysfunction of various metabolic systems. Some of these toxins participate in the disturbance of food breakdown and may downregulate other pathways, resulting in a reduced ability of free fatty acid breakdown. PD may even worsen metabolic functions, with complications such as: i) hyperglycaemia, caused by the use of PDF containing high concentrations of glucose; ii) hypernatremia, that is a result of short dialysate dwell times during the rapid exchanges of high-volume PD; iii) protein/amino acids loss into the dialysate, worsening the nutrition status of patients already depleted by CKD, and iv) hypercatabolism. Severe hypercatabolism caused by PD remains controversial and occurs because PD methods cannot provide an adequate dialysis dose for CKD patients[58]–[60]. For these reasons, an optimization of dialysis dose and nutritional counselling, together with the use of PD solutions without glucose, like icodextrin and amino acid based solutions, are some strategies to prevent and correct malnutrition when PD patients cannot comply with dietary requirements[59], [61], [62]. Likewise, the proteomic analysis of this particular case study revealed some clusters with relevant trends related with metabolic pathways, such as “metabolism of amino acid and derivatives” (cluster 3, Figure 9); “arginine and proline metabolism” and “phospholipid metabolism” (cluster 5, Figure 9); “pyruvate metabolism”; and “citric acid cycle TCA cycle” (cluster 10, Figure 9). All showed a decreasing trend.

Interestingly, as observed in case study 1, “class I MHC mediated antigen processing presentation” appears also as an enriched pathway. The quantitative levels of surface MHC expression is a determinant of antigen-presenting capacity. It was found that resting human peritoneal MCs (HPMCs) constitutively expressed MHC I molecules, but there was no detectable MHC II [63]. However, Shaw *et al*. suggested that normal HPMCs have a significant inherent

phagocytic activity, and can be induced to produce MHC II, and constitutively express costimulatory molecules. Moreover, they can present antigen to autologous memory T Lymphocytes[63]. Therefore, HPMCs equipped with phagocytic and antigen presenting machinery have an important role in intraperitoneal immunity[63]–[65], and for this reason a decreasing trend in this machinery may indicate a compromised immune response for future infection events.

In addition to the infectious peritonitis that this patient suffered, it is known that other factors such as, uraemia, high glucose concentrations in PDF, GDPs formed during heat sterilization, and the generation of AGEs, have all been implicated in ultrafiltration failure (UFF) development [66]. UFF is defined as failure to achieve at least 400 ml of net ultrafiltration during a 4 h dwell using 4.25% dextrose [67]. Four major causes of UFF have been described, such as, i) Highly effective peritoneal surface area, characterized by transition to a very rapid transport state with D/P creatinine >0.81; ii) Low osmotic conductance to glucose, characterized by attenuation of sodium sieving and decreased peritoneal free water clearance; iii) Low effective peritoneal surface area, manifests with decreases in the transport of both solute and water; and iv) High total peritoneal fluid loss rate, due to an increase in the rate of bulk absorption from the peritoneal cavity into lymphatics and into the local tissues[67].

Importantly, morphological and functional alterations in the PM, such as, local neoangiogenesis, vasculopathy, mesothelial to mesenchymal transition (MMT), and collagen deposition in the compact submesothelial ECM zone with subsequent PM thickening, are common in long-term PD patients. In this case study, cluster 6 (Figure 9) presents an increasing trend of enriched pathways related with ECM, such as, “matrisome”, “collagens” and “ECM matrix organization”. Additionally, “integrin3” pathway is also enriched. Specific integrin heterodimers preferentially bind to distinct ECM proteins to affect cell characteristics by signal transduction to the cell interior[68]. Integrins sense ECM-induced extracellular changes during pathological events, leading to cellular responses, which influence ECM remodelling[69]. β1 and β3 integrins serve essential roles in the progression of cancer-associated processes, including the initiation, proliferation, survival, migration and invasion[68]. Moreover, integrins regulate membrane trafficking and endocytosis, EMT, cell polarization, cytoskeletal rearrangements, activity and localization of MMPs [70].These enriched pathways observed for cluster 6 (Figure 9), can be understood in the context of some the aforementioned morphological alterations, and can translate clinically into faster small-solute transport most often due to a combination of a rapid disappearance of the osmotic gradient and diminished osmotic conductance of the PM, meaning that there is less osmosis even though a gradient is present. Both effects are associated with a functional decline in the peritoneum as a dialyzing membrane[66], [71]. There is evidence that the decrease in the peritoneal osmotic conductance is related to aquaporin-1 (AQP1) dysfunction [72] and that the acceleration of small-solute transfer is related to the thickening of

the collagen layer and high vascular density[66]. Importantly, in this case study, the enriched collagen pathway, presents several collagens with an increasing trend (see Supplementary Table 4), and that may lead later to UFF.

Interestingly, UFF can be present shortly after the start of PD, for instance due to MMT, or later. Late UFF develops in 21% of long-term patients and a reduction of both free water transport (FWT) and small pore fluid transport (SPFT) is likely to occur in the majority of long-term PD patients. Those patients developing encapsulating peritoneal sclerosis (EPS) should be considered as a separate subgroup, in which FWT is much more impaired than SPFT, probably due to interference of interstitial collagen-1 with the crystalloid osmotic gradient. This mechanism may also apply to other patients with reduced FWT[73]. Those with mainly impaired SPFT likely have a reduced hydrostatic filtration pressure due to vasculopathy. Therefore, measurement of peritoneal transport function should not only include netUF, but also separate determinations of FWT and SPFT to guide treatment options [73]. In this particular case study, a change in the profile transporter from high average to high was observed, and also creatinine clearance was <60 ml/min in the last time point. On the other hand, measurement of the effluent biomarker CA125 at the time of each PET showed an increase trend of this marker across time, indicating that there is no loss of mesothelial cell mass [74]. However, given the fact that the transcapillary movement of free water via aquaporin 1 accounts for 40 to 50% of total filtration across the PM, and that the aquaporin-1 function can be clinically estimated[67], it would be an important measure to improve the peritoneal function assessment.

In addition, another enriched pathway in cluster 6 (Figure 9) is the “regulation of insulin-like growth factor (IGF) transport and uptake by insulin-like growth factor binding proteins (IGFBPs)”. The circulating IGFs are in complexes with IGFBPs, increasing the half-life of IGFs in the body, modulating availability of IGFs to target receptors for IGFs, and acting as signalling molecules independently of IGFs. Although structurally very similar to insulin, the IGFs act in a very different way, whereas insulin is stored in a specific gland and released when needed, the IGFs are stored outside of cells with soluble binding proteins [75]. The IGFBPs regulate cell activity by sequestering IGFs away from the type I IGF receptor, they may inhibit mitogenesis, differentiation, survival, and other IGF-stimulated events. However, IGFBP proteolysis can reverse inhibition or generate IGFBP fragments with novel bioactivity[76]. In addition, IGFBP interaction with cell or matrix components may concentrate IGFs near their receptor, enhancing IGF activity[76]. Therefore, proteolysis has pivotal role regarding this pathway, with an increasing trend of MMP2 and PLG proteases. Morever, the peptidome analysis and protease prediction may be useful to get some insights regarding the IGFBP-regulated pathways. Remarkably, within the enriched pathways several IGFBP (IGFBP2, -3, -4, -5 and -6) present an increasing trend. A study published by Lee *et al.*[77], showed that the IGF1/IGFBP3 ratio was significantly associated with inflammatory markers in incident automated peritoneal dialysis

(APD). Considering that chronic inflammation is implicated in cardiovascular morbidity in end stage renal disease (ESRD) patients, the authors suggested that the estimation of IGF system activity and inflammation could be of clinical relevance[77]. Moreover, increased serum IGFBP3 in CKD patients, showed to be associated with decreased estimated glomerular filtration rate (eGFR) in both sexes[78]. In this case study, the patients presented a constant decrease of eGFR (Supplementary Table 2). Furthermore, it was demonstrated that adult dialysis patients have elevated IGF-I, IGFBP-1 and IGFBP-3 serum concentrations compared with subjects with normal renal function [79]. It was also suggested that extracorporeal losses (peritoneal and urinary) of IGF1 and IGFBP1 in adult continuous ambulatory PD (CAPD) do not influence their serum levels and that IGF1 may therefore be used as a marker of malnutrition[80].

Another cluster presenting an increasing trend is the Cluster 7, and some of the enriched pathways may be related with ischemic cardiomyopathy, which the patient has as comorbidity, such the muscle contraction and the hypertrophic cardiomyopathy pathways. Some of the myocardial markers within these pathways, such as, MYL2, MYL9, MYL3 and MYL1, are over expressed (Supplementary Table S4 and Table ESM 2). A study performed by Palomo-Piñón [76], suggested that inflammation and myocardial damage markers influence loss of residual renal function (RRF) in PD patients. Thus, it is interesting to observe that these myocardial markers that may influence the loss of RRF, can be also detected through the proteome analysis of the PDE, and with an increasing trend across time, suggesting aggravation of the cardiac condition during PD therapy, albeit not necessarily because of it.

Another interesting enriched pathway in cluster 7 (Figure 9) is “Basigin interactions”. Basigin (BSG) is a transmembrane glycoprotein that belongs to the Ig superfamily and is highly enriched on the surface of epithelial cells. The BSG has a role in intercellular interactions involved in various immunologic phenomena, differentiation, and development, but the major function is the stimulation of synthesis of several matrix metalloproteinases (MMPs). BSG also induces angiogenesis via stimulation of VEGF production and interacts with a variety of other proteins like caveolin-1, cyclophilins, integrins and annexin II that play important roles in cell proliferation, energy metabolism, migration, adhesion and motion [81], [82]. In addition to the BSG, Caveolin-1 (CAV), integrin beta-1 (ITGB1) and neural cell adhesion molecule L1 (L1CAM), are also within this enriched pathway supporting the aforementioned interactions, as can be seen in Table S4. Moreover, the “basigin interactions” pathway may be related with some enriched pathways already described for cluster 6, such as, “integrin3” and specially with “ECM matrix organization”, since BSG can stimulate synthesis of MMPs[82], [83] such as MMP2 and MMP15 that are found within this pathway. Higher dialysate levels of MMP2 are associated with PM dysfunction[84].

In contrast, to the clusters mentioned before, cluster 8 (Figure 9) presents a decreasing trend, with enriched pathways such as “prefolding mediated transfer of substrate to CCT/TRiC”,

through which unfolded actins and tubulins bound to prefoldin are transferred to CCT (chaperonin-containing t-complex polypeptide 1 (TCP-1 ring complex (TRiC, also called CCT)) via a docking mechanism[85]. This cylindrical complex contains a central cavity that binds to unfolded polypeptides and promote their folding in an ATP-dependent manner, sequestering the polypeptides from the cellular environment. Moreover, the TRiC is indispensable for cell survival because the folding of an essential subset of cytosolic proteins requires TRiC, and this function cannot be substituted by other chaperones[86], [87].Thus, CCT/TRiC plays a central role in maintaining cellular proteostasis and is also suggested to be involved in cell proliferation and tumor genesis[88]. Importantly, for the folding substrates that are dependent upon CCT for folding (obligate substrates), their functions are intrinsically linked to CCT folding activity. Therefore, if CCT fails to fold such a substrate correctly, then effects from the loss of function of the substrate could occur. Additionally, failure to fold substrate proteins could lead to a toxic gain of function where toxicity could arise from the formation of aggregates and misfolded proteins [89]. Following this line of thought, a decreasing trend of "prefolding mediated transfer of substrate to CCT/TRiC" may lead to formation of aggregates and misfolded proteins, gaining of toxicity and consequently PM injury.

Other enriched pathway within this cluster is the Platelet-derived growth factor receptor beta (PDGFRB) pathway. The PDGFRB pathway, consists in a signalling transduction pathway mainly via JAK/STAT, PI3K, phospholipase Cγ (PLC-γ), or mitogen-activated protein kinase (MAPK) pathways, promoting gene expression and mediating the biological functions of the PDGF isoforms, such as proliferation, migration, and survival [90]. MAPK and STAT3, both important for the signalling pathways described above, are present within the enriched PDGFRB pathway, cluster 8 (decreasing trend). However, it is already known that high glucose activates the p38 MAPK pathway in cultured human peritoneal MCs (HPMCs), playing a role in the pathogenesis of peritoneal fibrosis[91]. Nevertheless, the decreasing trend of the enriched PDGFRB, may be in part explained by the fact that Simvastatin was prescribed to this patient. Simvastatin is a drug with cholesterol-lowering action, but has been demonstrated to be capable of abrogating EMT changes in glucose-treated HPMCs and PDF-stimulated PD rats [92]. Notwithstanding the fact that statins abrogation of EMT, was mediated, at least in part, by inhibiting isoprenylation of small GTPases, it is possible that statins may exhibit this favourable effect via other mechanisms. In particular, EMT can be induced by a variety of cytokines or growth factors including TGF-β, angiotensin II, fibroblast growth factor-2, epidermal growth factor and importantly, the platelet-derived growth factor[92]. Interestingly, the statins were not being prescribed at the moment of the first time point, starting only to be administrated after the second time point of the study, which may explain the decrease trend of the PDGFRB pathways.

Even though our last time point was 3 months before the development of ultrafiltration failure, at this point the patient had already suffered a change of transporter profile from high

average to high and also creatinine clearance was < 60 (ml/min), being related with a worse prognosis. Additionally, at the proteomic level, we can pinpoint a decreasing trend for a panoply of metabolic pathways and protein homeostasis; and an increased trend for pathways related with the ECM. It is noteworthy to distinguish clusters 6 and 7 (Figure 9), in that ECM pathways in cluster 6 show an initial increase followed by a later stabilization, whereas cluster 7 increases constantly highlighting the worsening of the cardiac condition. On the other hand, for the clusters with decreasing trend, cluster 8 shows a tendency to stabilize, while clusters 3 and 10 decrease constantly, emphasizing the continuation of PD-related metabolic alterations over time. Nevertheless, with a three months' gap between our last time point and the time-to-event (UFF), it is no possible to create a strong hypothesis about the cause of UFF, however the proteomics analysis does reveal a continued aggravation of the cardiac co-morbidity as well as continued alteration of the metabolic profile, likely compounding to the progressive deterioration of the PM condition.

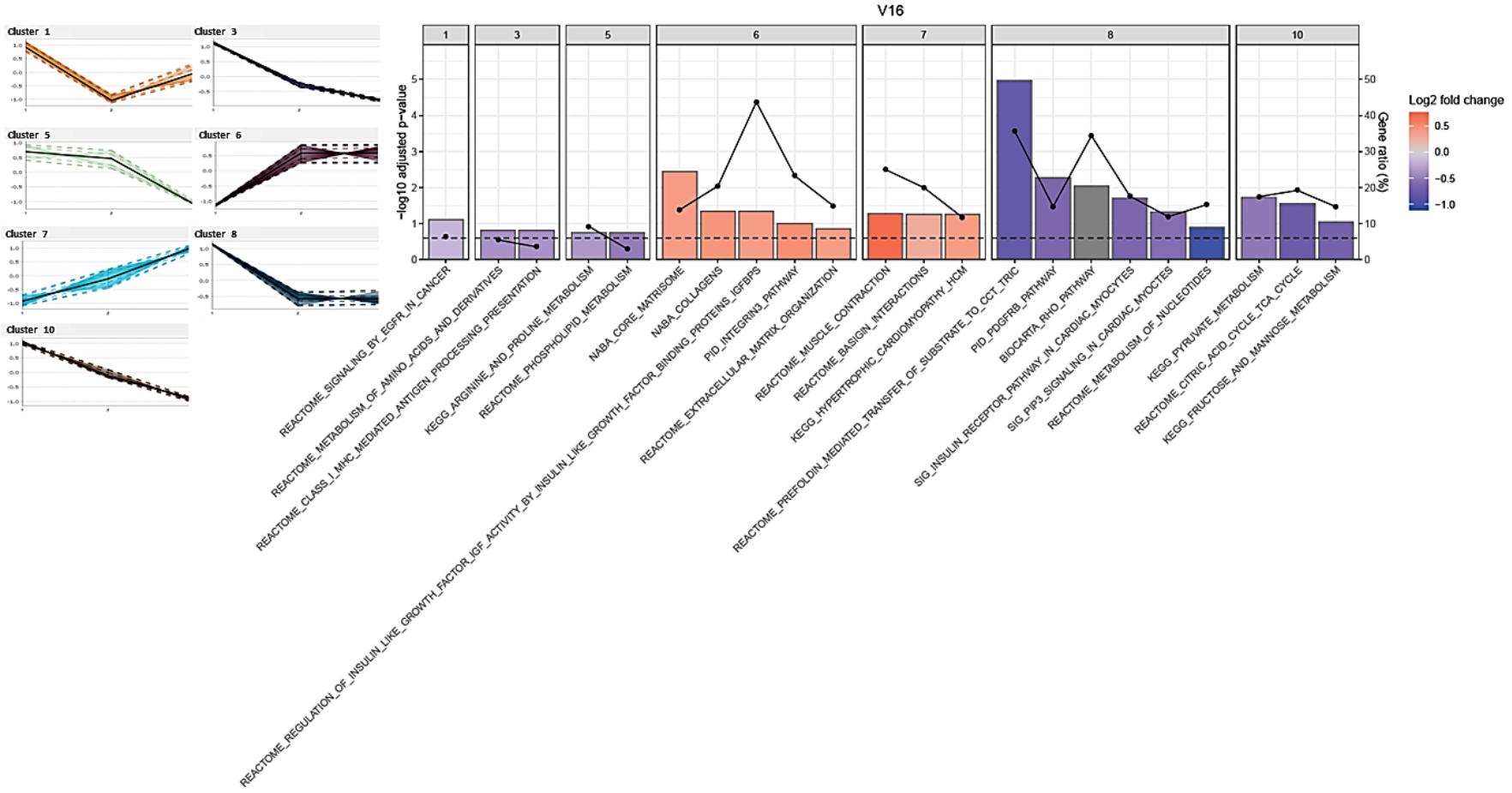

Figure 9- Case study 2 (V16)- Cluster trends (time profiles) and respective bar plot with the most significant (-log10 adjusted p-value) enriched pathways for each cluster. Bar heights represent the adjusted p-value for each pathway. The log2 fold change represents the median of the differences between all proteins enriched for that specific pathway at the last time-point and the same proteins at the first time-point. Blue means decrease, and red increase. The dots represent the number of proteins identified within the pathway in a specific cluster, divided by the total number of proteins identified in a specific pathway for this specific patient proteome background (universe). Dashed line represents the threshold of the p-adjusted value (0.25).

Case study 3- Patient with a good response to PD therapy

Patient P03 represents a clinical case of a man that initiated PD at age of 52 for the treatment of CKD due to hypertensive nephrosclerosis. This patient performed PD for more than 3 years. The peritoneal function, effluent biomarker CA125 and other clinical aspects such as serum albumin and PTH were assessed for each time point without any significant clinical alteration, with the exception of the creatinine clearance that was <60 (ml/min) for the last time-point. The patient is still performing PD therapy since the last time-point. More details for this patient can be seen in the Figure 10 and Supplementary Table S2.

Regarding proteomic analysis, some clusters have important pathways already discussed above in case studies 1 and 2, such as "Post translational protein modification" and "O-linked glycosylation of mucins", with an increasing trend (cluster 11, Figure 10); and "cytokine–cytokine receptor interaction" with and increasing/stabilizing trend (cluster 14, Figure 10). Within cluster 7 (Figure 10), with a moderately increasing trend, the pathways enriched and proteins therein may suggest a well-balanced matrix homeostasis, with regards to collagen formation, ECM organization and degradation. In the healthy peritoneum, MCs play an important role in the finely regulated but continuous processes of both synthesis and degradation of matrix within the peritoneal cavity. However, during disease states, metabolism of the matrix proteins and the basal lamina can become uncontrolled, leading to fibrosis and sclerosis[93]. Excessive matrix proteins can result from increased synthesis or reduced degradation. This balance is modulated by a family of specific MMPs, that when acting together are capable of degrading all the constituents of the basement membrane. Therefore, the identity and regulation of these MMPS, as well as their specific inhibitors, known as Tissue Inhibitors of Metalloproteinases' (TIMPs), are critical both in the normal turnover of the membrane constituents and during tissue injury that occurs during PD[93]. Therefore, in this particular case study, collagens and some MMPs such as, MMP2, MMP3 and MMP11 and their inhibitor, TIMP1, are found enriched within a steadily increasing trend over time, which may indicate a proteolytic/antiproteolytic balance.

A study performed by Hirahara *et al.*[15], investigated the potential of MMP and TIMPs as indicator of peritoneal injury. The peritoneal equilibration test (PET) results correlated with MMP2, MMP3 and TIMP-1 levels in the drained dialysate. However, correlation coefficients of the peritoneal solute transport rate were higher with the level of MMP-2 than with the levels of MMP3 or TIMP1. Moreover, MMP-3 level was biased by gender difference or the etiology of ESRD. The TIMP1 level was also biased by gender difference. Furthermore, expression of TIMP1 is induced by various factors, such as Il-1, TNF-α and TGF-β, whereas MMP2 is usually expressed constitutively. Therefore, MMP3 and TIMP1 might be more easily affected by various factors than MMP2. In addition, correlation coefficient between MMP2 and TIMP1 levels in the

dialysate was higher than between MMP2 and MMP3. This may be attributed to the local production of MMP2 and TIMP1 in the peritoneal tissues besides transport from circulation. Thus, given that MMP2 is produced in the peritoneum and directly degrades peritoneal tissue, MMP2 levels in the drainage may reflect injury to the peritoneum, and thus be a useful marker of peritoneal injury or change in peritoneal solute transport rate (PSTR) [15], [94]. Concerning our case study, given the steadily increasing trend overtime of both MMP2 and TIMP1, we could speculate that this suggests a proteolytic/antiproteolytic balance. Yet, a study published by Cho *et al.* [84] showed that dialysate levels of MMP2 and TIMP1 concentration increased with longer PD duration. Higher MMP-2 levels were associated with faster PSTR and future peritonitis risk. Administration of biocompatible solutions exerted no significant effect on dialysate levels of MMP-2 or TIMP-1, but did counteract the increase in PSTR and the risk of peritonitis associated with the use of standard PD solutions [84]. Thus, it is important to understand and distinguish the involvement of MMP2 and TIMP1, as a part of the important and continuous balanced process of both synthesis and degradation of matrix within the peritoneal cavity, because MMP/TIMP ratio often determines the extent of ECM protein degradation and tissue remodelling[95]. Therefore, different levels of the MMPs and TIMPs in the PDE may reflect a normal PM wound healing process, or a PM dysfunction associated to high levels of MMP2 [84].

Interestingly, the core matrisome pathway is enriched for both cluster 7 and cluster 10 (this latter with a decreasing trend) (Figure 10). It should be noted that proteins are not shared between different clusters, and proteins within clusters 7 and 10 are therefore different proteins despite belonging to the same enriched pathway, (Supplementary Table S5). Thus, for instance, whereas cluster 7 consists mainly of collagen proteins, in cluster 10 a wide variety of proteins are observed. The "ECM regulators" pathway enriched in cluster 14 (Figure 10), with an increasing/stabilizing trend, also supports the hypothesis that both synthesis and degradation of matrix are properly regulated, with the presence of some proteases within the pathway, such as, CTSF (Cathepsin F), MMP19 (Matrix Metalloproteinase-19), ADAMTS13 (a disintegrin and metalloproteinase with thrombospondin motifs 13); and also some inhibitors, such as SERPINF2 (Alpha-2-antiplasmin), SERPINA11 (Serpin A11) and ITIH3 (Inter-alpha-trypsin inhibitor heavy chain H3). Some of these proteases and protease inhibitors that have a pivotal role as ECM regulators play also a role in the complement and coagulation cascade.

"Complement and coagulation cascades" is one of the most frequently enriched pathways found across our patients' cohort (Table S5), and patient P03 is not an exception, presenting an increasing/stabilizing trend for this particular pathway (Cluster 14, Figure 10). Recently, Poppelaars *et al.* reviewed and summarized a comprehensive overview of the role of complement system in PD. The proposed mechanism of complement activation in PD patients, suggests that PD therapy decreases the expression of complement regulators produced and secreted by the MCs, such as CD55 and CD59, leading to local complement activation[96]. The cellular debris,

as a result of direct peritoneal damage by biocompatible PDFs, as well as antibodies against microorganisms could also contribute to local complement activation during PD. This activation results in the formation of anaphylatoxins (C3a, C5a), opsonins (C3b, iC3b), and the membrane attack complex (C5b-9)[96]. In this specific case study, complement factors such as C5 and C6, which are known to be produced and secreted by MCs [97] are found within the enriched "complement and coagulation cascades" pathway (cluster 14, Figure 10). Similarly, some anaphylatoxins, such as, C4A and C4B, both derived from proteolytic degradation of the complement C4, are also found, (Supplementary Table S5). In addition, the carboxypeptidase B2 (CPB2), responsible for the cleavage of biologically active peptides such as anaphylatoxins, is also found within the pathway. Moreover, C8A, C8B and C8G, which are constituents of the membrane attack complex, are also found enriched.

Importantly, complement activation leads to the influx of leukocytes, increases the production of thrombin anti-thrombin complexes and fibrin exudation on the surface of the injured peritoneum. In addition, complement activation during PD leads to peritoneum injury, can promote the progression to fibrosis after tissue injury and stimulate MCs to undergo EMT [96]. Interestingly, SERPINC1 (antithrombin-III) and SERPIND1 (heparin cofactor 2), are some thrombin inhibitors regulating coagulation cascades that are found within the pathway. In addition, SERPING1 (plasma protease C1 inhibitor) is also present, and plays a role in the regulation of complement activation, coagulation, fibrinolysis and the generation of kinins. Moreover, SERPINF2 (alpha-2-antiplasmin) and KNG1 (kininogen-1) are also some of the inhibitors found enriched in the complement and coagulation cascades pathways. On the other hand, PLAU (urokinase-type plasminogen activator) is responsible for the cleavage of the zymogen plasminogen to form the active enzyme plasmin and is also present within the pathway.

However, this finding of complement activation was not exclusively observed for this particular case study, given the fact that was one of the main enriched pathways found dysregulated across several patients. In addition, these findings are in line with recent studies published by Bartosova *et al.*[98] and Boehm *et al.*[99], where the analysis of peritoneal biopsy and peritoneal surface proteomes in model rats of chronic PD, showed an increased complement activation related with glucose exposure. In summary, complement has a pivotal role in preventing infections, however, complement dysregulation drives pathology and measurement of specific PDE complement biomarkers might predict poor outcome and patient survival, as suggested by Zelek *et al.*[100].

Therefore, it is interesting to observe that many of these proteins and proteases identified and enriched for these pathways orchestrate processes related with ECM, and complement coagulation cascades. Thus, the use of complement biomarkers in the management of PD could be particularly useful, together with implementation of strategies to protect the peritoneum and to enable long-term PD. These strategies may pass through the use of PDF supplemented with

Alanyl-Glutamine-mediated membrane protection[99], or through the inhibition of membrane complement regulators by using of anti-C5a complementary peptides, which have been shown to ameliorate acute peritoneal injury by the neutralization of Crry and CD59 [101]. Even though these suggested approaches were not yet tested in a large patient cohort, the follow-up of some complement biomarkers identified in our study (namely C4A, C4B, C8A, C8B and CPB2, etc.) could add more information about PM condition and could be helpful to prevent PM injury related with complement activation.

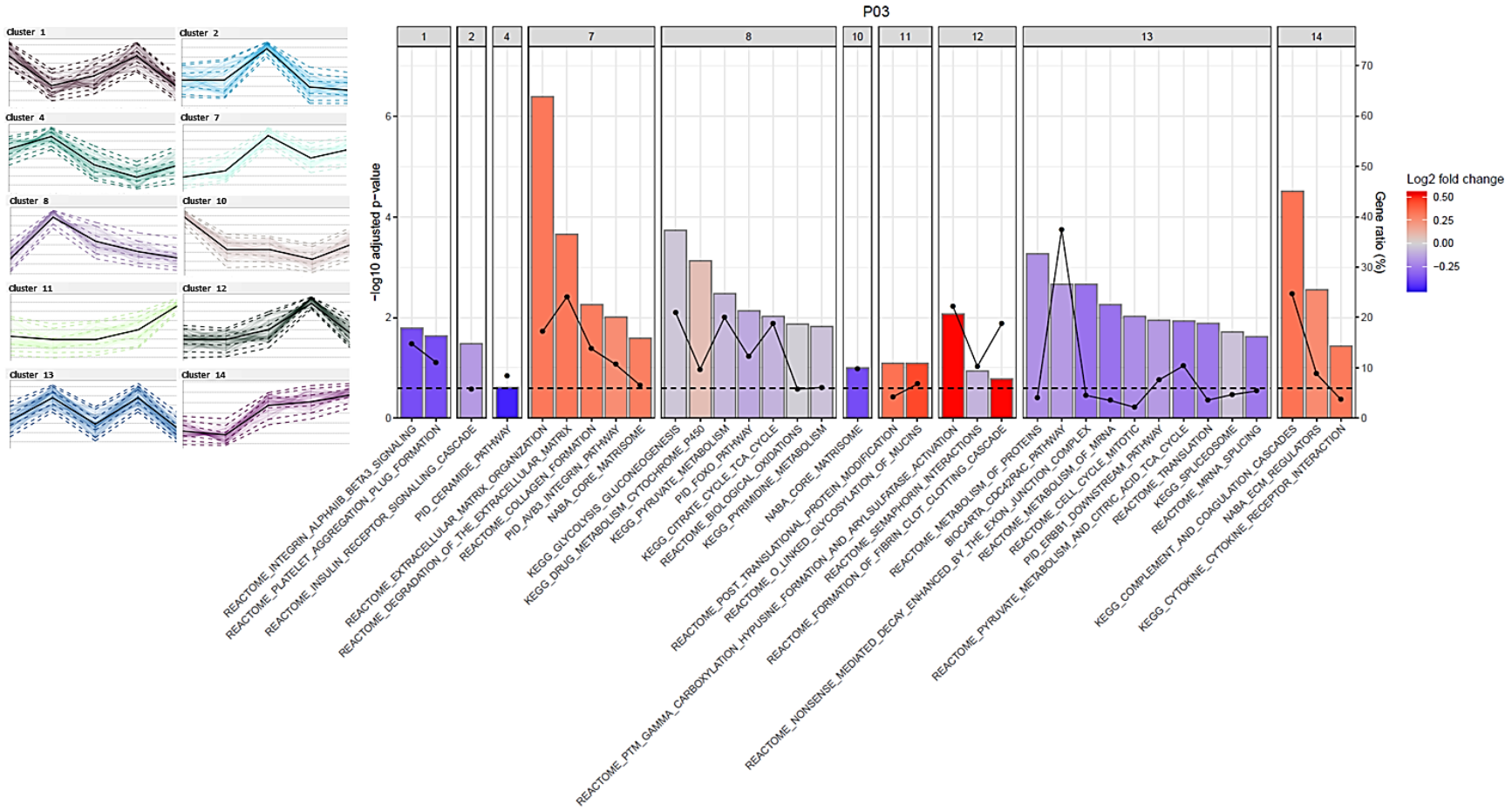

Figure 10- Case study 3- Cluster trends (time profiles) and respective bar plot with the most significant (-log10 adjusted p-value) enriched pathways for each cluster. Bar heights represent the adjusted p-value for each pathway. The log2 fold change represents the median of the differences between all proteins enriched for that specific pathway at the last time-point and the same proteins at the first time-point. Blue means decrease, and red increase. The dots represent the number of proteins identified within the pathway in a specific cluster, divided by the total number of proteins identified in a specific pathway for this specific patient proteome background (universe). Dashed line represents the threshold of the p-adjusted value (0.25).

4-Conclusions

This longitudinal study presented in a PD patients' cohort greatly increased the protein PDE coverage, giving new insights regarding PDE sample complexity. The analysis of longitudinal data performed for patients with three or more time points revealed that some of the most frequently significant pathways across patients are related with metabolic pathways, complement and coagulation cascades, ECM organization, formation of fibrin clot clotting cascade and integrin pathways. In addition, the need of a case by case patient treatment, and the possibility of identifying and following changes in the PM during long-term PD is here highlighted with three clinical case studies. Interestingly, our methodology used in parallel with PET measurements gave a holistic view of a patient´s condition, with the proteome analysis suggesting for patient case study 1, a diminished capacity of the peritoneal host response, with a decreasing trend of proteins within pathways of immune response, such as "class I MHC mediated antigen processing presentation" and the "Il-6, -7, pathway". For this particular case, the proteomic analysis revealed that, for instance, following the IL-6 levels could have been useful for a clinical decision. On the other hand, for case study 2, the longitudinal analysis pinpointed a decreasing trend for protein homeostasis and a panoply of metabolic pathways; and an increased trend for pathways related with extra cellular matrix (ECM). In contrast, case study 3 represents a good patient response to PD therapy, in that many of the proteins and proteases identified orchestrate and regulate the process of both synthesis and degradation of matrix within the peritoneal cavity what it may reflect a normal PM wound healing process. Even though our study represents more an exploratory than a biomarker discovery study, it has the potential to be applied to a larger stratified cohort of patients and performed in a context of clinical biomarker discovery. Moreover, this knowledge could help to guide and develop case-by-case interventions that may improve clinical outcome in an individual manner, allowing to distinguish patients that respond well to therapy from those who are at the highest risk for PD-related complications such as, episodes of peritonitis or ultrafiltration failure.

In addition, and to the best of our knowledge, this is the first analysis of PDE native peptides. The study of these naturally originated peptides through proteolytic activity of several proteases, is of great importance to shed some light on pathways at the "peptide level" that could be as much informative as the proteome. With this purpose, protease prediction analysis was performed to extend our knowledge about proteases that might be related with protein cleavage inside the peritoneum. Therefore, and as future prospects, the longitudinal analysis of the patients' peptidome has to be performed and the protease prediction inferred by the native peptide information interrogated. Lastly, the protease prediction, proteome and peptidome longitudinal study have to be put together so as to develop a more complete picture about biological processes occurring within the peritoneum.

Thereby, this study shed some light about the main molecular pathways associated with long-term PD, and contributed with valuable information for the proteomic and clinical research community in future studies using PDE samples.

5-Conflict of interest

The author declares no conflict of interest.

6-Acknowledgements

J. E. Araújo would like to thanks to J. Axelsson and S. Lundberg for the plasma dataset contribution and to S. Jorge for the help given with sample gathering and pre-treatment while he was working at SciLifeLab (Sweden). J. E. Araújo acknowledges the doctoral grant SFRH/BD/109201/2015 provided by Fundação para a Ciência e a Tecnologia Ministério da Educação e Ciência (FCT–MEC, Portugal). Dr. J. L. Capelo and Dr H. M Santos acknowledges Associated Laboratory for Sustainable Chemistry-Clean Processes and Technologies- LAQV which is financed by national funds from FCT/MEC (UID/QUI/50006/2013) and co-financed by the ERDF under the PT2020 Partnership Agreement (POCI-01-0145-FEDER-007265). J. E. Araújo, Dr. J. L. Capelo and Dr H. M. Santos acknowledges Proteomass Scientific Society. This work was supported by LehtiöLab.

7-Data Accessibility

Supplementary information can be found in the annex 1 and as Electronic Supplementary Material (ESM)

Figure S1-Bar chart representation of the total number/overlap of peptides and proteins identified between sets.

Figure S2-Venn diagrams comparison of the fragmentation techniques (CID and HCD-EthcD) applied for endogenous peptides analysis, with number of peptide sequences and parental proteins identified and proteases predicted.

Supplementary Material Tables

Table S1- Enriched pathways (terms) present across the patient's cohort. Each pathway (term), has the frequency, that means the number of times that a pathway appears across the patient's cohort, the patients that have that specific term, and the group (relation between the different pathways, if they are related the group number is the same).

Table S2- Clinical parameters assess during the PET for the longitudinal case study patients. The values highlighted are out of the reference range values for that specific parameter (described at the bottom of the table).

Table S3-Patient P01-Enriched pathways for each cluster with the respective Gene Ratio, Background ratio (Bg Ratio), p-value, p-adjust, q-value, Gene Id and counts (number of genes (proteins) per pathways). The highlighted pathways were the one selected for the bar plots graphs.

Table S4-Patient V16-Enriched pathways for each cluster with the respective Gene Ratio, Background ratio (Bg Ratio), p-value, p-adjust, q-value, Gene Id and counts (number of genes (proteins) per pathways). The highlighted pathways were the one selected for the bar plots graphs.

Table S5-Patient P03-Enriched pathways for each cluster with the respective Gene Ratio, Background ratio (Bg Ratio), p-value, p-adjust, q-value, Gene Id and counts (number of genes (proteins) per pathways). The highlighted pathways were the one selected for the bar plots graphs.

Electronic Supplementary Material Tables can be assessed at ProteomeXchange:

Project Name: In-Depth Analysis of Peritoneal Dialysis Effluent Proteome and Peptidome: A Longitudinal Follow-Up Study
Project accession: PXD016853
Username: reviewer78275@ebi.ac.uk

Table ESM1- Detailed clinical information of the patient's cohort.

Table ESM2- Table with all the proteins identified and quantified with TMT labelling for all patients.

Table ESM3- Protein ranking abundance, proteins ¬ quantified and summarized are ranked according to their MS1 intensities and divided into four groups –(non-)unique for PDE, (non-) shared across patients– with neuropathy plasma dataset proteins as background.

Table ESM4- Proteasix protease prediction analysis of the endogenous peptides acquired and identified with the CID fragmentation method.

Table ESM5- Proteasix protease prediction analysis of the endogenous peptides acquired and identified with the HCD-EThcD fragmentation method.

8-References

[1] S. J. Davies, "Peritoneal dialysis-current status and future challenges," *Nature Reviews Nephrology*. 2013.

[2] P. K. T. Li *et al.*, "Changes in the worldwide epidemiology of peritoneal dialysis," *Nature Reviews Nephrology*. 2017.

[3] A. K. Jain, P. Blake, P. Cordy, and A. X. Garg, "Global Trends in Rates of Peritoneal Dialysis," *J. Am. Soc. Nephrol.*, 2012.

[4] F. M. C. A. KGaA, "Fresenius Medical Care 2017. Annual Report," 2017.

[5] H. Terawaki, "Peritoneal Physiology and Peritoneal Membrane," in *The Essentials of Clinical Dialysis*, Y.-L. Kim and H. Kawanishi, Eds. Springer, 2018, pp. 153–161.

[6] S. J. Davies, "Peritoneal dialysis—current status and future challenges," *Nat. Rev. Nephrol.*, 2013.

[7] R. T. Krediet and D. G. Struijk, "Peritoneal changes in patients on long-term peritoneal dialysis," *Nat Rev Nephrol*, 2013.

[8] A. K. Al-Hwiesh *et al.*, "Changes in peritoneal membrane with different peritoneal dialysis solutions: Is there a difference?," *Hong Kong J. Nephrol.*, vol. 19, pp. 7–18, Oct. 2016.

[9] G. T. González-Mateo *et al.*, "Angiogenesis and Lymphangiogenesis in Peritoneal Dialysis," in *Aspects in Dialysis*, no. 7, 2018, pp. 133–163.

[10] J. Shi, M. Yu, and M. Sheng, "Angiogenesis and Inflammation in Peritoneal Dialysis: The Role of Adipocytes," *Kidney Blood Press. Res.*, vol. 42, no. 2, pp. 209–219, 2017.

[11] T. Duarte and C. Spencer, "Personalized Proteomics: The Future of Precision Medicine," *Proteomes*, 2016.

[12] B. Schaefer *et al.*, "Neutral pH and low–glucose degradation product dialysis fluids induce major early alterations of the peritoneal membrane in children on peritoneal dialysis," *Kidney Int.*, vol. 94, no. 2, pp. 419–429, Aug. 2018.

[13] M. A. Bajo, G. del Peso, and I. Teitelbaum, "Peritoneal Membrane Preservation," *Seminars in Nephrology*. 2017.

[14] D. Lopes Barreto and R. T. Krediet, "Current status and practical use of effluent biomarkers in peritoneal dialysis patients," *Am. J. Kidney Dis.*, 2013.

[15] I. Hirahara, M. Inoue, T. Umino, O. Saito, S. Muto, and E. Kusano, "Matrix metalloproteinase levels in the drained dialysate reflect the peritoneal solute transport rate: A multicentre study in Japan," *Nephrol. Dial. Transplant.*, 2011.

[16] C. Aufricht *et al.*, "Biomarker research to improve clinical outcomes of peritoneal dialysis: consensus of the European Training and Research in Peritoneal Dialysis (EuTRiPD) network," *Kidney International*. 2017.

[17] R. M. M. Branca *et al.*, "HiRIEF LC-MS enables deep proteome coverage and unbiased proteogenomics," *Nat. Methods*, 2014.

[18] J. E. Araújo *et al.*, "A cost-effective method to get insight into the peritoneal dialysate effluent proteome," *J. Proteomics*, vol. 145, pp. 207–213, 2016.

[19] I. A. Brewis and N. Topley, "Proteomics and peritoneal dialysis: Early days but clear potential," *Nephrology Dialysis Transplantation*. 2010.

[20] C. S. Hughes, S. Foehr, D. A. Garfield, E. E. Furlong, L. M. Steinmetz, and J. Krijgsveld, "Ultrasensitive proteome analysis using paramagnetic bead technology.,"

Mol. Syst. Biol., 2014.

[21] D. Kessner, M. Chambers, R. Burke, D. Agus, and P. Mallick, "ProteoWizard: Open source software for rapid proteomics tools development," *Bioinformatics*, 2008.

[22] S. Kim and P. A. Pevzner, "MS-GF+ makes progress towards a universal database search tool for proteomics," *Nat. Commun.*, 2014.

[23] L. Käll, J. D. Canterbury, J. Weston, W. S. Noble, and M. J. MacCoss, "Semi-supervised learning for peptide identification from shotgun proteomics datasets," *Nat. Methods*, 2007.

[24] P. DI Tommaso, M. Chatzou, E. W. Floden, P. P. Barja, E. Palumbo, and C. Notredame, "Nextflow enables reproducible computational workflows," *Nature Biotechnology*. 2017.

[25] H. L. Röst *et al.*, "OpenMS: A flexible open-source software platform for mass spectrometry data analysis," *Nature Methods*. 2016.

[26] Y. Perez-Riverol *et al.*, "The PRIDE database and related tools and resources in 2019: Improving support for quantification data," *Nucleic Acids Res.*, 2019.

[27] J. Klein, J. Eales, P. Zürbig, A. Vlahou, H. Mischak, and R. Stevens, "Proteasix: A tool for automated and large-scale prediction of proteases involved in naturally occurring peptide generation," *Proteomics*, 2013.

[28] J. Matuszkiewicz-Rowinska, "Update on fungal peritonitis and its treatment," in *Peritoneal Dialysis International*, 2009.

[29] A. Liberzon, A. Subramanian, R. Pinchback, H. Thorvaldsdóttir, P. Tamayo, and J. P. Mesirov, "Molecular signatures database (MSigDB) 3.0," *Bioinformatics*, 2011.

[30] G. Yu, L. G. Wang, Y. Han, and Q. Y. He, "ClusterProfiler: An R package for comparing biological themes among gene clusters," *Omi. A J. Integr. Biol.*, 2012.

[31] L. J. Pearson *et al.*, "Multiple extracellular vesicle types in peritoneal dialysis effluent are prominent and contain known biomarkers," *PLoS One*, 2017.

[32] R. Herzog *et al.*, "Effects of Alanyl-Glutamine Treatment on the Peritoneal Dialysis Effluent Proteome Reveal Pathomechanism-Associated Molecular Signatures," *Mol. Cell. Proteomics*, 2018.

[33] R. T. Krediet, D. G. Struijk, S. van Esch, and R. T. Krediet, "Assessment of the Peritoneum by Biomarkers in Peritoneal Effluent," *Perit. Dial. Man.*, pp. 27–34, 2018.

[34] M. Pernemalm *et al.*, "In-depth human plasma proteome analysis captures tissue proteins and transfer of protein variants across the placenta," *Elife*, vol. 8, 2019.

[35] M. Schrader, P. Schulz-Knappe, and L. D. Fricker, "Historical perspective of peptidomics," *EuPA Open Proteomics*, 2014.

[36] Z. W. Lai, A. Petrera, and O. Schilling, "The emerging role of the peptidome in biomarker discovery and degradome profiling," *Biological Chemistry*. 2015.

[37] R. Vitorino, "Digging Deep into Peptidomics Applied to Body Fluids," *Proteomics*. 2018.

[38] B. Magalhães *et al.*, "Reviewing Mechanistic Peptidomics in Body Fluids Focusing on Proteases," *Proteomics*. 2018.

[39] L. S. Aroeira *et al.*, "Epithelial to Mesenchymal Transition and Peritoneal Membrane Failure in Peritoneal Dialysis Patients: Pathologic Significance and Potential Therapeutic Interventions," *J. Am. Soc. Nephrol.*, 2007.

[40] A. Isaza-Restrepo, J. S. Martin-Saavedra, J. L. Velez-Leal, F. Vargas-Barato, and R. Riveros-Dueñas, "The peritoneum: Beyond the tissue - A review," *Front. Physiol.*, vol. 9, no. JUN, pp. 1–12, 2018.

[41] S. Mortier, N. H. Lameire, and A. S. De Vriese, "The effects of peritoneal dialysis solutions on peritoneal host defense," *Peritoneal Dialysis International*. 2004.

[42] R. Kazancioglu, "Peritoneal defense mechanisms - The effects of new peritoneal dialysis solutions," in *Peritoneal Dialysis International*, 2009.

[43] Y. C. Cheong, S. M. Laird, T. C. Li, J. B. Shelton, W. L. Ledger, and I. D. Cooke, "Peritoneal healing and adhesion formation/reformation," *Hum. Reprod. Update*, 2001.

[44] L. Holmdahl and M. L. Ivarsson, "The role of cytokines, coagulation, and fibrinolysis in peritoneal tissue repair," *European Journal of Surgery*. 1999.

[45] G. Garibotto *et al.*, "Effects of peritoneal dialysis on protein metabolism," *Nutrition, Metabolism and Cardiovascular Diseases*. 2013.

[46] A. Sofia *et al.*, "Acute effects of peritoneal dialysis on muscle protein turnover," *G. Ital. Nefrol.*, 2002.

[47] M. J. Kailemia, D. Park, and C. B. Lebrilla, "Glycans and glycoproteins as specific biomarkers for cancer," *Analytical and Bioanalytical Chemistry*. 2017.

[48] D. T. Tran and K. G. Ten Hagen, "Mucin-type o-glycosylation during development," *Journal of Biological Chemistry*. 2013.

[49] M. Sperandio, "Selectins and glycosyltransferases in leukocyte rolling in vivo," *FEBS Journal*. 2006.

[50] M. F. Ali, V. B. Chachadi, A. Petrosyan, and P. W. Chengs, "Golgi phosphoprotein 3 determines cell binding properties under dynamic flow by controlling golgi localization of core 2 N-acetylglucosaminyltransferase 1," *J. Biol. Chem.*, 2012.

[51] S. J. Hobbs and J. C. Nolz, "Regulation of T cell trafficking by enzymatic synthesis of O-glycans," *Frontiers in Immunology*. 2017.

[52] G. Marenzi, "Chronic kidney disease in acute coronary syndromes," *World J. Nephrol.*, 2012.

[53] X. Han *et al.*, "Statin in the treatment of patients with myocardial infarction: A meta-analysis," *Med. (United States)*, vol. 97, no. 12, pp. 10–13, 2018.

[54] G. M. Keating and B. Jarvis, "Carvedilol: A review of its use in chronic heart failure," *Drugs*. 2003.

[55] N. Bissessor and H. White, "Valsartan in the treatment of heart failure or left ventricular dysfunction after myocardial infarction," *Vascular Health and Risk Management*. 2007.

[56] S. M. Hurst *et al.*, "IL-6 and its soluble receptor orchestrate a temporal switch in the pattern of leukocyte recruitment seen during acute inflammation," *Immunity*, 2001.

[57] R. M. McLoughlin *et al.*, "IL-6 trans-signaling via STAT3 directs T cell infiltration in acute inflammation," *Proc. Natl. Acad. Sci. U. S. A.*, 2005.

[58] B. Stegmayr, "Dialysis procedures alter metabolic conditions," *Nutrients*. 2017.

[59] M. Gallieni, C. Musetti, A. Granata, L. Olivi, and S. Bertoli, "Metabolic consequences of peritoneal dialysis treatment," *Panminerva Med.*, 2009.

[60] C. R. Góes, M. N. Berbel, A. L. Balbi, and D. Ponce, "Approach to the metabolic implications of peritoneal dialysis in acute kidney injury," *Perit. Dial. Int.*, vol. 35, no. 4, pp. 397–405, 2015.

[61] H. L. Tjiong *et al.*, "Dialysate as food: Combined amino acid and glucose dialysate improves protein anabolism in renal failure patients on automated peritoneal dialysis," *J. Am. Soc. Nephrol.*, 2005.

[62] H. L. Tjiong, R. Swart, J. W. van den Berg, and M. W. Fieren, "Amino acid-based peritoneal dialysis solutions for malnutrition: New perspectives," *Perit. Dial. Int.*, 2009.

[63] T. J. Shaw *et al.*, "Human Peritoneal Mesothelial Cells Display Phagocytic and Antigen-Presenting Functions to Contribute to Intraperitoneal Immunity," *Int. J. Gynecol. Cancer*, 2016.

[64] M. T. Valle *et al.*, "Antigen-presenting function of human peritoneum mesothelial cells," *Clin. Exp. Immunol.*, 2008.

[65] M. J. Hausmann, B. Rogachev, M. Weiler, C. Chaimovitz, and A. Douvdevani, "Accessory role of human peritoneal mesothelial cells in antigen presentation and T-cell growth," *Kidney Int.*, 2000.

[66] A. R. Aguirre and H. Abensur, "Protective measures against ultrafiltration failure in peritoneal dialysis patients," *Clinics*. 2011.

[67] I. Teitelbaum, "Ultrafiltration failure in peritoneal dialysis: A pathophysiologic approach," *Blood Purif.*, vol. 39, no. 1–3, pp. 70–73, 2015.

[68] B. Pan, J. Guo, Q. Liao, and Y. Zhao, "β1 and β3 integrins in breast, prostate and pancreatic cancer: A novel implication (Review)," *Oncology Letters*. 2018.

[69] J. Schnittert, R. Bansal, G. Storm, and J. Prakash, "Integrins in wound healing, fibrosis and tumor stroma: High potential targets for therapeutics and drug delivery," *Adv. Drug Deliv. Rev.*, vol. 129, pp. 37–53, Apr. 2018.

[70] E. Madrazo, A. C. Conde, and J. Redondo-Muñoz, "Inside the cell: Integrins as new governors of nuclear alterations?," *Cancers (Basel).*, vol. 9, no. 7, pp. 1–17, 2017.

[71] A. M. Coester, W. Smit, D. G. Struijk, and R. T. Krediet, "Peritoneal function in clinical practice: The importance of follow-up and its measurement in patients. Recommendations for patient information and measurement of peritoneal function," *NDT Plus*. 2009.

[72] O. Devuyst and J. Ni, "Aquaporin-1 in the peritoneal membrane: Implications for water transport across capillaries and peritoneal dialysis," *Biochim. Biophys. Acta - Biomembr.*,

vol. 1758, no. 8, pp. 1078–1084, Aug. 2006.

[73] R. T. Krediet, "Ultrafiltration Failure Is a Reflection of Peritoneal Alterations in Patients Treated With Peritoneal Dialysis," *Front. Physiol.*, vol. 9, p. 1815, 2018.

[74] R. T. Krediet, "Dialysate cancer antigen 125 concentration as marker of peritoneal membrane status in patients treated with chronic peritoneal dialysis," *Perit. Dial. Int.*, 2001.

[75] J. Holly and C. Perks, "The role of insulin-like growth factor binding proteins," in *Neuroendocrinology*, 2006.

[76] S. M. Firth and R. C. Baxter, "Cellular actions of the insulin-like growth factor binding proteins," *Endocrine Reviews*. 2002.

[77] M. J. Lee *et al.*, "Association between the ratio of insulin-like growth factor-I to insulin-like growth factor binding protein-3 and inflammation in incident automated peritoneal dialysis patients," *Growth Horm. IGF Res.*, 2013.

[78] K. Dittmann *et al.*, "Association between serum insulin-like growth factor I or IGF-binding protein 3 and estimated glomerular filtration rate: results of a population-based sample.," *BMC Nephrol.*, 2012.

[79] P. Iglesias *et al.*, "Growth hormone, IGF-I and its binding protiens (IGFBP-1 and -3) in adult uraemic patients undergoing peritoneal dialysis and haemodialysis," *Clin. Endocrinol. (Oxf).*, 2004.

[80] A. Kagan, Y. Altman, Z. Zadik, and Y. Bar-Khayim, "Extracorporeal losses of insulin-like growth factor-I and insulin-like growth factor binding protein-3 in adult patients on CAPD.," *Adv. Perit. Dial.*, vol. 13, pp. 47–52, 1997.

[81] J. L. Jiang and J. Tang, "CD147 and its interacting proteins in cellular functions.," *Sheng Li Xue Bao*, 2007.

[82] G. D. Grass and B. P. Toole, "How, with whom and when: An overview of CD147-mediated regulatory networks influencing matrix metalloproteinase activity," *Biosci. Rep.*, 2016.

[83] R. Li, L. Huang, H. Guo, and B. P. Toole, "Basigin (murine EMMPRIN) stimulates matrix metalloproteinase production by fibroblasts," *J. Cell. Physiol.*, 2001.

[84] Y. Cho *et al.*, "Higher dialysate matrix metalloproteinase-2 levels are associated with peritoneal membrane dysfunction," *Perit. Dial. Int.*, 2016.

[85] E. A. McCormack, O. Llorca, J. L. Carrascosa, J. M. Valpuesta, and K. R. Willison, "Point mutations in a hinge linking the small and large domains of β-actin result in trapped folding intermediates bound to cytosolic chaperonin CCT," *J. Struct. Biol.*, 2001.

[86] T. Lopez, K. Dalton, and J. Frydman, "The Mechanism and Function of Group II Chaperonins," *Journal of Molecular Biology*. 2015.

[87] C. Spiess, A. S. Meyer, S. Reissmann, and J. Frydman, "Mechanism of the eukaryotic chaperonin: Protein folding in the chamber of secrets," *Trends in Cell Biology*. 2004.

[88] C. Boudiaf-Benmammar, T. Cresteil, and R. Melki, "The Cytosolic Chaperonin CCT/TRiC and Cancer Cell Proliferation," *PLoS One*, vol. 8, no. 4, pp. 1–10, 2013.

[89] J. Vallin and J. Grantham, “The role of the molecular chaperone CCT in protein folding and mediation of cytoskeleton-associated processes: implications for cancer cell biology,” *Cell Stress and Chaperones*. 2019.

[90] J. Andrae, R. Gallini, and C. Betsholtz, “Role of platelet-derived growth factors in physiology and medicine,” *Genes and Development*. 2008.

[91] Z. G. Xu *et al.*, “High glucose activates the p38 MAPK pathway in cultured human peritoneal mesothelial cells,” *Kidney Int.*, 2003.

[92] T. I. Chang *et al.*, “The effect of statin on epithelial-mesenchymal transition in peritoneal mesothelial cells,” *PLoS One*, 2014.

[93] S. Yung and T. Chan, “Peritoneal mesothelial cells and the extracellular matrix,” *Nephrology*, vol. 6, no. 6, pp. 250–258, 2001.

[94] I. Hirahara *et al.*, “Matrix metalloproteinase-2 as a superior biomarker for peritoneal deterioration in peritoneal dialysis,” *World J. Nephrol.*, 2016.

[95] X. Wang and R. A. Khalil, “Matrix Metalloproteinases, Vascular Remodeling, and Vascular Disease,” in *Advances in Pharmacology*, 2018.

[96] F. Poppelaars *et al.*, “The complement system in dialysis: A forgotten story?,” *Front. Immunol.*, vol. 9, no. JAN, pp. 1–12, 2018.

[97] G. Barbano *et al.*, “Peritoneal mesothelial cells produce complement factors and express CD59 that inhibits C5b-9-mediated cell lysis.,” *Adv. Perit. Dial.*, 1999.

[98] M. Bartosova *et al.*, “Complement activation in peritoneal dialysis⇓Induced arteriolopathy,” *J. Am. Soc. Nephrol.*, 2018.

[99] M. Boehm *et al.*, “The peritoneal surface proteome in a model of chronic peritoneal dialysis reveals mechanisms of membrane damage and preservation,” *Front. Physiol.*, 2019.

[100] W. Zelek *et al.*, “Complement biomarkers in the management of peritoneal dialysis,” *Immunobiology*, 2016.

[101] T. Mizuno *et al.*, “Anti-C5a complementary peptide ameliorates acute peritoneal injury induced by neutralization of Crry and CD59,” *Am. J. Physiol. - Ren. Physiol.*, 2013.

CHAPTER VII. CONCLUDING REMARKS AND FUTURE PERSPECTIVES

Peritoneal membrane failure in patients with end stage renal disease submitted to PD therapy cannot be predicted and does not occur in every patient in the same sequence and to the same extent. Moreover, long-term PD leads to morphological and functional alterations in the PM, reducing the lifespan of this dialysis up to five years, and forcing the replacement of PD by other RRT. Although a number of molecules have been identified to be involved on PM alterations, a global peptidomics/proteomics study to identify biomarkers of PM alterations has not been fully addressed yet.

Therefore, the present project aimed to develop longitudinal studies to unravel the evolution of the peptidome and proteome of the PDE with time, to identify specific molecular changes that can be particularly interesting for the understanding and early detection of long-term PM alterations. However, to achieve this goal, MS-based methods are needed to improve PDE proteome and peptidome analysis and to overcome some drawbacks that can arise from such a complex biological sample, and that can hamper the proteome and peptidome coverage. For this reason, this thesis focused also in the use of sample treatments and methodologies to reduce PDE sample complexity prior to MS analysis. Therefore, different methods of sample treatment were assessed with success as proteomics tools for getting insight into the PDE proteome and peptidome.

Unravelling the PDE proteome presents some challenges in terms of sample treatment, as PDE is a relatively diluted solution of proteins, with their concentrations spanning several orders of magnitude. Therefore, the first sample treatment step that needed to be tested and optimized was the PDE concentration of the highly diluted samples, using centrifugal concentrators. This was investigated in chapter IV, and applied in all studies (chapter I-VI) as sample concentration methodology. Another major concern, was how to deal with the HAP present in these complex samples. In order to overcome this problem, two different methodologies, consisting in the DTT-based equalization, an ACN-based depletion, were tested on PDE samples, and applied before the 1D and 2D methodologies, and MALDI-MS-based profiling, across the chapter III to V.

Particularly, for the chapters III and V, chemical assisted DTT-based equalization, ACN-based depletion and the use of the entire proteome were tested for the first time in PDE to investigate their performance to obtain MALDI-TOF-MS-based profiles in order to classify two groups of patients, namely patients with chronic glomerulonephritis and diabetic nephropathy. In addition, samples were trypsinated using a fast ultrasonic approach, the pool of peptides profiled using MALDI-MS, and then the sets of data generated were treated with free/open-source software by principal component analysis and hierarchical clustering. The results suggested DTT-based equalization is a more robust methodology when compared with the other two, as the patients were well grouped by principal component analysis or by hierarchical clustering. This result suggests that successful MALDI-MS-based profiling of PDE samples relies in the selection of an appropriate sample treatment to compress the complexity of the proteome appropriately. These studies demonstrated also that the introduction of MS-based profiling

can provide a powerful, fast, cheap and accurate tool to classify patients with renal failure, using PDE samples.

For the study presented in chapter IV, results of 1D and 2D gel electrophoresis methodologies, showed that the use of ACN and DTT over PDE to deplete HAP or to equalize the concentration of proteins, respectively, performs well and although the number and type of proteins identified are different, the annotation per gene ontology term reveals the same biological paths being affected for patients undergoing PD. Thus, the largest number of proteins lost through peritoneal dialysate belongs to the group of extracellular proteins involved in regulation processes through binding. However, for the searching of biomarkers, DTT seems to be the most promising of the two methods because it acts as an equalizer and it allows to interrogate more proteins in the same sample.

On the other hand, for the study present in chapter VI, the approach used to deal with the HAP was with the Agilent Human 14 Multiple Affinity Removal Column (MARS14) in order to chromatographically remove fourteen interfering HAP. In addition, the high-resolution peptide isoelectric focusing (HiRIEF) technique was novelty applied to PDE samples, allowing a reproducible fractionation and leading to a reduction of PDE sample complexity prior to LC-ESI- Orbitrap MS/MS analysis. This sample treatment approach, effectively expanded the dynamic range of the analysis, and culminated in the result of highest proteome coverage ever achieved for this complex sample. Moreover, a label-free quantitative approach was applied for the first time in the analysis of PDE endogenous peptides, representing the most complete peptidome coverage ever achieved. In addition, the endogenous peptides were analyzed for the prediction of the proteases that might be the origin of these peptides, giving insights about the most active proteases within the peritoneal cavity. Furthermore, this research constitutes the first proteome-based longitudinal study of PD patient cohort. However, there is still work in progress concerning the data analysis. Currently this study represents more an exploratory than a biomarker discovery study but, nevertheless, it has the potential to be applied to a larger stratified cohort of patients and performed in a context of clinical biomarker discovery, allowing to distinguish patients that respond well to therapy from those who are at the highest risk for PD-related complications such as, episodes of peritonitis or ultrafiltration failure.

In summary, the achievements and main remark conclusions of these studies are:

- The potential of PDE as a reservoir of clinical biomarkers that may help to identify patients with a highest risk for PD-related complications, is directly linked to the sample treatment which is crucial to achieve the analysis depth needed for the early detection of peritoneal changes in patients of long-term PD;
- The different methodologies to diminish/remove HAP and protein/peptides fractionation techniques assessed to improve the coverage of the proteome fraction have given a better notion about the PDE

proteome, revealing that the "plasma-like" concept used to describe this proteome is even more complex than previously thought.

- Functional categorization analysis of the PDE proteome showed that the identified proteins are involved in different biological processes such as cellular processes and regulation. The cellular compartment of these proteins are mostly from extracellular, cytoplasm and nucleus, probably originated from PM cell detachment, and concerning the molecular function they are mainly associated with binding and catalytic activity;

- The longitudinal data analysis revealed the most significant enriched pathways in the PD cohort related with metabolic pathways, complement and coagulation cascades, ECM organization, formation of fibrin clot clotting cascade and integrin pathways. This follow-up methodology used in parallel with PET measurements extended our knowledge about the pathophysiological biological processes occurring within the peritoneum;

- Despite the inherent challenges of PDE peptidome analysis, such as the range size of the endogenous peptides, charge state and origin from the activity of an array of often-unknown endogenous proteolytic enzymes, it was possible to identify and generate a list of peptides differentially expressed over time for all the PD patient cohort. The list of peptides was further submitted for protease prediction analysis. Importantly, 73% of the proteases predicted as involved in the generation of the native peptides were identified and quantified in the proteome analysis.

Regardless of the impressive amount of data generated, that will contribute with valuable information for the proteomic and clinical research community in future studies using PDE samples, some work and questions still need to be addressed. Therefore, some of the future perspective are:

- Data mining of the peptidome data, and further link of the longitudinal analysis results obtained for the peptidome, with the proteome longitudinal study, in order to have a more complete information about the occurring processes linked to the membrane evolution.

- Link the changes observed in the P3DEVOATLAS, with other medical variables of the peritoneal membrane and some candidate biomarkers present on PDE, such as, cancer antigen 125, plasminogen activator inhibitor 1, and interleukin 6, etc.

- Final elaboration of the P3DEVOATLAS, with biochemical and medical integration of all data obtained, potentially valuable for clinical diagnosis and prognosis. Elaboration of a panel of levels of proteins and /or peptides to be used and monitored as a quick indicator of the peritoneum status by selected/ multiple reaction monitoring mass spectrometry (SRM/MRM-MS).

ANNEX I. SUPPLEMENTARY INFORMATION FOR CHAPTER VI

Supplementary material

Figures

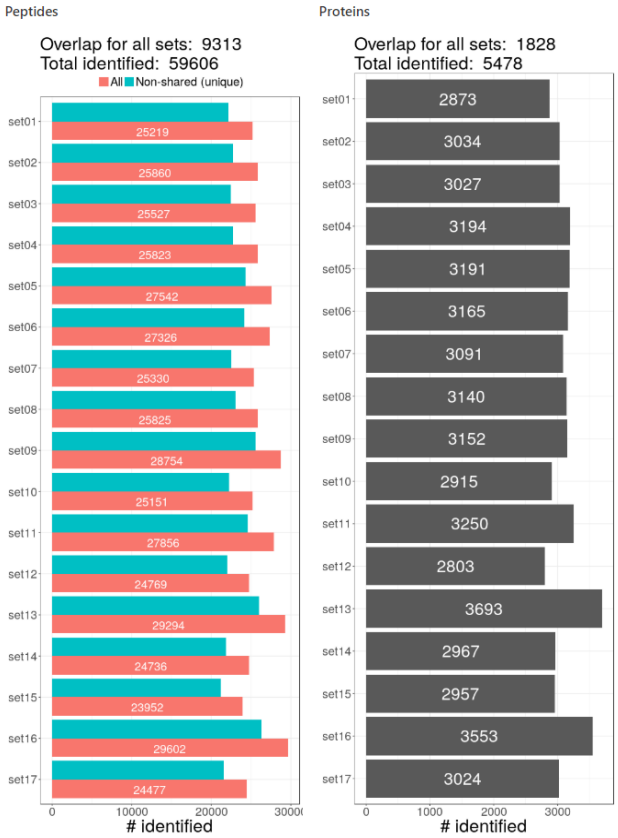

Figure S1- Bar chart representation of the total number/overlap of peptides and proteins identified between sets.

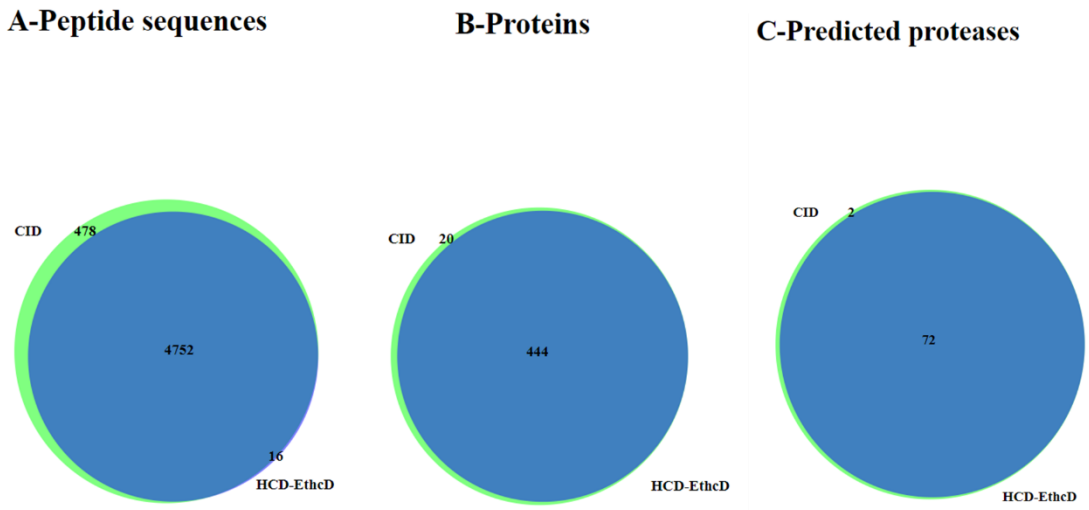

Figure S2-Venn diagrams comparison of the fragmentation techniques (CID and HCD-EthcD) applied for endogenous peptides analysis, with number of peptide sequences and parental proteins identified and proteases predicted.

Tables

Table S1-Enriched pathways (terms) present across the patient's cohort. Each pathway (term), has the frequency, that means the number of times that a pathway appears across the patients cohort, the patients that have that specific term, and the group (relation between the different pathways, if they are related the group number is the same).

Term	Frequency	Patients	Group
NABA_CORE_MATRISOME	27	P02,P03,P05,P06,P07,P09,P10,P11,P23,V02,V04,V14,V15,V16,V17,V19	1
KEGG_COMPLEMENT_AND_COAGULATION_CASCADES	24	P01,P02,P03,P05,P06,P07,P09,P10,P13,P15,P17,P18,P23,V02,V03,V07,V08,V14,V15,V19	2
NABA_ECM_GLYCOPROTEINS	23	P02,P03,P05,P06,P07,P09,P10,P11,P15,P18,P23,V14,V15,V16,V17,V19	1
REACTOME_CELL_CYCLE	22	P01,P02,P03,P05,P07,P11,P17,P21,P23,V02,V03,V04,V08,V16,V17,V19	3
KEGG_GLYCOLYSIS_GLUCONEOGENESIS	22	P01,P02,P03,P05,P07,P09,P10,P11,P13,P17,P23,V03,V08,V14,V16,V17,V18,V19	4
REACTOME_GLUCOSE_METABOLISM	22	P01,P02,P03,P05,P07,P09,P10,P13,P15,P17,P20,P23,V03,V08,V14,V15,V16,V17,V18,V19	4
REACTOME_CELL_CYCLE_MITOTIC	21	P01,P02,P03,P05,P07,P09,P11,P17,P23,V02,V03,V04,V08,V16,V17,V19	3
REACTOME_FORMATION_OF_FIBRIN_CLOT_CLOTTING_CASCADE	21	P01,P02,P03,P05,P06,P07,P09,P10,P13,P17,P18,P23,V02,V03,V07,V08,V14,V15,V19	5
REACTOME_METABOLISM_OF_RNA	21	P01,P02,P03,P04,P05,P07,P10,P11,P13,P18,P21,V02,V03,V04,V08,V16,V17,V19	6
PID_ERBB1_DOWNSTREAM_PATHWAY	21	P01,P02,P03,P05,P06,P07,P11,P20,P23,V02,V04,V08,V14,V16,V19	7
PID_INTEGRIN1_PATHWAY	20	P01,P02,P05,P06,P07,P10,P11,P15,P18,P21,V07,V08,V14,V15,V17,V18	8
REACTOME_METABOLISM_OF_MRNA	20	P01,P02,P03,P04,P05,P07,P10,P11,P13,P18,V02,V03,V04,V08,V16,V17,V19	6
BIOCARTA_MPR_PATHWAY	20	P02,P03,P04,P05,P06,P07,P09,P10,P11,P18,P20,P23,V04,V08,V14,V15,V16,V18,V19	9
BIOCARTA_CDC42RAC_PATHWAY	19	P02,P03,P04,P05,P06,P07,P09,P10,P11,P18,P20,P23,V04,V08,V14,V15,V16,V18,V19	9
PID_PDGFRB_PATHWAY	19	P02,P03,P05,P06,P07,P09,P11,P20,P23,V08,V14,V16,V17,V19	7
REACTOME_MRNA_PROCESSING	19	P02,P03,P04,P05,P07,P13,P17,P18,P20,P21,V03,V04,V08,V15,V19	10
REACTOME_MRNA_SPLICING	19	P02,P03,P04,P05,P07,P13,P17,P18,P20,P21,V04,V08,V15,V19	10
REACTOME_PROCESSING_OF_CAPPED_INTRON_CONTAINING_PRE_MRNA	19	P02,P03,P04,P05,P07,P13,P17,P18,P20,P21,V03,V04,V08,V15,V19	10
PID_NFAT_3PATHWAY	18	P01,P02,P03,P05,P06,P07,P11,P17,P20,P23,V02,V03,V08,V16,V17,V19	11
REACTOME_PROTEIN_FOLDING	18	P01,P02,P03,P04,P05,P07,P09,P11,P17,P21,P23,V03,V04,V08,V16,V17,V19	12
BIOCARTA_INTRINSIC_PATHWAY	18	P01,P02,P04,P05,P07,P09,P10,P13,P18,P23,V02,V03,V07,V08,V14,V15,V19	5
BIOCARTA_CHREBP2_PATHWAY	17	P01,P02,P03,P05,P06,P07,P17,P18,P20,P23,V02,V03,V08,V16,V17,V19	11
REACTOME_GLYCOLYSIS	17	P01,P02,P03,P05,P07,P09,P10,P13,P15,P17,V08,V14,V16,V17,V18,V19	4

REACTOME_PHASE_II_CONJUGATION	17	P01,P02,P03,P07,P10,P11,P15,V04,V08,V14,V15,V16,V17,V18,V19	13
BIOCARTA_CLASSIC_PATHWAY	17	P01,P03,P05,P06,P07,P09,P10,P15,P17,P18,P23,V07,V08,V14,V16,V19	2
KEGG_CELL_CYCLE	17	P01,P02,P03,P05,P06,P07,P11,P17,P18,P20,V02,V03,V08,V16,V17,V19	11
REACTOME_EXTRACELLULAR_MATRIX_ORGANIZATION	17	P02,P03,P05,P07,P10,P11,P17,V04,V08,V15,V16,V17,V18,V19	14
REACTOME_METABOLISM_OF_PROTEINS	16	P01,P03,P07,P11,P13,V02,V03,V04,V08,V17,V19	6
REACTOME_TRANSLATION	16	P01,P02,P03,P04,P05,P07,P10,P11,P13,P15,V03,V04,V08,V19	6
KEGG_ECM_RECEPTOR_INTERACTION	16	P01,P02,P05,P06,P07,P10,P11,P15,V07,V08,V15,V16,V17	8
REACTOME_BIOLOGICAL_OXIDATIONS	16	P01,P02,P03,P07,P10,P11,P15,V04,V07,V14,V15,V16,V18,V19	13
REACTOME_GLUCONEOGENESIS	16	P01,P02,P03,P05,P07,P09,P10,P13,P17,P20,V03,V08,V14,V17,V18,V19	4
NABA_ECM_REGULATORS	16	P01,P02,P03,P05,P07,P10,P11,P15,V04,V14,V15,V17,V19	15
REACTOME_COMPLEMENT_CASCADE	16	P01,P03,P05,P06,P07,P09,P10,P15,P17,P18,V07,V08,V15,V19	2
REACTOME_INFLUENZA_LIFE_CYCLE	16	P01,P02,P03,P04,P05,P11,P15,P18,V03,V04,V08,V16,V17,V19	6
PID_CDC42_PATHWAY	16	P02,P03,P04,P05,P06,P07,P09,P11,P18,P20,V08,V14,V15,V16,V18,V19	9
PID_RAC1_PATHWAY	16	P02,P03,P04,P05,P06,P07,P11,P18,P20,P23,V08,V14,V15,V16,V18,V19	9
PID_FOXO_PATHWAY	16	P02,P03,P05,P06,P07,P11,P15,P17,P18,P20,V02,V03,V08,V16,V17,V19	11
SIG_INSULIN_RECEPTOR_PATHWAY_IN_CARDIAC_MYOCYTES	16	P02,P03,P05,P06,P07,P11,P15,P17,P20,V02,V03,V08,V14,V16,V17,V19	11
ST_PHOSPHOINOSITIDE_3_KINASE_PATHWAY	16	P02,P03,P05,P06,P07,P15,P17,P18,P20,V02,V03,V08,V16,V17,V18,V19	11
REACTOME_3_UTR_MEDIATED_TRANSLATIONAL_REGULATION	15	P01,P02,P03,P04,P07,P10,P11,P15,P18,P20,V03,V04,V08,V19	6
REACTOME_MITOTIC_G2_G2_M_PHASES	15	P01,P02,P03,P05,P07,P11,P17,P23,V02,V03,V08,V16	16
KEGG_CITRATE_CYCLE_TCA_CYCLE	15	P01,P02,P03,P05,P07,P17,P23,V08,V15,V16,V17,V18,V19	17
KEGG_FRUCTOSE_AND_MANNOSE_METABOLISM	15	P01,P02,P03,P05,P07,P10,P17,P23,V08,V14,V15,V16,V17	4
KEGG_PYRUVATE_METABOLISM	15	P01,P02,P03,P05,P07,P10,P11,P13,P23,V14,V16,V17,V18,V19	18
REACTOME_CYTOSOLIC_TRNA_AMINOACYLATION	15	P01,P02,P03,P05,P07,P11,P17,P23,V08,V14,V16,V19	19
REACTOME_PYRUVATE_METABOLISM_AND_CITRIC_ACID_TCA_CYCLE	15	P01,P02,P03,P05,P11,P23,V04,V14,V15,V16,V17,V18,V19	17
REACTOME_TCA_CYCLE_AND_RESPIRATORY_ELECTRON_TRANSPORT	15	P01,P02,P03,P05,P07,P23,V04,V14,V15,V16,V17,V18,V19	20
REACTOME_INTRINSIC_PATHWAY	15	P01,P07,P10,P17,P18,P23,V02,V03,V07,V08,V14,V15,V16,V19	5
REACTOME_PLATELET_AGGREGATION_PLUG_FORMATION	15	P01,P02,P03,P06,P07,P09,P17,P20,P23,V03,V14,V15,V16,V18	21
BIOCARTA_RHO_PATHWAY	15	P02,P03,P04,P05,P07,P11,P20,P23,V04,V08,V14,V15,V16,V18,V19	9
KEGG_FC_GAMMA_R_MEDIATED_PHAGOCYTOSIS	15	P02,P03,P05,P06,P07,P10,P18,V04,V08,V14,V15,V16,V18,V19	7

KEGG_SPLICEOSOME	15	P02,P03,P04,P05,P06,P07,P13,P17,P21,V04,V08,V15,V19	10
PID_LKB1_PATHWAY	15	P02,P03,P05,P06,P07,P11,P17,P18,P20,V02,V03,V08,V16,V17,V19	11
REACTOME_METABOLISM_OF_AMINO_ACIDS_AND_DERIVATIVES	15	P02,P03,P05,P07,P09,P10,P13,P21,V08,V14,V16,V17,V18,V19	3
SIG_PIP3_SIGNALING_IN_CARDIAC_MYOCTES	15	P02,P03,P05,P06,P07,P15,P17,P18,P20,V02,V03,V08,V16,V17,V19	11
REACTOME_HIV_INFECTION	14	P01,P02,P05,P11,P17,P21,P23,V02,V03,V04,V08,V16,V17	3
REACTOME_LOSS_OF_NLP_FROM_MITOTIC_CENTROSOMES	14	P01,P02,P03,P05,P07,P11,P17,P23,V02,V03,V08,V16	16
REACTOME_RECRUITMENT_OF_MITOTIC_CENTROSOME_PROTEINS_AND_COMPLEXES	14	P01,P02,P03,P05,P07,P11,P17,P23,V02,V03,V08,V16	16
REACTOME_TRNA_AMINOACYLATION	14	P01,P02,P03,P05,P07,P11,P23,V08,V14,V16,V19	19
BIOCARTA_EXTRINSIC_PATHWAY	14	P01,P02,P03,P04,P05,P07,P09,P23,V02,V03,V07,V15,V17,V19	5
REACTOME_G1_S_TRANSITION	14	P01,P02,P03,P05,P07,P09,P21,V02,V03,V04,V08,V16,V17,V19	3
REACTOME_MITOTIC_G1_G1_S_PHASES	14	P01,P02,P03,P05,P07,P09,P21,V02,V03,V04,V08,V16,V17,V19	3
REACTOME_REGULATION_OF_MRNA_STABILITY_BY_PROTEINS_THAT_BIND_AU_RICH_ELEMENTS	14	P01,P02,P05,P07,P09,P11,V02,V04,V08,V16,V17,V19	3
REACTOME_METABOLISM_OF_NUCLEOTIDES	14	P02,P03,P05,P07,P15,V04,V08,V14,V15,V16,V17,V18,V19	22
REACTOME_PEPTIDE_CHAIN_ELONGATION	14	P02,P03,P04,P05,P07,P11,P15,P18,V03,V04,V08,V14,V19	6
PID_A6B1_A6B4_INTEGRIN_PATHWAY	13	P01,P07,P10,P17,P18,P20,V02,V08,V15,V17	23
REACTOME_PREFOLDIN_MEDIATED_TRANSFER_OF_SUBSTRATE_TO_CCT_TRIC	13	P01,P02,P03,P04,P23,V03,V04,V14,V16,V17,V19	12
KEGG_PENTOSE_PHOSPHATE_PATHWAY	13	P01,P02,P03,P05,P06,P07,P13,V08,V14,V16,V17,V18,V19	4
BIOCARTA_COMP_PATHWAY	13	P01,P03,P05,P06,P07,P10,P15,P18,P23,V07,V08,V19	2
BIOCARTA_AMI_PATHWAY	13	P01,P02,P03,P04,P05,P06,P07,P09,P23,V02,V03,V07,V15	5
REACTOME_COMMON_PATHWAY	13	P01,P02,P03,P04,P05,P06,P09,P23,V02,V03,V07,V15,V19	5
REACTOME_NONSENSE_MEDIATED_DECAY_ENHANCED_BY_THE_EXON_JUNCTION_COMPLEX	13	P01,P02,P03,P04,P05,P07,P11,P15,P18,V04,V08,V19	6
REACTOME_S_PHASE	13	P01,P02,P05,P07,P09,P21,V02,V03,V04,V08,V16,V17,V19	3
KEGG_AMINOACYL_TRNA_BIOSYNTHESIS	13	P02,P03,P05,P07,P17,P23,V08,V14,V16,V19	19
KEGG_RIBOSOME	13	P02,P03,P04,P05,P07,P11,P15,P18,V03,V04,V08,V19	6
PID_BETA_CATENIN_NUC_PATHWAY	13	P02,P03,P05,P06,P07,P11,P15,P20,V03,V08,V16,V17,V19	11
PID_INSULIN_GLUCOSE_PATHWAY	13	P02,P03,P05,P06,P07,P11,P17,P18,P20,V02,V16,V17,V19	11
NABA_COLLAGENS	13	P02,P03,P05,P07,P10,P11,P21,V08,V15,V16,V17,V19	14
PID_SYNDECAN_1_PATHWAY	13	P02,P03,P05,P07,P10,P11,P15,V03,V04,V08,V15,V16,V17	14

REACTOME_COLLAGEN_FORMATION	13	P02,P03,P05,P07,P10,P11,V08,V15,V16,V17,V19	14
BIOCARTA_LECTIN_PATHWAY	12	P01,P03,P06,P07,P10,P15,P17,P23,V07,V08,V19	2
REACTOME_ACTIVATION_OF_NF_KAPPAB_IN_B_CELLS	12	P01,P02,P05,P07,P09,P21,V02,V04,V08,V16,V17,V19	3
REACTOME_ANTIGEN_PROCESSING_UBIQUITINATION_PROTEASOME_DEGRADATION	12	P01,P02,P05,P07,P21,V02,V04,V08,V14,V16,V19	3
REACTOME_CYCLIN_E_ASSOCIATED_EVENTS_DURING_G1_S_TRANSITION_	12	P01,P02,P05,P07,P09,P21,V02,V04,V08,V16,V17,V19	3
REACTOME_DNA_REPLICATION	12	P01,P02,P03,P05,P07,V02,V03,V04,V08,V16,V17	3
REACTOME_DOWNSTREAM_SIGNALING_EVENTS_OF_B_CELL_RECEPTOR_BCR	12	P01,P02,P05,P07,P09,P21,V02,V04,V08,V16,V17,V19	3
REACTOME_HOST_INTERACTIONS_OF_HIV_FACTORS	12	P01,P02,P05,P09,P21,P23,V02,V03,V04,V08,V16,V17	3
REACTOME_REGULATION_OF_MITOTIC_CELL_CYCLE	12	P01,P02,P05,P07,P09,P21,V02,V04,V08,V16,V17,V19	3
REACTOME_SCF_BETA_TRCP_MEDIATED_DEGRADATION_OF_EMI1	12	P01,P02,P05,P07,P09,P21,V02,V04,V08,V16,V17,V19	3
REACTOME_SCFSKP2_MEDIATED_DEGRADATION_OF_P27_P21	12	P01,P02,P05,P07,P09,P21,V02,V04,V08,V16,V17,V19	3
REACTOME_SIGNALING_BY_WNT	12	P01,P02,P05,P07,P09,P21,V02,V04,V08,V16,V17,V19	3
REACTOME_SYNTHESIS_OF_DNA	12	P01,P02,P05,P07,P09,P21,V02,V03,V04,V08,V16,V17	3
REACTOME_INFLUENZA_VIRAL_RNA_TRANSCRIPTION_AND_REPLICATION	12	P03,P04,P05,P07,P11,P15,P18,V04,V08,V17,V19	6
KEGG_OOCYTE_MEIOSIS	11	P01,P02,P03,P05,P06,P07,P18,P20,V03,V08,V19	24
KEGG_CYSTEINE_AND_METHIONINE_METABOLISM	11	P01,P02,P07,P10,V04,V08,V16,V17,V18,V19	25
BIOCARTA_ACTINY_PATHWAY	11	P02,P04,P05,P06,P09,P20,V04,V08,V15,V16	9
KEGG_PATHOGENIC_ESCHERICHIA_COLI_INFECTION	11	P02,P03,P05,P06,P07,P10,P11,V14,V16,V19	26
REACTOME_INTEGRIN_ALPHAIIB_BETA3_SIGNALING	11	P02,P03,P07,P09,P20,P23,V03,V14,V16,V19	21
PID_MTOR_4PATHWAY	11	P02,P03,P05,P06,P07,P20,V02,V08,V16,V17,V19	11
REACTOME_MITOTIC_M_M_G1_PHASES	11	P02,P03,P05,P07,P09,V02,V03,V04,V08,V16,V17	3
REACTOME_REGULATION_OF_APOPTOSIS	11	P02,P05,P07,P09,P10,P21,V02,V03,V04,V08,V17	3
REACTOME_NCAM1_INTERACTIONS	11	P02,P03,P05,P07,P10,P11,P15,V08,V15,V16,V17	14
REACTOME_SRP_DEPENDENT_COTRANSLATIONAL_PROTEIN_TARGETING_TO_MEMBRANE	11	P03,P04,P05,P07,P11,P15,P18,V04,V08,V19	6
KEGG_FOCAL_ADHESION	10	P01,P02,P05,P07,P10,P21,V02,V15,V17	8
KEGG_GLUTATHIONE_METABOLISM	10	P01,P03,P05,P07,P09,P10,V16,V17,V18,V19	13
REACTOME_METABOLISM_OF_CARBOHYDRATES	10	P01,P05,P07,P10,P15,P17,V08,V14,V17,V18	27
KEGG_SYSTEMIC_LUPUS_ERYTHEMATOSUS	10	P01,P03,P06,P07,P10,P17,P23,V07,V16,V19	2

REACTOME_INNATE_IMMUNE_SYSTEM	10	P01,P05,P06,P09,P10,P18,V07,V08,V15,V16	28
REACTOME_CLASS_I_MHC_MEDIATED_ANTIGEN_PROCESSING_PRESENTATION	10	P01,P02,P05,P07,P11,P21,V04,V08,V16,V19	3
REACTOME_ER_PHAGOSOME_PATHWAY	10	P01,P02,P05,P07,P09,P21,V02,V04,V08,V17	3
KEGG_PURINE_METABOLISM	10	P02,P03,P05,P07,P11,P15,V08,V16,V18,V19	22
REACTOME_GLYCOSAMINOGLYCAN_METABOLISM	10	P02,P07,P10,P11,P20,V15,V16,V17,V18,V19	27
KEGG_SMALL_CELL_LUNG_CANCER	10	P05,P07,P09,P10,V08,V14,V15,V17,V18	23
PID_AVB3_INTEGRIN_PATHWAY	9	P01,P02,P03,P10,P11,V08,V15,V16,V17	14
PID_INTEGRIN3_PATHWAY	9	P01,P05,P07,P23,V03,V15,V16,V17	8
REACTOME_APOPTOSIS	9	P01,P02,P05,P07,P17,P23,V04,V08	3
KEGG_AMINO_SUGAR_AND_NUCLEOTIDE_SUGAR_METABOLISM	9	P01,P02,P03,P05,P07,P10,P17,V04,V18	29
KEGG_ARGININE_AND_PROLINE_METABOLISM	9	P01,P05,P07,P20,V03,V16,V17,V18,V19	30
KEGG_DRUG_METABOLISM_CYTOCHROME_P450	9	P01,P03,P07,P23,V04,V14,V17,V18,V19	13
REACTOME_PTM_GAMMA_CARBOXYLATION_HYPUSINE_FORMATION_AND_ARYLSULFATASE_ACTIVATION	9	P01,P03,P04,P05,P07,P23,V02,V03,V17	31
REACTOME_APC_C_CDC20_MEDIATED_DEGRADATION_OF_MITOTIC_PROTEINS	9	P02,P05,P09,P21,V02,V04,V08,V16,V17	3
REACTOME_APC_C_CDH1_MEDIATED_DEGRADATION_OF_CDC20_AND_OTHER_APC_C_CDH1_TARGETED_PROTEINS_IN_LATE_MITOSIS_EARLY_G1	9	P02,P05,P09,P21,V02,V04,V08,V16,V17	3
REACTOME_ASSEMBLY_OF_THE_PRE_REPLICATIVE_COMPLEX	9	P02,P05,P09,P21,V02,V04,V08,V16,V17	3
REACTOME_AUTODEGRADATION_OF_CDH1_BY_CDH1_APC_C	9	P02,P05,P09,P21,V02,V04,V08,V16,V17	3
REACTOME_AUTODEGRADATION_OF_THE_E3_UBIQUITIN_LIGASE_COP1	9	P02,P05,P09,P21,V02,V04,V08,V16,V17	3
REACTOME_CDK_MEDIATED_PHOSPHORYLATION_AND_REMOVAL_OF_CDC6	9	P02,P05,P09,P21,V02,V04,V08,V16,V17	3
REACTOME_CDT1_ASSOCIATION_WITH_THE_CDC6_ORC_ORIGIN_COMPLEX	9	P02,P05,P09,P21,V02,V04,V08,V16,V17	3
REACTOME_ORC1_REMOVAL_FROM_CHROMATIN	9	P02,P05,P09,P21,V02,V04,V08,V16,V17	3
REACTOME_P53_DEPENDENT_G1_DNA_DAMAGE_RESPONSE	9	P02,P05,P09,P21,V02,V04,V08,V16,V17	3
REACTOME_P53_INDEPENDENT_G1_S_DNA_DAMAGE_CHECKPOINT	9	P02,P05,P09,P21,V02,V04,V08,V16,V17	3
REACTOME_PURINE_METABOLISM	9	P02,P05,P07,P09,P15,V08,V14,V16,V18	22
REACTOME_SIGNALING_BY_THE_B_CELL_RECEPTOR_BCR	9	P02,P07,P09,P21,V02,V04,V08,V16,V17	3
REACTOME_SULFUR_AMINO_ACID_METABOLISM	9	P02,P03,P07,P09,P10,V04,V14,V17,V18	25
REACTOME_VIF_MEDIATED_DEGRADATION_OF_APOBEC3G	9	P02,P05,P09,P21,V02,V04,V08,V16,V17	3
REACTOME_SIGNALING_BY_PDGF	9	P02,P03,P07,P10,P11,P15,V08,V15,V18	32

REACTOME_HEMOSTASIS	9	P03,P07,P09,P10,P23,V03,V14,V15	33
REACTOME_MUSCLE_CONTRACTION	9	P10,P11,P15,P17,P21,V08,V16,V17,V19	34
REACTOME_ACTIVATION_OF_THE_MRNA_UPON_BINDING_OF_THE_CAP_BINDING_COMPLEX_AND_EIFS_AND_SUBSEQUENT_BINDING_TO_43S	8	P01,P03,P10,P11,P15,V04,V19	6
KEGG_APOPTOSIS	8	P01,P02,P03,P05,P07,P10,P11,V18	35
PID_TELOMERASE_PATHWAY	8	P01,P02,P05,P11,V14,V16,V17	36
SIG_CHEMOTAXIS	8	P01,P02,P07,P11,V08,V14,V16,V19	37
KEGG_METABOLISM_OF_XENOBIOTICS_BY_CYTOCHROME_P450	8	P01,P03,P07,P21,V04,V14,V17,V19	13
BIOCARTA_FIBRINOLYSIS_PATHWAY	8	P01,P02,P07,P09,P23,V15,V16,V19	5
REACTOME_POST_TRANSLATIONAL_PROTEIN_MODIFICATION	8	P01,P03,P05,P07,P23,V02,V17	38
KEGG_UBIQUITIN_MEDIATED_PROTEOLYSIS	8	P02,P21,V04,V14,V16,V18,V19	39
PID_GMCSF_PATHWAY	8	P02,P05,P07,P10,P20,V14,V16	40
SIG_REGULATION_OF_THE_ACTIN_CYTOSKELETON_BY_RHO_GTPASES	8	P02,P05,P07,P11,V03,V08,V14,V19	37
BIOCARTA_UCALPAIN_PATHWAY	8	P02,P03,P05,P18,V07,V16,V17,V19	41
PID_CASPASE_PATHWAY	8	P02,P03,P05,P07,P23,V08,V19	42
REACTOME_CELL_CYCLE_CHECKPOINTS	8	P02,P05,P09,P21,V02,V04,V08,V17	3
REACTOME_CROSS_PRESENTATION_OF_SOLUBLE_EXOGENOUS_ANTIGENS_ENDOSOMES	8	P02,P07,P21,V02,V04,V08,V16,V17	3
REACTOME_DESTABILIZATION_OF_MRNA_BY_AUF1_HNRNP_D0	8	P02,P05,P07,P09,V02,V04,V08,V19	3
REACTOME_M_G1_TRANSITION	8	P02,P05,P09,P21,V02,V04,V08,V17	3
REACTOME_REGULATION_OF_ORNITHINE_DECARBOXYLASE_ODC	8	P02,P05,P21,V02,V04,V08,V16,V17	3
PID_INTEGRIN2_PATHWAY	8	P02,P04,P05,P09,P10,V03,V07,V15	43
PID_UPA_UPAR_PATHWAY	8	P02,P03,P04,P09,P18,P23,V15,V19	44
KEGG_LYSOSOME	8	P02,P05,P07,P10,V04,V15,V17,V19	45
NABA_BASEMENT_MEMBRANES	8	P07,P09,P10,P11,V14,V15,V18	23
REACTOME_A_TETRASACCHARIDE_LINKER_SEQUENCE_IS_REQUIRED_FOR_GAG_SYNTHESIS	7	P01,P09,P10,V03,V16,V19	27
REACTOME_AXON_GUIDANCE	7	P01,P02,P07,V17,V18	46
REACTOME_DEVELOPMENTAL_BIOLOGY	7	P01,P02,P07,P17,V17,V18	46
REACTOME_HEPARAN_SULFATE_HEPARIN_HS_GAG_METABOLISM	7	P01,P05,P10,V15,V16,V17,V19	27
REACTOME_NGF_SIGNALLING_VIA_TRKA_FROM_THE_PLASMA_MEMBRANE	7	P01,P02,P05,P07,V14,V16,V18	32

KEGG_STARCH_AND_SUCROSE_METABOLISM	7	P01,P03,P05,P07,P17,V15,V19	47
BIOCARTA_LAIR_PATHWAY	7	P01,P06,P07,P10,V07,V15,V16	43
PID_MYC_ACTIV_PATHWAY	7	P01,P02,P03,P05,P11,V14,V19	48
KEGG_NEUROTROPHIN_SIGNALING_PATHWAY	7	P02,P05,P07,P18,V03,V08	49
PID_ERBB1_RECEPTOR_PROXIMAL_PATHWAY	7	P02,P05,P07,P10,V14,V16,V18	49
REACTOME_ANTIVIRAL_MECHANISM_BY_IFN_STIMULATED_GENES	7	P02,P05,P10,V02,V04,V16,V18	50
BIOCARTA_HIVNEF_PATHWAY	7	P02,P05,P07,P11,P23,V08	42
BIOCARTA_MCALPAIN_PATHWAY	7	P02,P05,P10,P11,V16,V17,V19	41
REACTOME_NCAM_SIGNALING_FOR_NEURITE_OUT_GROWTH	7	P02,P03,P07,P11,V08,V15,V17	14
REACTOME_FORMATION_OF_THE_TERNARY_COMPLEX_AND_SUBSEQUENTLY_THE_43S_COMPLEX	7	P03,P05,P15,P20,V03,V16,V19	6
REACTOME_CHYLOMICRON_MEDIATED_LIPID_TRANSPORT	7	P07,P09,P10,V14,V15,V17,V19	51
KEGG_CYTOKINE_CYTOKINE_RECEPTOR_INTERACTION	6	P01,P03,P18,V14,V16,V19	52
KEGG_T_CELL_RECEPTOR_SIGNALING_PATHWAY	6	P01,P02,P05,P10,V14,V18	53
REACTOME_SIGNALING_BY_INSULIN_RECEPTOR	6	P01,P03,P05,P17,V14,V19	54
ST_INTEGRIN_SIGNALING_PATHWAY	6	P01,P02,P11,P23,V15,V16	37
KEGG_TYROSINE_METABOLISM	6	P01,P03,V16,V17,V18	55
REACTOME_GLUTATHIONE_CONJUGATION	6	P01,P02,P07,P09,P10,V18	13
REACTOME_INITIAL_TRIGGERING_OF_COMPLEMENT	6	P01,P05,P07,P10,P18,V07	2
REACTOME_REGULATION_OF_COMPLEMENT_CASCADE	6	P01,P06,P10,V02,V15,V19	2
REACTOME_O_LINKED_GLYCOSYLATION_OF_MUCINS	6	P01,P03,P05,P07,V15,V19	56
REACTOME_SIGNALING_BY_ILS	6	P01,P02,P05,P15,P20,V16	40
REACTOME_GPCR_DOWNSTREAM_SIGNALING	6	P01,P10,P15,V04,V19	57
REACTOME_ADAPTIVE_IMMUNE_SYSTEM	6	P02,P21,V03,V08,V16	58
REACTOME_IMMUNE_SYSTEM	6	P02,P05,P07,V02,V07,V16	58
KEGG_VALINE_LEUCINE_AND_ISOLEUCINE_DEGRADATION	6	P02,P05,P10,P15,P23,V19	18
PID_AR_PATHWAY	6	P02,P05,V08,V14,V16,V19	59
PID_CERAMIDE_PATHWAY	6	P02,P03,P05,V14,V16	60
PID_ENDOTHELIN_PATHWAY	6	P02,P05,P07,V04,V18,V19	61
PID_LIS1_PATHWAY	6	P02,P07,V02,V03,V17	62

PID_VEGFR1_2_PATHWAY	6	P02,P05,V14,V16,V17,V18	63
REACTOME_ANTIGEN_PROCESSING_CROSS_PRESENTATION	6	P02,P07,P21,V04,V08,V17	3
REACTOME_SIGNALING_BY_ERBB2	6	P02,P05,P07,P09,V14,V18	32
REACTOME_SIGNALLING_BY_NGF	6	P02,P05,P07,P10,V16,V19	32
REACTOME_GLYCOSPHINGOLIPID_METABOLISM	6	P02,P11,P23,V04,V15,V17	64
REACTOME_SPHINGOLIPID_METABOLISM	6	P02,P07,P11,P23,V04,V17	64
KEGG_TRYPTOPHAN_METABOLISM	6	P05,P10,P13,P15,P20,V18	18
KEGG_TGF_BETA_SIGNALING_PATHWAY	6	P05,P10,P17,P23,V07,V19	65
REACTOME_STRIATED_MUSCLE_CONTRACTION	6	P06,P11,P15,P21,V16,V19	34
REACTOME_PLATELET_ACTIVATION_SIGNALING_AND_AGGREGATION	6	P07,P10,P23,V03,V15	33
REACTOME_RESPONSE_TO_ELEVATED_PLATELET_CYTOSOLIC_CA2_	6	P07,P10,P23,V03,V15	33
KEGG_DILATED_CARDIOMYOPATHY	6	P07,P11,V15,V16,V17,V19	66
REACTOME_LIPID_DIGESTION_MOBILIZATION_AND_TRANSPORT	6	P07,P23,V14,V15,V17,V19	51
REACTOME_LIPOPROTEIN_METABOLISM	6	P07,P10,V14,V15,V17,V19	51
REACTOME_G_ALPHA_S_SIGNALLING_EVENTS	6	P10,P15,P21,P23,V04,V19	67
REACTOME_DOWNSTREAM_SIGNAL_TRANSDUCTION	5	P01,P02,P05,P07,V18	32
BIOCARTA_MET_PATHWAY	5	P01,P02,P07,V14,V16	49
KEGG_INSULIN_SIGNALING_PATHWAY	5	P01,P02,P05,P07,P09	68
PID_MET_PATHWAY	5	P01,P02,P05,V14,V18	49
REACTOME_APOPTOTIC_EXECUTION_PHASE	5	P01,P07,P17,P23,V08	42
KEGG_ALANINE_ASPARTATE_AND_GLUTAMATE_METABOLISM	5	P01,P02,P05,V17,V18	30
KEGG_PRION_DISEASES	5	P01,P07,P10,P18,V07	69
KEGG_ANTIGEN_PROCESSING_AND_PRESENTATION	5	P01,P07,P21,V17,V19	70
REACTOME_UNFOLDED_PROTEIN_RESPONSE	5	P01,P07,P11,P17,V17	71
BIOCARTA_INTEGRIN_PATHWAY	5	P02,P05,P07,V03,V16	41
KEGG_PROPANOATE_METABOLISM	5	P02,P05,P07,P15,V18	18
KEGG_PYRIMIDINE_METABOLISM	5	P02,P03,P05,P07,V19	22
KEGG_VASCULAR_SMOOTH_MUSCLE_CONTRACTION	5	P02,P05,P10,V03,V19	24
REACTOME_SIGNALING_BY_EGFR_IN_CANCER	5	P02,P05,V14,V16,V18	32

REACTOME_SYNTHESIS_AND_INTERCONVERSION_OF_NUCLEOTIDE_DI_AND_TRIP HOSPHATES	5	P02,P03,P05,P07,V17	72
KEGG_CARDIAC_MUSCLE_CONTRACTION	5	P02,P11,P23,V16,V19	73
NABA_ECM_AFFILIATED	5	P02,P11,P15,V15	74
REACTOME_TRANSMEMBRANE_TRANSPORT_OF_SMALL_MOLECULES	5	P03,P05,P07,V03,V14	75
KEGG_REGULATION_OF_ACTIN_CYTOSKELETON	5	P05,P06,V14,V16,V19	76
PID_INTEGRIN_A4B1_PATHWAY	5	P05,P07,P10,V16,V17	77
NABA_PROTEOGLYCANS	5	P05,P17,V04,V14,V17	78
REACTOME_REGULATION_OF_INSULIN_LIKE_GROWTH_FACTOR_IGF_ACTIVITY_B Y_INSULIN_LIKE_GROWTH_FACTOR_BINDING_PROTEINS_IGFBPS	5	P06,P10,P21,P23,V16	79
REACTOME_INTEGRIN_CELL_SURFACE_INTERACTIONS	5	P07,P09,P15,P23,V15	8
KEGG_HYPERTROPHIC_CARDIOMYOPATHY_HCM	5	P11,V15,V16,V17,V19	66
KEGG_CELL_ADHESION_MOLECULES_CAMS	4	P01,P06,P07,P23	80
KEGG_PATHWAYS_IN_CANCER	4	P01,P09,P23	81
REACTOME_SIGNAL_TRANSDUCTION_BY_L1	4	P01,P02,P06,V18	82
KEGG_ERBB_SIGNALING_PATHWAY	4	P01,P02,V14,V18	32
KEGG_O_GLYCAN_BIOSYNTHESIS	4	P01,P02,P07,V19	56
KEGG_N_GLYCAN_BIOSYNTHESIS	4	P01,P17,P23,V19	38
BIOCARTA_BIOPEPTIDES_PATHWAY	4	P01,P02,P05,P23	40
PID_IL6_7_PATHWAY	4	P01,P05,P07,V15	83
PID_REG_GR_PATHWAY	4	P01,P02,P06,P20	84
REACTOME_DIABETES_PATHWAYS	4	P01,P17,P23,V17	71
REACTOME_GPCR_LIGAND_BINDING	4	P01,P10,P15,V19	57
KEGG_EPITHELIAL_CELL_SIGNALING_IN_HELICOBACTER_PYLORI_INFECTION	4	P02,P09,V03,V16	85
KEGG_LEUKOCYTE_TRANSENDOTHELIAL_MIGRATION	4	P02,P05,P15,V19	86
KEGG_VIBRIO_CHOLERAE_INFECTION	4	P02,P17,P18,V14	85
REACTOME_INTERFERON_SIGNALING	4	P02,P05,P10,V02	50
REACTOME_SIGNALING_BY_RHO_GTPASES	4	P02,P07,V16,V19	87
REACTOME_SIGNALING_BY_SCF_KIT	4	P02,P05,P07,V16	40
KEGG_ADHERENS_JUNCTION	4	P02,P05,V14,V16	88

KEGG_COLORECTAL_CANCER	4	P02,P05,V15,V19	81
KEGG_GALACTOSE_METABOLISM	4	P02,P05,P10,V14	47
PID_FAK_PATHWAY	4	P02,P05,P07,V17	49
REACTOME_MYD88_MAL_CASCADE_INITIATED_ON_PLASMA_MEMBRANE	4	P02,P05,P10,P17	28
REACTOME_NFKB_AND_MAP_KINASES_ACTIVATION_MEDIATED_BY_TLR4_SIGNALING_REPERTOIRE	4	P02,P05,P10,P17	28
REACTOME_RECYCLING_PATHWAY_OF_L1	4	P02,P05,V02,V19	82
REACTOME_TRAF6_MEDIATED_INDUCTION_OF_NFKB_AND_MAP_KINASES_UPON_TLR7_8_OR_9_ACTIVATION	4	P02,P05,P10,P17	28
REACTOME_DEGRADATION_OF_THE_EXTRACELLULAR_MATRIX	4	P02,P03,P17,V19	89
REACTOME_HDL_MEDIATED_LIPID_TRANSPORT	4	P02,P07,P18,V14	51
REACTOME_METABOLISM_OF_LIPIDS_AND_LIPOPROTEINS	4	P02,P07,P11,V18	90
REACTOME_PHOSPHOLIPID_METABOLISM	4	P02,P11,P23,V16	64
REACTOME_AMYLOIDS	4	P02,P07,P09,V03	91
REACTOME_ACTIVATION_OF_CHAPERONE_GENES_BY_XBP1S	4	P04,P07,P23,V17	71
BIOCARTA_NFAT_PATHWAY	4	P05,P23,V18,V19	92
REACTOME_DOWNSTREAM_SIGNALING_OF_ACTIVATED_FGFR	4	P05,P07,V14,V18	32
PID_TGFBR_PATHWAY	4	P07,P11,V04,V14	65
REACTOME_L1CAM_INTERACTIONS	4	P07,P17,V02,V15	82
REACTOME_CHONDROITIN_SULFATE_DERMATAN_SULFATE_METABOLISM	4	P10,V15,V17,V19	27
REACTOME_SIGNALING_BY_GPCR	4	P10,P15,V18,V19	57
KEGG_PANCREATIC_CANCER	3	P01,P23,V18	81
NABA_SECRETED_FACTORS	3	P01,V08,V19	52
PID_SHP2_PATHWAY	3	P01,P09,V19	93
BIOCARTA_AGR_PATHWAY	3	P01,V15,V17	41
KEGG_LEISHMANIA_INFECTION	3	P01,V15,V16	94
REACTOME_COSTIMULATION_BY_THE_CD28_FAMILY	3	P01,P02,V17	95
KEGG_TOLL_LIKE_RECEPTOR_SIGNALING_PATHWAY	3	P01,P05,P07	28
KEGG_WNT_SIGNALING_PATHWAY	3	P01,V15,V17	96
REACTOME_ANTIGEN_PRESENTATION_FOLDING_ASSEMBLY_AND_PEPTIDE_LOADING_OF_CLASS_I_MHC	3	P01,P07,V14	70

KEGG_AMYOTROPHIC_LATERAL_SCLEROSIS_ALS	3	P02,P05,V19	35
KEGG_PARKINSONS_DISEASE	3	P02,P05,V18	20
PID_IL12_2PATHWAY	3	P02,V04,V08	97
PID_IL2_1PATHWAY	3	P02,P05	40
REACTOME_CYTOKINE_SIGNALING_IN_IMMUNE_SYSTEM	3	P02,P05,P20	50
REACTOME_IRON_UPTAKE_AND_TRANSPORT	3	P02,P05,V16	85
ST_B_CELL_ANTIGEN_RECEPTOR	3	P02,P05,V14	53
KEGG_DRUG_METABOLISM_OTHER_ENZYMES	3	P02,P05,V15	98
KEGG_HUNTINGTONS_DISEASE	3	P02,V16,V19	20
KEGG_LYSINE_DEGRADATION	3	P02,P10,V17	18
KEGG_RENAL_CELL_CARCINOMA	3	P02,P10,V14	49
PID_THROMBIN_PAR1_PATHWAY	3	P02,V15,V19	61
REACTOME_ACTIVATED_TLR4_SIGNALLING	3	P02,P05,P17	28
REACTOME_GOLGI_ASSOCIATED_VESICLE_BIOGENESIS	3	P02,P04,V19	99
REACTOME_MEMBRANE_TRAFFICKING	3	P02,V14,V19	99
REACTOME_TRIF_MEDIATED_TLR3_SIGNALING	3	P02,P05,P10	28
REACTOME_SEMAPHORIN_INTERACTIONS	3	P03,P07,V15	100
REACTOME_INTEGRATION_OF_ENERGY_METABOLISM	3	P03,P05,V19	67
KEGG_GLIOMA	3	P03,V18,V19	101
KEGG_VIRAL_MYOCARDITIS	3	P04,P10,V16	102
PID_NECTIN_PATHWAY	3	P04,P11,V19	103
BIOCARTA_MAPK_PATHWAY	3	P05,P10,V14	104
KEGG_BLADDER_CANCER	3	P05,P17,P23	105
KEGG_GAP_JUNCTION	3	P05,V14,V19	24
KEGG_MELANOGENESIS	3	P05,P23,V16	24
KEGG_P53_SIGNALING_PATHWAY	3	P05,P21,V14	106
PID_RHOA_PATHWAY	3	P05,V08,V14	107
KEGG_NOD_LIKE_RECEPTOR_SIGNALING_PATHWAY	3	P05,V16,V17	108
PID_AP1_PATHWAY	3	P05,V04,V14	109

KEGG_VASOPRESSIN_REGULATED_WATER_REABSORPTION	3	P07,P23,V03	110
REACTOME_CLASS_B_2_SECRETIN_FAMILY_RECEPTORS	3	P07,P10,P15	67
KEGG_NATURAL_KILLER_CELL_MEDIATED_CYTOTOXICITY	3	P10,V14,V16	53
REACTOME_ASPARAGINE_N_LINKED_GLYCOSYLATION	3	P10,P17,P23	38
KEGG_TIGHT_JUNCTION	3	P10,V04,V19	86
REACTOME_SEMA4D_IN_SEMAPHORIN_SIGNALING	3	P10,P18,V19	100
REACTOME_SEMA4D_INDUCED_CELL_MIGRATION_AND_GROWTH_CONE_COLLAPSE	3	P10,P13,V19	100
KEGG_AXON_GUIDANCE	3	P10,P17,V19	46
KEGG_HEMATOPOIETIC_CELL_LINEAGE	3	P15,V08,V15	111
PID_NCADHERIN_PATHWAY	3	V08,V15,V19	103
PID_TCPTP_PATHWAY	2	P01,V19	112
REACTOME_HS_GAG_BIOSYNTHESIS	2	P01,P07	27
REACTOME_HS_GAG_DEGRADATION	2	P01,V17	27
PID_CXCR4_PATHWAY	2	P01,P02	113
PID_INSULIN_PATHWAY	2	P01,V18	68
PID_RET_PATHWAY	2	P01,P02	49
REACTOME_DEADENYLATION_DEPENDENT_MRNA_DECAY	2	P01,V16	114
REACTOME_INSULIN_RECEPTOR_SIGNALLING_CASCADE	2	P01,P03	54
KEGG_ALZHEIMERS_DISEASE	2	P01,P05	20
REACTOME_METABOLISM_OF_VITAMINS_AND_COFACTORS	2	P01,P06	115
KEGG_B_CELL_RECEPTOR_SIGNALING_PATHWAY	2	P02,P05	53
PID_BCR_5PATHWAY	2	P02,P05	53
PID_IL4_2PATHWAY	2	P02,P09	116
PID_KIT_PATHWAY	2	P02,P05	40
SIG_BCR_SIGNALING_PATHWAY	2	P02,P05	53
KEGG_BETA_ALANINE_METABOLISM	2	P02,P15	18
PID_ILK_PATHWAY	2	P02,V02	117
PID_NETRIN_PATHWAY	2	P02,P05	49
PID_P38_MK2_PATHWAY	2	P02,V08	11

REACTOME_ADVANCED_GLYCOSYLATION_ENDPRODUCT_RECEPTOR_SIGNALING	2	P02,V18	118
REACTOME_NEURONAL_SYSTEM	2	P02,V04	119
KEGG_SNARE_INTERACTIONS_IN_VESICULAR_TRANSPORT	2	P02,P23	120
PID_P75_NTR_PATHWAY	2	P03,V03	121
PID_HNF3A_PATHWAY	2	P04,P10	122
BIOCARTA_ECM_PATHWAY	2	P05,V15	41
KEGG_LONG_TERM_POTENTIATION	2	P05,V14	24
KEGG_VEGF_SIGNALING_PATHWAY	2	P05,V04	53
PID_CMYB_PATHWAY	2	P05,V18	123
PID_P73PATHWAY	2	P05,V15	124
PID_SYNDECAN_2_PATHWAY	2	P05,P07	125
REACTOME_DNA_REPAIR	2	P05,V16	126
REACTOME_GASTRIN_CREB_SIGNALLING_PATHWAY_VIA_PKC_AND_MAPK	2	P05,P10	57
REACTOME_P75_NTR_RECEPTOR_MEDIATED_SIGNALLING	2	P05,V03	121
REACTOME_SIGNALING_BY_ERBB4	2	P05,V18	32
REACTOME_SIGNALING_BY_FGFR	2	P05,V18	32
REACTOME_SIGNALING_BY_FGFR_IN_DISEASE	2	P05,P07	32
REACTOME_G_ALPHA_Q_SIGNALLING_EVENTS	2	P05,P10	57
REACTOME_TOLL_RECEPTOR_CASCADES	2	P05,P07	28
ST_ADRENERGIC	2	P05,V18	127
PID_DELTA_NP63_PATHWAY	2	P05,V19	128
REACTOME_IMMUNOREGULATORY_INTERACTIONS_BETWEEN_A_LYMPHOID_AND_A_NON_LYMPHOID_CELL	2	P06,P07	80
REACTOME_REGULATION_OF_INSULIN_SECRETION	2	P07,V19	67
KEGG_ARRHYTHMOGENIC_RIGHT_VENTRICULAR_CARDIOMYOPATHY_ARVC	2	P07,P11	66
REACTOME_ADHERENS_JUNCTIONS_INTERACTIONS	2	P07,V02	129
REACTOME_CELL_CELL_COMMUNICATION	2	P07,V18	129
REACTOME_CELL_CELL_JUNCTION_ORGANIZATION	2	P07,V02	129
REACTOME_CELL_JUNCTION_ORGANIZATION	2	P07,V02	129
KEGG_PROSTATE_CANCER	2	P09,V16	101

REACTOME_SIGNALING_BY_ROBO_RECEPTOR	2	P10,V18	130
REACTOME_CHONDROITIN_SULFATE_BIOSYNTHESIS	2	P10,V19	27
WNT_SIGNALING	2	P11,V18	96
PID_AVB3_OPN_PATHWAY	2	P15,P23	131
REACTOME_SIGNALING_BY_NOTCH	2	P18,V04	132
KEGG_ENDOCYTOSIS	2	P21,V04	133
PID_ERA_GENOMIC_PATHWAY	2	P21,P23	122
PID_AJDISS_2PATHWAY	2	P23,V19	88
PID_FRA_PATHWAY	2	P23,V18	109
REACTOME_KERATAN_SULFATE_DEGRADATION	2	V04,V17	78
REACTOME_CITRIC_ACID_CYCLE_TCA_CYCLE	2	V15,V16	17
REACTOME_KERATAN_SULFATE_KERATIN_METABOLISM	2	V17,V19	78
PID_LYMPH_ANGIOGENESIS_PATHWAY	1	P01	134
REACTOME_PI3K_CASCADE	1	P01	54
REACTOME_CLASS_A1_RHODOPSIN_LIKE_RECEPTORS	1	P01	57
BIOCARTA_P38MAPK_PATHWAY	1	P02	104
KEGG_CHEMOKINE_SIGNALING_PATHWAY	1	P02	113
PID_LYSOPHOSPHOLIPID_PATHWAY	1	P02	61
REACTOME_GROWTH_HORMONE_RECEPTOR_SIGNALING	1	P02	40
KEGG_CHRONIC_MYELOID_LEUKEMIA	1	P02	81
KEGG_FATTY_ACID_METABOLISM	1	P02	18
PID_ERBB2_ERBB3_PATHWAY	1	P02	53
PID_TRKR_PATHWAY	1	P02	49
REACTOME_HIV_LIFE_CYCLE	1	P02	126
REACTOME_LYSOSOME_VESICLE_BIOGENESIS	1	P02	99
REACTOME_FORMATION_OF_TUBULIN_FOLDING_INTERMEDIATES_BY_CCT_TRIC	1	P04	12
BIOCARTA_SALMONELLA_PATHWAY	1	P05	9
KEGG_PORPHYRIN_AND_CHLOROPHYLL_METABOLISM	1	P05	135
PID_FCER1_PATHWAY	1	P05	53

PID_HIF1_TFPATHWAY	1	P05	136
PID_IFNG_PATHWAY	1	P05	40
REACTOME_FRS2_MEDIATED_CASCADE	1	P05	54
REACTOME_NEPHRIN_INTERACTIONS	1	P05	137
PID_ATF2_PATHWAY	1	P07	138
REACTOME_CELL_SURFACE_INTERACTIONS_AT_THE_VASCULAR_WALL	1	P07	139
REACTOME_FACTORS_INVOLVED_IN_MEGAKARYOCYTE_DEVELOPMENT_AND_PLATELET_PRODUCTION	1	P09	140
PID_PTP1B_PATHWAY	1	P09	112
KEGG_PPAR_SIGNALING_PATHWAY	1	P10	90
PID_P53_DOWNSTREAM_PATHWAY	1	P10	106
PID_ECADHERIN_NASCENT_AJ_PATHWAY	1	P11	103
REACTOME_PPARA_ACTIVATES_GENE_EXPRESSION	1	P11	90
REACTOME_SMOOTH_MUSCLE_CONTRACTION	1	P17	34
KEGG_NEUROACTIVE_LIGAND_RECEPTOR_INTERACTION	1	P23	141
REACTOME_TRANSPORT_TO_THE_GOLGI_AND_SUBSEQUENT_MODIFICATION	1	P23	38
BIOCARTA_PROTEASOME_PATHWAY	1	V02	3
KEGG_PROTEASOME	1	V02	3
REACTOME_MHC_CLASS_II_ANTIGEN_PRESENTATION	1	V03	58
BIOCARTA_EIF4_PATHWAY	1	V04	114
KEGG_MAPK_SIGNALING_PATHWAY	1	V04	142
PID_NOTCH_PATHWAY	1	V04	132
REACTOME_APOPTOTIC_CLEAVAGE_OF_CELLULAR_PROTEINS	1	V08	42
KEGG_NICOTINATE_AND_NICOTINAMIDE_METABOLISM	1	V14	143
REACTOME_FATTY_ACID_TRIACYLGLYCEROL_AND_KETONE_BODY_METABOLISM	1	V14	90
KEGG_GLYCEROLIPID_METABOLISM	1	V14	144
PID_ARF6_TRAFFICKING_PATHWAY	1	V15	145
REACTOME_OTHER_SEMAPHORIN_INTERACTIONS	1	V15	146
KEGG_PROGESTERONE_MEDIATED_OOCYTE_MATURATION	1	V16	101

PID_VEGFR1_PATHWAY	1	V16	63
REACTOME_EGFR_DOWNREGULATION	1	V16	32
REACTOME_TCR_SIGNALING	1	V16	95
PID_GLYPICAN_1PATHWAY	1	V16	147
PID_EPHA_FWDPATHWAY	1	V16	148
REACTOME_BASIGIN_INTERACTIONS	1	V16	139
KEGG_OTHER_GLYCAN_DEGRADATION	1	V17	149
PID_SYNDECAN_4_PATHWAY	1	V17	125
PID_TXA2PATHWAY	1	V17	61
KEGG_ARACHIDONIC_ACID_METABOLISM	1	V18	150
KEGG_MELANOMA	1	V18	101
ST_FAS_SIGNALING_PATHWAY	1	V18	151
PID_PI3KCI_AKT_PATHWAY	1	V19	11
REACTOME_KERATAN_SULFATE_BIOSYNTHESIS	1	V19	78
REACTOME_TRANS_GOLGI_NETWORK_VESICLE_BUDDING	1	V19	99

Table S2-Clinical parameters assess during the PET for the longitudinal case study patients. The values highlighted are out of the reference range values for that specific parameter (described at the bottom of the table).

Patient	PD duration (months)	PD duration (years)	D/P_{creat_240min}	Profile Transporter	Peritoneal UF (mL/4h)	Diuresis	Creatinine clearance (mL/min)	Kt/v	Serum albumin (mg/dL)	CA 125 (kU/L)	PTH (pg/mL)	eGFR (mL/min)	Diabetes	Total episodes of peritonitis until PET	Incidence (number/year)
P01	1	0,1	0,9	H	500	900	144,07	2,53	3,5	38,9	402	8,18	0	0	0,000
	6	0,5	0,69	H.A.	835	1480	104,51	2,15	3,6	42,8	238	8	0	0	0,000
	13	1,0	0,928	H.	600	1520	144,58	2,17	3,2	38,8	234	11,68	0	0	0,000
	25	2,1	0,67	H.A.	760	1070	110	2,07	3,5	45,1	125	8,39	0	1	0,472
	39	3,3	0,74	H.A.	350	990	107,39	1,9	3,7	39,9	422	7,88	0		0,306
P03	1	0,1	0,76	H.A.	700	460	66,39	2,05	3,9	6	151	1,73	0	0	0,000
	7	0,5	0,81	H.	620	1180	79,31	2,3	3,7	26,2	194	4,53	0	0	0,000
	19	1,6	0,71	H.A.	425	1500	79,05	2,25	4,3	28,9	466	6,16	0	0	0,000
	31	2,6	0,59	L.A.	570	1500	83,84	2,32	4,4	37,4	504,6	6,89	0	0	0,000
	45	3,7	0,6	L.A.	940	950	55,8	1,7	3,9	31,3	463,4	3,81	0	0	0,000
V16	14	1,1	0,73	H.A.	915	2260	71,39	2,1	3,7	6	1029	5,22	0	1	0,878
	27	2,3	0,78	H.A.	486	2000	68,39	1,95	3,8	12,7	696	3,63	0	1	0,443
	40	3,3	0,84	H.	919	2000	56,69	1,94	3,7	23,8	46	2	0	1	0,301
				Reference values	**>400**	***N/A**	**>60**	**1,7**	**>3,0**	****N/A**	**<800**				

* the higher the better

** descending profile may indicate loss of MCs lining layer

Table S3- Patient P01-Enriched pathways for each cluster with the respective Gene Ratio, Background ratio (Bg Ratio), p-value, p-adjust, q-value, Gene Id and counts (number of genes (proteins) per pathways). The highlighted pathways were the one selected for the bar plots graphs.

Cluster	Description	GeneRatio	BgRatio	pvalue	p.adjust	qvalue	geneID	Count
1	KEGG_CYTOKINE_CYTOKINE_RECEPTOR_INTERACTION	9/53	54/1513	0,00006	0,01510	0,01364	KITLG/CNTFR/PDGFRB/IFNAR1/INHBB/CSF1/TGFBR2/VEGFA/CCL25	9
1	REACTOME_HS_GAG_BIOSYNTHESIS	4/53	10/1513	0,00024	0,02898	0,02618	SDC1/NDST1/GPC1/AGRN	4
1	PID_INTEGRIN3_PATHWAY	6/53	31/1513	0,00052	0,04165	0,03763	SDC1/PDGFRB/TGFBR2/VEGFA/COL4A1/CYR61	6
1	PID_TCPTP_PATHWAY	4/53	17/1513	0,00228	0,13673	0,12353	LMAN1/PDGFRB/CSF1/VEGFA	4
1	REACTOME_AXON_GUIDANCE	9/53	91/1513	0,00340	0,16297	0,14725	CLTA/GPC1/NCK1/MAP2K1/PLXND1/HFE2/AP2A1/COL4A1/AGRN	9
1	REACTOME_HS_GAG_DEGRADATION	3/53	10/1513	0,00409	0,16378	0,14798	SDC1/GPC1/AGRN	3
1	KEGG_PANCREATIC_CANCER	3/53	11/1513	0,00549	0,17251	0,15586	MAP2K1/TGFBR2/VEGFA	3
1	REACTOME_HEPARAN_SULFATE_HEPARIN_HS_GAG_METABOLISM	4/53	22/1513	0,00615	0,17251	0,15586	SDC1/NDST1/GPC1/AGRN	4
1	KEGG_T_CELL_RECEPTOR_SIGNALING_PATHWAY	3/53	12/1513	0,00714	0,17251	0,15586	CD8A/NCK1/MAP2K1	3
1	PID_AVB3_INTEGRIN_PATHWAY	5/53	36/1513	0,00719	0,17251	0,15586	SDC1/CSF1/TGFBR2/VEGFA/COL4A1	5
1	REACTOME_DEVELOPMENTAL_BIOLOGY	9/53	104/1513	0,00835	0,18213	0,16456	CLTA/GPC1/NCK1/MAP2K1/PLXND1/HFE2/AP2A1/COL4A1/AGRN	9
1	KEGG_CELL_ADHESION_MOLECULES_CAMS	6/53	54/1513	0,00981	0,19274	0,17414	SDC1/CD8A/VCAM1/SIGLEC1/CD99/PDCD1LG2	6
1	REACTOME_A_TETRASACCHARIDE_LINKER_SEQUENCE_IS_REQUIRED_FOR_GAG_SYNTHESIS	3/53	14/1513	0,01124	0,19274	0,17414	SDC1/GPC1/AGRN	3
1	REACTOME_SIGNAL_TRANSDUCTION_BY_L1	3/53	14/1513	0,01124	0,19274	0,17414	CLTA/MAP2K1/AP2A1	3
1	KEGG_PATHWAYS_IN_CANCER	6/53	58/1513	0,01380	0,21840	0,19733	KITLG/PDGFRB/MAP2K1/TGFBR2/VEGFA/COL4A1	6
1	NABA_SECRETED_FACTORS	7/53	76/1513	0,01456	0,21840	0,19733	KITLG/SCUBE3/INHBB/CSF1/VEGFA/CCL25/CRLF1	7
1	PID_SHP2_PATHWAY	3/53	16/1513	0,01646	0,23239	0,20997	PDGFRB/MAP2K1/VEGFA	3
1	REACTOME_DOWNSTREAM_SIGNAL_TRANSDUCTION	3/53	17/1513	0,01950	0,24632	0,22255	PDGFRB/NCK1/MAP2K1	3
1	REACTOME_NGF_SIGNALLING_VIA_TRKA_FROM_THE_PLASMA_MEMBRANE	3/53	17/1513	0,01950	0,24632	0,22255	CLTA/MAP2K1/AP2A1	3
3	REACTOME_O_LINKED_GLYCOSYLATION_OF_MUCINS	5/87	15/1513	0,00107	0,24924	0,24924	B3GNT7/GALNT10/GCNT1/MUC16/B3GNT9	5
4	REACTOME_CELL_CYCLE	11/91	35/1513	0,00000	0,00068	0,00058	LMNB1/PSMC2/NPM1/YWHAG/NUDC/PPP2R2A/HSP90AA1/PCNA/PSME1/SKP1/TUBB4B	11
4	BIOCARTA_AMI_PATHWAY	7/91	14/1513	0,00001	0,00068	0,00058	PROC/FGB/AHSP/F2/FGG/PROS1/F10	7
4	PID_MYC_ACTIV_PATHWAY	8/91	23/1513	0,00003	0,00170	0,00144	EIF2S1/CAD/NPM1/HSPA4/NCL/HSP90AA1/HSPD1/PTMA	8
4	REACTOME_UNFOLDED_PROTEIN_RESPONSE	7/91	19/1513	0,00006	0,00231	0,00196	EIF2S1/IGFBP1/CALR/SEC31A/HDGF/KHSRP/HSP90B1	7
4	REACTOME_METABOLISM_OF_PROTEINS	17/91	104/1513	0,00008	0,00251	0,00213	F9/PROC/EEF1B2/EIF2S1/PDIA3/F2/PABPC1/TCP1/CALR/EEF1A1/HSPD1/SEC31A/PFDN4/PROS1/TUBB4B/F10/RPS3	17

4	REACTOME_FORMATION_OF_FIBRIN_CLOT_CLOTTING_CASCADE	7/91	24/1513	0,00034	0,00989	0,00839	F9/PROC/FGB/F2/FGG/PROS1/F10	7
4	PID_IL6_7_PATHWAY	5/91	13/1513	0,00062	0,01510	0,01280	IL6/STAT3/FGG/STAT1/HSP90B1	5
4	REACTOME_CLASS_I_MHC_MEDIATED_ANTIGEN_PROCESSING_PRESENTATION	8/91	41/1513	0,00232	0,04532	0,03843	UBE2M/UBE2K/PSMC2/PDIA3/CALR/SEC31A/PSME1/SKP1	8
4	BIOCARTA_FIBRINOLYSIS_PATHWAY	4/91	11/1513	0,00292	0,05344	0,04531	SERPINB2/FGB/F2/FGG	4
4	BIOCARTA_EXTRINSIC_PATHWAY	6/91	10/1513	0,00001	0,00068	0,00058	PROC/FGB/F2/FGG/PROS1/F10	6
4	REACTOME_COMMON_PATHWAY	6/91	11/1513	0,00001	0,00107	0,00091	PROC/FGB/F2/FGG/PROS1/F10	6
4	REACTOME_CELL_CYCLE_MITOTIC	9/91	30/1513	0,00003	0,00170	0,00144	PSMC2/YWHAG/NUDC/PPP2R2A/HSP90AA1/PCNA/PSME1/SKP1/TUBB4B	9
4	BIOCARTA_INTRINSIC_PATHWAY	7/91	18/1513	0,00004	0,00175	0,00149	F9/PROC/FGB/F2/FGG/PROS1/F10	7
4	REACTOME_PTM_GAMMA_CARBOXYLATION_HYPUSINE_FORMATION_AND_ARYLSULFATASE_ACTIVATION	5/91	12/1513	0,00040	0,01064	0,00902	F9/PROC/F2/PROS1/F10	5
4	REACTOME_DIABETES_PATHWAYS	8/91	39/1513	0,00165	0,03722	0,03155	EIF2S1/IGFBP1/F2/CALR/SEC31A/HDGF/KHSRP/HSP90B1	8
4	REACTOME_MITOTIC_G1_G1_S_PHASES	5/91	16/1513	0,00182	0,03801	0,03222	PSMC2/PPP2R2A/PCNA/PSME1/SKP1	5
4	REACTOME_S_PHASE	4/91	14/1513	0,00770	0,13266	0,11248	PSMC2/PCNA/PSME1/SKP1	4
4	KEGG_ANTIGEN_PROCESSING_AND_PRESENTATION	5/91	23/1513	0,01000	0,15452	0,13101	PDIA3/HSPA4/CALR/HSP90AA1/PSME1	5
4	REACTOME_G1_S_TRANSITION	4/91	15/1513	0,01002	0,15452	0,13101	PSMC2/PCNA/PSME1/SKP1	4
4	REACTOME_ANTIGEN_PROCESSING_UBIQUITINATION_PROTEASOME_DEGRADATION	5/91	24/1513	0,01204	0,17637	0,14954	UBE2M/UBE2K/PSMC2/PSME1/SKP1	5
4	REACTOME_POST_TRANSLATIONAL_PROTEIN_MODIFICATION	8/91	54/1513	0,01321	0,18438	0,15632	F9/PROC/PDIA3/F2/CALR/SEC31A/PROS1/F10	8
4	REACTOME_INFLUENZA_LIFE_CYCLE	5/91	25/1513	0,01435	0,18863	0,15993	CLTC/CALR/HSP90AA1/RAN/RPS3	5
4	REACTOME_METABOLISM_OF_MRNA	7/91	46/1513	0,01757	0,18863	0,15993	PSMC2/PABPC1/PPP2R2A/RBM8A/PSME1/KHSRP/RPS3	7
4	REACTOME_METABOLISM_OF_RNA	7/91	46/1513	0,01757	0,18863	0,15993	PSMC2/PABPC1/PPP2R2A/RBM8A/PSME1/KHSRP/RPS3	7
4	BIOCARTA_BIOPEPTIDES_PATHWAY	3/91	10/1513	0,01855	0,18863	0,15993	STAT3/F2/STAT1	3
4	KEGG_TOLL_LIKE_RECEPTOR_SIGNALING_PATHWAY	3/91	10/1513	0,01855	0,18863	0,15993	IL6/STAT1/SPP1	3
4	PID_TELOMERASE_PATHWAY	3/91	10/1513	0,01855	0,18863	0,15993	NCL/HNRNPC/HSP90AA1	3
4	REACTOME_DNA_REPLICATION	4/91	18/1513	0,01955	0,18863	0,15993	PSMC2/NUDC/PCNA/PSME1	4
4	REACTOME_ER_PHAGOSOME_PATHWAY	4/91	18/1513	0,01955	0,18863	0,15993	PSMC2/PDIA3/CALR/PSME1	4
4	REACTOME_HOST_INTERACTIONS_OF_HIV_FACTORS	5/91	27/1513	0,01982	0,18863	0,15993	PSMC2/NPM1/PSME1/SKP1/RAN	5
4	KEGG_PATHWAYS_IN_CANCER	8/91	58/1513	0,01996	0,18863	0,15993	LAMC1/IL6/STAT3/LAMB2/HSP90AA1/STAT1/FGFR1/HSP90B1	8
4	KEGG_CELL_CYCLE	3/91	11/1513	0,02442	0,21041	0,17839	YWHAG/PCNA/SKP1	3
4	KEGG_WNT_SIGNALING_PATHWAY	3/91	11/1513	0,02442	0,21041	0,17839	SFRP2/CTNNBIP1/SKP1	3

4	REACTOME_PREFOLDIN_MEDIATED_TRANSFER_OF_SUBSTRATE_TO_CCT_TRIC	3/91	11/1513	0,02442	0,21041	0,17839	TCP1/PFDN4/TUBB4B	3
4	PID_REG_GR_PATHWAY	4/91	20/1513	0,02823	0,21566	0,18285	IL6/HSP90AA1/FGG/STAT1	4
4	REACTOME_REGULATION_OF_MRNA_STABILITY_BY_PROTEINS_THAT_BIND_AU_RICH_ELEMENTS	4/91	20/1513	0,02823	0,21566	0,18285	PSMC2/PABPC1/PSME1/KHSRP	4
4	REACTOME_HIV_INFECTION	5/91	30/1513	0,03034	0,21566	0,18285	PSMC2/NPM1/PSME1/SKP1/RAN	5
4	REACTOME_ANTIGEN_PRESENTATION_FOLDING_ASSEMBLY_AND_PEPTIDE_LOADING_OF_CLASS_I_MHC	3/91	12/1513	0,03116	0,21566	0,18285	PDIA3/CALR/SEC31A	3
4	REACTOME_NONSENSE_MEDIATED_DECAY_ENHANCED_BY_THE_EXON_JUNCTION_COMPLEX	4/91	21/1513	0,03331	0,21566	0,18285	PABPC1/PPP2R2A/RBM8A/RPS3	4
4	REACTOME_SIGNALING_BY_ILS	4/91	21/1513	0,03331	0,21566	0,18285	IL6/STAT3/STAT1/SKP1	4
4	PID_INTEGRIN3_PATHWAY	5/91	31/1513	0,03451	0,21566	0,18285	LAMC1/FGB/FGG/SDC4/SPP1	5
4	REACTOME_ACTIVATION_OF_NF_KAPPAB_IN_B_CELLS	3/91	13/1513	0,03878	0,21566	0,18285	PSMC2/PSME1/SKP1	3
4	REACTOME_CYCLIN_E_ASSOCIATED_EVENTS_DURING_G1_S_TRANSITION_	3/91	13/1513	0,03878	0,21566	0,18285	PSMC2/PSME1/SKP1	3
4	REACTOME_DOWNSTREAM_SIGNALING_EVENTS_OF_B_CELL_RECEPTOR_BCR	3/91	13/1513	0,03878	0,21566	0,18285	PSMC2/PSME1/SKP1	3
4	REACTOME_LOSS_OF_NLP_FROM_MITOTIC_CENTROSOMES	3/91	13/1513	0,03878	0,21566	0,18285	YWHAG/HSP90AA1/TUBB4B	3
4	REACTOME_MITOTIC_G2_G2_M_PHASES	3/91	13/1513	0,03878	0,21566	0,18285	YWHAG/HSP90AA1/TUBB4B	3
4	REACTOME_PLATELET_AGGREGATION_PLUG_FORMATION	3/91	13/1513	0,03878	0,21566	0,18285	FGB/F2/FGG	3
4	REACTOME_RECRUITMENT_OF_MITOTIC_CENTROSOME_PROTEINS_AND_COMPLEXES	3/91	13/1513	0,03878	0,21566	0,18285	YWHAG/HSP90AA1/TUBB4B	3
4	REACTOME_REGULATION_OF_MITOTIC_CELL_CYCLE	3/91	13/1513	0,03878	0,21566	0,18285	PSMC2/PSME1/SKP1	3
4	REACTOME_SCF_BETA_TRCP_MEDIATED_DEGRADATION_OF_EMI1	3/91	13/1513	0,03878	0,21566	0,18285	PSMC2/PSME1/SKP1	3
4	REACTOME_SCFSKP2_MEDIATED_DEGRADATION_OF_P27_P21	3/91	13/1513	0,03878	0,21566	0,18285	PSMC2/PSME1/SKP1	3
4	REACTOME_SYNTHESIS_OF_DNA	3/91	13/1513	0,03878	0,21566	0,18285	PSMC2/PCNA/PSME1	3
4	REACTOME_TRANSLATION	5/91	32/1513	0,03901	0,21566	0,18285	EEF1B2/EIF2S1/PABPC1/EEF1A1/RPS3	5
4	PID_A6B1_A6B4_INTEGRIN_PATHWAY	4/91	23/1513	0,04497	0,24293	0,20597	LAMC1/YWHAG/LAMB2/CD9	4
4	REACTOME_A_TETRASACCHARIDE_LINKER_SEQUENCE_IS_REQUIRED_FOR_GAG_SYNTHESIS	3/91	14/1513	0,04726	0,24293	0,20597	DCN/BGN/SDC4	3
4	REACTOME_INTRINSIC_PATHWAY	3/91	14/1513	0,04726	0,24293	0,20597	F9/F2/F10	3
4	REACTOME_SIGNALING_BY_WNT	3/91	14/1513	0,04726	0,24293	0,20597	PSMC2/PSME1/SKP1	3
5	PID_ERBB1_DOWNSTREAM_PATHWAY	6/60	30/1513	0,00085	0,20734	0,19939	PPP2R1A/SFN/ARPC5/ARPC1B/YWHAZ/PPP5C	6
8	REACTOME_GPCR_LIGAND_BINDING	15/219	40/1513	0,00022	0,06851	0,06851	OXT/NPY/RAMP3/APP/PPBP/INSL5/PENK/GAST/GIP/FZD6/PYY/CGA/GCG/MLN/C3AR1	15
8	REACTOME_GPCR_DOWNSTREAM_SIGNALING	14/219	43/1513	0,00186	0,20174	0,20174	OXT/NPY/RAMP3/APP/PPBP/INSL5/PENK/GAST/GIP/PYY/CGA/GCG/MLN/C3AR1	14
8	REACTOME_CLASS_A1_RHODOPSIN_LIKE_RECEPTORS	11/219	30/1513	0,00197	0,20174	0,20174	OXT/NPY/APP/PPBP/INSL5/PENK/GAST/PYY/CGA/MLN/C3AR1	11

10	PID_INSULIN_PATHWAY	4/35	10/1513	0,00005	0,00705	0,00617	CRK/INSR/EIF4EBP1/PTPN11	4
10	REACTOME_INSULIN_RECEPTOR_SIGNALLING_CASCADE	3/35	16/1513	0,00517	0,20565	0,17992	CRK/INSR/EIF4EBP1	3
10	REACTOME_TRANSLATION	4/35	32/1513	0,00545	0,20565	0,17992	EIF4H/RPL4/EIF4EBP1/EIF3A	4
10	REACTOME_SIGNALING_BY_INSULIN_RECEPTOR	3/35	17/1513	0,00618	0,20565	0,17992	CRK/INSR/EIF4EBP1	3
10	REACTOME_ACTIVATION_OF_THE_MRNA_UPON_BINDING_OF_THE_CAP_BINDING_COMPLEX_AND_EIFS_AND_SUBSEQUENT_BINDING_TO_43S	3/35	18/1513	0,00730	0,20565	0,17992	EIF4H/EIF4EBP1/EIF3A	3
10	REACTOME_METABOLISM_OF_PROTEINS	7/35	104/1513	0,00801	0,20565	0,17992	GALNT5/GALNT7/EIF4H/HSPA9/RPL4/EIF4EBP1/EIF3A	7
10	PID_MET_PATHWAY	3/35	20/1513	0,00988	0,21120	0,18479	CRK/EIF4EBP1/PTPN11	3
10	PID_CXCR4_PATHWAY	3/35	22/1513	0,01292	0,21120	0,18479	ITGA2/CRK/PTPN11	3
10	ST_INTEGRIN_SIGNALING_PATHWAY	3/35	22/1513	0,01292	0,21120	0,18479	VASP/ITGA2/CRK	3
10	REACTOME_AXON_GUIDANCE	6/35	91/1513	0,01578	0,21120	0,18479	VASP/ANK1/MYH10/ITGA2/COL5A2/EVL	6
13	REACTOME_PREFOLDIN_MEDIATED_TRANSFER_OF_SUBSTRATE_TO_CCT_TRIC	7/77	11/1513	0,00000	0,00005	0,00005	CCT3/CCT7/CCT6A/CCT5/CCT8/CCT2/CCT4	7
13	KEGG_ECM_RECEPTOR_INTERACTION	9/77	50/1513	0,00066	0,06183	0,05773	LAMB1/VTN/LAMA4/TNC/GP5/THBS2/COL5A1/LAMA2/COL5A3	9
13	KEGG_FOCAL_ADHESION	11/77	81/1513	0,00193	0,07516	0,07017	LAMB1/VTN/LAMA4/TNC/CAPN2/PAK2/TLN1/THBS2/COL5A1/LAMA2/COL5A3	11
13	REACTOME_PROTEIN_FOLDING	7/77	15/1513	0,00000	0,00044	0,00041	CCT3/CCT7/CCT6A/CCT5/CCT8/CCT2/CCT4	7
13	KEGG_OOCYTE_MEIOSIS	5/77	18/1513	0,00152	0,07516	0,07017	YWHAH/YWHAE/PRKACA/CALML3/PPP3CA	5
13	REACTOME_APOPTOSIS	7/77	37/1513	0,00201	0,07516	0,07017	PSME2/VIM/PSMB1/PAK2/PLEC/HIST1H1B/FAS	7
13	PID_INTEGRIN1_PATHWAY	8/77	48/1513	0,00225	0,07516	0,07017	LAMB1/VTN/LAMA4/TNC/CSPG4/THBS2/COL5A1/LAMA2	8
13	KEGG_APOPTOSIS	4/77	13/1513	0,00312	0,07516	0,07017	CAPN2/PRKACA/FAS/PPP3CA	4
13	REACTOME_LOSS_OF_NLP_FROM_MITOTIC_CENTROSOMES	4/77	13/1513	0,00312	0,07516	0,07017	YWHAE/PRKACA/TUBB/DYNC1H1	4
13	REACTOME_MITOTIC_G2_G2_M_PHASES	4/77	13/1513	0,00312	0,07516	0,07017	YWHAE/PRKACA/TUBB/DYNC1H1	4
13	REACTOME_RECRUITMENT_OF_MITOTIC_CENTROSOME_PROTEINS_AND_COMPLEXES	4/77	13/1513	0,00312	0,07516	0,07017	YWHAE/PRKACA/TUBB/DYNC1H1	4
13	REACTOME_CELL_CYCLE_MITOTIC	6/77	30/1513	0,00319	0,07516	0,07017	PSME2/PSMB1/YWHAE/PRKACA/TUBB/DYNC1H1	6
13	BIOCARTA_AGR_PATHWAY	4/77	14/1513	0,00421	0,08503	0,07938	LAMA4/PAK2/UTRN/LAMA2	4
13	PID_NFAT_3PATHWAY	4/77	14/1513	0,00421	0,08503	0,07938	YWHAH/YWHAE/PRKACA/PPP3CA	4
13	PID_A6B1_A6B4_INTEGRIN_PATHWAY	5/77	23/1513	0,00490	0,08674	0,08098	LAMB1/LAMA4/YWHAH/YWHAE/LAMA2	5
13	REACTOME_METABOLISM_OF_PROTEINS	12/77	104/1513	0,00490	0,08674	0,08098	CCT3/RPS12/CCT7/MAN2A1/CCT6A/CCT5/CCT8/EIF4A1/CCT2/PROZ/F7/CCT4	12
13	REACTOME_CELL_CYCLE	6/77	35/1513	0,00711	0,11828	0,11043	PSME2/PSMB1/YWHAE/PRKACA/TUBB/DYNC1H1	6
13	PID_TELOMERASE_PATHWAY	3/77	10/1513	0,01174	0,18462	0,17236	YWHAE/XRCC6/XRCC5	3

13	REACTOME_APOPTOTIC_EXECUTION_PHASE	4/77	19/1513	0,01341	0,19975	0,18649	VIM/PAK2/PLEC/HIST1H1B	4
13	BIOCARTA_CHREBP2_PATHWAY	3/77	11/1513	0,01556	0,20178	0,18838	YWHAH/YWHAE/PRKACA	3
13	SIG_CHEMOTAXIS	3/77	11/1513	0,01556	0,20178	0,18838	ARHGAP1/PAK2/ACTR2	3
13	REACTOME_HIV_INFECTION	5/77	30/1513	0,01569	0,20178	0,18838	PSME2/PSMB1/PAK2/XRCC6/XRCC5	5
13	KEGG_ALZHEIMERS_DISEASE	4/77	21/1513	0,01917	0,23583	0,22017	CAPN2/CALML3/FAS/PPP3CA	4
14	KEGG_GLYCOLYSIS_GLUCONEOGENESIS	13/124	29/1513	0,00000	0,00002	0,00001	ALDOA/LDHB/TPI1/ENO2/ENO1/GALM/ADH5/AKR1A1/ALDH1A3/ ALDH9A1/PGK1/PGM2/LDHA	13
14	KEGG_PYRUVATE_METABOLISM	8/124	16/1513	0,00001	0,00073	0,00065	LDHB/HAGH/AKR1B1/GRHPR/ALDH9A1/GLO1/MDH1/LDHA	8
14	KEGG_GLUTATHIONE_METABOLISM	8/124	21/1513	0,00013	0,00378	0,00337	GSR/GSS/LAP3/GSTT1/GSTM3/IDH1/GSTO1/GSTP1	8
14	KEGG_DRUG_METABOLISM_CYTOCHROME_P450	7/124	10/1513	0,00000	0,00019	0,00017	GSTT1/GSTM3/ADH5/ALDH1A3/GSTO1/AOX1/GSTP1	7
14	REACTOME_GLUCOSE_METABOLISM	10/124	27/1513	0,00002	0,00111	0,00099	ALDOA/PYGB/TPI1/ENO2/ENO1/UGP2/GOT1/PGK1/PGM2/MDH1	10
14	KEGG_METABOLISM_OF_XENOBIOTICS_BY_CYTOCHROME_P450	6/124	10/1513	0,00004	0,00158	0,00141	GSTT1/GSTM3/ADH5/ALDH1A3/GSTO1/GSTP1	6
14	KEGG_CITRATE_CYCLE_TCA_CYCLE	6/124	12/1513	0,00017	0,00378	0,00337	ACO2/IDH1/ACO1/FH/SUCLG2/MDH1	6
14	REACTOME_PYRUVATE_METABOLISM_AND_CITRIC_ACID_TCA_CYCLE	6/124	12/1513	0,00017	0,00378	0,00337	LDHB/ACO2/IDH1/FH/SUCLG2/LDHA	6
14	REACTOME_GLUCONEOGENESIS	7/124	17/1513	0,00020	0,00415	0,00370	ALDOA/TPI1/ENO2/ENO1/GOT1/PGK1/MDH1	7
14	KEGG_FRUCTOSE_AND_MANNOSE_METABOLISM	6/124	13/1513	0,00029	0,00519	0,00462	ALDOA/TPI1/PHPT1/AKR1B1/MPI/TSTA3	6
14	KEGG_AMINO_SUGAR_AND_NUCLEOTIDE_SUGAR_METABOLISM	7/124	18/1513	0,00031	0,00519	0,00462	GNPDA1/MPI/UGDH/UGP2/PGM2/TSTA3/PGM3	7
14	REACTOME_PHASE_II_CONJUGATION	7/124	19/1513	0,00046	0,00658	0,00586	GSS/AHCY/UGDH/CNDP2/UGP2/GSTO1/GSTP1	7
14	REACTOME_TCA_CYCLE_AND_RESPIRATORY_ELECTRON_TRANSPORT	6/124	14/1513	0,00047	0,00658	0,00586	LDHB/ACO2/IDH1/FH/SUCLG2/LDHA	6
14	KEGG_CYSTEINE_AND_METHIONINE_METABOLISM	5/124	10/1513	0,00062	0,00805	0,00718	LDHB/AHCY/GOT1/MPST/LDHA	5
14	REACTOME_GLYCOLYSIS	5/124	12/1513	0,00169	0,01938	0,01728	ALDOA/TPI1/ENO2/ENO1/PGK1	5
14	REACTOME_BIOLOGICAL_OXIDATIONS	7/124	23/1513	0,00169	0,01938	0,01728	GSS/AHCY/UGDH/CNDP2/UGP2/GSTO1/GSTP1	7
14	REACTOME_METABOLISM_OF_CARBOHYDRATES	15/124	82/1513	0,00188	0,02027	0,01807	ALDOA/PYGB/TPI1/ENO2/ENO1/PGLS/GLCE/ARSB/GUSB/UGP2/GOT1/PGK1/PGM2/TKT/MDH1	15
14	KEGG_ARGININE_AND_PROLINE_METABOLISM	5/124	13/1513	0,00257	0,02612	0,02329	LAP3/ASS1/CKB/ALDH9A1/GOT1	5
14	KEGG_ALANINE_ASPARTATE_AND_GLUTAMATE_METABOLISM	4/124	10/1513	0,00612	0,05334	0,04756	ADSL/ASS1/GOT1/NIT2	4
14	KEGG_TYROSINE_METABOLISM	4/124	10/1513	0,00612	0,05334	0,04756	ADH5/ALDH1A3/GOT1/AOX1	4
14	REACTOME_GLUTATHIONE_CONJUGATION	4/124	10/1513	0,00612	0,05334	0,04756	GSS/CNDP2/GSTO1/GSTP1	4
14	REACTOME_TRNA_AMINOACYLATION	5/124	16/1513	0,00713	0,05933	0,05290	TARS/KARS/PPA2/PPA1/YARS	5
14	REACTOME_METABOLISM_OF_VITAMINS_AND_COFACTORS	4/124	11/1513	0,00902	0,07173	0,06395	NAMPT/PDXK/GSTO1/QPRT	4
14	KEGG_STARCH_AND_SUCROSE_METABOLISM	5/124	17/1513	0,00945	0,07207	0,06426	PYGB/GUSB/UGDH/UGP2/PGM2	5

14	KEGG_PENTOSE_PHOSPHATE_PATHWAY	4/124	14/1513	0,02254	0,16501	0,14712	ALDOA/PGLS/PGM2/TKT	4
14	REACTOME_CYTOSOLIC_TRNA_AMINOACYLATION	4/124	15/1513	0,02883	0,20295	0,18094	TARS/KARS/PPA1/YARS	4
15	KEGG_COMPLEMENT_AND_COAGULATION_CASCADES	25/135	62/1513	0,00000	0,00000	0,00000	CPB2/SERPIND1/C5/C8G/C4BPB/C3/F12/C9/C6/KLKB1/F13A1/KNG1/C1S/C8A/C4BPA/F13B/SERPINC1/C8B/CFI/MASP2/F11/C4A/C4B/CFB/CFH	25
15	REACTOME_INNATE_IMMUNE_SYSTEM	17/135	61/1513	0,00001	0,00038	0,00037	LBP/C5/C8G/C4BPB/C3/C9/C6/C1S/PLCG2/C8A/C4BPA/C8B/CFI/MASP2/C4A/CFB/CFH	17
15	REACTOME_FORMATION_OF_FIBRIN_CLOT_CLOTTING_CASCADE	8/135	24/1513	0,00070	0,01948	0,01888	F12/KLKB1/F13A1/KNG1/F13B/SERPINC1/F11/GP1BA	8
15	NABA_ECM_REGULATORS	22/135	124/1513	0,00084	0,02105	0,02040	SERPINA7/SERPIND1/MMP2/F12/ADAMTS8/SULF1/PZP/F13A1/KNG1/ITIH4/ITIH1/SERPINA4/CST2/CTSF/CPN2/SERPINA6/ITIH2/F13B/SERPINC1/ADAMTS13/SERPINA3/MASP2	22
15	REACTOME_COMPLEMENT_CASCADE	15/135	28/1513	0,00000	0,00000	0,00000	C5/C8G/C4BPB/C3/C9/C6/C1S/C8A/C4BPA/C8B/CFI/MASP2/C4A/CFB/CFH	15
15	BIOCARTA_COMP_PATHWAY	10/135	19/1513	0,00000	0,00008	0,00008	C5/C3/C9/C6/C1S/C8A/MASP2/C4A/C4B/CFB	10
15	BIOCARTA_LECTIN_PATHWAY	8/135	12/1513	0,00000	0,00008	0,00008	C5/C3/C9/C6/C8A/MASP2/C4A/C4B	8
15	KEGG_SYSTEMIC_LUPUS_ERYTHEMATOSUS	11/135	25/1513	0,00000	0,00016	0,00015	C5/C8G/C3/C9/C6/C1S/C8A/C8B/HLA-DPA1/C4A/C4B	11
15	BIOCARTA_CLASSIC_PATHWAY	8/135	14/1513	0,00001	0,00029	0,00028	C5/C3/C9/C6/C1S/C8A/C4A/C4B	8
15	REACTOME_REGULATION_OF_COMPLEMENT_CASCADE	7/135	12/1513	0,00002	0,00073	0,00070	C4BPB/C3/C4BPA/CFI/C4A/CFB/CFH	7
15	KEGG_PRION_DISEASES	9/135	23/1513	0,00008	0,00235	0,00228	C5/C8G/C9/C6/SOD1/BAX/NCAM1/C8A/C8B	9
15	REACTOME_INITIAL_TRIGGERING_OF_COMPLEMENT	5/135	13/1513	0,00376	0,08676	0,08407	C3/C1S/MASP2/C4A/CFB	5
15	KEGG_N_GLYCAN_BIOSYNTHESIS	5/135	14/1513	0,00543	0,10749	0,10416	ST6GAL1/MGAT1/MAN2A2/MAN1C1/B4GALT1	5
15	REACTOME_INTRINSIC_PATHWAY	5/135	14/1513	0,00543	0,10749	0,10416	F12/KLKB1/KNG1/F11/GP1BA	5
15	BIOCARTA_LAIR_PATHWAY	4/135	10/1513	0,00832	0,14406	0,13960	C5/C3/C6/KNG1	4
15	REACTOME_COSTIMULATION_BY_THE_CD28_FAMILY	4/135	10/1513	0,00832	0,14406	0,13960	CSK/ICOSLG/PTPN6/HLA-DPA1	4
15	KEGG_LEISHMANIA_INFECTION	5/135	16/1513	0,01024	0,16683	0,16166	TGFB1/C3/NCF4/PTPN6/HLA-DPA1	5

Table S4- Patient V16-Enriched pathways for each cluster with the respective Gene Ratio, Background ratio (Bg Ratio), p-value, p-adjust, q-value, Gene Id and counts (number of genes (proteins) per pathways). The highlighted pathways were the one selected for the bar plots graphs.

Cluster	Description	GeneRatio	BgRatio	pvalue	p.adjust	qvalue	geneID	Count
1	KEGG_PROGESTERONE_MEDIATED_OOCYTE_MATURATION	5/108	11/1659	0,0004	0,0762	0,0712	GNAI2/MAPK3/MAP2K1/HSP90AB1/HSP90AA1	5
1	REACTOME_SIGNALING_BY_EGFR_IN_CANCER	7/108	24/1659	0,0006	0,0762	0,0712	CLTA/EPS15L1/MAPK3/MAP2K1/AP2B1/HGS/HSP90AA1	7
1	KEGG_HUNTINGTONS_DISEASE	6/108	19/1659	0,0009	0,0762	0,0712	NDUFAB1/CLTA/BAX/AP2B1/CREB3L2/HIP1	6
1	PID_CERAMIDE_PATHWAY	5/108	13/1659	0,0009	0,0762	0,0712	MAPK3/BAX/MAP2K1/BID/TRADD	5
1	PID_VEGFR1_2_PATHWAY	6/108	23/1659	0,0027	0,1816	0,1697	MAPK3/MAP2K1/HSP90AB1/HGS/HSP90AA1/PTPN11	6
1	PID_VEGFR1_PATHWAY	4/108	11/1659	0,0039	0,1892	0,1768	MAPK3/HSP90AA1/PTPN11/NRP2	4
1	REACTOME_EGFR_DOWNREGULATION	4/108	11/1659	0,0039	0,1892	0,1768	CLTA/EPS15L1/AP2B1/HGS	4
1	KEGG_NATURAL_KILLER_CELL_MEDIATED_CYTOTOXICITY	6/108	26/1659	0,0052	0,1892	0,1768	MAPK3/IFNAR1/MAP2K1/BID/PTPN11/HLA-A	6
1	KEGG_NOD_LIKE_RECEPTOR_SIGNALING_PATHWAY	4/108	12/1659	0,0056	0,1892	0,1768	CCL2/MAPK3/HSP90AB1/HSP90AA1	4
1	PID_GMCSF_PATHWAY	4/108	12/1659	0,0056	0,1892	0,1768	CCL2/MAPK3/MAP2K1/PTPN11	4
1	KEGG_PROSTATE_CANCER	5/108	20/1659	0,0075	0,2165	0,2022	MAPK3/MAP2K1/HSP90AB1/CREB3L2/HSP90AA1	5
1	BIOCARTA_MET_PATHWAY	4/108	13/1659	0,0077	0,2165	0,2022	MAPK3/MAP2K1/MET/PTPN11	4
1	KEGG_MELANOGENESIS	4/108	14/1659	0,0102	0,2469	0,2307	GNAI2/MAPK3/MAP2K1/CREB3L2	4
1	REACTOME_INTRINSIC_PATHWAY	4/108	14/1659	0,0102	0,2469	0,2307	F9/KLKB1/F10/F11	4
3	REACTOME_METABOLISM_OF_AMINO_ACIDS_AND_DERIVATIVES	11/98	62/1659	0,0007	0,1558	0,1332	DLD/PSMD5/AHCY/GCLC/PSMA6/FAH/PSMB1/PSPH/NQO1/HIBCH/SMS	11
3	REACTOME_CLASS_I_MHC_MEDIATED_ANTIGEN_PROCESSING_PRESENTATION	9/98	50/1659	0,0020	0,1558	0,1332	PSMD5/PSMA6/BLMH/PSMB1/SEC23A/UBE2N/UBA7/UBE2L3/SEC31A	9
3	REACTOME_ANTIGEN_PROCESSING_UBIQUITINATION_PROTEASOME_DEGRADATION	7/98	32/1659	0,0020	0,1558	0,1332	PSMD5/PSMA6/BLMH/PSMB1/UBE2N/UBA7/UBE2L3	7
3	REACTOME_DNA_REPLICATION	6/98	24/1659	0,0021	0,1558	0,1332	PSMD5/PSMA6/PSMB1/PPP2R1A/PCNA/PAFAH1B1	6
3	REACTOME_GLUCOSE_METABOLISM	6/98	28/1659	0,0047	0,1996	0,1706	PPP2R1A/UGP2/PGK1/GBE1/MDH1/ALDOA	6
3	REACTOME_CELL_CYCLE_MITOTIC	7/98	37/1659	0,0048	0,1996	0,1706	PSMD5/PSMA6/PSMB1/YWHAE/PPP2R1A/PCNA/PAFAH1B1	7
3	REACTOME_G1_S_TRANSITION	5/98	20/1659	0,0049	0,1996	0,1706	PSMD5/PSMA6/PSMB1/PPP2R1A/PCNA	5
3	REACTOME_MITOTIC_G1_G1_S_PHASES	5/98	21/1659	0,0062	0,1996	0,1706	PSMD5/PSMA6/PSMB1/PPP2R1A/PCNA	5
3	REACTOME_METABOLISM_OF_MRNA	9/98	59/1659	0,0064	0,1996	0,1706	PSMD5/RPS12/PSMA6/PSMB1/DDX6/PPP2R1A/KHSRP/LSM4/EIF4A1	9
3	REACTOME_ADAPTIVE_IMMUNE_SYSTEM	14/98	117/1659	0,0070	0,1996	0,1706	C3/PSMD5/CSK/VASP/PSMA6/BLMH/PSMB1/SEC23A/UBE2N/PPP2R1A/UBA7/UBE2L3/SEC31A/PLCG2	14
3	REACTOME_REGULATION_OF_ORNITHINE_DECARBOXYLASE_ODC	4/98	14/1659	0,0072	0,1996	0,1706	PSMD5/PSMA6/PSMB1/NQO1	4

3	REACTOME_METABOLISM_OF_RNA	9/98	61/1659	0,0080	0,2027	0,1732	PSMD5/RPS12/PSMA6/PSMB1/DDX6/PPP2R1A/KHSRP/LSM4/EIF4A1	9
3	REACTOME_MITOTIC_M_M_G1_PHASES	5/98	23/1659	0,0093	0,2173	0,1857	PSMD5/PSMA6/PSMB1/PPP2R1A/PAFAH1B1	5
3	REACTOME_BIOLOGICAL_OXIDATIONS	5/98	24/1659	0,0112	0,2272	0,1942	AHCY/GCLC/ADH1B/UGP2/GSTP1	5
3	REACTOME_CELL_CYCLE	7/98	43/1659	0,0112	0,2272	0,1942	PSMD5/PSMA6/PSMB1/YWHAE/PPP2R1A/PCNA/PAFAH1B1	7
3	REACTOME_SIGNALING_BY_WNT	4/98	16/1659	0,0120	0,2277	0,1946	PSMD5/PSMA6/PSMB1/PPP2R1A	4
3	KEGG_GLUTATHIONE_METABOLISM	5/98	25/1659	0,0134	0,2388	0,2041	GCLC/IDH1/GPX4/GSTP1/SMS	5
3	PID_ERBB1_DOWNSTREAM_PATHWAY	6/98	35/1659	0,0146	0,2404	0,2054	ARPC3/YWHAE/EGFR/ARPC2/PPP2R1A/ACTR2	6
3	BIOCARTA_ACTINY_PATHWAY	3/98	10/1659	0,0177	0,2404	0,2054	ARPC3/ARPC2/ACTR2	3
3	REACTOME_SYNTHESIS_OF_DNA	4/98	18/1659	0,0185	0,2404	0,2054	PSMD5/PSMA6/PSMB1/PCNA	4
3	REACTOME_IMMUNE_SYSTEM	19/98	199/1659	0,0197	0,2404	0,2054	C3/PSMD5/CSK/VASP/PSMA6/BLMH/PSMB1/C9/IL18/SEC23A/UBE2N/PPP2R1A/UBA7/UBE2L3/SEC31A/PLCG2/C8B/CFI/EIF4A1	19
3	REACTOME_PHASE_II_CONJUGATION	4/98	19/1659	0,0223	0,2404	0,2054	AHCY/GCLC/UGP2/GSTP1	4
3	REACTOME_S_PHASE	4/98	19/1659	0,0223	0,2404	0,2054	PSMD5/PSMA6/PSMB1/PCNA	4
3	REACTOME_DEADENYLATION_DEPENDENT_MRNA_DECAY	3/98	11/1659	0,0233	0,2404	0,2054	DDX6/LSM4/EIF4A1	3
3	REACTOME_INTEGRIN_ALPHAIIB_BETA3_SIGNALING	3/98	11/1659	0,0233	0,2404	0,2054	CSK/FGB/FGG	3
3	REACTOME_TCR_SIGNALING	3/98	11/1659	0,0233	0,2404	0,2054	CSK/VASP/UBE2N	3
3	REACTOME_METABOLISM_OF_NUCLEOTIDES	5/98	29/1659	0,0248	0,2404	0,2054	ADK/CMPK1/GART/GMPS/TXNRD1	5
3	REACTOME_HOST_INTERACTIONS_OF_HIV_FACTORS	5/98	30/1659	0,0284	0,2404	0,2054	PSMD5/PSMA6/PSMB1/RAN/PPIA	5
3	BIOCARTA_CDC42RAC_PATHWAY	3/98	12/1659	0,0298	0,2404	0,2054	ARPC3/ARPC2/ACTR2	3
3	BIOCARTA_FIBRINOLYSIS_PATHWAY	3/98	12/1659	0,0298	0,2404	0,2054	SERPINB2/FGB/FGG	3
3	BIOCARTA_MPR_PATHWAY	3/98	12/1659	0,0298	0,2404	0,2054	ARPC3/ARPC2/ACTR2	3
3	KEGG_TYROSINE_METABOLISM	3/98	12/1659	0,0298	0,2404	0,2054	MIF/FAH/ADH1B	3
3	REACTOME_SIGNALING_BY_THE_B_CELL_RECEPTOR_BCR	4/98	21/1659	0,0315	0,2404	0,2054	PSMD5/PSMA6/PSMB1/PLCG2	4
3	KEGG_EPITHELIAL_CELL_SIGNALING_IN_HELICOBACTER_PYLORI_INFECTION	4/98	22/1659	0,0368	0,2404	0,2054	CSK/EGFR/PLCG2/ATP6V1G1	4
3	KEGG_CYSTEINE_AND_METHIONINE_METABOLISM	3/98	13/1659	0,0371	0,2404	0,2054	AHCY/SMS/LDHA	3
3	REACTOME_ANTIVIRAL_MECHANISM_BY_IFN_STIMULATED_GENES	3/98	13/1659	0,0371	0,2404	0,2054	UBE2N/UBA7/EIF4A1	3
3	REACTOME_GLYCOLYSIS	3/98	13/1659	0,0371	0,2404	0,2054	PPP2R1A/PGK1/ALDOA	3
3	REACTOME_LOSS_OF_NLP_FROM_MITOTIC_CENTROSOMES	3/98	13/1659	0,0371	0,2404	0,2054	YWHAE/PPP2R1A/PAFAH1B1	3
3	PID_PDGFRB_PATHWAY	6/98	43/1659	0,0375	0,2404	0,2054	CSK/ARPC3/YWHAE/ARPC2/PPP2R1A/ACTR2	6

3	REACTOME_INNATE_IMMUNE_SYSTEM	8/98	67/1659	0,0400	0,2404	0,2054	C3/C9/UBE2N/PPP2R1A/UBA7/PLCG2/C8B/CFI	8
3	KEGG_GLYCOLYSIS_GLUCONEOGENESIS	5/98	33/1659	0,0412	0,2404	0,2054	DLD/ADH1B/PGK1/LDHA/ALDOA	5
3	REACTOME_HIV_INFECTION	5/98	33/1659	0,0412	0,2404	0,2054	PSMD5/PSMA6/PSMB1/RAN/PPIA	5
3	ST_INTEGRIN_SIGNALING_PATHWAY	4/98	23/1659	0,0426	0,2404	0,2054	VASP/ZYX/PLCG2/ACTR2	4
3	KEGG_CITRATE_CYCLE_TCA_CYCLE	3/98	14/1659	0,0452	0,2404	0,2054	DLD/IDH1/MDH1	3
3	REACTOME_APC_C_CDC20_MEDIATED_DEGRADATION_OF_MITOTIC_PROTEINS	3/98	14/1659	0,0452	0,2404	0,2054	PSMD5/PSMA6/PSMB1	3
3	REACTOME_APC_C_CDH1_MEDIATED_DEGRADATION_OF_CDC20_AND_OTHER_APC_C_CDH1_TARGETED_PROTEINS_IN_LATE_MITOSIS_EARLY_G1	3/98	14/1659	0,0452	0,2404	0,2054	PSMD5/PSMA6/PSMB1	3
3	REACTOME_ASSEMBLY_OF_THE_PRE_REPLICATIVE_COMPLEX	3/98	14/1659	0,0452	0,2404	0,2054	PSMD5/PSMA6/PSMB1	3
3	REACTOME_AUTODEGRADATION_OF_CDH1_BY_CDH1_APC_C	3/98	14/1659	0,0452	0,2404	0,2054	PSMD5/PSMA6/PSMB1	3
3	REACTOME_AUTODEGRADATION_OF_THE_E3_UBIQUITIN_LIGASE_COP1	3/98	14/1659	0,0452	0,2404	0,2054	PSMD5/PSMA6/PSMB1	3
3	REACTOME_CDK_MEDIATED_PHOSPHORYLATION_AND_REMOVAL_OF_CDC6	3/98	14/1659	0,0452	0,2404	0,2054	PSMD5/PSMA6/PSMB1	3
3	REACTOME_CDT1_ASSOCIATION_WITH_THE_CDC6_ORC_ORIGIN_COMPLEX	3/98	14/1659	0,0452	0,2404	0,2054	PSMD5/PSMA6/PSMB1	3
3	REACTOME_ORC1_REMOVAL_FROM_CHROMATIN	3/98	14/1659	0,0452	0,2404	0,2054	PSMD5/PSMA6/PSMB1	3
3	REACTOME_P53_DEPENDENT_G1_DNA_DAMAGE_RESPONSE	3/98	14/1659	0,0452	0,2404	0,2054	PSMD5/PSMA6/PSMB1	3
3	REACTOME_P53_INDEPENDENT_G1_S_DNA_DAMAGE_CHECKPOINT	3/98	14/1659	0,0452	0,2404	0,2054	PSMD5/PSMA6/PSMB1	3
3	REACTOME_PLATELET_AGGREGATION_PLUG_FORMATION	3/98	14/1659	0,0452	0,2404	0,2054	CSK/FGB/FGG	3
3	REACTOME_RECRUITMENT_OF_MITOTIC_CENTROSOME_PROTEINS_AND_COMPLEXES	3/98	14/1659	0,0452	0,2404	0,2054	YWHAE/PPP2R1A/PAFAH1B1	3
3	REACTOME_VIF_MEDIATED_DEGRADATION_OF_APOBEC3G	3/98	14/1659	0,0452	0,2404	0,2054	PSMD5/PSMA6/PSMB1	3
3	KEGG_UBIQUITIN_MEDIATED_PROTEOLYSIS	3/98	15/1659	0,0542	0,2450	0,2093	UBE2N/UBA7/UBE2L3	3
3	REACTOME_ACTIVATION_OF_NF_KAPPAB_IN_B_CELLS	3/98	15/1659	0,0542	0,2450	0,2093	PSMD5/PSMA6/PSMB1	3
3	REACTOME_CROSS_PRESENTATION_OF_SOLUBLE_EXOGENOUS_ANTIGENS_ENDOSOMES	3/98	15/1659	0,0542	0,2450	0,2093	PSMD5/PSMA6/PSMB1	3
3	REACTOME_CYCLIN_E_ASSOCIATED_EVENTS_DURING_G1_S_TRANSITION_	3/98	15/1659	0,0542	0,2450	0,2093	PSMD5/PSMA6/PSMB1	3
3	REACTOME_DOWNSTREAM_SIGNALING_EVENTS_OF_B_CELL_RECEPTOR_BCR	3/98	15/1659	0,0542	0,2450	0,2093	PSMD5/PSMA6/PSMB1	3
3	REACTOME_MITOTIC_G2_G2_M_PHASES	3/98	15/1659	0,0542	0,2450	0,2093	YWHAE/PPP2R1A/PAFAH1B1	3
3	REACTOME_PYRUVATE_METABOLISM_AND_CITRIC_ACID_TCA_CYCLE	3/98	15/1659	0,0542	0,2450	0,2093	DLD/IDH1/LDHA	3
3	REACTOME_REGULATION_OF_MITOTIC_CELL_CYCLE	3/98	15/1659	0,0542	0,2450	0,2093	PSMD5/PSMA6/PSMB1	3
3	REACTOME_SCF_BETA_TRCP_MEDIATED_DEGRADATION_OF_EMI1	3/98	15/1659	0,0542	0,2450	0,2093	PSMD5/PSMA6/PSMB1	3

3	REACTOME_SCFSKP2_MEDIATED_DEGRADATION_OF_P27_P21	3/98	15/1659	0,0542	0,2450	0,2093	PSMD5/PSMA6/PSMB1	3
3	REACTOME_REGULATION_OF_MRNA_STABILITY_BY_PROTEINS_THAT_BIND_AU_RICH_ELEMENTS	4/98	25/1659	0,0556	0,2479	0,2118	PSMD5/PSMA6/PSMB1/KHSRP	4
5	KEGG_ARGININE_AND_PROLINE_METABOLISM	5/101	14/1659	0,0010	0,1739	0,1645	LAP3/ASS1/ALDH2/ACY1/ALDH7A1	5
5	REACTOME_PHOSPHOLIPID_METABOLISM	6/101	22/1659	0,0015	0,1739	0,1645	ARSA/HEXB/ARSB/PLD3/PLD4/CHKB	6
6	NABA_CORE_MATRISOME	38/223	145/1659	0,0000	0,0036	0,0035	IGFBP5/NID2/MXRA5/COL1A1/SPARC/IGFBP2/COL21A1/LAMA5/EMILIN2/CILP/COL5A3/FRAS1/TNC/SLIT1/IGFBP4/SPON2/CILP2/IGFBP7/COL1A2/COL14A1/COL6A2/IGFBP6/LAMB2/PODN/FBN1/THBS4/PRELP/MFAP5/MEPE/SMOC1/COL6A1/MMRN2/COL16A1/COL5A2/EMILIN1/IGFBP3/LTBP1/HMCN2	38
6	NABA_COLLAGENS	9/223	19/1659	0,0003	0,0443	0,0432	COL1A1/COL21A1/COL5A3/COL1A2/COL14A1/COL6A2/COL6A1/COL16A1/COL5A2	9
6	NABA_ECM_GLYCOPROTEINS	27/223	108/1659	0,0006	0,0443	0,0432	IGFBP5/NID2/MXRA5/SPARC/IGFBP2/LAMA5/EMILIN2/CILP/FRAS1/TNC/SLIT1/IGFBP4/SPON2/CILP2/IGFBP7/IGFBP6/LAMB2/FBN1/THBS4/MFAP5/MEPE/SMOC1/MMRN2/EMILIN1/IGFBP3/LTBP1/HMCN2	27
6	REACTOME_REGULATION_OF_INSULIN_LIKE_GROWTH_FACTOR_IGF_ACTIVITY_BY_INSULIN_LIKE_GROWTH_FACTOR_BINDING_PROTEINS_IGFBPS	7/223	13/1659	0,0006	0,0443	0,0432	MMP2/IGFBP5/IGFBP2/IGFBP4/IGFBP6/PLG/IGFBP3	7
6	KEGG_ECM_RECEPTOR_INTERACTION	15/223	47/1659	0,0007	0,0443	0,0432	COL1A1/LAMA5/SDC1/COL5A3/TNC/COL1A2/COL6A2/SDC2/LAMB2/DAG1/THBS4/COL6A1/SDC4/COL5A2/CD44	15
6	PID_SYNDECAN_1_PATHWAY	10/223	26/1659	0,0012	0,0587	0,0572	TGFB1/COL1A1/LAMA5/SDC1/COL1A2/COL14A1/COL6A2/COL6A1/COL16A1/COL5A2	10
6	PID_INTEGRIN3_PATHWAY	10/223	28/1659	0,0023	0,0971	0,0947	COL1A1/SDC1/TNC/COL1A2/FBN1/PDGFB/PLAUR/TGFBR2/VEGFA/SDC4	10
6	REACTOME_EXTRACELLULAR_MATRIX_ORGANIZATION	13/223	44/1659	0,0036	0,1363	0,1330	MMP2/MMP15/COL1A1/COL21A1/TIMP2/COL5A3/COL1A2/COL14A1/COL6A2/PLG/COL6A1/COL16A1/COL5A2	13
6	PID_GLYPICAN_1PATHWAY	5/223	10/1659	0,0060	0,1839	0,1794	TGFB1/APP/TGFBR2/VEGFA/PRNP	5
6	REACTOME_NCAM1_INTERACTIONS	6/223	14/1659	0,0065	0,1839	0,1794	COL1A1/COL1A2/COL6A2/COL6A1/COL5A2/PRNP	6
6	PID_AVB3_INTEGRIN_PATHWAY	10/223	32/1659	0,0068	0,1839	0,1794	COL1A1/SDC1/COL1A2/COL14A1/COL6A2/TGFBR2/COL6A1/VEGFA/COL16A1/COL5A2	10
6	KEGG_CYTOKINE_CYTOKINE_RECEPTOR_INTERACTION	15/223	58/1659	0,0074	0,1839	0,1794	RELT/TGFB1/CCL24/TNFRSF13B/CD27/VEGFC/PPBP/TNFRSF21/PDGFB/PDGFA/TGFBR2/VEGFA/TNFRSF19/CXCL12/TNFSF12	15
6	REACTOME_GLYCOSAMINOGLYCAN_METABOLISM	12/223	44/1659	0,0104	0,2285	0,2229	SDC1/SLC9A1/B3GNT2/SDC2/CSGALNACT1/PRELP/SDC4/CHST3/EXT1/ST3GAL6/CD44/B3GNT7	12
6	REACTOME_COLLAGEN_FORMATION	9/223	29/1659	0,0107	0,2285	0,2229	COL1A1/COL21A1/COL5A3/COL1A2/COL14A1/COL6A2/COL6A1/COL16A1/COL5A2	9
7	REACTOME_MUSCLE_CONTRACTION	12/229	29/1659	0,0002	0,0520	0,0509	MYL2/MYL9/MYL3/MYL1/MYLK/TPM2/CALD1/TPM3/DES/MYH11/MYH8/TNNT1	12
7	KEGG_CARDIAC_MUSCLE_CONTRACTION	8/229	15/1659	0,0003	0,0520	0,0509	MYL2/ATP1B3/MYL3/MYH7/CACNA2D1/TPM2/ATP1B1/TPM3	8
7	REACTOME_BASIGIN_INTERACTIONS	6/229	10/1659	0,0008	0,0557	0,0546	ATP1B3/ITGB1/BSG/CAV1/ATP1B1/L1CAM	6
7	REACTOME_STRIATED_MUSCLE_CONTRACTION	8/229	17/1659	0,0009	0,0557	0,0546	MYL2/MYL3/MYL1/TPM2/TPM3/DES/MYH8/TNNT1	8
7	KEGG_DILATED_CARDIOMYOPATHY	10/229	25/1659	0,0010	0,0557	0,0546	MYL2/MYL3/ITGB1/TTN/MYH7/CACNA2D1/TPM2/TPM3/EMD/DES	10

7	KEGG_HYPERTROPHIC_CARDIOMYOPATHY_HCM	10/229	25/1659	0,0010	0,0557	0,0546	MYL2/MYL3/ITGB1/TTN/MYH7/CACNA2D1/TPM2/TPM3/EMD/DES	10
7	REACTOME_A_TETRASACCHARIDE_LINKER_SEQUENCE_IS_REQUIRED_FOR_GAG_SYNTHESIS	6/229	12/1659	0,0029	0,1361	0,1332	DCN/B3GAT3/CSPG4/BGN/HSPG2/AGRN	6
7	PID_INTEGRIN_A4B1_PATHWAY	7/229	16/1659	0,0033	0,1361	0,1332	MYH2/VCAM1/CRK/ITGB1/IGSF8/THBS2/JAM2	7
7	REACTOME_HEPARAN_SULFATE_HEPARIN_HS_GAG_METABOLISM	8/229	21/1659	0,0047	0,1631	0,1597	DCN/HS6ST1/B3GAT3/CSPG4/BGN/HSPG2/AGRN/EXT2	8
7	KEGG_VIRAL_MYOCARDITIS	10/229	30/1659	0,0049	0,1631	0,1597	MYH1/MYH2/CXADR/CD55/EIF4G1/CAV1/MYH7/MYH11/MYH8/HLA-B	10
7	PID_EPHA_FWDPATHWAY	5/229	10/1659	0,0067	0,2013	0,1971	EPHA1/EPHA4/CRK/EPHA7/EPHA6	5
8	REACTOME_PREFOLDIN_MEDIATED_TRANSFER_OF_SUBSTRATE_TO_CCT_TRIC	10/293	10/1659	0,0000	0,0000	0,0000	TUBA4A/CCT7/CCT6A/CCT5/CCT8/CCT3/CCT2/TCP1/ACTB/CCT4	10
8	REACTOME_PROTEIN_FOLDING	10/293	13/1659	0,0000	0,0009	0,0008	TUBA4A/CCT7/CCT6A/CCT5/CCT8/CCT3/CCT2/TCP1/ACTB/CCT4	10
8	PID_PDGFRB_PATHWAY	19/293	43/1659	0,0000	0,0052	0,0047	MAPK1/YWHAQ/YWHAH/ACTN4/ARPC1B/ACTR3/STAT3/IQGAP1/ARHGDIA/YWHAB/YWHAG/YWHAZ/GRB2/SFN/ARPC5/ARPC4/LYN/DNM2/PTPRJ	19
8	BIOCARTA_RHO_PATHWAY	11/293	19/1659	0,0001	0,0089	0,0080	VCL/PFN1/ARPC1B/ACTR3/CFL1/ARHGAP1/TLN1/ARHGEF1/ARPC5/GSN/ARPC4	11
8	KEGG_SYSTEMIC_LUPUS_ERYTHEMATOSUS	13/293	26/1659	0,0001	0,0106	0,0095	C5/C8G/ACTN4/C6/FCGR3B/C1S/ACTN2/FCGR3A/C1QC/ACTN1/C4A/C4B/H2AFY	13
8	PID_RAC1_PATHWAY	10/293	17/1659	0,0002	0,0106	0,0095	ARPC1B/ACTR3/STAT3/IQGAP1/ARHGDIA/CFL1/PAK2/ARPC5/NCF2/ARPC4	10
8	PID_FOXO_PATHWAY	8/293	12/1659	0,0002	0,0131	0,0117	YWHAQ/CAT/YWHAH/YWHAB/YWHAG/YWHAZ/SFN/XPO1	8
8	PID_BETA_CATENIN_NUC_PATHWAY	9/293	15/1659	0,0003	0,0142	0,0127	YWHAQ/YWHAH/YWHAB/YWHAG/YWHAZ/SFN/MMP9/XPO1/VCAN	9
8	PID_ERBB1_DOWNSTREAM_PATHWAY	15/293	35/1659	0,0004	0,0179	0,0160	MAPK1/YWHAQ/YWHAH/ARPC1B/ACTR3/STAT3/IQGAP1/CAPN2/YWHAB/YWHAG/YWHAZ/GRB2/SFN/ARPC5/ARPC4	15
8	REACTOME_PURINE_METABOLISM	9/293	16/1659	0,0005	0,0200	0,0179	ADSL/ATIC/CAT/HPRT1/IMPDH2/PNP/ADSS/ADA/APRT	9
8	SIG_INSULIN_RECEPTOR_PATHWAY_IN_CARDIAC_MYOCYTES	9/293	16/1659	0,0005	0,0200	0,0179	MAPK1/YWHAQ/YWHAH/YWHAB/YWHAG/YWHAZ/GRB2/SFN/CAP1	9
8	BIOCARTA_CHREBP2_PATHWAY	7/293	11/1659	0,0009	0,0297	0,0266	YWHAQ/YWHAH/YWHAB/FASN/YWHAG/YWHAZ/PRKAR1A	7
8	SIG_PIP3_SIGNALING_IN_CARDIAC_MYOCTES	8/293	15/1659	0,0018	0,0485	0,0434	YWHAQ/YWHAH/YWHAB/YWHAG/YWHAZ/PAK2/GRB2/SFN	8
8	BIOCARTA_MPR_PATHWAY	7/293	12/1659	0,0018	0,0485	0,0434	MAPK1/ARPC1B/ACTR3/PRKAR1A/ARPC5/CAP1/ARPC4	7
8	ST_PHOSPHOINOSITIDE_3_KINASE_PATHWAY	7/293	12/1659	0,0018	0,0485	0,0434	YWHAQ/YWHAH/YWHAB/YWHAG/YWHAZ/GRB2/SFN	7
8	KEGG_PATHOGENIC_ESCHERICHIA_COLI_INFECTION	10/293	22/1659	0,0022	0,0573	0,0512	YWHAQ/TUBA4A/ARPC1B/YWHAZ/NCL/HCLS1/TUBB/ACTB/ARPC5/ARPC4	10
8	PID_NFAT_3PATHWAY	8/293	16/1659	0,0030	0,0726	0,0649	YWHAQ/YWHAH/KPNB1/YWHAB/YWHAG/YWHAZ/SFN/XPO1	8
8	REACTOME_SIGNALING_BY_SCF_KIT	7/293	13/1659	0,0033	0,0745	0,0666	MAPK1/STAT3/YWHAB/GRB2/MMP9/PTPN6/LYN	7
8	KEGG_AMINOACYL_TRNA_BIOSYNTHESIS	8/293	17/1659	0,0048	0,1042	0,0932	IARS2/SARS/AARS/KARS/YARS/CARS/LARS/HARS	8
8	PID_LKB1_PATHWAY	7/293	14/1659	0,0055	0,1082	0,0967	YWHAQ/YWHAH/CAB39/YWHAB/YWHAG/YWHAZ/SFN	7

8	PID_CDC42_PATHWAY	9/293	21/1659	0,0060	0,1082	0,0967	MAPK1/ARPC1B/ACTR3/IQGAP1/ARHGDIA/CFL1/PAK2/ARPC5/ARPC4	9
8	KEGG_CELL_CYCLE	6/293	11/1659	0,0060	0,1082	0,0967	YWHAQ/YWHAH/YWHAB/YWHAG/YWHAZ/SFN	6
8	PID_INSULIN_GLUCOSE_PATHWAY	6/293	11/1659	0,0060	0,1082	0,0967	YWHAQ/YWHAH/YWHAB/YWHAG/YWHAZ/SFN	6
8	REACTOME_METABOLISM_OF_NUCLEOTIDES	11/293	29/1659	0,0073	0,1262	0,1128	NME1/ADSL/GSR/ATIC/CAT/HPRT1/IMPDH2/PNP/ADSS/ADA/APRT	11
8	KEGG_PENTOSE_PHOSPHATE_PATHWAY	7/293	15/1659	0,0088	0,1346	0,1204	ALDOC/PGD/TALDO1/ALDOB/PGM2/G6PD/TKT	7
8	KEGG_ADHERENS_JUNCTION	10/293	26/1659	0,0094	0,1346	0,1204	VCL/MAPK1/ACTN4/IQGAP1/ACP1/ACTB/ACTN2/ACTN1/PTPN6/PTPRJ	10
8	KEGG_PURINE_METABOLISM	11/293	30/1659	0,0098	0,1346	0,1204	NME1/ADSL/NME3/ATIC/HPRT1/IMPDH2/PNP/ADSS/ADA/APRT/ITPA	11
8	PID_ERBB1_RECEPTOR_PROXIMAL_PATHWAY	6/293	12/1659	0,0103	0,1346	0,1204	MAPK1/STAT3/TLN1/GRB2/GSN/PTPN6	6
8	SIG_CHEMOTAXIS	6/293	12/1659	0,0103	0,1346	0,1204	ACTR3/CFL1/ARHGAP1/PAK2/GDI2/GDI1	6
8	BIOCARTA_INTEGRIN_PATHWAY	8/293	19/1659	0,0108	0,1346	0,1204	VCL/MAPK1/CAPNS1/CAPN1/TLN1/GRB2/ACTN2/ACTN1	8
8	KEGG_LEISHMANIA_INFECTION	8/293	19/1659	0,0108	0,1346	0,1204	MAPK1/FCGR3B/ITGB2/NCF2/FCGR3A/NCF4/PTPN6/ITGAM	8
8	REACTOME_NGF_SIGNALLING_VIA_TRKA_FROM_THE_PLASMA_MEMBRANE	8/293	19/1659	0,0108	0,1346	0,1204	MAPK1/DUSP3/STAT3/CLTC/YWHAB/GRB2/PRKAR1A/DNM2	8
8	REACTOME_TRNA_AMINOACYLATION	8/293	19/1659	0,0108	0,1346	0,1204	IARS2/SARS/AARS/KARS/YARS/CARS/LARS/HARS	8
8	REACTOME_INFLUENZA_LIFE_CYCLE	12/293	35/1659	0,0128	0,1517	0,1356	RPS16/IPO5/CLTC/KPNB1/RPS15A/CALR/RPS2/RPS21/RPSA/XPO1/RPS18/RPS3	12
8	REACTOME_SIGNALLING_BY_NGF	11/293	31/1659	0,0129	0,1517	0,1356	MAPK1/DUSP3/STAT3/CLTC/ARHGDIA/YWHAB/ADAM17/ARHGEF1/GRB2/PRKAR1A/DNM2	11
8	REACTOME_FORMATION_OF_THE_TERNARY_COMPLEX_AND_SUBSEQUENTLY_THE_43S_COMPLEX	7/293	16/1659	0,0134	0,1532	0,1370	RPS16/RPS15A/RPS2/RPS21/RPSA/RPS18/RPS3	7
8	REACTOME_SIGNALING_BY_ILS	9/293	24/1659	0,0163	0,1728	0,1545	MAPK1/IL6/STAT3/YWHAB/YWHAZ/GRB2/PTPN6/CASP1/LYN	9
8	BIOCARTA_MCALPAIN_PATHWAY	6/293	13/1659	0,0164	0,1728	0,1545	MAPK1/CAPNS1/CAPN1/CAPN2/TLN1/PRKAR1A	6
8	PID_AR_PATHWAY	6/293	13/1659	0,0164	0,1728	0,1545	APPL1/HNRNPA1/XRCC6/GSN/XRCC5/PA2G4	6
8	KEGG_REGULATION_OF_ACTIN_CYTOSKELETON	19/293	67/1659	0,0185	0,1816	0,1624	VCL/MAPK1/PFN1/ACTN4/ARPC1B/IQGAP1/ITGA2/ITGB2/CFL1/PAK2/ARHGEF1/ACTB/ARPC5/MSN/ACTN2/GSN/ACTN1/ARPC4/ITGAM	19
8	BIOCARTA_ACTINY_PATHWAY	5/293	10/1659	0,0194	0,1816	0,1624	ARPC1B/ACTR3/ARPC5/PSMA7/ARPC4	5
8	PID_TELOMERASE_PATHWAY	5/293	10/1659	0,0194	0,1816	0,1624	MAPK1/NCL/HNRNPC/XRCC6/XRCC5	5
8	REACTOME_SIGNALING_BY_RHO_GTPASES	5/293	10/1659	0,0194	0,1816	0,1624	ARHGDIB/ARHGDIA/ARHGAP1/GDI2/GDI1	5
8	REACTOME_CYTOSOLIC_TRNA_AMINOACYLATION	7/293	17/1659	0,0194	0,1816	0,1624	SARS/AARS/KARS/YARS/CARS/LARS/HARS	7
8	KEGG_GLYCOLYSIS_GLUCONEOGENESIS	11/293	33/1659	0,0211	0,1934	0,1729	ALDOC/GAPDH/LDHB/ENO1/ACSS2/HK3/ADH5/PGAM1/ALDOB/PGM2/HK1	11
8	REACTOME_REGULATION_OF_MRNA_STABILITY_BY_PROTEINS_THAT_BIND_AU_RICH_ELEMENTS	9/293	25/1659	0,0216	0,1936	0,1731	PSMA3/PSMD10/HSPA8/YWHAB/YWHAZ/TNPO1/PSMA7/XPO1/ELAVL1	9
8	BIOCARTA_CLASSIC_PATHWAY	6/293	14/1659	0,0245	0,2145	0,1918	C5/C6/C1S/C1QC/C4A/C4B	6

8	PID_MTOR_4PATHWAY	7/293	18/1659	0,0271	0,2323	0,2077	MAPK1/YWHAQ/YWHAH/YWHAB/YWHAG/YWHAZ/SFN	7
8	KEGG_FC_GAMMA_R_MEDIATED_PHAGOCYTOSIS	9/293	26/1659	0,0281	0,2361	0,2111	MAPK1/ARPC1B/CFL1/ARPC5/FCGR3A/GSN/ARPC4/LYN/DNM2	9
8	BIOCARTA_LAIR_PATHWAY	5/293	11/1659	0,0305	0,2369	0,2119	C5/IL6/C6/KNG1/ITGB2	5
8	BIOCARTA_UCALPAIN_PATHWAY	5/293	11/1659	0,0305	0,2369	0,2119	CAPNS1/CAPN1/TLN1/ACTN2/ACTN1	5
8	REACTOME_DNA_REPAIR	5/293	11/1659	0,0305	0,2369	0,2119	RPA3/DDB1/XRCC6/RPA2/XRCC5	5
8	REACTOME_IRON_UPTAKE_AND_TRANSPORT	5/293	11/1659	0,0305	0,2369	0,2119	CP/ATP6V1A/ATP6V1B2/ATP6V1C1/FTL	5
10	KEGG_PYRUVATE_METABOLISM	7/106	18/1659	0,0001	0,0187	0,0185	AKR1B1/GRHPR/MDH2/ALDH9A1/ME1/GLO1/HAGH	7
10	REACTOME_CITRIC_ACID_CYCLE_TCA_CYCLE	5/106	10/1659	0,0002	0,0279	0,0276	ACO2/MDH2/FH/SUCLG1/SUCLG2	5
10	KEGG_CITRATE_CYCLE_TCA_CYCLE	5/106	14/1659	0,0012	0,0900	0,0890	ACO2/MDH2/FH/SUCLG1/SUCLG2	5
10	KEGG_FRUCTOSE_AND_MANNOSE_METABOLISM	5/106	14/1659	0,0012	0,0900	0,0890	TPI1/SORD/PFKL/AKR1B1/AKR1B10	5
10	REACTOME_PYRUVATE_METABOLISM_AND_CITRIC_ACID_TCA_CYCLE	5/106	15/1659	0,0017	0,1026	0,1014	ACO2/MDH2/FH/SUCLG1/SUCLG2	5
10	REACTOME_TCA_CYCLE_AND_RESPIRATORY_ELECTRON_TRANSPORT	5/106	18/1659	0,0042	0,2089	0,2065	ACO2/MDH2/FH/SUCLG1/SUCLG2	5

Table S5- Patient P03-Enriched pathways for each cluster with the respective Gene Ratio, Background ratio (Bg Ratio), p-value, p-adjust, q-value, Gene Id and counts (number of genes (proteins) per pathways). The highlighted pathways were the one selected for the bar plots graphs.

Cluster	Description	GeneRatio	BgRatio	pvalue	p.adjust	qvalue	geneID	Count
1	REACTOME_INTEGRIN_ALPHAIIB_BETA3_SIGNALING	4/36	11/1407	1,1E-04	1,6E-02	1,5E-02	RAP1B/FGB/FGG/APBB1IP	4
1	REACTOME_PLATELET_AGGREGATION_PLUG_FORMATION	4/36	14/1407	3,0E-04	2,3E-02	2,2E-02	RAP1B/FGB/FGG/APBB1IP	4
2	REACTOME_INSULIN_RECEPTOR_SIGNALLING_CASCADE	5/58	15/1407	2,2E-04	3,3E-02	3,1E-02	CAB39/EIF4B/YWHAB/EIF4G1/CRK	5
2	REACTOME_SIGNALING_BY_INSULIN_RECEPTOR	5/58	16/1407	3,1E-04	3,3E-02	3,1E-02	CAB39/EIF4B/YWHAB/EIF4G1/CRK	5
4	PID_CERAMIDE_PATHWAY	4/71	11/1407	1,5E-03	2,4E-01	2,4E-01	MAPK1/IGF1/PAWR/PDGFA	4
4	KEGG_GLIOMA	4/71	12/1407	2,2E-03	2,4E-01	2,4E-01	MAPK1/IGF1/PDGFA/CALML5	4
7	REACTOME_EXTRACELLULAR_MATRIX_ORGANIZATION	15/85	41/1407	2,7E-09	4,1E-07	3,9E-07	MMP11/TIMP1/MMP2/PCOLCE/COL6A3/PCOLCE2/MMP3/COL3A1/PLG/COL12A1/COL6A1/COL5A1/KLKB1/COL1A2/PRSS1	15
7	REACTOME_DEGRADATION_OF_THE_EXTRACELLULAR_MATRIX	7/85	13/1407	2,9E-06	2,2E-04	2,1E-04	MMP11/TIMP1/MMP2/MMP3/PLG/KLKB1/PRSS1	7
7	NABA_COLLAGENS	7/85	20/1407	9,4E-05	4,7E-03	4,5E-03	COL6A3/COL3A1/COL12A1/COL6A6/COL6A1/COL5A1/COL1A2	7
7	REACTOME_COLLAGEN_FORMATION	8/85	28/1407	1,5E-04	5,6E-03	5,3E-03	PCOLCE/COL6A3/PCOLCE2/COL3A1/COL12A1/COL6A1/COL5A1/COL1A2	8
7	PID_AVB3_INTEGRIN_PATHWAY	8/85	31/1407	3,2E-04	9,8E-03	9,3E-03	VCL/COL6A3/COL3A1/COL12A1/COL6A1/ANGPTL3/COL5A1/COL1A2	8
7	REACTOME_NCAM1_INTERACTIONS	5/85	14/1407	9,3E-04	2,4E-02	2,2E-02	COL6A3/COL3A1/COL6A1/COL5A1/COL1A2	5
7	NABA_CORE_MATRISOME	18/85	141/1407	1,2E-03	2,6E-02	2,4E-02	PCOLCE/COL6A3/PCOLCE2/COL3A1/PRG2/ADIPOQ/COL12A1/PRELP/RSPO1/COL6A6/COL6A1/ECM1/NTNG1/COL5A1/SPARC/FRAS1/LUM/COL1A2	18
7	PID_SYNDECAN_1_PATHWAY	6/85	25/1407	2,8E-03	5,4E-02	5,1E-02	COL6A3/COL3A1/COL12A1/COL6A1/COL5A1/COL1A2	6
7	PID_P75_NTR_PATHWAY	4/85	13/1407	5,8E-03	9,9E-02	9,3E-02	RTN4R/MMP3/PLG/ADAM17	4
7	REACTOME_NCAM_SIGNALING_FOR_NEURITE_OUT_GROWTH	5/85	21/1407	6,7E-03	1,0E-01	9,7E-02	COL6A3/COL3A1/COL6A1/COL5A1/COL1A2	5
7	REACTOME_SIGNALING_BY_PDGF	6/85	30/1407	7,5E-03	1,0E-01	9,8E-02	COL6A3/COL3A1/PLG/COL6A1/COL5A1/COL1A2	6
7	NABA_ECM_REGULATORS	14/85	118/1407	8,8E-03	1,1E-01	1,1E-01	MMP11/TIMP1/MMP2/SERPINF1/SERPINA4/MMP3/PLG/ADAM17/SERPINA7/SERPINA5/SERPINA6/SERPINA3/MASP2/PRSS1	14
7	KEGG_TYROSINE_METABOLISM	3/85	10/1407	1,9E-02	2,2E-01	2,1E-01	FAH/HPD/DBH	3
8	KEGG_GLYCOLYSIS_GLUCONEOGENESIS	13/141	29/1407	1,0E-06	1,9E-04	1,5E-04	ADH1B/DLD/TPI1/ENO2/ENO1/ADH5/AKR1A1/ALDH1A3/ALDOA/ALDH9A1/PGAM1/PGK1/PGM2	13
8	KEGG_DRUG_METABOLISM_CYTOCHROME_P450	7/141	10/1407	8,2E-06	7,6E-04	6,2E-04	ADH1B/GSTT1/GSTM3/ADH5/ALDH1A3/AOX1/GSTP1	7
8	KEGG_PYRUVATE_METABOLISM	8/141	16/1407	5,4E-05	3,3E-03	2,7E-03	DLD/AKR1B1/GRHPR/MDH2/ALDH9A1/GLO1/HAGH/MDH1	8
8	REACTOME_GLUCONEOGENESIS	8/141	17/1407	9,3E-05	3,6E-03	3,0E-03	TPI1/ENO2/ENO1/MDH2/ALDOA/PGAM1/PGK1/MDH1	8
8	REACTOME_GLUCOSE_METABOLISM	10/141	26/1407	9,7E-05	3,6E-03	3,0E-03	TPI1/ENO2/ENO1/MDH2/ALDOA/UGP2/PGAM1/PGK1/PGM2/MDH1	10

8	KEGG_METABOLISM_OF_XENOBIOTICS_BY_CYTOCHROME_P450	6/141	10/1407	1,4E-04	4,2E-03	3,5E-03	ADH1B/GSTT1/GSTM3/ADH5/ALDH1A3/GSTP1	6
8	PID_FOXO_PATHWAY	6/141	11/1407	2,8E-04	7,3E-03	6,0E-03	YWHAQ/YWHAH/YWHAE/YWHAG/YWHAZ/SOD2	6
8	KEGG_CITRATE_CYCLE_TCA_CYCLE	6/141	12/1407	5,1E-04	9,4E-03	7,7E-03	DLD/ACO2/IDH1/ACO1/MDH2/MDH1	6
8	PID_LKB1_PATHWAY	6/141	12/1407	5,1E-04	9,4E-03	7,7E-03	YWHAQ/YWHAH/YWHAE/YWHAG/YWHAZ/EZR	6
8	REACTOME_GLYCOLYSIS	6/141	12/1407	5,1E-04	9,4E-03	7,7E-03	TPI1/ENO2/ENO1/ALDOA/PGAM1/PGK1	6
8	REACTOME_BIOLOGICAL_OXIDATIONS	8/141	22/1407	7,9E-04	1,3E-02	1,1E-02	ADH1B/MAT2B/GCLC/GSS/AHCY/MAT2A/UGP2/GSTP1	8
8	PID_MTOR_4PATHWAY	7/141	18/1407	1,1E-03	1,5E-02	1,3E-02	YWHAQ/YWHAH/YWHAE/EIF4A1/YWHAG/CYCS/YWHAZ	7
8	KEGG_PYRIMIDINE_METABOLISM	6/141	14/1407	1,4E-03	1,5E-02	1,3E-02	DPYD/NME1/NT5C/CMPK1/AK3/TXNRD1	6
8	PID_NFAT_3PATHWAY	6/141	14/1407	1,4E-03	1,5E-02	1,3E-02	YWHAQ/YWHAH/YWHAE/YWHAG/YWHAZ/PPP3CA	6
8	SIG_INSULIN_RECEPTOR_PATHWAY_IN_CARDIAC_MYOCYTES	6/141	14/1407	1,4E-03	1,5E-02	1,3E-02	YWHAQ/YWHAH/YWHAE/YWHAG/YWHAZ/SERPINB6	6
8	KEGG_CELL_CYCLE	5/141	10/1407	1,6E-03	1,5E-02	1,3E-02	YWHAQ/YWHAH/YWHAE/YWHAG/YWHAZ	5
8	KEGG_TYROSINE_METABOLISM	5/141	10/1407	1,6E-03	1,5E-02	1,3E-02	ADH1B/MIF/ADH5/ALDH1A3/AOX1	5
8	PID_INSULIN_GLUCOSE_PATHWAY	5/141	10/1407	1,6E-03	1,5E-02	1,3E-02	YWHAQ/YWHAH/YWHAE/YWHAG/YWHAZ	5
8	REACTOME_PHASE_II_CONJUGATION	7/141	19/1407	1,6E-03	1,5E-02	1,3E-02	MAT2B/GCLC/GSS/AHCY/MAT2A/UGP2/GSTP1	7
8	BIOCARTA_CHREBP2_PATHWAY	5/141	11/1407	2,6E-03	2,3E-02	1,9E-02	YWHAQ/YWHAH/YWHAE/YWHAG/YWHAZ	5
8	ST_PHOSPHOINOSITIDE_3_KINASE_PATHWAY	5/141	11/1407	2,6E-03	2,3E-02	1,9E-02	YWHAQ/YWHAH/YWHAE/YWHAG/YWHAZ	5
8	REACTOME_METABOLISM_OF_NUCLEOTIDES	8/141	26/1407	2,7E-03	2,3E-02	1,9E-02	DPYD/NME1/NT5C/AMPD2/CMPK1/AK1/GART/TXNRD1	8
10	NABA_ECM_GLYCOPROTEINS	23/147	102/1407	1,6E-04	4,3E-02	4,2E-02	AGRN/NID2/COCH/LAMA4/IGFBP5/FGL2/PXDN/EMILIN2/LAMC1/CILP/LTBP2/NID1/MMRN1/SPARCL1/FNDC1/THBS4/MFAP5/MEPE/SMOC1/SRPX/EMILIN1/FBLN2/LTBP1	23
10	NABA_CORE_MATRISOME	27/147	141/1407	7,5E-04	1,0E-01	9,9E-02	AGRN/DCN/NID2/COCH/LAMA4/IGFBP5/FGL2/PXDN/EMILIN2/LAMC1/CILP/LTBP2/NID1/MMRN1/SPARCL1/FNDC1/THBS4/MFAP5/COL4A2/MEPE/SMOC1/COL15A1/SRPX/EMILIN1/FBLN2/LTBP1/PRG4	27
11	REACTOME_POST_TRANSLATIONAL_PROTEIN_MODIFICATION	8/55	52/1407	6,4E-04	8,0E-02	7,7E-02	MUC16/ARSA/RPN2/ARSB/GALNT1/B3GNT8/GALNT6/MAN1B1	8
11	REACTOME_O_LINKED_GLYCOSYLATION_OF_MUCINS	4/55	13/1407	1,2E-03	8,0E-02	7,7E-02	MUC16/GALNT1/B3GNT8/GALNT6	4
12	REACTOME_PTM_GAMMA_CARBOXYLATION_HYPUSINE_FORMATION_AND_ARYLSULFATASE_ACTIVATION	6/88	12/1407	3,5E-05	8,5E-03	8,1E-03	F9/PROC/F2/PROZ/F10/F7	6
12	REACTOME_SEMAPHORIN_INTERACTIONS	7/88	27/1407	9,4E-04	1,1E-01	1,1E-01	PLXND1/SEMA6D/RHOA/PTPRC/CFL1/PAK2/TLN1	7
12	BIOCARTA_EXTRINSIC_PATHWAY	4/88	10/1407	2,2E-03	1,6E-01	1,6E-01	PROC/F2/F10/F7	4
12	REACTOME_FORMATION_OF_FIBRIN_CLOT_CLOTTING_CASCADE	6/88	24/1407	2,7E-03	1,6E-01	1,6E-01	F9/PROC/F13A1/F2/F10/F7	6
12	REACTOME_COMMON_PATHWAY	4/88	11/1407	3,4E-03	1,6E-01	1,6E-01	PROC/F13A1/F2/F10	4
12	BIOCARTA_AMI_PATHWAY	4/88	12/1407	4,8E-03	2,0E-01	1,9E-01	PROC/F2/F10/F7	4

13	REACTOME_METABOLISM_OF_PROTEINS	21/101	100/1407	2,5E-06	5,4E-04	4,4E-04	RPS12/CCT7/UGGT1/CCT6A/CCT5/CCT8/CCT3/HSPA9/EEF2/RPL4/PABPC1/MPI/EEF1A1/EIF5A/HSPD1/GANAB/CS/RPS21/RPS3A/RPSA/ACTB	21
13	REACTOME_PREFOLDIN_MEDIATED_TRANSFER_OF_SUBSTRATE_TO_CCT_TRIC	6/101	10/1407	2,0E-05	2,2E-03	1,8E-03	CCT7/CCT6A/CCT5/CCT8/CCT3/ACTB	6
13	BIOCARTA_CDC42RAC_PATHWAY	6/101	11/1407	4,1E-05	2,2E-03	1,8E-03	ARPC5/ARPC1B/ACTR3/ARPC2/ACTR2/ARPC4	6
13	BIOCARTA_MPR_PATHWAY	6/101	11/1407	4,1E-05	2,2E-03	1,8E-03	ARPC5/ARPC1B/ACTR3/ARPC2/ACTR2/ARPC4	6
13	REACTOME_NONSENSE_MEDIATED_DECAY_ENHANCED_BY_THE_EXON_JUNCTION_COMPLEX	8/101	21/1407	5,0E-05	2,2E-03	1,8E-03	RPS12/RPL4/PABPC1/PPP2R1A/PPP2R2A/RPS21/RPS3A/RPSA	8
13	REACTOME_PEPTIDE_CHAIN_ELONGATION	7/101	18/1407	1,3E-04	4,7E-03	3,9E-03	RPS12/EEF2/RPL4/EEF1A1/RPS21/RPS3A/RPSA	7
13	REACTOME_INFLUENZA_LIFE_CYCLE	8/101	24/1407	1,5E-04	4,7E-03	3,9E-03	RPS12/CLTC/KPNB1/RPL4/RPS21/RPS3A/RPSA/RAN	8
13	REACTOME_PROTEIN_FOLDING	6/101	14/1407	2,2E-04	5,6E-03	4,6E-03	CCT7/CCT6A/CCT5/CCT8/CCT3/ACTB	6
13	REACTOME_METABOLISM_OF_MRNA	10/101	39/1407	2,6E-04	5,6E-03	4,6E-03	PSMD5/RPS12/RPL4/PABPC1/PPP2R1A/PPP2R2A/RPS21/RPS3A/RPSA/KHSRP	10
13	REACTOME_METABOLISM_OF_RNA	10/101	39/1407	2,6E-04	5,6E-03	4,6E-03	PSMD5/RPS12/RPL4/PABPC1/PPP2R1A/PPP2R2A/RPS21/RPS3A/RPSA/KHSRP	10
13	REACTOME_CELL_CYCLE	8/101	26/1407	2,8E-04	5,6E-03	4,6E-03	PSMD5/HSPA2/PRKACA/PPP2R1A/PPP2R2A/TUBB/PCNA/PAFAH1B1	8
13	PID_RAC1_PATHWAY	6/101	16/1407	5,2E-04	9,4E-03	7,7E-03	ARPC5/ARPC1B/ACTR3/ARPC2/ACTR2/ARPC4	6
13	REACTOME_CELL_CYCLE_MITOTIC	7/101	22/1407	5,6E-04	9,4E-03	7,7E-03	PSMD5/PRKACA/PPP2R1A/PPP2R2A/TUBB/PCNA/PAFAH1B1	7
13	BIOCARTA_RHO_PATHWAY	6/101	17/1407	7,6E-04	1,1E-02	9,2E-03	ARPC5/ARPC1B/ACTR3/ARPC2/ACTR2/ARPC4	6
13	PID_CDC42_PATHWAY	6/101	17/1407	7,6E-04	1,1E-02	9,2E-03	ARPC5/ARPC1B/ACTR3/ARPC2/ACTR2/ARPC4	6
13	PID_ERBB1_DOWNSTREAM_PATHWAY	8/101	30/1407	8,3E-04	1,1E-02	9,4E-03	ARPC5/ARPC1B/ACTR3/ARPC2/PPP2R1A/PPP2R2A/ACTR2/ARPC4	8
13	REACTOME_PYRUVATE_METABOLISM_AND_CITRIC_ACID_TCA_CYCLE	5/101	12/1407	9,1E-04	1,2E-02	9,7E-03	LDHB/IDH2/CS/FH/LDHA	5
13	REACTOME_TRANSLATION	8/101	31/1407	1,1E-03	1,3E-02	1,1E-02	RPS12/EEF2/RPL4/PABPC1/EEF1A1/RPS21/RPS3A/RPSA	8
13	KEGG_AMINOACYL_TRNA_BIOSYNTHESIS	5/101	13/1407	1,4E-03	1,6E-02	1,3E-02	SARS/DARS/TARS/KARS/YARS	5
13	KEGG_PATHOGENIC_ESCHERICHIA_COLI_INFECTION	6/101	19/1407	1,5E-03	1,6E-02	1,3E-02	ARPC5/ARPC1B/ARPC2/TUBB/ACTB/ARPC4	6
13	KEGG_SPLICEOSOME	6/101	20/1407	2,0E-03	2,0E-02	1,6E-02	HSPA2/HNRNPU/PCBP1/HSPA6/HNRNPC/HNRNPK	6
13	REACTOME_CYTOSOLIC_TRNA_AMINOACYLATION	5/101	14/1407	2,1E-03	2,0E-02	1,6E-02	SARS/DARS/TARS/KARS/YARS	5
13	REACTOME_TCA_CYCLE_AND_RESPIRATORY_ELECTRON_TRANSPORT	5/101	14/1407	2,1E-03	2,0E-02	1,6E-02	LDHB/IDH2/CS/FH/LDHA	5
13	REACTOME_MRNA_SPLICING	6/101	21/1407	2,6E-03	2,4E-02	2,0E-02	HNRNPA2B1/HNRNPU/PCBP1/HNRNPC/DHX9/HNRNPK	6
13	REACTOME_TRNA_AMINOACYLATION	5/101	15/1407	2,9E-03	2,5E-02	2,1E-02	SARS/DARS/TARS/KARS/YARS	5
13	REACTOME_MRNA_PROCESSING	6/101	22/1407	3,4E-03	2,8E-02	2,3E-02	HNRNPA2B1/HNRNPU/PCBP1/HNRNPC/DHX9/HNRNPK	6
13	REACTOME_PROCESSING_OF_CAPPED_INTRON_CONTAINING_PRE_MRNA	6/101	22/1407	3,4E-03	2,8E-02	2,3E-02	HNRNPA2B1/HNRNPU/PCBP1/HNRNPC/DHX9/HNRNPK	6

13	KEGG_RIBOSOME	5/101	16/1407	4,0E-03	3,1E-02	2,6E-02	RPS12/RPL4/RPS21/RPS3A/RPSA	5
13	REACTOME_3_UTR_MEDIATED_TRANSLATIONAL_REGULATION	6/101	24/1407	5,5E-03	3,5E-02	2,9E-02	RPS12/RPL4/PABPC1/RPS21/RPS3A/RPSA	6
13	BIOCARTA_CHREBP2_PATHWAY	4/101	11/1407	5,6E-03	3,5E-02	2,9E-02	FASN/PRKACA/PPP2R1A/PPP2R2A	4
13	REACTOME_FORMATION_OF_THE_TERNARY_COMPLEX_AND_SUBSEQUENTLY_THE_43S_COMPLEX	4/101	11/1407	5,6E-03	3,5E-02	2,9E-02	RPS12/RPS21/RPS3A/RPSA	4
13	REACTOME_LOSS_OF_NLP_FROM_MITOTIC_CENTROSOMES	4/101	11/1407	5,6E-03	3,5E-02	2,9E-02	PRKACA/PPP2R1A/TUBB/PAFAH1B1	4
13	REACTOME_MITOTIC_G1_G1_S_PHASES	4/101	11/1407	5,6E-03	3,5E-02	2,9E-02	PSMD5/PPP2R1A/PPP2R2A/PCNA	4
13	REACTOME_MITOTIC_G2_G2_M_PHASES	4/101	11/1407	5,6E-03	3,5E-02	2,9E-02	PRKACA/PPP2R1A/TUBB/PAFAH1B1	4
13	REACTOME_RECRUITMENT_OF_MITOTIC_CENTROSOME_PROTEINS_AND_COMPLEXES	4/101	11/1407	5,6E-03	3,5E-02	2,9E-02	PRKACA/PPP2R1A/TUBB/PAFAH1B1	4
13	REACTOME_ACTIVATION_OF_THE_MRNA_UPON_BINDING_OF_THE_CAP_BINDING_COMPLEX_AND_EIFS_AND_SUBSEQUENT_BINDING_TO_43S	5/101	18/1407	7,0E-03	4,0E-02	3,3E-02	RPS12/PABPC1/RPS21/RPS3A/RPSA	5
13	REACTOME_INFLUENZA_VIRAL_RNA_TRANSCRIPTION_AND_REPLICATION	5/101	18/1407	7,0E-03	4,0E-02	3,3E-02	RPS12/RPL4/RPS21/RPS3A/RPSA	5
13	REACTOME_SRP_DEPENDENT_COTRANSLATIONAL_PROTEIN_TARGETING_TO_MEMBRANE	5/101	18/1407	7,0E-03	4,0E-02	3,3E-02	RPS12/RPL4/RPS21/RPS3A/RPSA	5
13	KEGG_CITRATE_CYCLE_TCA_CYCLE	4/101	12/1407	7,9E-03	4,3E-02	3,6E-02	ACLY/IDH2/CS/FH	4
13	REACTOME_DNA_REPLICATION	4/101	12/1407	7,9E-03	4,3E-02	3,6E-02	PSMD5/PPP2R1A/PCNA/PAFAH1B1	4
13	PID_PDGFRB_PATHWAY	7/101	37/1407	1,4E-02	7,3E-02	6,0E-02	ARPC5/ARPC1B/ACTR3/ARPC2/PPP2R1A/ACTR2/ARPC4	7
13	PID_NFAT_3PATHWAY	4/101	14/1407	1,4E-02	7,5E-02	6,1E-02	KPNB1/PRKACA/CASP3/RAN	4
13	KEGG_STARCH_AND_SUCROSE_METABOLISM	4/101	16/1407	2,3E-02	1,2E-01	9,7E-02	GBE1/PYGB/UGDH/HK1	4
13	REACTOME_TRANSMEMBRANE_TRANSPORT_OF_SMALL_MOLECULES	5/101	24/1407	2,4E-02	1,2E-01	1,0E-01	ATP6V1A/PRKACA/FTL/HK1/TF	5
13	REACTOME_INTEGRATION_OF_ENERGY_METABOLISM	4/101	17/1407	2,9E-02	1,4E-01	1,2E-01	ACLY/FASN/PRKACA/PPP2R1A	4
13	REACTOME_G1_S_TRANSITION	3/101	10/1407	3,0E-02	1,4E-01	1,2E-01	PSMD5/PPP2R1A/PCNA	3
13	REACTOME_MITOTIC_M_M_G1_PHASES	3/101	11/1407	3,9E-02	1,8E-01	1,5E-01	PSMD5/PPP2R1A/PAFAH1B1	3
13	KEGG_FC_GAMMA_R_MEDIATED_PHAGOCYTOSIS	4/101	20/1407	5,0E-02	2,3E-01	1,9E-01	ARPC5/ARPC1B/ARPC2/ARPC4	4
13	REACTOME_FATTY_ACID_TRIACYLGLYCEROL_AND_KETONE_BODY_METABOLISM	3/101	13/1407	6,1E-02	2,7E-01	2,2E-01	ACLY/FASN/ME1	3
13	REACTOME_BIOLOGICAL_OXIDATIONS	4/101	22/1407	6,7E-02	2,9E-01	2,4E-01	ALDH1A1/UGDH/CNDP2/GCLM	4
13	REACTOME_SIGNALLING_BY_NGF	4/101	22/1407	6,7E-02	2,9E-01	2,4E-01	CLTC/PRKACA/CASP3/PPP2R1A	4
13	KEGG_ENDOCYTOSIS	5/101	32/1407	7,4E-02	3,1E-01	2,5E-01	CHMP4B/HSPA2/CLTC/HSPA6/RAB11B	5
13	KEGG_INSULIN_SIGNALING_PATHWAY	4/101	23/1407	7,7E-02	3,2E-01	2,6E-01	PYGB/FASN/PRKACA/HK1	4
13	REACTOME_NGF_SIGNALLING_VIA_TRKA_FROM_THE_PLASMA_MEMBRANE	3/101	15/1407	8,7E-02	3,5E-01	2,8E-01	CLTC/PRKACA/PPP2R1A	3

13	REACTOME_REGULATION_OF_MRNA_STABILITY_BY_PROTEINS_THAT_BIND_AU_RICH_ELEMENTS	3/101	15/1407	8,7E-02	3,5E-01	2,8E-01	PSMD5/PABPC1/KHSRP	3
13	KEGG_PYRUVATE_METABOLISM	3/101	16/1407	1,0E-01	4,0E-01	3,3E-01	LDHB/ME1/LDHA	3
13	REACTOME_GLUCOSE_METABOLISM	4/101	26/1407	1,1E-01	4,2E-01	3,5E-01	GBE1/PYGB/PRKACA/PPP2R1A	4
13	KEGG_AMINO_SUGAR_AND_NUCLEOTIDE_SUGAR_METABOLISM	3/101	17/1407	1,2E-01	4,4E-01	3,6E-01	MPI/UGDH/HK1	3
13	REACTOME_ANTIGEN_PROCESSING_UBIQUITINATION_PROTEASOME_DEGRADATION	3/101	18/1407	1,3E-01	5,0E-01	4,1E-01	PSMD5/UBE2N/TPP2	3
13	KEGG_GLYCOLYSIS_GLUCONEOGENESIS	4/101	29/1407	1,5E-01	5,0E-01	4,1E-01	LDHB/GALM/HK1/LDHA	4
13	REACTOME_PHASE_II_CONJUGATION	3/101	19/1407	1,5E-01	5,0E-01	4,1E-01	UGDH/CNDP2/GCLM	3
13	ST_INTEGRIN_SIGNALING_PATHWAY	3/101	19/1407	1,5E-01	5,0E-01	4,1E-01	CSE1L/ACTR3/ACTR2	3
13	KEGG_CYSTEINE_AND_METHIONINE_METABOLISM	2/101	10/1407	1,6E-01	5,0E-01	4,1E-01	LDHB/LDHA	2
13	KEGG_WNT_SIGNALING_PATHWAY	2/101	10/1407	1,6E-01	5,0E-01	4,1E-01	PRKACA/PPP2R1A	2
13	REACTOME_GLUTATHIONE_CONJUGATION	2/101	10/1407	1,6E-01	5,0E-01	4,1E-01	CNDP2/GCLM	2
13	REACTOME_MYD88_MAL_CASCADE_INITIATED_ON_PLASMA_MEMBRANE	2/101	10/1407	1,6E-01	5,0E-01	4,1E-01	UBE2N/PPP2R1A	2
13	REACTOME_REGULATION_OF_APOPTOSIS	2/101	10/1407	1,6E-01	5,0E-01	4,1E-01	PSMD5/CASP3	2
13	REACTOME_SULFUR_AMINO_ACID_METABOLISM	2/101	10/1407	1,6E-01	5,0E-01	4,1E-01	CNDP2/GCLM	2
13	REACTOME_TRAF6_MEDIATED_INDUCTION_OF_NFKB_AND_MAP_KINASES_UPON_TLR7_8_OR_9_ACTIVATION	2/101	10/1407	1,6E-01	5,0E-01	4,1E-01	UBE2N/PPP2R1A	2
13	PID_HIF1_TFPATHWAY	3/101	20/1407	1,7E-01	5,2E-01	4,3E-01	HK1/TF/LDHA	3
13	REACTOME_HOST_INTERACTIONS_OF_HIV_FACTORS	3/101	20/1407	1,7E-01	5,2E-01	4,3E-01	PSMD5/KPNB1/RAN	3
13	REACTOME_ACTIVATED_TLR4_SIGNALLING	2/101	11/1407	1,8E-01	5,4E-01	4,5E-01	UBE2N/PPP2R1A	2
13	REACTOME_FACTORS_INVOLVED_IN_MEGAKARYOCYTE_DEVELOPMENT_AND_PLATELET_PRODUCTION	2/101	11/1407	1,8E-01	5,4E-01	4,5E-01	CAPZA1/PRKACA	2
13	SIG_CHEMOTAXIS	2/101	11/1407	1,8E-01	5,4E-01	4,5E-01	ACTR3/ACTR2	2
13	KEGG_GLUTATHIONE_METABOLISM	3/101	21/1407	1,9E-01	5,5E-01	4,5E-01	IDH2/GCLM/G6PD	3
13	REACTOME_METABOLISM_OF_AMINO_ACIDS_AND_DERIVATIVES	5/101	44/1407	2,0E-01	5,8E-01	4,8E-01	PSMD5/GLUD1/CNDP2/PHGDH/GCLM	5
13	KEGG_PURINE_METABOLISM	3/101	22/1407	2,1E-01	5,8E-01	4,8E-01	AK2/ATIC/ADSS	3
13	KEGG_VASOPRESSIN_REGULATED_WATER_REABSORPTION	2/101	12/1407	2,1E-01	5,8E-01	4,8E-01	PRKACA/RAB11B	2
13	REACTOME_DESTABILIZATION_OF_MRNA_BY_AUF1_HNRNP_D0	2/101	12/1407	2,1E-01	5,8E-01	4,8E-01	PSMD5/PABPC1	2
13	REACTOME_HIV_INFECTION	3/101	23/1407	2,3E-01	6,2E-01	5,1E-01	PSMD5/KPNB1/RAN	3
13	KEGG_APOPTOSIS	2/101	13/1407	2,4E-01	6,2E-01	5,1E-01	PRKACA/CASP3	2
13	KEGG_FRUCTOSE_AND_MANNOSE_METABOLISM	2/101	13/1407	2,4E-01	6,2E-01	5,1E-01	MPI/HK1	2

13	REACTOME_PURINE_METABOLISM	2/101	13/1407	2,4E-01	6,2E-01	5,1E-01	ATIC/ADSS	2
13	REACTOME_SIGNALING_BY_FGFR	2/101	13/1407	2,4E-01	6,2E-01	5,1E-01	PRKACA/PPP2R1A	2
13	REACTOME_METABOLISM_OF_LIPIDS_AND_LIPOPROTEINS	6/101	59/1407	2,4E-01	6,3E-01	5,2E-01	APOC3/ACLY/FASN/PRKACA/PITPNB/ME1	6
14	KEGG_COMPLEMENT_AND_COAGULATION_CASCADES	17/99	59/1407	1,6E-07	3,1E-05	2,9E-05	C4A/SERPING1/CPB2/SERPIND1/C5/C8G/F12/C6/KNG1/SERPINF2/C8A/CFH/SERPINC1/C8B/PLAU/C4B/CFB	17
14	NABA_ECM_REGULATORS	21/99	118/1407	2,9E-05	2,8E-03	2,6E-03	HRG/SERPING1/SERPIND1/F12/PZP/KNG1/ITIH4/ITIH1/CTSF/CPN2/SERPINF2/SERPINA11/ADAMTSL2/ITIH2/AGT/SERPINC1/HTRA1/ADAMTS13/PLAU/ITIH3/MMP19	21
14	REACTOME_COMPLEMENT_CASCADE	8/99	26/1407	2,5E-04	1,6E-02	1,5E-02	C4A/C5/C8G/C6/C8A/CFH/C8B/CFB	8
14	BIOCARTA_LECTIN_PATHWAY	5/99	12/1407	8,3E-04	3,7E-02	3,4E-02	C4A/C5/C6/C8A/C4B	5
14	KEGG_CYTOKINE_CYTOKINE_RECEPTOR_INTERACTION	10/99	47/1407	1,1E-03	3,7E-02	3,4E-02	TGFB1/GHR/EGFR/CSF1R/PRL/INHBC/LEP/MET/IL6ST/FAS	10
14	KEGG_SYSTEMIC_LUPUS_ERYTHEMATOSUS	7/99	25/1407	1,2E-03	3,7E-02	3,4E-02	C4A/C5/C8G/C6/C8A/C8B/C4B	7
14	BIOCARTA_COMP_PATHWAY	6/99	19/1407	1,3E-03	3,7E-02	3,4E-02	C4A/C5/C6/C8A/C4B/CFB	6
14	BIOCARTA_CLASSIC_PATHWAY	5/99	14/1407	1,9E-03	4,6E-02	4,2E-02	C4A/C5/C6/C8A/C4B	5
14	PID_UPA_UPAR_PATHWAY	6/99	23/1407	3,9E-03	8,5E-02	7,9E-02	GPLD1/TGFB1/LRP1/EGFR/ITGB1/PLAU	6
14	REACTOME_HEMOSTASIS	15/99	116/1407	1,2E-02	2,4E-01	2,2E-01	HRG/SERPING1/TGFB1/APOB/F12/THBS1/KNG1/MERTK/ITGB1/CLU/SERPINF2/SERPINC1/L1CAM/PLAU/SLC3A2	15